Regional-Scale Flows in Complex Terrain: An Observational and Numerical Investigation

by James E. Bossert

Colorado State University

DEPARTMENT OF ATMOSPHERIC SCIENCE

PAPER NO. 472

Regional-Scale Flows in Complex Terrain: An Observational and Numerical Investigation

by

James E. Bossert

Department of Atmospheric Science

Colorado State University

Fort Collins, CO 80523

Research Supported by

The National Science Foundation

under grant ATM-8610796

Air Force Office of Scientific Research

under contract F49620-85-C-0077DEF

National Aeronautics and Space Administration

under grant NAGW601

and

Army Research Office

under contract DAAL03-86-K-0175

Atmospheric Science Paper No. 472

ABSTRACT

REGIONAL-SCALE FLOWS IN COMPLEX TERRAIN: AN OBSERVATIONAL AND NUMERICAL INVESTIGATION

An observational program has been conducted to obtain information concerning thermally-driven flows in complex terrain on meso-β to meso-α scales (100 - 500 km). Data were collected from remote surface observing systems at exposed mountaintop locations throughout the state of Colorado, over the summers of 1984-1988. These field experiments have been called the Rocky Mountain Peaks Experiments (ROMPEX). The observations from ROMPEX have been supplemented with data from other remote surface networks, special soundings, upper-air observations, and radar and lightning strike information to provide an adequate description of the flows and weather of interest.

The observations have shown the development of a recurrent "regional-scale" circulation system across the Colorado mountain barrier, operating on a diurnal time scale. The basic structure of the flow system consists of a daytime inflow phase toward the mountains along the Continental Divide, and a nocturnal outflow away from this high terrain. Long-term averages show this circulation system to be the dominant wind pattern at several high altitude stations, revealing its climatological significance. Attention has been focused upon the nocturnal phase of the circulation system along the western slope of the mountain barrier. Here, the winds are particularly strong and from a southeasterly direction, which is generally counter to the upper-level winds, and onset abruptly in early evening with steady flow thereafter. Soundings have shown this nocturnal current to be shallow and within a distinct stable air mass. Convective storms are found to enhance this southeasterly flow regime.

Numerical simulations have been performed with the Colorado State University Regional Atmospheric Modelling System (CSU-RAMS) to provide further insight into the physical mechanisms forcing the observed regional-scale circulation system. The model simulations include both idealized two- and three-dimensional experiments, as well as a three-dimensional case study experiment using actual data for the initialization. The three-dimensional simulations use two-way interactive grid nesting and a realistic representation of topography over the region of interest.

The idealized three-dimensional experiment showed that thermal forcing over realistic topography in conditions of negligible, or weak ambient flow, is capable of producing many of the flow features observed throughout the diurnal cycle. This experiment further showed how the deep mountain-plains solenoid along and above the Front Range crest evolves in late afternoon into a shallower density current, which then propagates westward over the mountains of the western slope. This unexpected flow phenomenon is the primary process responsible for the strong nocturnal southeasterly winds found in observations. Sensitivity experiments show that the particular terrain configuration through an east-west cross-section of the Colorado mountains is important to the generation of this unusual circulation. The strong thermal gradient produced by differential heating of the topography is the primary driving force in the density current evolution. Coriolis influence maintains the steady nocturnal south-southeast winds over the western slope. Additional experiments show that the diurnally evolving regional-scale circulation system over the Colorado Rocky Mountains is a robust feature which can occur over a range of ambient flow and stratification conditions. Soil moisture experiments reveal that wet soil along the eastern slope and dry along the western slope aids the development of the westward propagating density current.

The diurnal evolution of the circulation system on the case study day was in fair agreement with many of the observed circulation features. This experiment also revealed that synoptic-scale forcing can influence the development of the regional-scale circulations in preferential regions along the eastern slope of the mountain barrier. As a result of the numerical experiments four phases of the thermally forced regional-scale diurnal circulation system have been identified. These consist of a daytime mountain boundary layer

development phase, a late afternoon transitional phase, an evening propagating density current phase, and a late night adjustment phase.

James E. Bossert
Department of Atmospheric Science
Colorado State University
Fort Collins, Colorado 80523
Fall, 1990

ACKNOWLEDGEMENTS

I am especially grateful for the support and guidance of Dr. William R. Cotton for providing me with the environment and resources necessary to complete the modeling phase of this research. I would like to thank my co-advisor Dr. Thomas B. McKee for his valuable suggestions and assistance throughout the course of this work. To Dr. Elmar R. Reiter, who supported me through the observational portion of this research work, I also extend my gratitude. The comments and participation of my other committee members, Drs. Richard H. Johnson and Jack E. Cermak, are also appreciated.

The author is truly indebted to Carolyn Bossert for her unfaltering encouragement during the various phases of this research, and for her skillful layout and editing of the manuscript. Brenda Thompson is recognized for her advice and assistance in the manuscript preparation. Thanks are also extended to Lucy McCall and Judy Sorbie-Dunn, both of whom assisted in the development of several figures within this report.

Special thanks are extended to those who personally endured many hardships to help me collect data in some very remote locations and occasionally late into the night. None of the observational research could have been obtained without the counsel and dedicated effort of John D. Sheaffer. Others I would like to acknowledge are Jerome M. Schmidt, Qi Hu, James F. Bresch, Richard C. Fleming, and Richard Graw.

The opportunity to conduct field research over the years within the high mountain terrain of Colorado was made possible by many personnel within the U.S. Forest Service, the Bureau of Land Management, and at various ski resorts around the state of Colorado, who were instrumental in approving site locations for our monitoring equipment. I also extend my thanks to the personnel in the Atmospheric Processes Group at the Los Alamos National Laboratory, NOAA-PROFS, the Bureau of Reclamation, the Boise Interagency

Fire Center, the United States Geological Survey, and the Data Support Section at NCAR for providing me with valuable data for this study.

The numerical portion of this dissertation was made possible through the guidance of Drs. Craig J. Tremback and Robert Walko. The assistance in the development of several simulations by Peter Q. Olsson is gratefully acknowledged. This study was improved tremendously by discussions, suggestions, and criticisms from Jerome Schmidt, John D. Sheaffer, Peter Olsson, Michael Moran, Ray McAnelly, and Michael Meyers.

This research was sponsored by the NASA under grant NAGW601, by the National Science Foundation under grant ATM-86-10796, by the Air Force Office of Scientific Research, Air Force Systems Command, grant F49620-85-C-0077DEF, by the U.S. Department of Energy Atmospheric Studies in Complex Terrain (ASCOT) Program under the University of California, Los Alamos National Laboratory subcontract 9-X38-5759V-1, and finally by Army Research Office under contract #DAAL03-86-K-0175. Much of the computing was performed at the National Center for Atmospheric Research (NCAR). NCAR is sponsored by the National Science Foundation.

TABLE OF CONTENTS

LIST OF FIGURES

LIST OF TABLES

Chapter 1

INTRODUCTION

For more than a century, man has endeavored to understand the pervasive wind circulations which occur in regions of sloping terrain (Fournet 1840; Hann 1878). Early observations showed that air motion down the slopes was a dependable phenomenon at night, while a general up the slope wind was the rule by day. Despite the apparent simplicity of this diurnal flow regime, a working theoretical explanation eluded early meteorologists until the development of Bjerknes' circulation theorem (Jeffreys 1922; Wenger 1923). These early theories were greatly expanded upon in later years (Ekhart 1934, 1944; Burger and Ekhart 1937; Wagner 1938; Defant 1949) to include more complicated and realistic forcing mechanisms over the slopes, and also include the circulations within mountain-valleys. With more recent observational evidence, we now recognize the importance of thermal forcing in complex terrain regions on all scales, from those of small slopes and mountain-valleys, up to the largest plateau land masses (Reiter and Tang 1984).

While most of the research attention to date has been focused upon thermally-driven flows along small scale slopes, and within mountain-valleys (micro-α to meso-β scales), some observations are available which show that terrain-induced flows can also be found on meso-β to meso-α scales (20 - 2000 km), provided a strong signal is induced by the underlying topography. For example, in South Africa, Tyson and Preston-Whyte (1972) described a diurnally-oscillating circulation system which evolves in winter between the Natal coast and the Drakensburg Plateau, a horizontal distance of 200 km. These authors called this circulation system the "mountain-plain" wind, to distinquish it from the smaller scale mountain-valley winds above which this wind regime occurs. In the United States, prominent, thermally-forced circulation systems with horizontal scales over 100 km have been found in both winter and summer in Washington state (Staley 1957; Mass 1982) and

along the Colorado Front Range in summer (Dirks 1969; Banta and Cotton 1981; Smith and McKee 1983; Toth and Johnson 1985). Given that these flows can cover a large topographic region in scale, they are regarded here as "regional-scale" flow systems as a convenient way to separate them from smaller-scale mountain-valley flows, or larger scale thermally forced wind systems which can encompass whole plateau areas (Tang and Reiter 1984).

Along the Front Range of the Rocky Mountains, a primary feature of this flow system is a thermally-forced mountain-plains solenoid, which has been shown to be an important factor in the development of convective storms (Tripoli and Cotton 1989a,b; Tremback 1990), which can then propagate eastward and evolve into large mesoscale convective complexes over the Great Plains. These convective complexes bring a high percentage of the total summer rainfall to the Midwest. In Washington state, these regional-scale flow systems have been associated with an increase in nocturnal precipitation over the Puget Sound region (Mass 1982). While these studies point out the implications of regional-scale flows concerning the convergence and transport of moisture, the potential impacts of these flows can easily be extended to questions of pollutant transport, forest fire control, mesoscale weather forecasting, and low-level or small aircraft safety in mountainous terrain. Most of these topics have received little research attention.

While the above studies might suggest that the regional-scale flows have been adequately studied, in actuality the available literature reveals that, at present, a dearth of knowledge exists on these "regional-scale" flows (see Barry 1981; and Atkinson 1981). On the whole, the limited knowledge we do possess regarding regional-scale circulation systems has generally been obtained as a secondary concern within studies whose primary focus involves some other meteorological flow or process. Thus, detailed evidence regarding the nature of these circulation systems in complex terrain is largely unknown, despite the proven and potential importance of these flow systems.

This lack of information is not surprising, given the difficulties inherent in analyzing flow regimes on scales significantly below those observable with the standard rawinsonde network. Only in recent years, with the advent of portable observing systems capable of operating in remote locations, has detailed observation of regional-scale flows been possible. Even still, these remote surface-based networks can provide only a two-dimensional view

of the flow system, leaving their full three-dimensional structure a mystery. The fact that these regional-scale wind systems are often attached to topography features which cover vast regions of remote, complex terrain provides an additional complication.

In this dissertation, an attempt is made to provide a detailed, three-dimensional investigation of thermally-induced meso-β to meso-α scale wind systems which occur across the Colorado Rocky Mountain barrier. The Front Range mountain-plains solenoid comprises the eastern branch of this flow system. In this regard, this study is the most ambitious attempt thus far at providing a comprehesive examination of thermally-induced wind systems on these larger mesoscales. While adequate evidence of these flow systems has been shown along the eastern slope of the Colorado Front Range as described above, only sketchy evidence (Whiteman 1980; Barr and Clements 1981; Bader *et al.* 1987) has been available over the western slope until recently (Reiter *et al.* 1987a; Bossert and Reiter 1987; Bossert *et al.* 1989). The purpose of the study is to answer some basic questions regarding the structure of this flow system and the primary mechanisms forcing its diurnal evolution over these larger scales. In this way we can understand whether these flow systems behave like simple slope flows, or are the result of more complex regional-scale dynamics and energy transfers.

The tools available to accomplish these goals include both observational and numerical analyses. The observational data from various mountaintop stations have been used to successfully diagnose the horizontal and vertical structure of this wind regime, as well as provide some climatological data on its frequency of occurrence. From these data, a peculiar component of this regional-scale wind system has been discovered. This is a strong southeasterly nocturnal outflow wind at the mountaintop level over western Colorado. The numerical modelling of these flows has demonstrated the complex nature through which they redistribute mass and energy across the mountain barrier throughout the diurnal cycle. The results from this study have allowed us to document the three-dimensional structure of a largely unknown yet prominent circulation system within the hierarchy of thermally-forced flows over high terrain.

In the following chapters literature concerning the hierarchical order of thermally-induced flows within complex terrain is reviewed (Chapter 2). This literature review is

meant to provide a perspective of thermally-driven winds within which the regional-scale flows are an important component. After this literature review, we will describe the design of (Chapter 3), and observations obtained from (Chapter 4), a field program which was conducted over the Colorado Rocky Mountains during the summers of 1984-1988, with the intention of documenting regional-scale circulations over this complex terrain region. To obtain additional insight into the regional-scale flows beyond what the observations alone can provide, numerical experiments will be presented which include idealized experiments dealing strictly with the influence of important physical processes on the evolution of the regional-scale flows (Chapter 5), and a case study experiment (Chapter 6) which attempts to simulate conditions for an actual day when the observations indicated a strong regional-scale signal. Finally, we summarize the results of this study through a conceptual model of the thermally-forced flows across the entire Colorado mountain barrier, and then draw several key conclusions regarding these flow systems, based upon the results of this study (Chapter 7).

Chapter 2

SUMMARY OF PRIOR RESEARCH

In this chapter we discuss the nature and interrelationships of thermally-forced circulations in mountainous terrain over the various spatial and temporal scales on which they can occur. Understanding the range of thermally-forced flows is imperative to the central theme of this dissertation, which is to observationally and numerically examine the nature of regional-scale flows over the mountains of Colorado. Essential to this effort will be an examination of the classical works regarding thermal forcing in complex terrain, for these studies represent the foundation upon which all contemporary results are based. It seems appropriate to begin this review with the most fundamental flow within the hierarchy of thermally-forced circulations, the slope flows. While terrain slopes can cover great horizontal distances, here we are only concerned with slopes on micro-α to meso-γ scales (1-20 km). These are the scales over which most observational data have been taken and at which existing theories are applicable. Investigation of larger-scale slopes and their resulting circulations is the major goal of the present study.

2.1 Slope Flows

2.1.1 General concepts

The slope flow regime consists of an anabatic (upslope) and katabatic (downslope) wind found over any inclined surface that is heated or cooled. The driving mechanism of these flows is the buoyancy which results from diabatic forcing of the inclined surface relative to the unaffected atmosphere some horizontal distance away from the slope. The buoyancy generates a hydrostatic pressure difference which induces horizontal motion from the atmosphere toward (away from) the slope for heating (cooling) and upward (downward) motion due to the positive (negative) buoyancy of a parcel located near the slope. Thus,

daytime heating of the slope induces lower pressure in the air layer near the slope, with ascending and toward the slope motion resulting in upslope (anabatic) flow. Nocturnal radiative cooling at the slope surface creates the opposite effect. Colder and denser than the unaffected environmental air, parcels near the surface become negatively buoyant. This results in flow downward and away from the slope constituting the downslope (katabatic) wind regime. A more detailed explanation of this process can be found in Atkinson (1981).

2.1.2 Early studies

European scientists were among the first to attempt an explanation of the physics behind slope flows. Much of the early work on slope winds was begun around the turn of the century by German speaking meteorologists, and was essentially qualitative in nature. Several more notable theoretical papers can be found in the inter-war era. Jeffreys (1922) discussed the baroclinic nature of the slope wind, whose speed he found to vary directly with horizontal temperature gradient and terrain slope. Similar results were obtained by Wenger (1923), who applied Bjerknes' circulation theorem to a heated slope and determined upslope accelerations. The observed characteristics of slope flows also received much attention during this time (Heywood 1933; Moll 1935; Jelinek 1937a,b; Burger and Ekhart 1937). These studies revealed many of the now well-known features of the slope wind regime: the start of the upslope and downslope winds shortly after sunrise and sunset, respectively; the speed maximum of the flow near the slope surface; and the shallow nature of slope winds.

More detailed and quantitative theories of slope winds were developed during and just following World War II. These studies were analytical in nature and generally considered only highly idealized slopes and flow structure. One of the most durable of these theories was that of Prandtl (1942). He assumed that cooling of the slope created a temperature deficit and resulting buoyancy force. This buoyancy force is assumed to be balanced by frictional effects. With these assumptions Prandtl was able to obtain an analytical expression for steady flow down an infinite slope. Defant (1949) expanded upon Prandtl's work to include the non-stationary case. Good agreement was found by Defant (1951) between Prandtl's model and the observed downslope winds on the sidewalls of the Inn Valley in Austria. Prandtl (1952) extended his theory of downslope flows to also include the upslope case.

This produced the unexpected result that the upslope wind speed was independent of the slope angle. Figure 2.1 shows the vertical profile of the wind and temperature perturbation associated with Prandtl's solution for upslope flow.

Fleagle (1950) incorporated a dynamic term d^2u/dt^2 to obtain a time-dependent analytical equation, analogous to that of a damped linear oscillator with a constant force, to examine the surging observed in nocturnal downslope flows. His solutions showed that as the flow moves down the slope, adiabatic warming results in an opposing pressure gradient force which slows the flow until radiational cooling can overcome the adverse pressure gradient and continue the downslope acceleration. Following a direction similar to Fleagle, Petkovsek and Hocevar (1971) developed an antitriptic model, where friction balances the pressure gradient, to obtain an expression for the drainage velocity.

2.1.3 Recent theoretical and observational research

The early theoretical studies with highly simplified analytical models were valuable in that they allow one to examine, in a direct way, the response of the slope flow system to changes in the forcing parameters. However, these models still leave many questions regarding slope flows unanswered. In particular, these models are incapable of simulating the complex time-dependent vertical structure of the drainage flow, changes in slope, and changes in the radiative characteristics of the surface. In addition, most of these analytical models consider only the nocturnal downslope flow. The daytime upslope winds have been little studied, mainly due to their highly turbulent nature. Upslope winds can also be difficult to distinguish from more regional airflow in well-mixed boundary-layers (Barry 1981). However, the advent of computers enabled Orville (1968) to develop a numerical model of upslope flow based upon a horizontal vorticity equation. The aim of this modeling effort was to examine stability effects upon the upslope circulation. Mahrer and Pielke (1977a) successfully simulated large-scale upslope and downslope flow in two-dimensions using a hydrostatic, primitive equation model (Pielke 1974).

The vast improvement in measurement systems and computer speed over the last several decades has greatly enhanced our ability to observe and model complex terrain flows. Observational data include several studies using instrumented towers over simple slopes

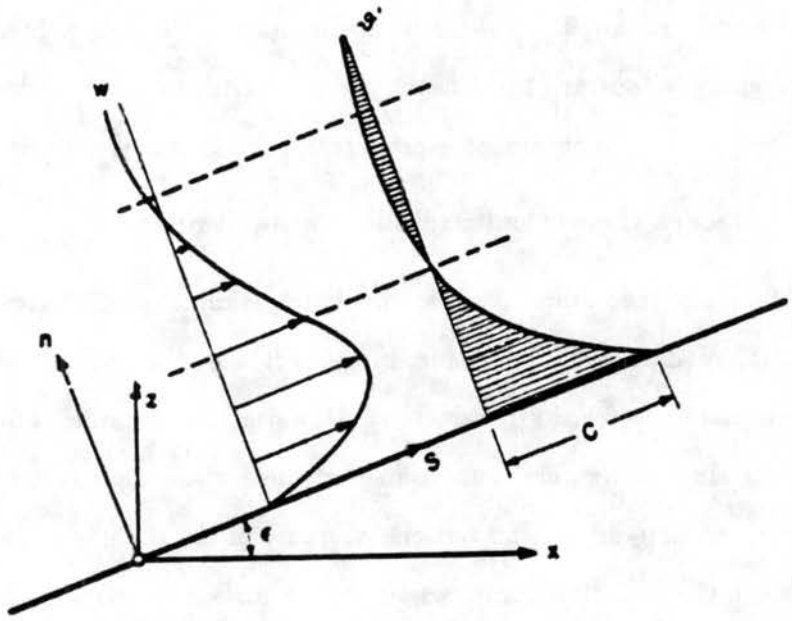

Figure 2.1: Schematic profiles (normal to the slope) of the wind speed u and potential temperature θ'.

(Manins and Sawford 1979a; Doran and Horst 1981; Mahrt and Larsen 1982) to obtain detailed vertical and temporal information on nocturnal slope flow behavior. Much of this research is oriented toward understanding transport and dispersion processes in complex terrain, as stable drainage flows will tend to trap atmospheric pollutants close to the ground. Upslope winds have still been largely neglected, however, several studies have discussed the complex development of upslope flows within a mountain-valley. Egger (1981) further enhanced Prandtl's model to include variable surface forcing, and obtained quasi-analytical solutions which showed that the effects of localized slope heating can extend over a large horizontal and vertical distance above the slope, strongly influencing the thermal structure of the valley. Similar results were obtained by Bader and McKee (1983) who simulated the early transient behavior over the slopes early in the heating cycle, where stable pockets develop over the valley sidewalls. These stable pockets temporarily block the slope flow and force transient cross-valley circulations which can destabilize the valley boundary layer.

Recent theoretical research on slope flows has continued to focus mainly upon the development of one-dimensional models of drainage flows with more realistic inclusion of the force balances, based upon more detailed observational data. Manins and Sawford (1979b) used a set of equations, vertically averaged over the katabatic flow depth, to examine the effects of ambient stratification and cooling along the slope on downslope flow development. This averaging method was employed in the hydraulic theory of Ellison and Turner (1959) in their study of turbulent entrainment into stratified flows. One of the principal conclusions in the steady solutions of Manins and Sawford was that shear-induced entrainment of ambient air into the katabatic layer is the main retarding force on the flow, and that surface stress is relatively unimportant.

Doran and Horst (1983) found that Manins and Sawford's layer averaged approach produced ambiguities in the specification of katabatic flow from ambient flow. Thus, these authors developed a simple numerical model where the eddy diffusivity is related to the local turbulent kinetic energy. Their model showed some skill in reproducing the observed structure of nocturnal drainage flows down the slopes of Rattlesnake Mountain in central Washington. Further investigations by these authors (Horst and Doran 1986) of the momentum balance of the Rattlesnake Mountain katabatic flow suggested that the surface

stress was up to three times stronger than the interfacial stress and is the dominant retarding force. This stands in contrast to Manins and Sawford's conclusions. Some of this discrepancy may be due to the different drag coefficients assumed in each study.

An even more general one-dimensional model of katabatic flow was developed by Fitzjarrald (1984), using an approach similar to that of Manins and Sawford (1979b). He found that the onset of katabatic winds is very sensitive to the cooling rate on the slope and the retarding effect of opposing ambient flow. His results provide a theoretical basis for the observed delay in drainage flows in a humid tropical location with reduced nocturnal cooling and opposing easterly tradewinds. More recent one-dimensional model studies by Arritt and Pielke (1987) and Kondo and Sato (1988) have also examined ambient wind effects on drainage flows. A comparison of the simulated temperature and downslope velocity from Arritt and Pielke (1987) with observations from Rattlesnake Mountain (Doran and Horst 1983) is shown in Fig. 2.2.

The research results described above have treated slope flows as a singular entity within complex terrain. However, observations of slope flows generally result from field experiments investigating thermally-driven wind systems over larger areas in complex terrain, often encompassing a mountain valley. This type of experiment provides a greater opportunity to study the complicated relationships between thermally-driven flows of different scales. At this juncture we will consider the broader role of the slope circulations as the most basic component within a structured, hierarchical order of flows in complex terrain. Hence, we now "move up a scale" and consider the mountain-valley (meso-γ to meso-β) scale and its associated slope, and mountain and valley wind systems.

2.2 Mountain-Valley Flows

2.2.1 General concepts

Two fundamental components of complex topography available for thermal forcing are the valley floor and the sidewall slopes. The air within the valley will be directly influenced by the flows along the sidewall slopes. However, the larger-scale of the valley allows for a more complex response to thermal forcing. The simplest way to discuss this effect is by considering a mountain-valley which empties out onto a flat plain. The volume of air

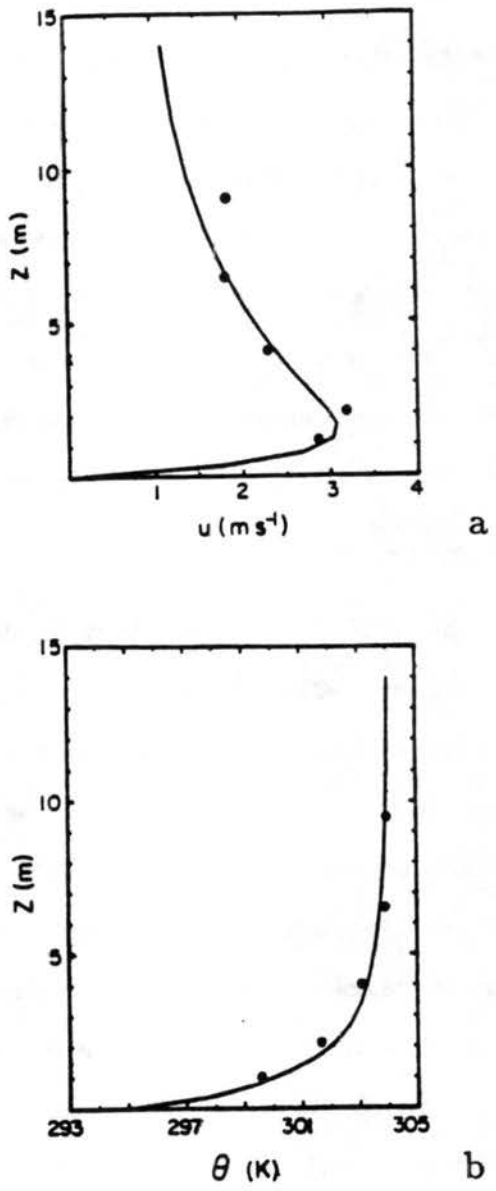

Figure 2.2: Predicted (a) velocity and (b) potential temperature profiles for 1-2 July 1980 at Rattlesnake Mountain (solid curves) compared to observed data (dots).

contained within the valley up to ridgetop is considerably less than that over the plain for the same height, and can be assessed by calculating a "topographic amplification factor" (Steinacker 1984; McKee and O'Neal 1989). The incident and outgoing radiation through a slab located over the valley or plain will be approximately equal, causing the valley to experience a higher amplitude diurnal temperature wave than the air over the plain. Thus, stronger daytime heating of the valley air mass generates higher temperatures which in turn induce lower pressure within the valley relative to the plain. The resulting horizontal pressure gradient generates a wind acceleration toward the valley. This daytime "upvalley" wind blows into the valley from the adjacent plains. At night, when the valley air mass is colder than that over the plain, the pressure gradient reverses and the mountain or "downvalley" wind blows from the valley toward the plain.

2.2.2 Early conceptual models

The conceptual model of the mountain-valley circulation system described above was first developed by Wagner (1938), who also discussed the interaction between the slope winds on the valley sidewalls and the mountain-valley winds. This early work by Wagner was later summarized in the now classic diagram of Defant (1949, 1951). The conceptual model of the interaction between flow regimes (Fig. 2.3) begins at sunrise, when heating on the valley sidewalls gives rise to shallow upslope circulations. At this time winds in the valley are downvalley, due to the cold, denser air that remains there relative to the plain. The action of the upslope winds removes mass from the bottom of the valley, which is replaced by warmer air from above the stable valley air mass. In the mid-morning hours, increased heating enhances the mass overturning process generated by the upslope flows, removing the cold stable air within the valley, equalizing the hydrostatic pressure between valley and plain and eliminating the downvalley wind. A neutral lapse rate is then established which allows the upslope flows and their return currents to freely circulate air within the valley.

The continuation of heating beyond this point induces an excess temperature perturbation within the valley relative to the plain. This generates upvalley flow, which reaches its peak velocity in the early afternoon. The upslope winds continue, but are reduced in

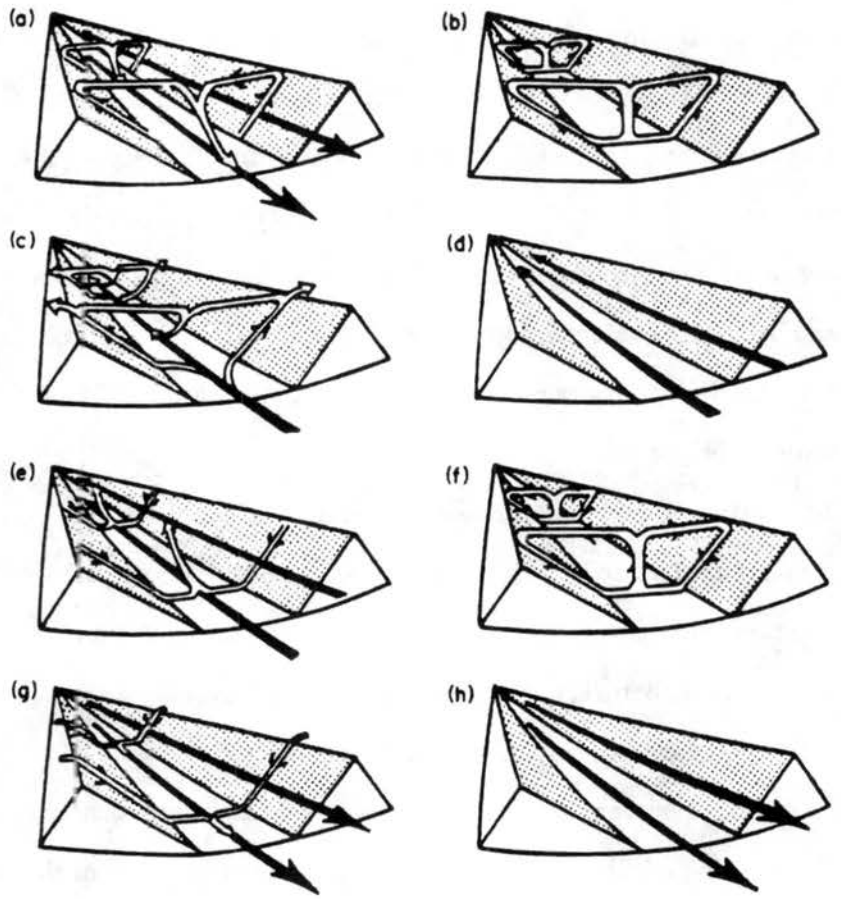

Figure 2.3: Schematic illustration of the diurnal variation of air currents in a valley. (From Defant, 1949.) (a) sunrise; onset of upslope winds (white arrows), continuation of mountain wind (black arrows). Valley cold, plains warm. (b) Mid-morning; strong slope winds, transition from mountain wind to valley wind. Valley temperature same as plains. (c) Noon to early afternoon; diminishing slope winds, fully developed valley wind. Valley warmer than plains. (d) Late afternoon; slope winds have ceased, valley wind continues. Valley continues warmer than plains. (e) Evening; onset of downslope winds, diminishing valley wind. Valley only slightly warmer than plain. (f) Early night; well-developed downslope winds, transition from valley wind to mountain wind. Valley and plains at same temperature. (g) Middle of night; downslope winds continue, mountain wind fully developed. Valley colder than plains. (h) Late night to morning; downslope winds have ceased, mountain wind fills valley. Valley colder than plains.

velocity due to the more homogeneous temperature structure within the valley. These upslope winds also extend over the ridges which encompass the valley. In the late afternoon, the upslope flow stops as surface heating diminishes. The upvalley winds continue unabated since the overall air temperature within the valley continues to be higher than that over the adjacent plains. In early evening, as the slopes of the valley cool and downslope motion begins, a redistribution of mass occurs within the valley. This process, along with the advection of cooler air into the valley, eventually combine to dissipate the upvalley wind. Only the downslope winds remain until further cooling of the valley relative to the plain initiates the downvalley wind in late evening. The downvalley and downslope winds continue until near sunrise, when the downslope winds begin to die out. The cold air within the valley maintains the downvalley wind, however, and at sunrise the upslope winds return and the whole process begins anew.

The Wagner-Defant mountain-valley circulation model provides a simple generalized conceptual framework to describe the interaction of slope and valley flows. It is important to keep in mind that this model is a highly simplified explanation of an often complex three-dimensional flow structure, and that many important processes are not accounted for. Some of these processes are: 1) the radiative characteristics of the valley floor and sidewalls, which will be influenced by vegetative cover, snow cover, and soil moisture; 2) cross-valley winds caused by shading effects of one sidewall, due to the orientation of the valley relative to the solar path; 3) the complex geometry of the valley and surrounding ridges; 4) the influence of larger-scale thermally-induced winds and gradient level winds along with their shear and wave characteristics. Each of these will directly impact the mountain-valley circulation at a given location.

2.2.3 Further developments upon early studies

Many others have expanded upon the basic conceptual model put forth by Wagner to try and accommodate some of the important processes listed above. For example, Gleeson (1951, 1953) provided a theory for the development of cross-valley winds, which arise from the differential heating of each slope due to solar orientation relative to the valley. Gleeson

included Coriolis terms in his analytical model, a rarity in theoretical studies of slope and mountain-valley winds.

A conceptual model of the effects of differential heating across the Dischma Valley in Switzerland was given by Urfer-Henneberger (1970). This model (Fig. 2.4), based upon extensive observations, provides a more realistic picture of the diurnal flow evolution within the mountain valley than does the Wagner-Defant model. The figure shows the complex three-dimensional structure which develops within the valley when all or part of one sidewall receives radiation while the other remains shaded. Strong cross-valley winds can develop, and a helical pattern can be found in the main up- or downvalley flow. In a study of the vertical structure of the winds within and above the mountain-valley, Buettner and Thyer (1966) noted the presence of anti-valley and anti-mountain winds above the ridges containing the Carbon River Valley in Washington. These anti-winds, which must exist from continuity considerations, were found to occupy the layer between the mountain or valley wind and the overlying gradient flow. Their direction was often somewhere in between those of the low-level thermally-forced flow and the synoptic-scale flow, suggesting that these winds encompassed a transitional layer between the two regimes. The speeds of the anti-winds were generally light, perhaps contributing to the lack of prior observations of these winds.

The effects of ambient flow from a cross-valley direction on the mountain-valley circulation has been studied analytically by Tang (1976) and numerically by Carlson and Foster (1986a,b), showing a strong interaction between these winds and the slope winds on the windward and lee slopes. Thermal stratification of the mountain-valley regime and the effects of slope winds in recirculating the mass within the stable core of the mountain wind has been extensively studied (Whiteman and McKee 1977; Whiteman 1980; Whiteman and McKee 1982). These authors found that the dissipation of the stable air within the valley during the morning transition phase is largely controlled by the action of the upslope winds, which transport mass from the bottom of the stable core up the sidewall slopes, causing a lowering of the inversion top and adiabatic warming of the stable core. This process appears to be responsible for the dissipation of the stable air within the valley, along with shear-induced mixing of stable air at the top of the inversion by ambient flow (Davidson

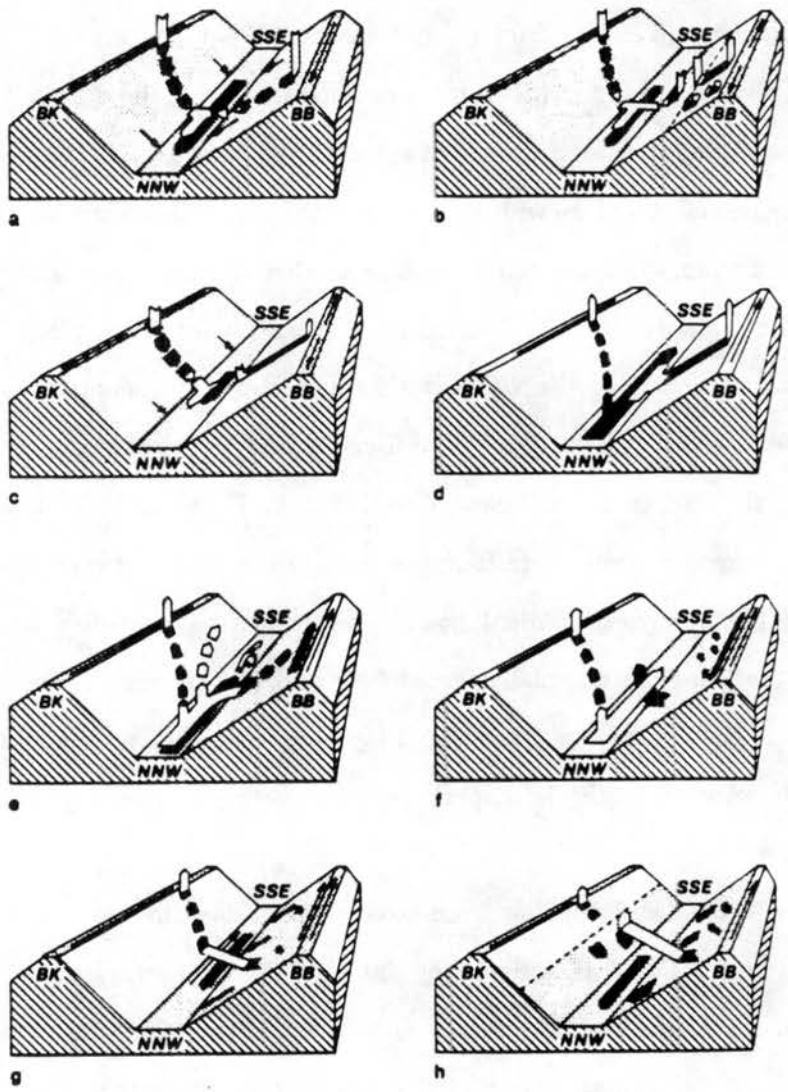

Figure 2.4: Model of the mountain-valley wind system in the Dischma Valley, Switzerland. (From Urfer-Henneberger, 1970.) (a) Midnight to sunrise on the eastern slope; (b) Sunrise on the upper east slope; (c) Whole east slope in sunlight; (d) Whole valley in sunlight, onset of valley wind; (e) West slope receiving more solar radiation than east slope; (f) Solar radiation only tangential to east slope; (g) Sunset on east slope and valley floor; (h) After sunset on the lower west slope.

and Rao 1958; Lenschow *et al.* 1979). In addition, Ayer (1961) describes how the lack of continued source air for the cold downvalley flow after the initiation of heating will reduce the volume of cold air within the valley, allowing the stable core to lower in height and eventually drain away.

Numerical simulations of the mountain-valley regime have also been conducted. Thyer (1966) employed a vorticity equation approach to undertake a rather ambitious study of slope and valley circulations in a three-dimensional framework. Unfortunately, his model became computationally unstable after only two minutes of integration time. Nevertheless, Thyer obtained reasonable results with upslope flow up the sidewall slopes of the valley, an upvalley wind up to 500 m AGL, and an "anti-valley" wind above. For the nocturnal case these flow features were reversed, all in reasonable agreement with observations. Bader and McKee (1983) were able to confirm Whiteman's (1980) hypotheses of valley inversion destruction, using a two-dimensional version of the nonhydrostatic Colorado State Cloud/Mesoscale Model (Tripoli and Cotton 1982). McNider and Pielke (1984) used a hydrostatic model to simulate slope and mountain-valley flows. Their results showed that the model was capable of simulating mountain-valley flows within the Gore Valley of Colorado, as observed by Whiteman (1980). These authors also discuss the nature of the valley wind as a secondary circulation dependent upon the slope flows and valley geometry, with cooling of the valley atmosphere forced by upward motion over the center of the valley, due to the convergence of the downslope flows.

2.2.4 Recent experimental research

The research noted above has contributed greatly to furthering our knowledge of mountain-valley flows beyond that of the Wagner-Defant model. Much additional information regarding the entire slope-mountain-valley wind system has been obtained in recent years as a result of several large field experiments in Europe and the United States.

One of the earliest of these was the Slope Wind Experiment Innsbruck 1978 (HAWEI) which used balloon soundings, aircraft measurements, and surface stations along each slope of the Inn Valley, Austria, to investigate the wind and temperature fields associated with the slope and mountain-valley wind (Brehm and Freytag 1982). Similar equipment, plus

tethered balloons and acoustic sounders, were deployed in the much smaller Dischma Valley of Switzerland during the DISKUS experiment in 1980. Data from this experiment were of sufficient resolution to allow the construction of three-dimensional temperature fields for certain time periods (Hennemuth 1985), in which definite thermal asymmetries appear. The nature of heat transport in the mountain valley from energy budget considerations was also addressed by Hennemuth. From this it was possible to establish that a mountain energy cascade exists, by which heat is exported out of the slope wind layer by ascending motion, and heat is imported to the valley atmosphere by descending motion over the stable valley air mass. Thus, we have a heat transport from smaller to larger-scales. Further observational results from the DISKUS experiment can be found in Egger (1983); and Hennemuth and Schmidt (1985). More recent, and of much larger-scale, was the 1982 MERKUR experiment. The experimental area encompassed the Inn Valley from Innsbruck northeastward to the Alpine forelands near Munich. Although the temporal and spatial resolution of the experimental stations was rather coarse, Freytag (1985) was able to examine the various terms in the valley energy budget, and show the importance of advective processes in producing the mountain and valley wind regimes. A recent summary of the results of the various European mountain-valley experiments is given by Vergeiner and Dreiseitl (1987).

The most extensive observational program of the mountain-valley regime to date was the Department of Energy's Atmospheric Studies in Complex Terrain (ASCOT) field experiment in September and October of 1984 in the Brush Creek Valley of western Colorado. This experiment included a long list of participants from many institutions and a vast array of state-of-the-art observing equipment. Details of the experiment can be found in Clements *et al.* (1989a).

Using five energy budget stations Whiteman *et al.* (1989a,b) examined the radiation and surface energy budget differences between ridge, valley, and slope sites. These authors found that shading effects between the slope sites produced cross-valley flows. The diurnal heating and cooling cycle also generates a clockwise rotation of the winds on the east facing slope and a counterclockwise rotation on the west facing slope. The cross-valley and downvalley shape of the Brush Creek nocturnal drainage wind was investigated by Clements *et al.* (1989b). The downvalley shape closely resembled a Prandtl profile, while the cross-valley

shape was found to be parabolic, leading to the term "Prandtl-parabolic wind field" for the drainage within the valley. The authors discuss that previous estimates of the drainage wind mass flux by Whiteman and Barr (1986) could be up to 43 percent too high by assuming horizontally homogeneous flow across the valley.

Stone and Hoard (1989) analyze the velocity fluctuations within the Brush Creek drainage wind using variance, coherence, and phase spectra. This study expands on the work of others (i.e. Fleagle 1950; McNider 1982; Gryning *et al.* 1985). These observations show that the time-scale of the fluctuations are an order of magnitude greater than those associated with turbulent eddy motion, suggesting the presence of internal gravity waves within the flow.

Flows within a tributary canyon to the main Brush Creek canyon have also been extensively studied (Coulter *et al.* 1989; Shinn *et al.* 1989; Porch *et al.* 1989). The flow within a tributary and its interaction with the main valley flow is very complex, as demonstrated in Fig. 2.5, from Coulter *et al.* (1989). The figure shows ambient southwesterly air from sources external to the valley moving across the top of Brush Creek (BC) exchanging momentum with air from within the valley drainage flow. Some of this external flow descends within the tributary (PC, UPC), producing enhanced subsidence within the tributary flow. This increases the efficiency of the tributary as a source of drainage air. As this air within the tributary drains toward Brush Creek, some of it exits the tributary as an elevated jet, producing confluence between this elevated jet and the main valley drainage jet.

These results point to the importance of the external wind field in determining the nature of the tributary and valley drainage flow. Further observations of this influence is provided by Barr and Orgill (1989), who examine the effects of radiation, clouds, and external wind speed upon the strength and depth of the Brush Creek drainage flow. They found a fairly good inverse relationship between the external wind speed and the top of the drainage wind layer. These authors also examine the cross-valley component of the drainage flow in Brush Creek from tethersonde profiles to show the influence of the external wind in inducing secondary circulations within the drainage wind. Figure 2.6 gives several examples of the cross-valley flow for different external wind conditions and the proposed streamlines associated with the observed winds. It is obvious from the figure that the external wind

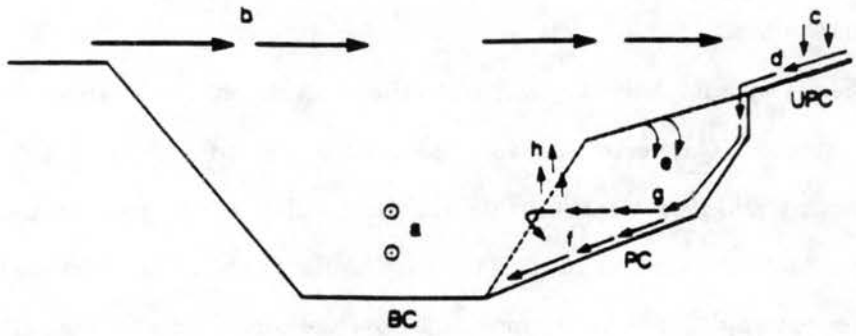

Figure 2.5: Schematic of the flow regime within Pack Canyon (PC) suggested by the data with opposing (southwesterly) external winds. The dashed line indicates the position of the south wall of PC. (a) Drainage down Brush Creek Canyon. (b) External opposing flow above the ridges. (c) Subsidence above upper PC. (d) Drainage from upper PC. (e) Air from the opposing flow entrained into PC. (f) Drainage from sidewalls and floor of PC. (g) Elevated drainage exiting PC over south wall of PC. (h) Ascending air created by convergence of Brush Creek and PC flows.

regime can dramatically influence the resulting drainage flow. This influence will depend upon the amount of shear-induced mixing between the external and valley wind. Another important influence can be lee waves which evolve over the ridges surrounding the valley. Depending upon the wavelength of the lee wave (λ) relative to the cross-valley width (W), this interaction will vary from short waves ($\lambda/W < 1$) which will separate at the ridge and travel across the valley, to flow which separates at the ridge and skips over the valley ($\lambda/W > 1$) (Hunt *et al.* 1978; Lee *et al.* 1987). However, when $\lambda/W \sim 1$ the lee-wave pattern will be in resonance with the terrain shape and the external wind can penetrate deeply into the valley, even completely scouring the valley drainage flow (Pielke 1985).

Another contribution from the ASCOT study involves the fate of the drainage flows beyond Brush Creek. Using tethersondes and a portable monostatic sodar, Neff and King (1989) analyzed the disposition of the Brush Creek drainage flow as it is incorporated within the larger air sheds of Roan Creek and the Colorado River above DeBeque Canyon, which cuts through the Book Cliffs escarpment. One of the principal results from this study was the identification of a pooling of drainage flows up to an elevation of 1800 m above sea level (MSL) by the Book Cliffs escarpment into the basin upstream from DeBeque Canyon. This pooling resulted in elevated drainage flows entering the basin from tributary drainages such as Roan Creek. These elevated flows overlay a dense, surface based air mass with light winds. The drainage flows eventually fill the basin to the height of the escarpment at which time the pooled air overflows the basin.

The ASCOT observations point to the necessity of observing a larger domain to achieve a more complete understanding of the flow in complex terrain. For example, Neff and King (1989) describe Doppler lidar observations which suggested that the accumulated drainage air within the pool can "back up" into Brush Creek, effectively blocking the Brush Creek drainage flow. Thus, drainage may weaken or shut-off in otherwise favorable conditions (i.e. clear skies, weak ambient flow), but a lack of information regarding downstream effects would make this anomalous condition very puzzling to the researcher. Here again, we arrive at a point where it is necessary to move up a scale to obtain a more general understanding of thermally-forced flows in complex terrain. This observation leads us to the next topic of this review, the basinwide and regional-scale thermally-driven winds.

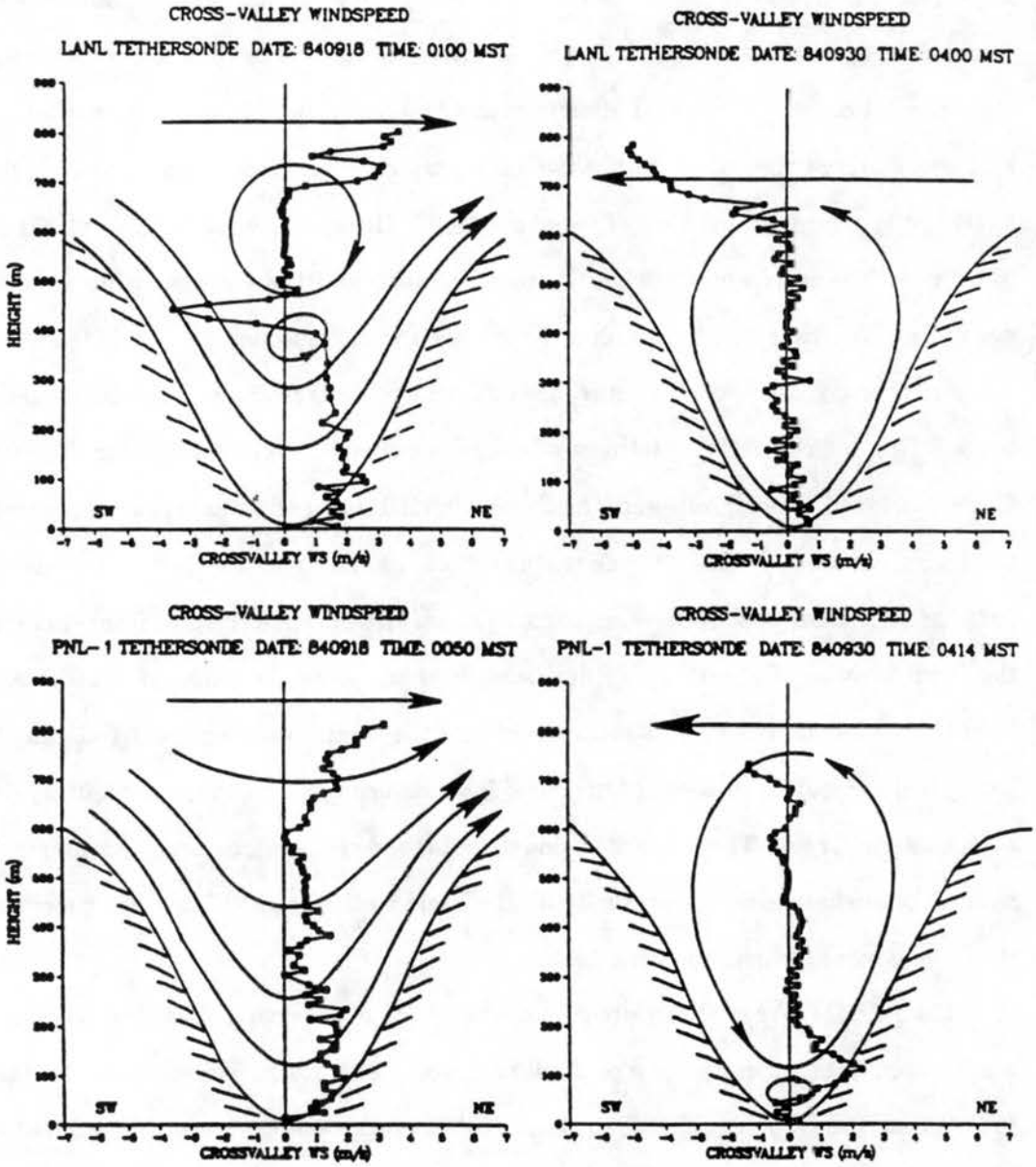

Figure 2.6: Characteristic cross-valley wind profiles with suggested streamlines for two experimental nights at a narrow and a wide position in Brush Creek.

2.3 Regional-Scale Flows

2.3.1 General concepts

The review of research on regional-scale flows will involve an examination of two types of flows: basin-wide studies of thermally-driven flows, and "mountain-plain" circulation systems. Basin-wide studies tend to look at the wind field over a region encompassing several valleys in complex terrain, or a large drainage basin. However, the winds are often from surface observations at a variety of station elevations, with little information on the vertical structure of the wind field provided. Mountain-plain circulation studies are generally two-dimensional in nature (the x-z plane) yielding information on the vertical structure but still limited in scope by neglecting horizontal flow variations.

A dearth of research exists on thermally-forced flows occurring at scales larger than mountain-valley flows. This situation is obviated by a cursory inspection of the sections on regional-scale flows contained in Barry's (1981) and Atkinson's (1981) books on mountain and mesoscale circulations. Much of this is certainly due to the difficulty in obtaining detailed observations at these scales. This situation will be discussed further in the following chapter. It is the purpose of this dissertation to expand our knowledge base of thermally-forced flows on horizontal meso-β to meso-α scales (20 - 2000 km).

While the history of research on thermally-forced flows over complex terrain has focused upon slope and mountain-valley circulations, the existence of similarly forced wind regimes on larger horizontal scales appears to have been known for some time (Burger and Ekhart 1937). To define these larger-scale flows, consider a large mountain barrier, extending over several hundred kilometers horizontally, without any large valleys or subranges. To further simplify matters, we can assume that the large-scale wind field is quiescent, and the insolation is strong. Then the heating that occurs over the slopes of the mountain range will hydrostatically produce low pressure over the slopes relative to the free air some horizontal distance away, in much the same way as the small-scale slope winds are generated, as discussed in Section 2.1.

An additional complication for these larger-scale slopes, however, is the horizontal scale L of the heated slopes relative to the Rossby radius of deformation ($L_r = NH/f$),

where $N = [g/\bar{\theta}(d\bar{\theta}/dz)^{1/2}]$ is the Brunt-Vaisala frequency, H is the depth of the resulting circulation, and f is the Coriolis parameter. For typical summertime mid-latitude conditions with $\bar{\theta} = 330°\text{C}$, $d\bar{\theta}/dz = \sim 2.0 - 4.0°\text{Ckm}^{-1}$, $N \sim 10^{-2}\text{s}^{-1}$, $H \sim 4000$ m, and $f \sim 10^{-4}\text{s}^{-1}$; $L_r \sim 300 - 500$ km, with the lower value corresponding to the weaker stability. The ratio L/L_r will determine the atmospheric response to heating over the slope. For $L/L_r > 1$, Coriolis influence dominates and the wind field, attempting to achieve a balanced state, will adjust to the low pressure induced by the heating, causing a low level cyclonic circulation and compensating upper level anticyclonic circulation. The temporal variability of solar heating will generally prevent the attainment of geostrophic balance.

When $L/L_r << 1$, Coriolis effects are relatively unimportant, the mass field will adjust to the wind field. A thermally-direct circulation will result, with heating driving convergent flow toward the crest of the mountains in the low-levels, and a compensating divergent flow away from the mountain crest at upper levels. Most mountain ranges within the Rocky Mountain massif have length scales L much less than L_r, however, thermally-induced flows across the Colorado Front Range, or which encompass several ranges can approach L_r. Variations in the depth of the thermally-forced circulation and ambient stratification will also affect the adjustment process, whereas the time-scale of thermally-forced flows in summer ($\sim$ 10 hours), which is greater than a half-pendulum day at 40°N, will also exert a geostrophically-balanced response on the resulting circulation system. For now, however, we will assume that the length of the heated slope is small relative to the Rossby radius of deformation, reserving the consideration of larger elevated land areas until the next section.

Of course, the previous discussion is a gross oversimplification of the actual situation. In practice, it would be very difficult to find a mountain range with such smooth slopes. Numerous valleys and ridges can always be found over mountain ranges of the scales considered here. These topographic features will produce their own circulation systems, as described in previous sections, greatly complicating the flow regime over the mountain barrier. Insolation variations between the slopes and soil/vegetation differences on each side of the mountain barrier will produce an asymmetry in the amount of heating and in the resulting wind circulations. Surface characteristics will certainly be inhomogeneous over the scales of the mountain barrier, inducing perturbations upon the regional-scale winds. Even light

winds due to weak synoptic-scale pressure gradients will influence the development of the regional-scale flow. Given these more realistic conditions, it is clear that the regional-scale wind field will result from the interaction of many processes operating on a wide variety of temporal and spatial scales. Thus, we might expect these flows to be difficult to interpret from standard meteorological observing equipment, or only appear in areas where the forcing from a particular process is particularly strong. These factors undoubtedly provide some explanation for the lack of observations of regional-scale flows appearing in the literature to date.

2.3.2 Basin studies

Several recent studies have described the wind field over a particular region or basin, the horizontal dimensions of which qualify the resulting wind fields as regional-scale. Astling (1984) used a surface network of meteorological stations along, and to the west of, the Wasatch Range of northern Utah to describe the diurnally varying convergent and divergent wind patterns and their relationship to thunderstorm frequency over the region. A similar study was conducted by Mass (1982) over the Puget Sound region in Washington. He found the diurnally varying summertime wind field over this region to be pronounced in the lowest 5 kPa. In addition, the convergence and divergence fields associated with the interaction of the sea-breeze and topographic winds were found to provide a possible explanation for the observed diurnal variations in precipitation frequency over the area.

Over the Front Range, Smith and McKee (1983) and Toth and Johnson (1985) used data from the National Atmospheric and Oceanic Administration's (NOAA) Program for Regional Observing and Forecasting Services (PROFS) mesoscale network to investigate the diurnal evolution of the wind field over the South Platte Basin. Toth and Johnson found an early morning downslope to upslope transition zone occurring in the foothills of the Front Range which then propagates eastward with time (Fig. 2.7a). Local confluence was located along the major ridges at midday. These areas are also the preferred regions for afternoon thunderstorm activity. In late afternoon, a similar transition zone, now from upslope to downslope flow, develops along the Front Range and propagates eastward with time

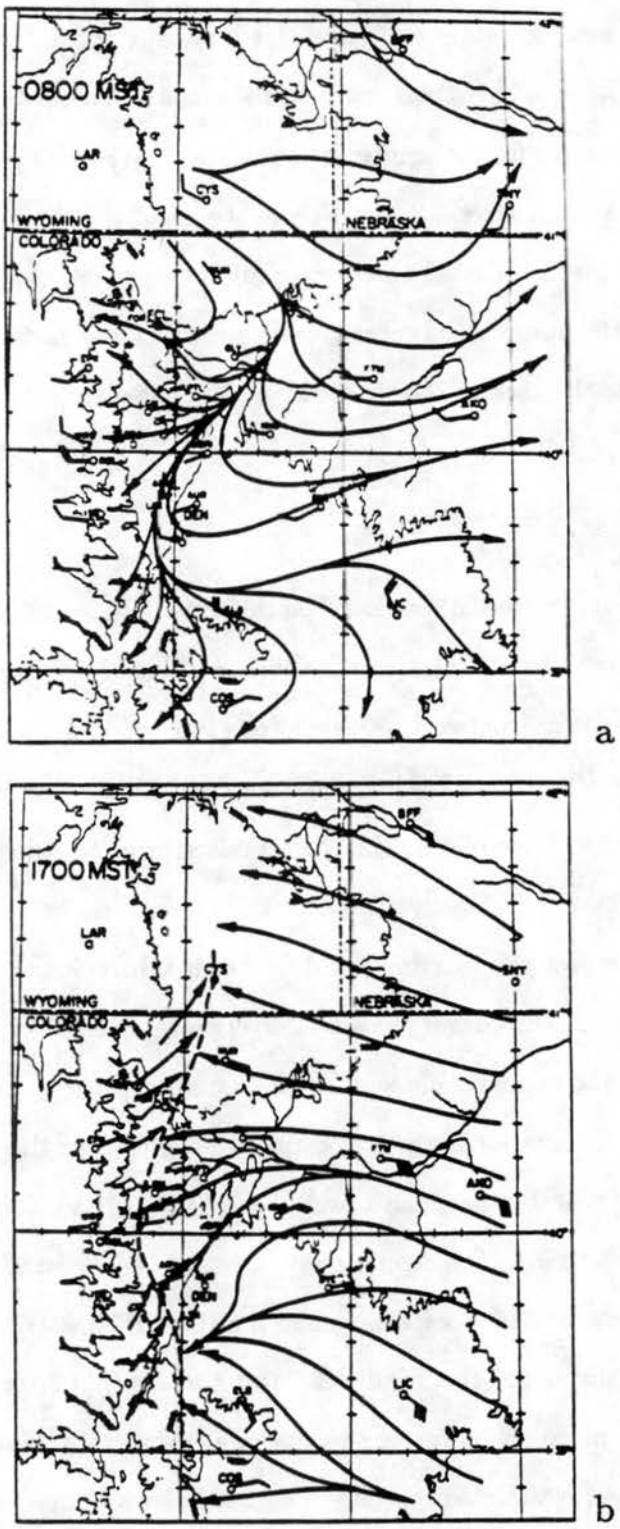

Figure 2.7: NOAA-PROFS mesonet station surface streamline analyses for July 1981 (a) 0800 MST; (b) 1700 MST.

(Fig. 2.7b). This pattern often develops in conjunction with the movement of thunderstorms from the mountains toward the plains.

Several other studies have investigated basin-wide flows within the complex terrain of Colorado. Banta and Cotton (1981), Cotton *et al.* (1982), and Banta (1984) have examined the boundary layer circulations which develop over the South Park area, located between the Front Range and Mosquito Range in central Colorado, during dry conditions with moderate westerly winds. South Park is a relatively flat intermountain basin at 280C m MSL, approximately 50 km wide and 80 km long. Banta (1984) describes the morning formation of upslope winds in a shallow mixed layer underneath the nocturnal surface-based inversion. This shallow upslope flow interacts with post-frontal westerly flow from over the ridgetop of the Mosquito Range to produce a lee-side convergence zone near the base of the mountains. The convergence zone is the region of earliest cumuli formation. With continued heating, the deep westerly winds mix out the shallow upslope flow along a boundary which propagates eastward with time. After the dissipation of the upslope flow, the afternoon wind regime begins, consisting of deep westerly flow over the South Park region.

2.3.3 Mountain-plain circulations

Investigations of mountain-plain circulations have the advantage of providing information about the vertical structure of regional-scale flows and their relationship with smaller-scale slope and mountain-valley flows. The hierarchical structure of these flow regimes has been nicely portrayed by Tyson and Preston-Whyte (1972) (Fig. 2.8), based upon data from their study of thermally-induced flows between the Drakensburg and the Indian Ocean in South Africa. In the figure we find slope flows, mountain-valley flows, and their associated anti-winds, overlain by the mountain-plain wind, for two different valley orientations. Mountain-plain circulations have been the subject of several numerical investigations, dating back to Dirks (1969), who used a two-dimensional hydrostatic model to describe the mountain-plain circulation which develops with heating over the Colorado Front Range. He noted the development of a two-cell system to this circulation, with a subsidence zone just to the east of the Front Range slope. This zone may account for the suppression of convection over this area, noted by other investigators (e.g., Crow 1969; Wetzel 1973; Henz

1974). The initiation of orographically generated cumulus convection over the Front Range, and their progressive development into mesoscale convective systems of varying intensity further to the east has been studied in some detail (Cotton *et al.* 1982; Knupp and Cotton 1982a,b; Cotton *et al.* 1983; Wetzel *et al.* 1983). The association between the upslope circulation and the initiation of convective clouds over the Front Range has recently been simulated by Banta (1986), on smaller-scales over the South Park region, and over the entire Front Range slope by Tripoli and Cotton (1989a,b) and in similar topography in Montana by Tremback (1990).

Several studies have also noted regional-scale winds over the Rocky Mountain slope in western Colorado. Whiteman (1980) discusses the presence of "up-incline" winds in his observations of mountain-valley flows in western Colorado. These up-incline winds appear to be the daytime branch of the mountain-plain circulation over the western slope of the Colorado Rockies. Barr and Clements (1981) noted the presence of a layer of nocturnal easterly winds between 3 and 4 km over the Piceance Basin of western Colorado. These authors speculated that this wind could have been a mesoscale flow generated by the higher terrain to the east. Based upon data from the 1984 ASCOT experiment, Bader *et al.* (1987) simulated the 800 m deep nocturnal drainage flow emanating from the high plateau area to the east of Brush Creek. The horizontal and vertical scale of the simulated downslope flow suggest that it may be the nocturnal branch of the mountain-plain circulation over the western slope of Colorado.

Further evidence of regional-scale flows across the mountain barrier in Colorado has been presented in Reiter *et al.* (1987a), who analysed winds at various mountaintop locations over the state, and in more detail by Bossert and Reiter (1987) and Bossert *et al.* (1989). These data from mountaintop locations have allowed the formulation of a more complete conceptual picture of the wind field on the regional-scale across the Colorado mountain barrier. Even at horizontal scales of several hundred kilometers, winds in the mountain boundary layer show considerable coherence, particularly at night over both the western and eastern slopes of the mountains. Vertically, it appears that the structure of the flow is similar to that suggested by Tyson and Preston-Whyte (1972), as shown in Fig. 2.8. Since the goal of this dissertation is to provide an extensive observational and numerical

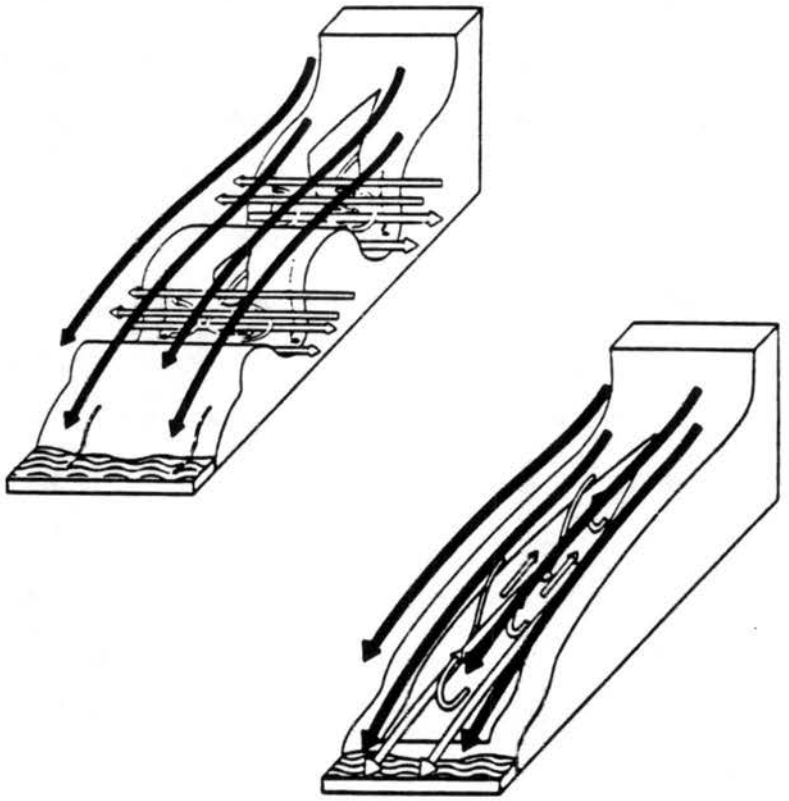

Figure 2.8: Schematic model of nocturnal air flow over the eastern plateau slopes of Natal in winter with valleys at right angles to the slope between Drakensburg and the ocean (upper), and with valleys parallel to the slope (lower).

analysis of the nature of regional-scale flows over the Colorado mountain barrier, a more detailed description of their structure is delayed until later chapters.

2.4 Plateau-Scale Flows

2.4.1 General concepts

In this section, we examine the literature which discusses the effects of thermal forcing over topography on the largest horizontal (synoptic) scales. The primary regions where these effects can be found are the Tibetan Plateau in central Asia, the Western Plateau in North America, and to a lesser extent South Africa and the Antarctic continent. Other large areas of elevated landmass such as the Alps or Caucauses in the Northern Hemisphere, or the Andes in the Southern Hemisphere, are too small in horizontal extent to be included here. Due to the large horizontal area of these plateaus, they generally greatly exceed the Rossby radius, resulting in a geostrophically-balanced atmospheric response to the heating. This large-scale response will dramatically influence the wave motions which, when appropriately averaged, constitute the atmospheric general circulation. In this regard, these thermal influences are of paramount importance to atmospheric dynamicists who specialize in large-scale problems, and to general circulation modelers. The extensive overlap of plateau-scale heating into other subdisciplines requires us to restrict our literature survey to only those papers relevant to flows over the plateau itself, ignoring the downstream effects of these flows on the general circulation.

2.4.2 The Tibetan Plateau

Much of the early research on plateau heating effects concerned the interaction of the Tibetan Plateau and the Indian Monsoon circulation (Koteswaram 1958). Limited observational data revealed that heating over the Tibetan Plateau produced an elevated heat source resulting in a low-level cyclonic circulation above the plateau surface ($\sim$ 60 kPa) and an upper level anticyclonic circulation ($\sim$ 10 kPa) (Flohn 1965, 1968). The strong upper-level anticyclone over the Tibetan highlands was known to have an "anchoring" effect upon the Tropical Easterly Jet over the Indian Monsoon region (Koteswaram 1958). However, it was uncertain whether the strong atmospheric heating over the plateau was primarily

due to surface sensible heating, or latent heat released from strong, persistent convective storms over the Assam and southeastern Tibet regions (Rangarajan 1963). Additional data to determine the nature of the heating were unavailable, however, until the late 1970s, when the Summer Monsoon Experiment, conducted from 1 May to 31 August 1979, allowed a more quantitative assessment of the role of plateau heating.

The meteorology of the Tibetan Plateau has been described by Chinese scientists, as summarized by Yeh *et al.* (1979). Unfortunately, these studies were written in Chinese. A brief review of some of this research was published in the Bulletin of the American Meteorological Society in 1981. Yeh (1981) determined the summer circulation over the plateau from observations. This circulation consists of a prominent boundary layer heat low, with several embedded mesoscale vortices (Fig. 2.9). The relationship between these low level vortices generated over the Tibetan Plateau and severe weather outbreaks downstream in China was investigated by Tao and Ding (1981). Surrounding the thermal low over the plateau is a belt of higher pressure, which forms a dome over the plateau heat low with increasing altitude (Yeh 1981). This structure is consistent with a warm core low forced by surface heating. The upper level anticyclone reaches its highest intensity near 15 kPa. Associated with this thermal circulation is a strong meridional circulation in the low levels toward the plateau from the south over India and Bangladesh, and toward the plateau in the mid-levels from northern China. This convergent flow at low-levels over the plateau produces several strong vertical circulation cells, with rising motion and numerous convective storms resulting over the plateau.

The role of the Tibetan Plateau as a huge elevated heat and cold source to the atmosphere was described by Gao *et al.* (1981). These authors show the diurnal and seasonal variations of the circulation over the plateau to be quite dramatic. The plateau acts as an atmospheric heat source from March through September, and as a cold source from October through February. A strong seasonal monsoon circulation is associated with this diabatic variability. To a lesser extent, variations in the amount of atmospheric heating over the plateau also occur on diurnal time-scales, with a strong intensification of the heat low and upper level anticyclone occurring between the morning and evening radiosonde observations at stations located on the plateau. A case study of the changing role of the Tibetan Plateau

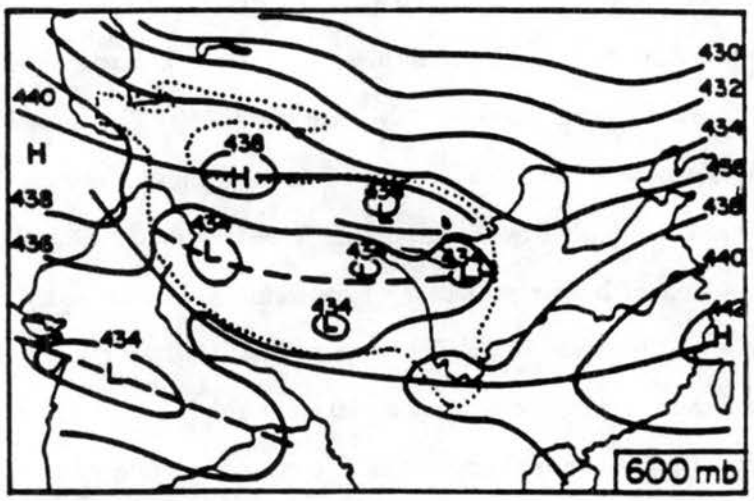

Figure 2.9: Mean 60 kPa geopotential height contours in July over the period 1961-70. Dashed lines: troughs; dolid: ridges; dotted: outline of the Tibetan Plateau. (After Gao *et al.* 1981 and Yeh *et al.* 1979).

from a cold source to heat source during the transition season (April) was investigated by Reiter and Gao (1982). This paper shows that in addition to an increase in sensible and latent heating over the plateau, horizontal advection and large-scale sinking are a significant component of the observed warming, especially in the middle levels of the atmosphere. Also, development of the heat low in the planetary boundary layer over the plateau may be augmented by "foehn-like" flow conditions from the high mountains which surround the Tibetan Plateau in a semicircular arc.

Using rawinsonde data obtained during the summer monsoon experiment (MONEX), several researchers have attempted to provide more quantitative information on the atmospheric heat source over the Tibetan Plateau (Luo and Yanai 1983, 1984; Nitta 1983; Chen *et al.* 1985). Luo and Yanai (1984) calculated the heat and moisture budgets within four sub-regions of the Tibetan Plateau. They found a strong regional variation in the disposition of the heat source between latent and sensible heating, with sensible the primary heat source in the dry western area of the plateau, and latent dominating in the very wet southeastern area. The sensible heating of the upper atmosphere is achieved by dry thermal convection originating near the surface, which has very high potential temperature values, and penetrating through a deep mixed layer up to the 30-40 kPa level. Latent heat is released in the prevalent cumulus convection over southeastern Tibet, which results from the advection of moist low-level air into the southern and eastern plateau region. In the eastern plateau region a mean heating rate of $\sim 3°K\ day^{-1}$ was calculated for the 20-50 kPa layer.

Numerical modeling of the circulations induced by the Tibetan Plateau and their effect upon the general circulation have been undertaken with a general circulation model (i.e. Hahn and Manabe 1975), with large-scale models (Kuo and Qian 1981; 1982), a mesoscale model (Shen *et al.* 1986), and with idealized models (Sang and Reiter 1982a,b; Egger 1987). Kuo and Qian (1981) found the daily mean vertical circulation over the plateau to be characterized by ascending motion, in general agreement with observations (Fig. 2.10).

2.4.3 The Western Plateau

In the Western Hemisphere, the region from northern Mexico to southern Canada in the south-north direction, and from the Cascades and Sierra Nevada ranges to the Front

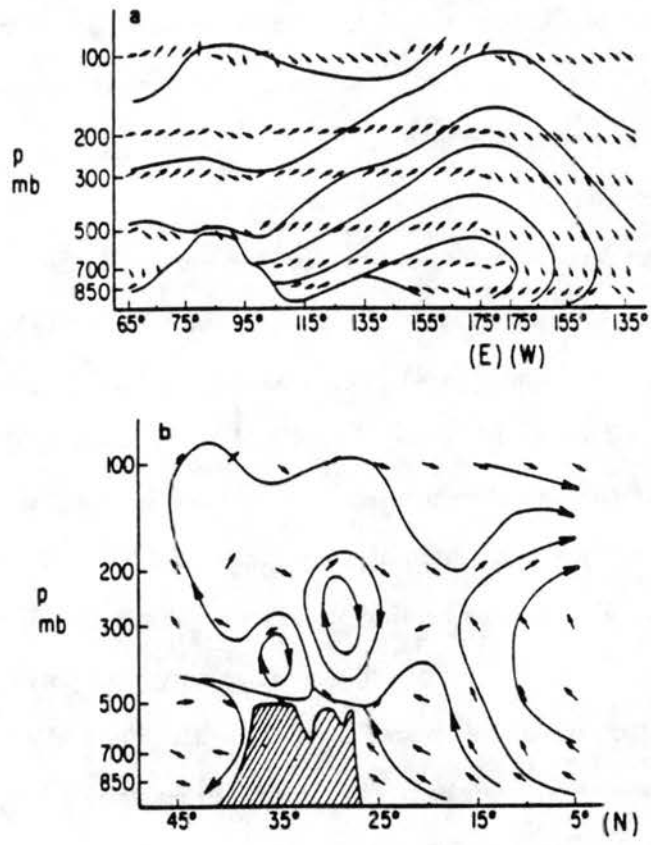

Figure 2.10: Observed mean vertical circulations in July. (a) Over a west-east plane at 35°N; (b) Through a north-south plane at 90°E. Vertical velocity magnified by 500 in (a) and 200 in (b).

Range of the Rocky Mountains in the west-east direction has been named the "Western Plateau" (Tang and Reiter, 1984). The center of this plateau is the Great Basin region of Nevada and Utah, with a mean elevation of $\sim$ 1500 m, significantly lower in mean elevation than the Tibetan Plateau. Tang and Reiter describe the similarities and differences between the plateau monsoon circulations of the Tibetan and Western Plateaus. As noted above for the Tibetan Plateau, the Western Plateau also acts as a seasonally dependent, elevated atmospheric heat or cold source. This can be readily observed by comparing height and temperature fields over the surface of the plateau (85 kPa) between July and December. This low-level seasonal thermal variation has an associated monsoonal circulation, with cyclonic flow up to 1 km deep around the periphery of the plateau in summer, and the reverse in winter.

Tang and Reiter (1984) contend that the low-level jet (LLJ) over the Great Plains is included within this summer plateau monsoon circulation. The LLJ phenomenon has been described by many authors (i.e. Means 1954; Blackadar 1957; Bonner 1968; Bonner and Paegle 1970) and attributed to several primary forcing mechanisms including frictional decoupling of the boundary layer (Blackadar 1957), and adjustment effects caused by thermal forcing of the sloping terrain east of the Rocky Mountains (Lettau 1967; Holton 1967; McNider and Pielke 1981). Wexler (1961) also claims that the LLJ is primarily a result of the position of the Bermuda subtropical high, which is generated largely by processes other than heating of the elevated plateau. Tang and Reiter's analyses show the development of an additional southerly LLJ associated with the summertime plateau monsoon. This LLJ extends from the Gulf of California into the Great Basin, and could be linked with the import of tropical moisture into this region. This moisture source is more locally described as the "Arizona Monsoon" (Bryson and Lowry 1955; Green and Sellers 1964) and is associated with widespread convective precipitation over the dry southwestern U.S. (Brenner 1974; Hales 1974; Houghton 1979; Maddox 1981; Culverwell 1982; among others).

Similar comparisons between the Tibetan and Western Plateaus have been made with respect to summertime circulation patterns on a diurnal time-scale (Reiter and Tang 1984). Similar to the Tibetan Plateau (Gao *et al.* 1981), a distinct amplification of the low-level heat low and corresponding upper level anticyclonic circulation can also be found over the

Western Plateau by comparing height differences between morning and evening soundings at 85 kPa and 10 kPa. In addition, by analyzing three-hour vector changes in the resultant winds at 85 kPa from stations over the plateau and the neighboring Great Plains, distinct diurnal patterns emerge over a widespread region, consisting of inflow toward the plateau by day (Fig. 2.11a) and outflow away from the plateau by night (Fig. 2.11b). This circulation system is especially pronounced over the central Rocky Mountains and western Great Plains. This response, driven by the diurnal heating and cooling of the Western Plateau, appears to be in phase with many of the regional-scale flows over the Colorado Rocky Mountains, as discussed in Section 2.3. However, it is difficult to assess the respective roles of mesoscale and large-scale diabatic processes in producing these circulation patterns from the available data.

An additional phenomenon created by heating the Western Plateau landmass is the creation of deep elevated mixed layers (Carlson *et al.* 1983). This mixed layer consists of an elevated warm bubble, due to the vertical mixing of sensible heat from the plateau surface, similar to conditions over the Tibetan Plateau described by Luo and Yanai (1984). This elevated mixed layer has been shown to produce conditions favorable for the development of severe storms as it is advected eastward by the large-scale flow (Benjamin and Carlson 1986; Benjamin 1986; Farrell and Carlson 1989).

2.5 Summary of Thermally-Forced Flows in Complex Terrain

The purpose of the previous sections was to provide a review of observational, theoretical, and numerical literature concerning the nature of thermal forcing over mountainous regions and the circulations which result from this forcing, over the entire range of complex terrain scales. From this review, it is apparent that thermally-forced flows can be found from the smallest depressions in topography up to the largest plateau complexes, and over every intermediate scale which is characteristic of the underlying topography. What emerges from this realization is that a continuum of complex terrain flows exist, with the dominant circulation resulting from the characteristics of the terrain, and also from the interaction of flows occurring on a variety of scales. Because of this scale selection, a natural hierarchy

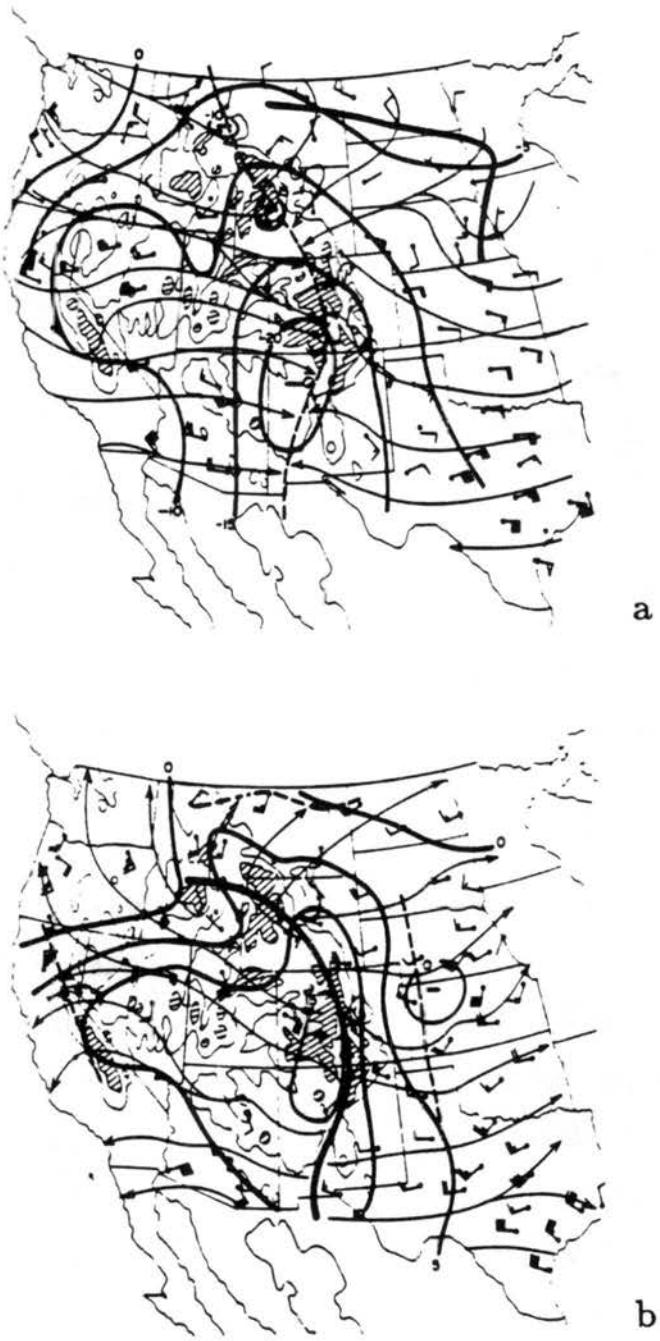

Figure 2.11: Three-hour changes of the 85 kPa surface (in geopotential meters, solid lines of medium thickness), three-hour vector changes of the resultant winds (barbs on arrows are exaggerated by a factor of five, i.e., a short barb is 0.2 ms^{-1}, etc.) and streamlines of these vector changes (thin solid lines). Axes of convergent and divergect centers are indicated by heavy dashed and solid lines, respectively. Time changes are (a) 1400-1100; (b) 2300-2000 MST.

of thermally-forced flows over complex terrain evolves, and these have been somewhat arbitrarily categorized in the previous sections as slope, mountain-valley, regional-scale, and plateau-scale flows. Thus, within the large-scale plateau with its associated low-level heat low and surrounding cyclonic circulation, we find regional-scale flows between the individual mountain ranges and adjacent plains located within the plateau; mountain-valley flows operating within the various river valleys of the plateau mountain ranges; and also slope flows on the sidewalls of the mountain valleys, and over the complex smaller slopes of the mountain ranges embedded within the plateau.

In practice, we need to distinguish between the different thermally-forced flow regimes, to aid in observational analyses and to allow for simplifying assumptions to the governing equations. However, in nature the distinction between these flows by horizontal scale is difficult at best, since interactions between thermally-forced flows on all scales, and also between synoptic-scale winds can be expected, particularly under well-mixed daytime conditions. The distinction between flow regimes may be somewhat more plausible at night, when more localized and shallow flows will exist, often decoupled from thermal flows and ambient winds of different scale by their particular thermal structure.

The foregoing arguments are intended to remind us that while we may attempt to categorize thermally-forced flows by the particular spatial and temporal dimensions specific to each, the real atmosphere is oblivious to such an arrangement. Understandably, this creates substantial difficulties in distinguishing between flow regimes when analyzing observational data. This problem becomes increasingly acute as we take measurements over larger horizontal and vertical scales in complex terrain in an attempt to observe more regional-scale flow behavior. At these larger scales, the interference created by the interaction of other thermally-driven circulations, as well as from winds driven by synoptic pressure gradients, can mask the signal of the flow of interest, contributing to their elusiveness. This situation is augmented by the difficulties inherent in devising a field program capable of observing flows over large distances in mountainous terrain, but of much smaller dimensions than the standard rawinsonde network. By considering these observational problems, it is easy to understand why a dearth of knowledge currently exists regarding thermally-driven flows in complex terrain on regional-scales. The following study is an attempt to overcome these

obstacles and provide some detailed information on the evolution, horizontal and vertical structure, and forcing mechanisms relating to thermally-driven regional-scale circulation systems in mountainous terrain.

Chapter 3

EXPERIMENTAL DESIGN

In response to the current lack of data for thermally-forced flows over complex terrain between the mountain valley (meso-γ to meso-β) and synoptic-scales, an observational program was designed to obtain information on larger mesoscale flow systems over the central Rocky Mountains. This observational program, known as the Rocky Mountain Peaks Experiment (ROMPEX), was conducted over the summers of 1984-1988, by personnel from Colorado State University, under the direction of Professor Elmar R. Reiter, with additional assistance during the larger 1985 phase of the experiment by scientists from the Los Alamos National Laboratory.

The goals of the ROMPEX experiments were to monitor the wind field at mountaintop during the summer season, analyze the departure of these winds from the overlying synoptic-scale flow, and determine surface energy budgets in several high altitude complex terrain locations. The primary method of data collection was through numerous surface stations placed at remote mountaintop sites, equipped with instrumentation to record basic meteorological parameters. At a smaller number of surface energy budget sites, solar and terrestrial radiation components and soil temperature and moisture were also measured. Additional data from a wide variety of sources was acquired to supplement the ROMPEX observations. In this chapter, a description of the site locations, equipment deployed, and data obtained for the 1984-1988 ROMPEX experiments will be presented. Results from the analysis of these data will then be given in the following chapters.

3.1 Preliminary Experiment - 1984

Mountaintop observations began as part of an ongoing investigation of surface energy budgets in complex terrain. This occurred when monitoring equipment consisting of a

"radiation" station and a "tower" station were relocated on 30 July 1984 from Colorado State University's Pingree Park facility, where surface energy budget data over a dissolving snowpack had been obtained (Sheaffer and Reiter 1987), to a site known as Mount Werner, at the top of the Steamboat Ski Resort near Steamboat Springs, Colorado. Together, the radiation and tower stations provide a means of estimating the various terms in the surface energy budget equation. These stations have been used successfully in several remote locations around the world (Smith 1986a,b; Smith *et al.* 1986; Sheaffer and Reiter 1987; Reiter *et al.* 1987a,b). A description of the radiation and tower station instrumentation deployed during the 1984 experiment is provided next. The Mt. Werner station was in operation until 1 September 1984 and is described in Section 3.2.

3.1.1 The radiation station

Figure 3.1 gives a schematic representation of the framework and instrumentation which constitutes the radiation station, originally designed by Eric Smith, Chris Johnson-Pasqua, and Charlie Wilkins at Colorado State University. The instrumentation and its specifications are described in Table 3.1. A set of two pyranometers and one pyrgeometer were mounted side by side on a steel plate, one set pointing upward and the other downward, to measure the downwelling and upwelling solar and terrestrial radiation fluxes. In addition, the visible portion of the solar spectrum was computed by the Campbell Scientific datalogger by subtracting the colored glass (near-infrared) pyranometer from the clear glass (total) pyranometer. The pyranometers and pyrgeometers were sampled every 60 seconds and average values computed every 15 minutes. All other instrumentation is self-explanatory, perhaps with the exception of the soil moisture blocks. These blocks were found to provide only a qualitative picture of soil moisture, as their measured resistance was a highly non-linear function of soil moisture, and varied considerably with soil type and the age of the blocks.

3.1.2 The tower station

In Fig. 3.2, a schematic of the tower station is shown, which was also developed at Colorado State University. Table 3.2 gives the relevant equipment information. The Gill

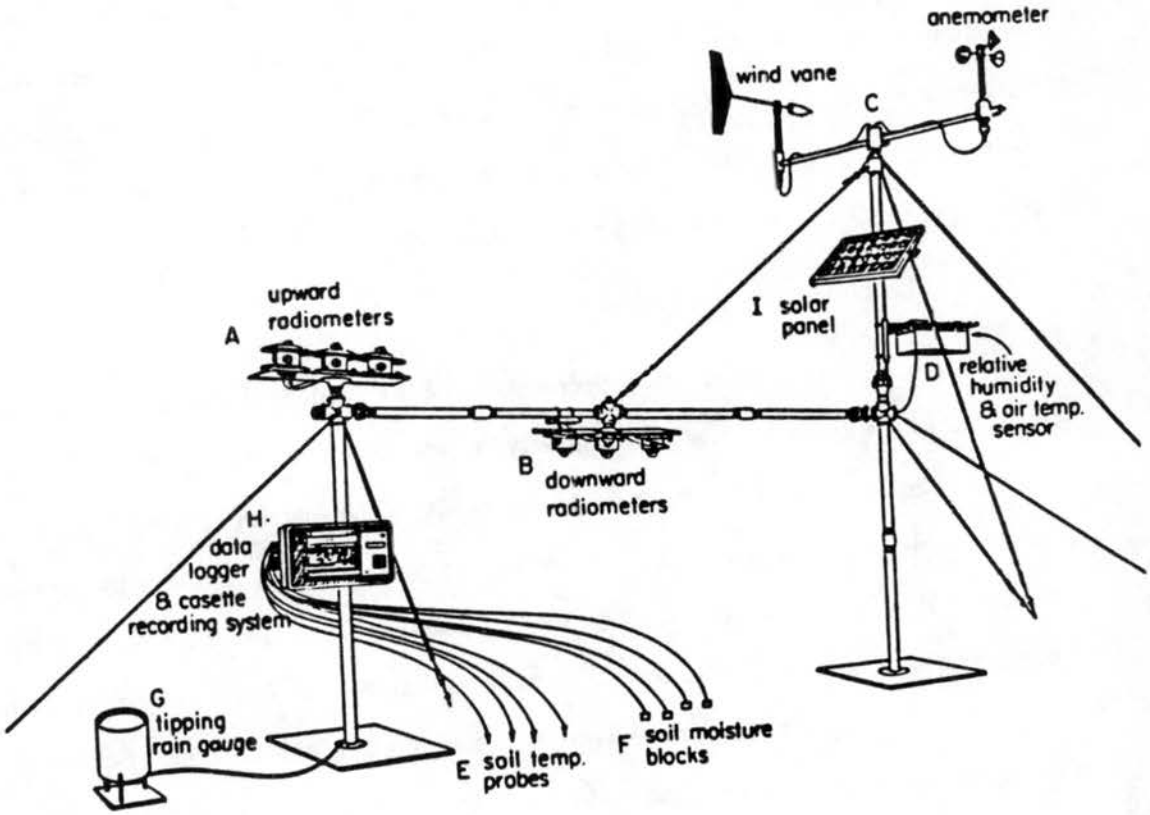

Figure 3.1: Schematic illustration of the radiation station.

Table 3.1: RADIATION STATION INSTRUMENTATION

Instrument	Comments/Specifications
Two Eppley precision spectral pyranometers with quartz (W6-295) inner and outer hemispheres	Measuring the 0.2- to 4.0 micron range of solar radiation to 1% accuracy
Two Eppley precision spectral pyranometers with colored glass (R68-Schott) outer hemisphere	Measuring the 0.7- to 4.0 micron range of solar radiation to 1% accuracy
Two Eppley precision spectral pyranometers with silicon hemispheres and sink-dome thermistors	Measuring the 2.0 to 50.0 micron terrestrial radiation to 1% accuracy
Campbell Scientific (CSI) cup anemometer and wind vane (model 014A and 024A)	Measuring wind speed to 0.25 m/s and wind direction to within 5 degrees at 3 m above the surface
CSI 207 thermistor and hygristor	At 2.5 m, temperature to 0.2 degrees C and relative humidity within 5%
Six CSI soil thermistors placed at 1.25, 2.5, 5.0, 10.0, 20.0, and 40.0 cm depth	Reliability varies with soil type
Four CSI CEL-WFD-7 ceramic soil moisture blocks placed at 1.25, 5.0, 20.0, and 40.0 cm depth	Reliability varies with age and soil type
CSI R62501 tipping rain gauge	1.0-mm sensitivity
CSI CR-7 data logger	Computes 15-minute average values from 5-second scans and records maximum, minimum, and average values on magnetic cassette tape

Table 3.2: TOWER STATION INSTRUMENTATION

Instrument	Comments/Specifications
Three R. M. Young 27005J-Gill U-V-W propeller anemometers at 3 m	Horizontal wind direction varies with angle of attack, wind speed to within 0.05 m/s
Campbell Scientific (CSI) 207 thermistor and hygristor	At 2.5 m, temperature to within 0.2 degrees C, and relative humidity to within 5%
CSI CR-7 data logger	Computes 5-minute average values from 2-second scan interval data and records data on magnetic cassette tape

U-V-W anemometers originally had low threshold polystyrene propellers, which were susceptible to hail damage and breakage in high wind situations at the mountaintop sites. These propellers were replaced with a much more durable polypropylene version. The anemometer base had to be checked occasionally for rotation from the vertical, particularly after high wind events. The thermistors were very reliable provided they were adequately sheltered from precipitation. The hygristor plate was quite fragile, also requiring shelter from the elements, and was checked occasionally and replaced after each field season. A problem arose from the sheltering of the thermistor/hygristor couplet. The "bird-cage" type shelters traditionally used were found to seriously damp the turbulent fluctuations measured, which are necessary to obtain turbulence statistics for temperature and moisture flux measurements. In an attempt to minimize this effect, a smaller "hat" type shelter was devised, which improved the measurements, but greatly increased the vulnerability of the thermistor/hygristor sensors to wetting from precipitation, which often arrives in violent squalls at high altitude. Data loss occurred when the sensors got wet, and this problem was acute during rainy "monsoonal" periods in July of the ROMPEX-85 experiment. Thus, in later experiments the highly protective "bird-cage" style shelters were used exclusively.

The radiation and tower stations became the standard monitoring systems used at various sites during all the following ROMPEX experiments. However, because the U-V-W

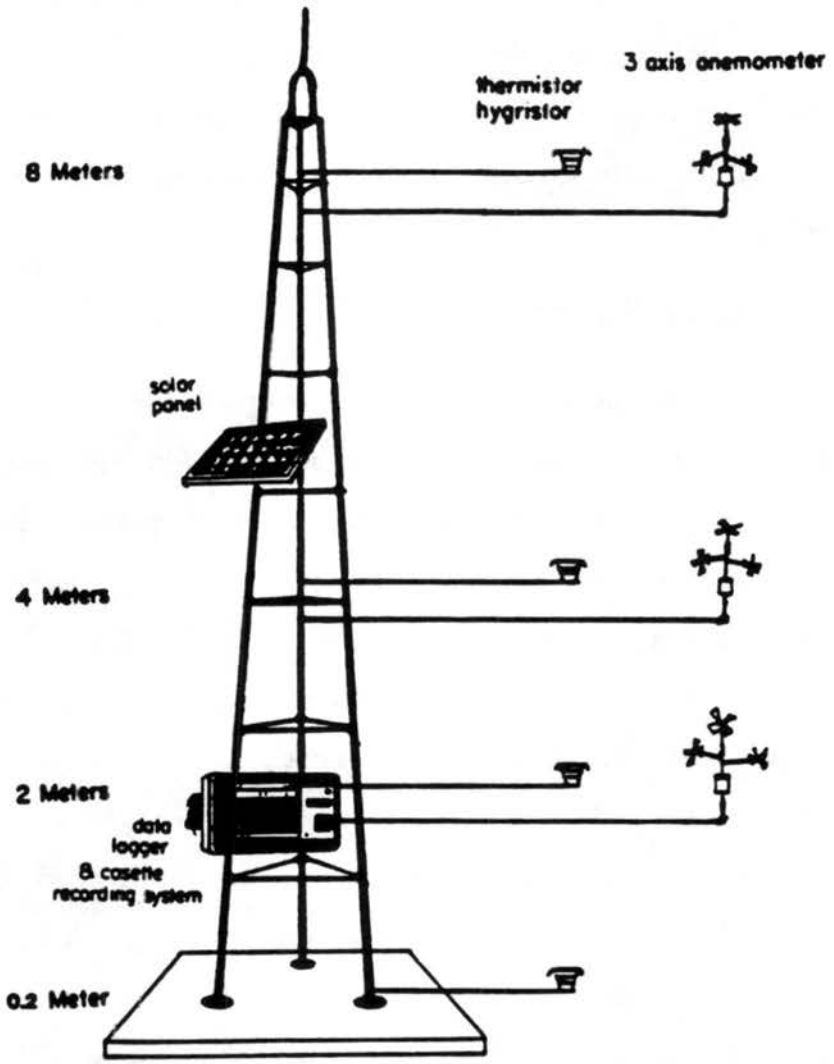

Figure 3.2: Schematic illustration of the tower station.

anemometers lacked sufficient resolution to obtain meaningful eddy correlation statistics, the radiation and tower stations were deployed separately in subsequent experiments and used only to measure basic meteorological parameters. This allowed more sites to be included in the study. The only significant modifications to the radiation and tower station descriptions in Tables 3.1 and 3.2 were the addition of a piezo-barometer to the radiation station at Mt. Werner in late summer of 1987, and the use of a single U-V-W anemometer, at the 3 m level, and thermistor/hygristor couplet (at $\sim$ 2.5 m) on the tower station, when it was deployed separately.

3.2 The Mount Werner Site

The original purpose for relocating the energy budget station (tower and radiation stations) during the summer of 1984 was to obtain surface flux measurements at a mountaintop location. For this purpose the Mount Werner site was ideal, due to its high altitude setting in the Park Range (3207 m), relatively easy access up a four-wheel drive road, and secure location within the Steamboat ski area. In addition, the site was flat, with a nearly unobstructed field of view for the radiometers, and had excellent wind exposure. From a regional-scale perspective, this exposure was due to the isolated location of the Park Range in northwestern Colorado, well removed from higher ranges 80 km to the south and 60 km to the east. Since Mt. Werner is the highest peak of the southern Park Range, the local-scale exposure is also favorable. A three-dimensional perspective of the mountain is provided in Fig. 3.3. The mountain has $\sim$ 20 degree slopes in three directions, falling over 1000 m to the Yampa River Valley and the town of Steamboat Springs to the west, and $\sim$ 200 m in elevation to the east towards more rolling terrain within the Park Range. Immediately to the south of the site, the slope drops 70 m in elevation to the principal ridgeline of the western Park Range. The site was largely devoid of trees and shrubs, with a heavy carpet of subalpine flowering plants and grasses. Figure 3.4 is a photograph of the radiation station in operation at the Mt. Werner site, during an airsonde launch in 1987.

Given the ideal conditions for observing wind phenomena at Mt. Werner, along with the establishment of a Colorado State University cloud physics laboratory atop Mt. Werner

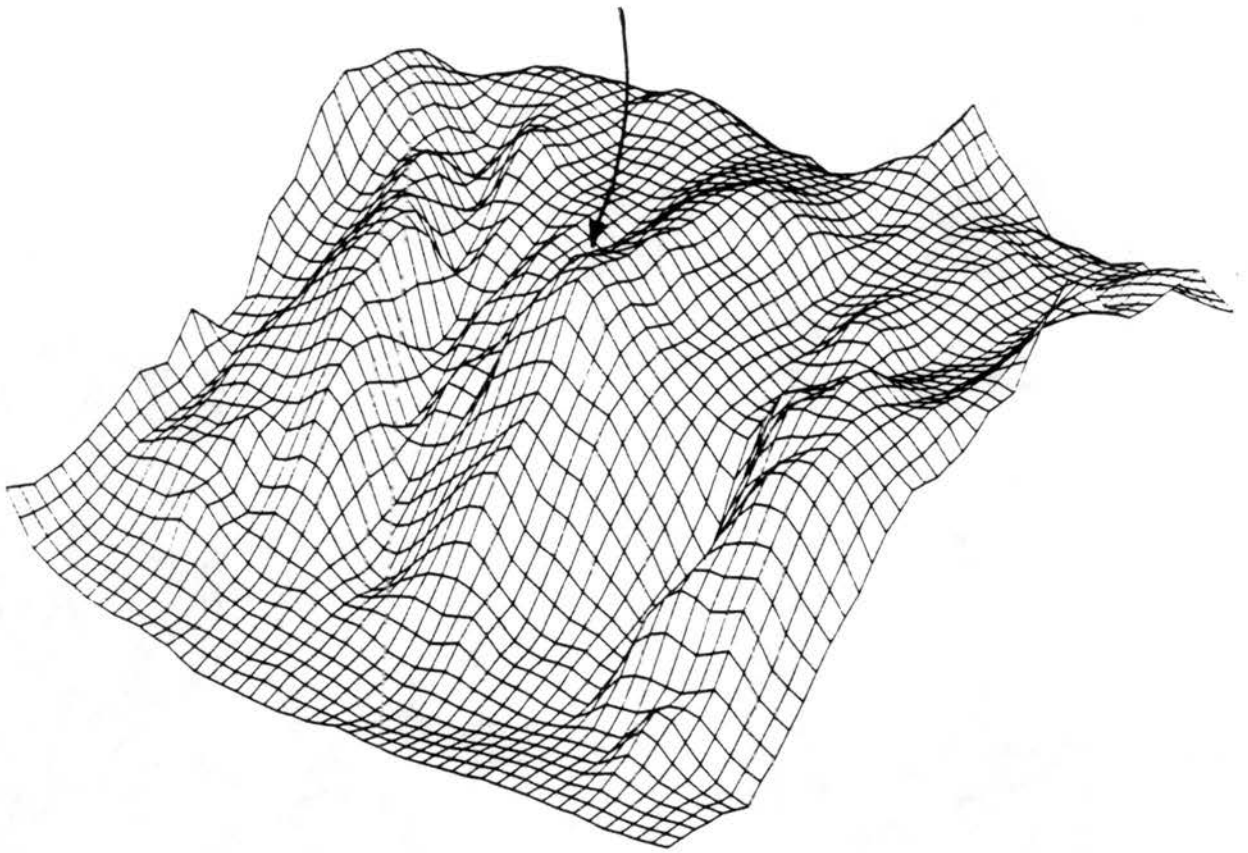

Figure 3.3: Schematic illustration of the three-dimensional topography in the vicinity of the Mount Werner station. Site location marked by arrow. Topography resolution is 30 seconds (~1 km).

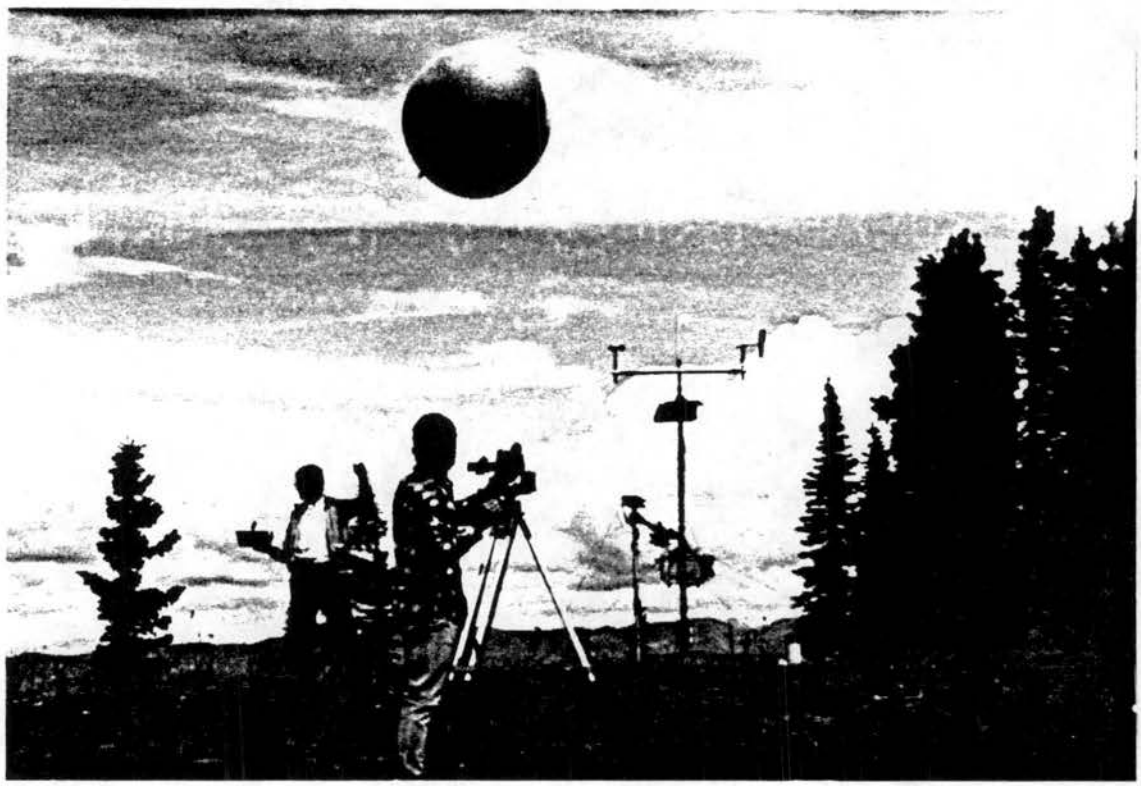

Figure 3.4: Photograph of the Mount Werner site during an airsonde release. Radiation station is in the center backround.

in September 1984, we were compelled to consider this site as our base station for future experiments, both from a scientific and practical standpoint. In fact, observations were taken at this site over portions of the five summer and fall seasons of 1984-1988. This continuous record has enabled us to establish a wind, temperature, and radiation climatology for this site, which will be discussed in the next chapter.

3.3 Extensive Field Observations - ROMPEX-85

3.3.1 Experiment development

From discussions in April 1985 between scientists from Colorado State University and the Los Alamos National Laboratory, a collaborative field experiment was organized to observe winds at the mountaintop level over an extensive area of the central Rocky Mountains. This experiment would involve the deployment of instrumentation on remote mountaintop sites across this complex terrain region. The unconventional nature of the experiment produced some unique siting requirements. The primary concern was to locate sites with adequate exposure to regional-scale winds. This meant finding mountaintop areas relatively unaffected by larger topographic features, which would produce unknown wind blocking and channeling effects, and unobstructed by large trees or rocks which could affect the local wind field. Additional requirements included vehicle access and security, since a significant amount of expensive monitoring equipment would be left at each site. These requirements imposed rather serious limitations on potential site locations.

The requirements of exposure, access, and security had all been met at the Mt. Werner site, located within the Steamboat ski area, during the preliminary 1984 field experiment. Thus, it seemed appropriate to search for other sites within ski resorts, which are generously distributed throughout the central Rocky Mountains. After locating existing ski resorts on a map and examining the topographic features specific to each, several potential sites were discovered. Negotiations then began with ski resort and U.S. Forest Service personnel to obtain permission to examine and possibly deploy equipment within these areas. Notably, in nearly all cases these individuals were very cooperative and accommodating. Plans were then made to stage a site reconnaissance investigation. In addition to the ski area

locations, several other potential sites were found within National Forest and National Park boundaries.

3.3.2 Site locations

From early on in the reconnaissance and deployment phase, it was clear that finding sites with the attributes of Mt. Werner would be extremely difficult. Many potentially ideal sites were either within established wilderness areas or otherwise inaccessible by vehicle, which would require carrying heavy equipment up a mountain or placing the equipment by helicopter, both deemed impractical. Other potential sites were too close to frequented roadways and trails, making the equipment vulnerable to tampering or target practice. These considerations, along with time, budget, and personnel constraints led to the activation of several less than ideal sites. Nevertheless, 16 stations were eventually deployed by personnel from CSU and the Los Alamos National Laboratory, with additional equipment and assistance provided by the U.S. Forest Service. Information concerning all of the sites set up specifically during the ROMPEX-85 experiment is provided in Table 3.3. Four other high altitude stations described in Table 3.3 (MI, WD, RO, SQ), in operation prior to the ROMPEX-85 experiment, were incorporated into the primary data base of the experiment.

The table shows that station elevations ranged from Mesa Verde National Park (MV) at 2610 m to Pikes Peak (PP) at 4297 m. Instrumentation at each station also varied significantly, from the Los Alamos stations where only wind speed, wind direction, and temperature were recorded, to the CSU flux tower at Crested Butte, which measured the U-V-W wind components, temperature, and humidity at four levels up to 20 m. The spatial locations of all of these sites relative to the regional topography is given in Fig. 3.5. Also shown are the daytime winds during 16 August 1985, a rare case when all stations experienced strong winds from a westerly direction, due to fast upper level flow. As shown in the figure, the spatial dimensions of the ROMPEX-85 experiment were vast, reaching over 600 km from southern Wyoming to northern New Mexico in the north-south direction and over 300 km in the east-west direction from Cuchara ski resort (CU) in eastern Colorado to Mesa Verde (MV) in southwestern Colorado. Additional information regarding the ROMPEX-85 experiment can be found in Reiter *et al.* (1987a).

Table 3.3: ROMPEX-85 STATIONS

No.	Station	ID	Elevation (msl)	Parameters Observed
1.	Mt. Werner	MW	3207	A
2.	Flat Tops	FT	3441	A
3.	Vail Mtn.	VA	3350	A
4.	Powderhorn	PW	2987	B
5.	Crested Butte	CB	3352	A
6.	Monarch Pass	MP	3597	B
7.	Pikes Peak	PP	4297	B
8.	Crested Butte Tower	CT	3382	D
9.	Elk Mountain	EK	3383	B
10.	Rocky Mtn. Natl. Pk.	RM	3660	B
11.	Cuchara	CU	3290	B
12.	Wolf Creek Pass	WC	3590	C
13.	Purgatory	PG	3200	C
14.	Mesa Verde	MV	2610	C
15.	Santa Fe Mtn.	SF	3660	C
16.	Mt. San Antonio	MS	3320	C
17.	Ward	WD	3048	E
18.	Rollinsville	RV	2749	E
19.	Squaw Mtn.	SQ	3505	E
20.	Mines Peak	MI	3650	B

Station Designation:

Stations 1-8:	operated by E. R. Reiter and staff, Colorado State University
Stations 9-10:	provided by D. Fox, U.S. Forest Service, Fort Collins, CO
Stations 11-16:	operated by W. Clements and staff, Los Alamos National Laboratory
Stations 17-19:	operated by PROFS-NOAA, Environmental Research Laboratory, Boulder, CO
Station 20:	operated by T. VonderHaar and staff, Colorado State University

Parameter Index:

A: radiation station
B: wind speed, wind direction, temperature, and humidity
C: wind speed, wind direction, and temperature
D: tower station: U-V-W at three levels: temperature and humidity at four levels
E: wind speed, wind direction, temperature, humidity, pressure, solar radiation, rainfall

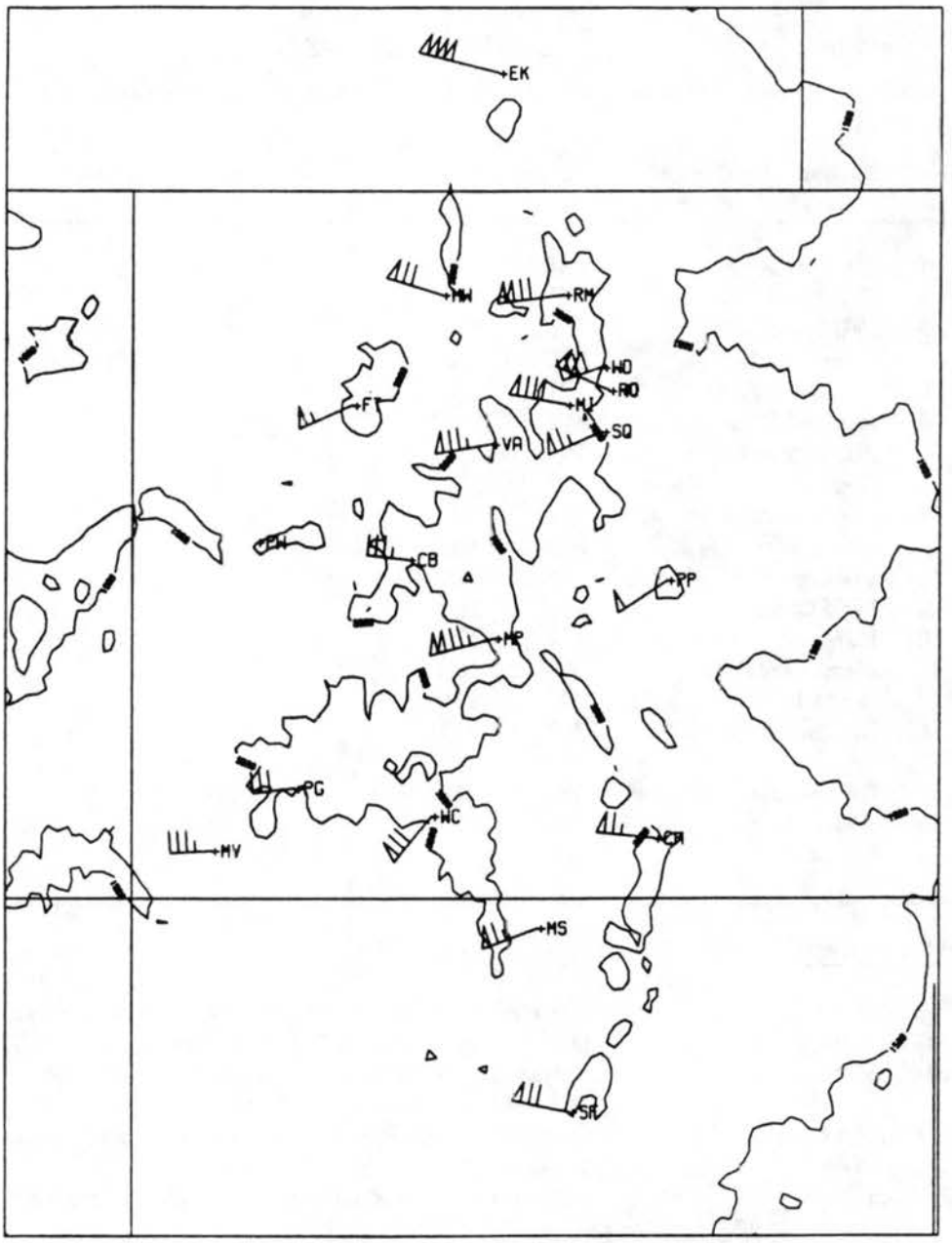

Figure 3.5: Geographic location of the 20 ROMPEX-85 sites. Topography contours at 1500 and 3000 msl. Wind data is for 3-hour afternoon average (1200-1500 MST) 16 August 1985. Wind barbs denote 1 ms^{-1}, flags denote 5 ms^{-1}.

3.4 Additional Data Sources

3.4.1 Supplemental 1985 data

Data from the widely spaced ROMPEX-85 experiment allowed only a preliminary examination of mesoscale flow patterns over the central Rocky Mountain region. Further resources were required to obtain more quantitative knowledge of these flows. To supplement the ROMPEX-85 data set, additional data were acquired from a wide variety of sources. A description of the data parameters, month and years obtained, and the agency providing the data is given in Table 3.4. Several stations from other remote networks were particularly useful for augmenting the ROMPEX-85 surface station network. In fact, two of the PROFS stations, Squaw Mountain (SQ in Fig. 3.5) and Rollinsville (RO in Fig. 3.5), became a part of the primary ROMPEX data set for all five summer seasons of operation (1984-1988).

All of the data from these remote networks were thoroughly scrutinized for obvious errors. Radar summaries were of some value in determining storm locations, important for assessing the effects of convective outflows on the mountaintop data. However, radar coverage is poor over north-central and northwestern Colorado. Thus, Automatic Lightning Detection System (ALDS) lightning strike data provided an additional source of information for locating convective storms over the mountainous terrain comprising the ROMPEX study area. National Meteorological Center upper air data were especially useful for determining the atmospheric structure over the study region. This was done primarily with rawinsonde data from Grand Junction and Denver. Hardcopies of satellite images, and surface and upper air charts, were also available from the Department of Atmospheric Science at CSU. These were used to assess the general synoptic conditions which prevailed during the ROMPEX experiments.

3.4.2 Further observations at Mt. Werner

Preliminary analysis of the ROMPEX-85 data, along with the supplemental data from other sources, provided information on the nature of mesoscale flows over the central Rocky Mountains and their interaction with convection and synoptic-scale winds. To further describe these flows, a scaled down experiment was planned to investigate a smaller region

Table 3.4: SUPPLEMENTAL DATA SOURCES

Data Type	Dates	Agency
ADP Upper Air	15 June – 15 Sept 1985 1 Aug – 31 Aug 1986 1 June – 15 Sept 1987	National Meteorological Center
National Radar Summary	August 1984 July – Aug 1985	National Meteorological Center
Automatic Lightning Detection System (ALDS) (lightning strikes)	July – Sept 1985 July – Sept 1986 June – Sept 1987	Boise Interagency Fire Center
<u>From Remote Surface Station Networks:</u>		
PROFS meso-net (22 stations in CO)	Aug 1984 July – Sept 1985 July – Sept 1986 June – Sept 1987	National Oceanic and Atmospheric Administration
Buffalo Pass, CO plus 7 stations in CO	Aug 1984 July – Sept 1985 July – Sept 1986 June – Sept 1987	Bureau of Reclamation
Remote Automated Weather System (RAWS) (11 stations in CO, WY)	July – Sept 1985 July – Sept 1986 June – Sept 1987	Boise Interagency Fire Center
Rabbit Ears Pass, CO	May 1984 – Oct 1987	U.S. Geological Survey

across north-central Colorado. This experiment was conducted in 1987 and is described in the next section.

Other commitments to conduct a surface energy budget experiment in Tibet precluded any significant field effort over the ROMPEX study region in 1986. However, in an effort to retain the continuity of observations at the Mt. Werner site, which had now been operational for portions of two summer seasons (1984-1985), this site was reactivated on 19 July 1986 with a radiation station. The station then ran continuously until its removal on 3 October 1986.

In preparation for the Tibetan Plateau Meteorological Experiment (TIPMEX-86; see Reiter *et al.* 1987b), all of the radiometers were recalibrated during the spring of 1986. The pyrgeometers were calibrated following the method of Albrecht *et al.* (1976), and the pyranometers were calibrated in a side-by-side experiment, which demonstrated that all instrument readings were within 1 % of each other. This does not seem exceptional, since all of the radiometers were only two years old, and had generally seen only several months of use. In addition to the reactivation of the Mt. Werner site in 1986, airsonde equipment (brought back from the TIPMEX-86 experiment) was acquired for several days, in an effort to investigate the vertical structure of the nocturnal winds over the Mt. Werner site.

Another minor experimental program was instituted in 1988; again to maintain continuity of summer measurements at the primary ROMPEX site of Mt. Werner, and to examine wind and temperature relationships between that mountaintop site and a site 10 km away and 1000 m lower in the Yampa River Valley. This experiment began on 10 June 1988 and ended 6 October 1988. The Mt. Werner site was instrumented for the fifth season with a radiation station, while the lower site at Brunner Draw was equipped with a modified tower station measuring winds, temperature, and humidity. In addition, both the mountaintop and valley stations were instrumented with piezo-barometers during September 1988, to investigate pressure differences due to thermal forcing.

3.5 A Transect Experiment - ROMPEX-87

3.5.1 Experiment development

Data acquired during the ROMPEX-85 field experiment revealed the presence of an organized regional-scale circulation system, operating across the western and eastern slopes of the Colorado mountain barrier. This circulation system was particularly pronounced across a region of north-central Colorado encompassing the 1985 mountaintop stations of Mt. Werner, Vail Mountain, Squaw Mountain, and Rollinsville (MW, VA, SQ, and RO in Fig. 3.5). Observations suggested that the wind phenomenon under study was centered over the high mountain barrier of the Front Range. Thus, it seemed appropriate to set-up a transect of stations between MW and SQ, to gain additional insight into the origins of the regional winds and the physical mechanisms responsible for their initiation. Actual field operations began on 8 June 1987 when the Mt. Werner base site was deployed with a radiation station. Looking southeast from the summit of Mt. Werner toward the Front Range, it was easy to spot several exposed mountaintop sites that would be excellent locations for the Mt. Werner to Squaw Mountain transect study.

3.5.2 Site description

Site selection involved many hours of driving on dirt roads and studying maps to arrive at possible site locations. After choosing prospective sites, all on federal land, local land managers were contacted to obtain permission for the deployment of equipment at the remote locations. As in 1985, we were again impressed by the interest and cooperation we received for our project. Upon receiving the necessary paperwork in early July 1987 authorizing our site selection, arrangements were made to set-up three remote mountaintop sites around Middle Park.

The first site was raised on National Forest land in the Williams Fork mountains on 7 July 1987. The site was in a clearing on a sub-peak of the range, on the southern flank of Middle Park. At the site were several large microwave relay structures, which attested to the exposure of the site, and also provided service road access. However, surrounding the clearing was a dense conifer forest, which continued down the gradual mountain slopes. In

an attempt to get above the damping influence of the forest, a 10 meter tower was erected at the site, and a Gill U-V-W anemometer placed at the 10 meter level. This put the instrument approximately at the top of the surrounding trees. The thermistor/hygristor couplet was placed at the 2.5 meter level. A photograph of the tower at the Williams Fork site is provided in Fig. 3.6.

The second site, Elk Mountain, was located on a southerly spur of the Rabbit Ears range 10 km north of Middle Park. The absolute summit of the mountain was equipped on 8 July 1987. The above treeline location provided excellent exposure. West of the summit, a very gradual ($\sim$ 5 degree) mountain slope lead to treeline, 400 meters away. East of the site, the mountain dropped off abruptly into a 75 meter cliff, below which a more gradual slope led to treeline. The ridgeline of the mountain itself was fairly continuous in both the north and south directions for several hundred meters. A photograph of the Elk Mountain site is given in Fig. 3.7.

On 9 July 1987, the third site in the Middle Park area was equipped. The location was Whiteley Peak, a striking peak of volcanic origins 30 km northwest of the center of Middle Park and 25 km southeast of the Mt. Werner site. A photograph of Whiteley Peak (Fig. 3.8) gives an indication of the dramatic rise of the mountain 600 meters above the valley floor. This abrupt rise and the isolated nature of the peak seemed to provide an excellent opportunity to measure the regional-scale airstream in a relatively unobstructed manner. After hauling a heavy datalogger, a 3 m tower section, and loaded backpacks up the steep, rocky slopes, the summit of Whiteley peak was equipped with remote wind, temperature, and humidity monitoring instrumentation. A photograph of the Whiteley Peak site is shown in Fig. 3.9. The site, while ideal in its exposed isolated location, had near vertical 100 m cliffs to the north and west, with 30° to 40° slopes to the south and east. We anticipated that this non-uniformity in slope and aspect would create some potentially serious local flow deflections, particularly during well-mixed daytime conditions. However, from our primary interest in nocturnal flow conditions, and the lack of terrain uniformity in virtually all mountain peak locations, we concluded that this site, as well as the others, were satisfactory for the experiment.

Figure 3.6: Photograph of the ROMPEX-87 Williams Peak station.

Figure 3.7: Photograph of the ROMPEX-87 Elk Mountain station.

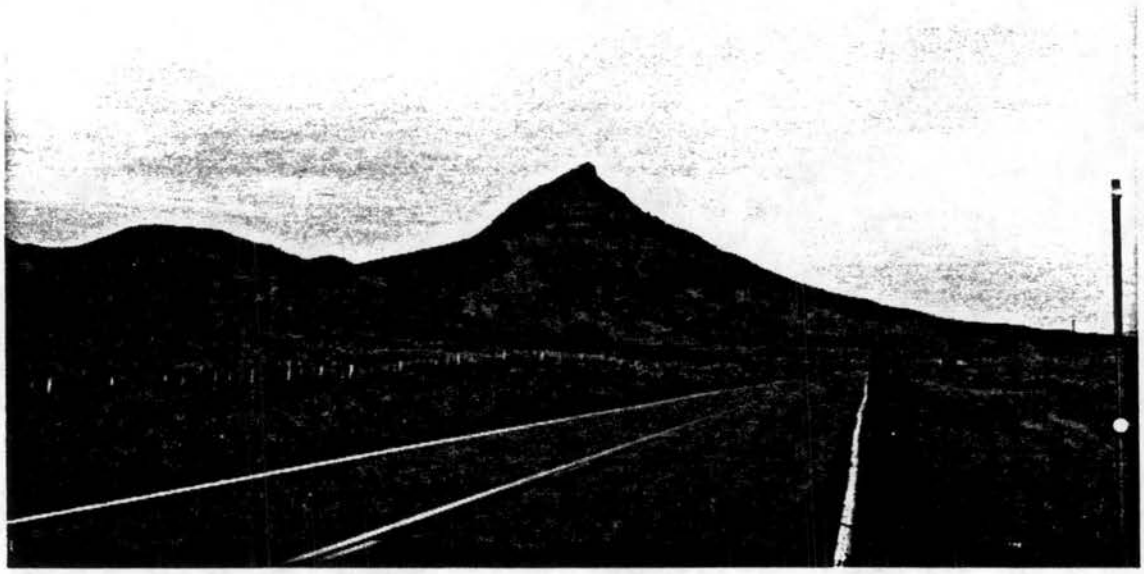

Figure 3.8: Photograph of Whiteley Peak from the northwest.

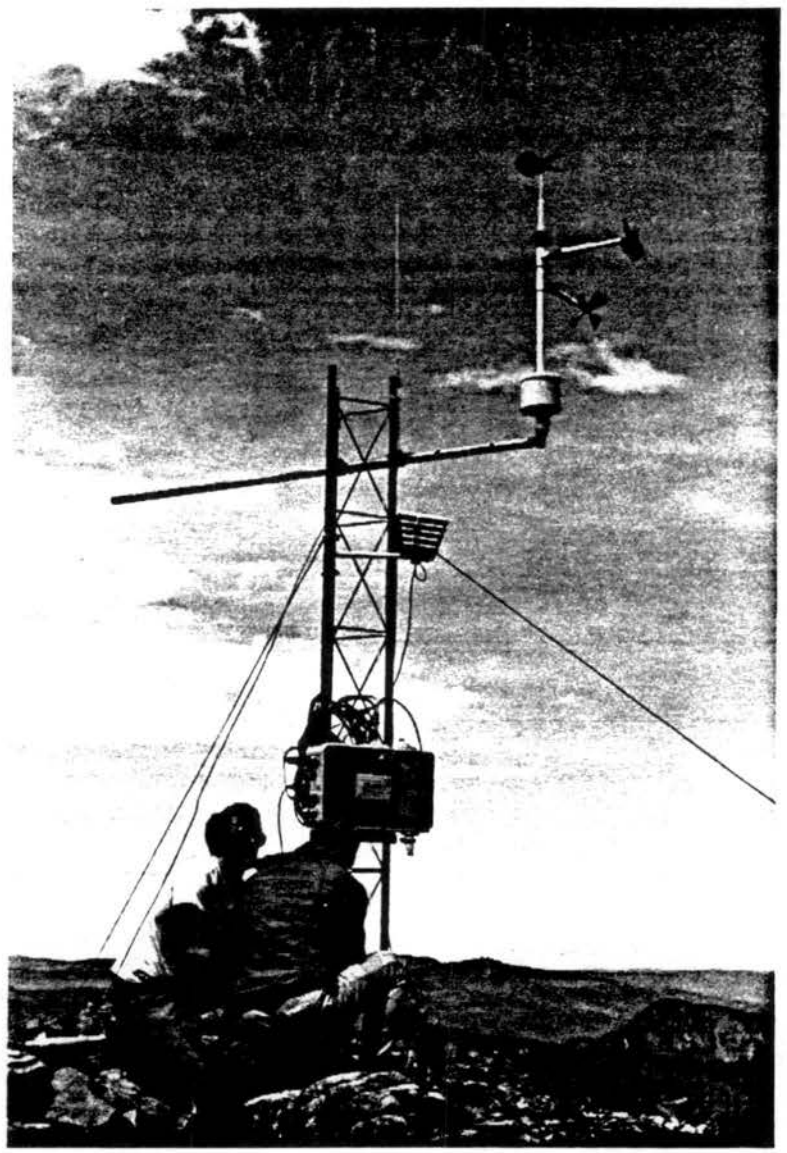

Figure 3.9: Photograph of the ROMPEX-87 Whiteley Peak station.

3.5.3 Data description

The four mountaintop sites specifically instrumented as part of the ROMPEX-87 experiment by personnel from CSU were combined with data from the Rollinsville and Squaw Mountain stations of the PROFS network and a remote station operated by the Bureau of Reclamation at Buffalo Pass, 10 km north of Mt. Werner, to obtain the primary data set analyzed in the following chapter. An additional site in Brunner Draw, located in the Yampa River Valley 10 km southwest of Mt. Werner, was also equipped as part of the ROMPEX-87 experiment. However, due to equipment problems and low elevation, data from this station are not used in the following analysis. Table 3.5 lists the pertinent information regarding the primary monitoring stations and the data available for the ROMPEX-87 field study. The geographical locations of the ROMPEX-87 sites are given in Fig. 3.10, relative to the regional topography. Additional surface, upper air, radar, and lightning strike data were also obtained to supplement the primary ROMPEX data base. These sources were described in section 3.4.1 and are also discussed in Bossert *et al.* (1989).

3.5.4 Special soundings

A further goal of the ROMPEX-87 field experiment was to investigate the vertical structure of the nocturnal regional-scale wind circulation over the study region. To accomplish this task required sounding equipment capable of providing high resolution wind, temperature, and humidity data at remote locations at night. These formidable requirements were met with a portable Airsonde^R sounding system developed by scientists at NCAR, and thoroughly tested during the TIPMEX-86 experiment in the rigorous conditions of the Tibetan Plateau. In 1987, this system was unavailable until early August.

The Airsonde system consists of a sonde measuring pressure, temperature, and humidity. The sonde transmits a signal which is received at the ground by a special transceiver. Output from the transceiver is ported to a small computer, with peripheral devices consisting of a printer and hard disk which provide a real time hardcopy and automatic storage of the sounding. Power is supplied by rechargeable NiCad batteries. The sonde is lifted by a 100 gm balloon filled with helium and tracked by theodolite to obtain winds. During

Table 3.5: ROMPEX-87 STATIONS

No.	Station	ID	Elevation (msl)	Dates of Operation	Parameters Observed
1.	Mt. Werner	MW	3207	8 June – 2 Oct	A
2.	Williams Peak	WL	3300	7 July – 10 Sept	B
3.	Elk Mountain	EM	3481	8 July – 10 Sept	B
4.	Whiteley Peak	WP	3081	9 July – 11 Sept	B
5.	Brunner Draw	BD	2110	17 Aug – 2 Oct	A
6.	Squaw Mtn.	SQ	3505	June – Sept	C
7.	Rollinsville	RO	2749	June – Sept	C
8.	Rabbit Ears	RE	3017	June – Oct	A
9.	Buffalo Pass	BP	3219	June – Sept	D

Station Designation:

Stations 1-5:	operated by E. R. Reiter and staff, Colorado State University
Stations 6-7:	PROFS-NOAA, Environmental Research Laboratory, Boulder, CO
Station 8:	operated by U.S. Geological Survey, Denver, CO
Station 9:	operated by Bureau of Reclamation, Denver, CO

Parameter Index:

A: radiation station (several configurations used at different stations)
B: U-V-W winds, temperature, and humidity
C: wind speed, wind direction, temperature, humidity, pressure, solar radiation, and rainfall
D: wind speed, wind direction, temperature, humidity, pressure, and rainfall

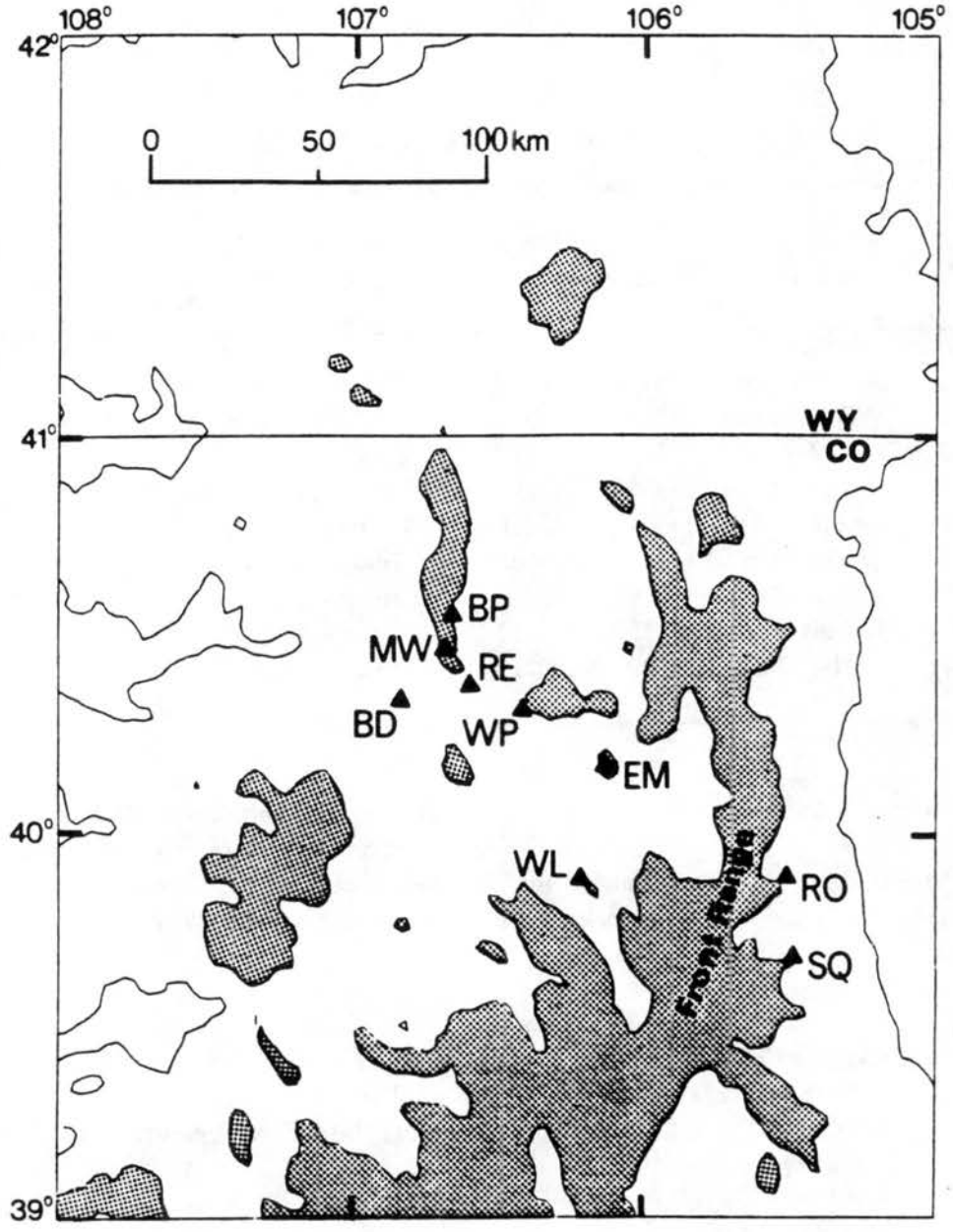

Figure 3.10: Geographic location of ROMPEX-87 stations and two-letter identifiers. Topographic contours are 2000 and 3000 msl. Areas above 3000 msl are shaded.

nighttime releases, small lights powered by battery cells were attached to the bottom of the sonde.

This sounding system was encased in styrofoam in a small table and could be easily loaded into the back of a truck for field soundings at various locations, provided the surface pressure could be accurately determined. Surface pressure was obtained by taking one sonde and calibrating it relative to an accurate barometric reading either at CSU or at the Mt. Werner base station. This sonde was then used as a reference to calibrate the sondes used over the course of an evening. This portable sounding system was used from a variety of locations during the summer and early fall of 1987. A total of twenty-six soundings were obtained under a variety of regional- and large-scale flow conditions. The information obtained from these launches provided detailed observations of the vertical structure of the regional wind field over the ROMPEX-87 study area.

3.6 Experiment Summary

The preceding sections have described the design and implementation of a series of field experiments initiated over the high terrain of the Colorado Rocky Mountains. Some emphasis was placed on detailing the difficulties in adequate site location and equipment deployment, which is inherent to an experiment of this nature. However, the data acquired from these experiments demonstrates the feasibility of conducting field operations at remote locations over a vast region, with limited personnel, observing equipment, and financial resources.

With these data, it has been possible to document systematic circulation patterns at mountaintop, resulting from diabatic forcing within the mountain boundary layer. Detailed analyses of circulation systems at these larger mesoscales have been previously unavailable, particularly west of the Continental Divide. Hence, the ROMPEX dataset provides a significant step forward in our ability to understand and describe the hierarchical structure of thermally-forced flows over complex terrain. This is of paramount importance in determining transport processes and in improving weather forecasting over large mountain regions.

Chapter 4

OBSERVATIONS OF REGIONAL-SCALE FLOWS OVER THE NORTH-CENTRAL ROCKY MOUNTAINS

In this chapter, the summertime meteorology of the mountaintop environment within the north-central Rocky Mountains is examined with data obtained during the Rocky Mountain Peaks Experiments and from additional sources, both described in the previous chapter. Given the very complex terrain and broad horizontal scale of the ROMPEX study region, it is reasonable to expect that many complicated wind patterns can develop as a result of synoptic-scale, regional-scale, and local-scale forcing mechanisms. One of the goals of this study is to unravel these combined effects and thereby decipher the regional-scale signal. This will be attempted by examining the horizontal and vertical structure of the winds at mountaintop over both diurnal and monthly temporal scales, and also by analyzing these flows during moist conditions, with abundant convection over the mountains, and during dry periods, when diurnal heating and cooling effects are optimized. Additional observational data will be presented in conjunction with numerical results in appropriate sections of the following two chapters.

4.1 Interdiurnal Flow Structure

This section has two primary goals: 1) to introduce the salient features of a diurnally reversing, regional-scale flow at mountaintop; 2) to demonstrate the spatial coherence of the regional-scale flow on each slope of the principal mountain barrier. The most effective way to accomplish this analysis is to examine time-series plots which show the interdiurnal flow structure at the various stations within the ROMPEX network.

4.1.1 The diurnal signal at Mt. Werner

In Chapter 2, many studies of diurnally reversing, thermally-driven flow systems were discussed. From this sparse body of research, it would be difficult to anticipate the summer season wind behavior at a mountaintop station in western Colorado. Perhaps the best guess would be to assume that an exposed high altitude site should closely follow the large-scale flow at a similar level, observed from the nearest rawinsonde station. However, the initial wind observations retrieved from the Mt. Werner station in August 1984 were very unexpected. Figure 4.1 shows a week-long period during the month over which a recurrent, diurnally oscillating flow was apparent. The flow varied between turbulent daytime northwesterly winds and very steady nocturnal east to southeast flow (Fig. 4.1a). The onset time of the easterly flow was somewhat variable, occurring between 1600 MST and 2200 MST, revealing that the onset is apparently not fixed to local sunset ($\sim$ 1900 MST). The nightly easterly winds seemed quite unusual given that the 70 kPa flow at Grand Junction, 200 km to the southwest, was from a westerly direction during most of this period. Moreover, the nocturnal easterly winds were very powerful (Fig. 4.1b), with gusts exceeding 20 ms^{-1} on 4 out of the 7 nights within this time-series. The strongest winds occurred around midnight, well into the nocturnal wind regime.

The nocturnal wind regime during this period often appeared very abruptly, with a 180° wind direction shift and strong easterly flow occurring within one hour of time. Figure 4.1 shows that the strong east-southeast flow often lasted many hours, or even the entire nocturnal period. On these occasions, the wind shift back to daytime northwesterly flow occurs over several hours, and is associated with the onset of morning heating. These evening wind reversal events at Mt. Werner were observed on 25 out of 33 days in which the station was in operation during 1984. Needless to say, our curiosity was raised by this dramatic, recurrent phenomenon. Our interest in the future ROMPEX experiments became focused upon describing the spatial and temporal characteristics of this strong nocturnal flow, and the physical mechanisms leading to its development.

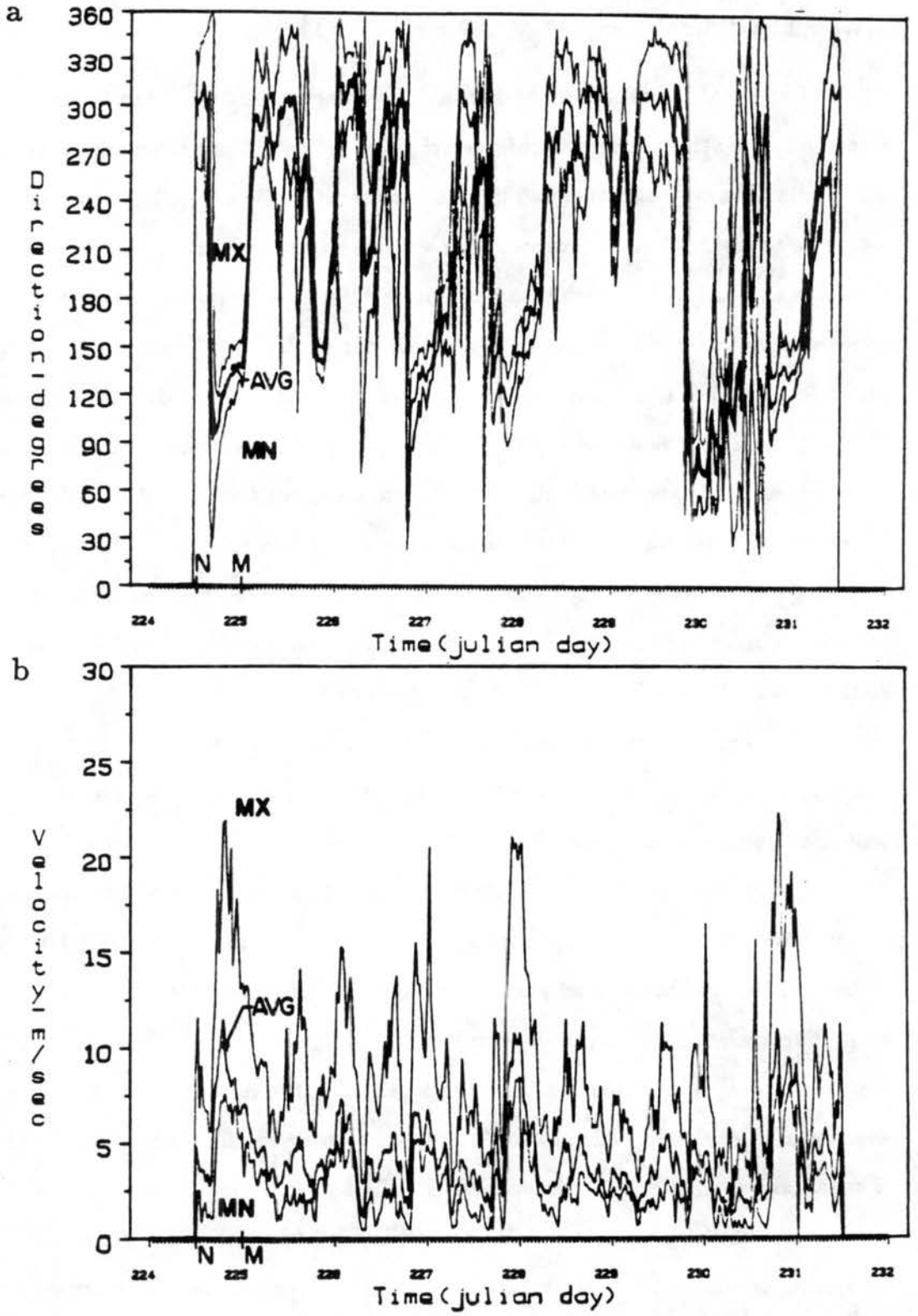

Figure 4.1: Maximum, average, and minimum (a) wind direction and (b) wind speed for 30 minute averaged intervals during Julian Days 225-232 (12-19 August) 1984. The "N" and "M" on the abscissa denote noon and midnight, respectively.

4.1.2 Horizontal flow structure-1985

During summer 1985, numerous mountaintop sites were instrumented to establish the regional aspects of the unusual nocturnal flow phenomenon detected at Mt. Werner in 1984. From the flow strength at Mt. Werner, and its peaktop location, it was inferred that this wind regime was not induced by local forcing, but was instead the result of a broader, regional-scale circulation system emanating from the higher topography to the south and east. This hypothesis was confirmed during the ROMPEX-85 experiment by comparing time-series of wind direction data from several stations located in similar locations relative to the regional topography. Figure 4.2 shows a comparison of the hourly-averaged wind direction behavior between the Squaw Mountain and Rollinsville stations (SQ and RO in Fig. 3.5) and the Mt. Werner and Vail Mountain sites (MW and VA in Fig. 3.5), during a ten-day period of July 1985. A simple three-point smoother (Haltiner and Williams 1980; p. 393) has been applied to the data to reduce small temporal fluctuations in wind direction, thereby enhancing the diurnal cycles.

The high altitude eastern slope stations of SQ and RO (Fig. 4.2a), which are 40 km apart, exhibit highly correlated diurnal wind direction cycles over this ten-day period. The winds at these two sites are seen to reverse between daytime easterly upslope winds and nocturnal downslope flow from a westerly direction, in agreement with the results of Toth and Johnson (1985). The wind direction begins to veer gradually toward a northerly direction at both stations shortly after the onset of morning heating, showing the link between thermal forcing and the rotation of the flow to an upslope component. The upslope flow begins around noon and generally lasts for several hours during the early afternoon. The wind vector again veers gradually back toward nocturnal westerly flow in late afternoon. The onset of the nocturnal wind regime generally occurs near local sunset ($\sim$ 1900 MST), but is quite variable within the time-series. The timing of the onset and shut-off of each flow regime is similar between the stations, particularly on days 10, 15, 16, and 17. The onset of upslope flow is generally 1-4 hours earlier at SQ than at RO, despite the higher altitude location of the SQ station.

The western slope stations of VA and MW (Fig. 4.2b) are also remarkably well-correlated ($r = 0.73$), especially for two mountaintop stations located 100 km apart over

complex terrain. Both stations undergo a diurnal flow reversal from daytime west-to-northwest upslope winds to nocturnal east-to-southeast downslope flow on each day within the time-series. The transition from the daytime to nocturnal regime often occurs abruptly, within one hour. The transition back to the daytime westerly upslope wind regime flow also occurs quickly, usually as a result of morning heating. These flow characteristics are similar to those described in Fig. 4.1 for the MW station during August 1984. On most of the days in this series the shift from westerly to easterly winds occurs 1-2 hours earlier at VA than MW. This earlier shift at VA would support the hypothesis that the nocturnal flow is of regional-scale proportions, and emanates from the direction of the high mountain barrier, which is geographically much closer to VA than MW. The time of the daytime/nocturnal regime wind shift is quite variable from day-to-day, occurring as early as 1700 MST on the 15th and 18th at VA, and as late as 2400 MST on the 13th, but usually within 1-2 hours of local sunset.

The above figure describes a recurrent, widespread diurnally forced flow regime across north-central Colorado, which shows a characteristic "inflow" pattern toward the Front Range by day and "outflow" pattern away from the high mountains by night. This circulation system appears as a coherent flow across the north-central Colorado mountain barrier (Fig. 4.2), suggesting a meso-β to meso-α horizontal extent. At this scale, the circulation can be defined as "regional", as it encompasses an area exceeding even the largest mountain valleys, but is still contained within the plateau or synoptic-scales. The ten-day time series over which this recurrent pattern occurs, and the day-to-day coherence of this wind system over large horizontal distances, suggests that this flow is not an anomalous feature. In fact at MW, the inflow/outflow diurnal wind signal occurs in varying degrees on well over half the days of recorded observations.

4.2 The Influence of Convection on Regional-Scale Flows

A peculiar characteristic of the July 1985 time-series discussed above was that it encompassed a moist period within the data record, during which significant convective activity occurred. Since strong convective storms can produce their own mesoscale circulations, it

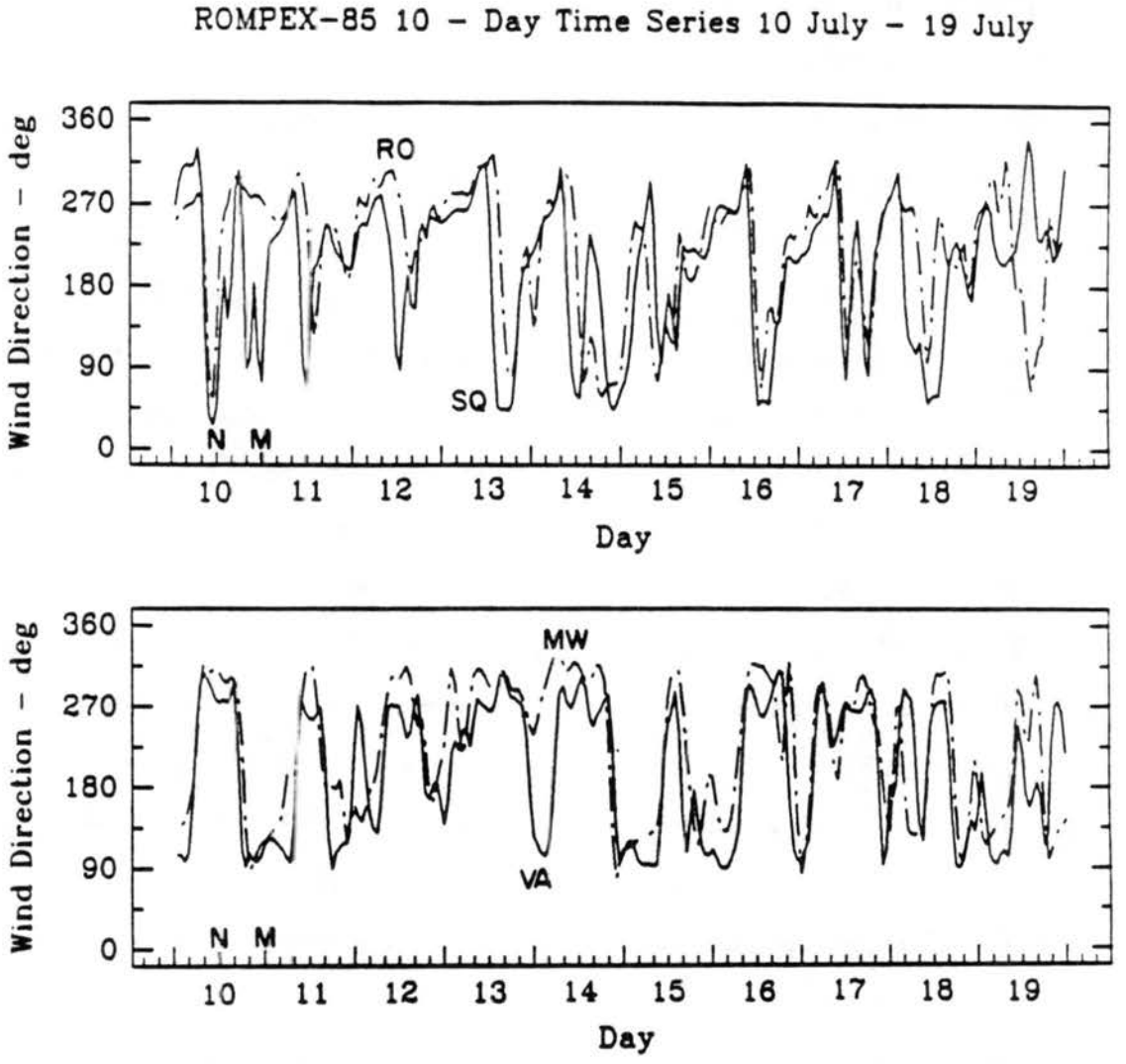

Figure 4.2: Hourly averaged wind direction at (a) two east slope stations (SQ, and RO); (b) two west slope stations (VA and MW) for the period 10-19 July 1985. The "N" and "M" on the abscissa denote noon and midnight, respectively.

seems appropriate here to examine how convective storms may influence the regional-scale wind field.

Convective storms of varying intensity occur frequently in summer over the north central Colorado mountains. Along the eastern slope of the Front Range, radar data has shown that the early development of cumulus clouds are due to "hot spots" (Wetzel 1973; Henz 1974) caused by preferential convergence of the upslope flows by local topography variations. Banta (1984) attributed the development of storms in South Park just east of the Mosquito Range to a lee-side convergence zone, produced when westerly flow from over the mountains meets the upslope flow generated over the basin. Banta and Schaaf (1987) used satellite imagery to traceback convective storms over the mountains of Colorado to their geographic location of origin for different large-scale flow regimes. Climatological studies of storm development over the Colorado Rockies have also been conducted with satellite imagery (Klitch *et al.* 1985) and lightning strike data (Lopez and Holle 1986).

Over the South Park region, the downdrafts and outflows associated with strong convective storms were studied by Knupp (1985) using Doppler radar. Gust fronts and density currents resulting from thunderstorm outflows have been investigated observationally by Charba (1974) and Goff (1976); in numerical simulations by Mitchell and Hovermale (1977) and Droegemeier and Wilhelmson (1987); and in the laboratory by Simpson (1969) and Simpson and Britter (1980). Through the production of strong outflow winds over the high mountain terrain caused by downdrafts associated with precipitation evaporation, deep convective storms could significantly perturb the thermally-forced flows generated over the ROMPEX study area. Convective modification of the mountain boundary layer air mass could be a factor in the wind behavior shown in the time-series of the previous section. However, without adequate radar data over western Colorado, and lacking high temporal and spatial resolution satellite imagery, the extent of this role has been difficult to assess.

4.2.1 An examination of convective storm location

One means of qualitatively inferring convective storm activity over the Colorado mountains is with data from the Automatic Lightning Detection System (ALDS), which provides the latitude/longitude location of positive lightning ground strokes, as observed with a

network of detectors which cover most of the inter-mountain west. These data have been shown by Lopez and Holle (1986) to be a reasonably accurate method of detecting and tracking strong convective activity. The ALDS data is used here to examine the geographic development of convective activity over the ROMPEX-85 network. Figure 4.3 shows the hourly-averaged number of strikes in each 0.167° latitude-longitude sector for the 23-day period from 9 - 31 July 1985. This extended period encompasses the ten-day time-series shown in Fig. 4.2, and with the additional days, provides a longer-term average. Frequent strong convective storms were observed over the Colorado mountains during this time-span, providing an opportunity to examine, in an averaged sense, the effects of convection on the regional-scale environment and associated circulation systems.

The averaged number of strikes between 1200 and 1300 MST (Fig. 4.3a) reveals the early development of storms just to the east of the Front Range crest, over the Mosquito Range west of South Park, and extending in an arc along the high terrain between the Front Range and the Flat Tops in western Colorado. The early storm activity along the Front Range during this period is in agreement with that shown in a longer term study by Lopez and Holle (1986). These storms result from convergence of low-level flow, induced by heating of the east and west slopes. Evidence of this convergent flow can be inferred from the time-series in Fig. 4.2, and is also seen during this 23-day period in the averaged diurnal wind cycle at individual stations. For instance, at the Squaw Mt. (SQ) station (Fig. 4.4a) the wind vector begins to rotate from thermal forcing by 0800 MST. The upslope flow is well developed by 1200 MST, and continues at SQ until 1500 MST on the average, when a wind shift to southwesterly flow occurs. At the Mt. Werner station (MW), the winds remain westerly throughout the daytime during this 23-day July period (Fig. 4.4b). Together, the opposing upslope flow systems on each side of the main mountain barrier forms the lower branch of a deep mountain-plains solenoid with a vertical branch near the crest of the Front Range.

The formation of convective clouds as a result of this solenoidal forcing is reflected in the solar radiation and precipitation amounts at SQ. Between 1000 and 1100 MST the incoming solar radiation at SQ (Fig. 4.5a) begins a dramatic decrease from clear-sky values, revealing the extent of cloud buildup over the site. During the next hour, when upslope flow

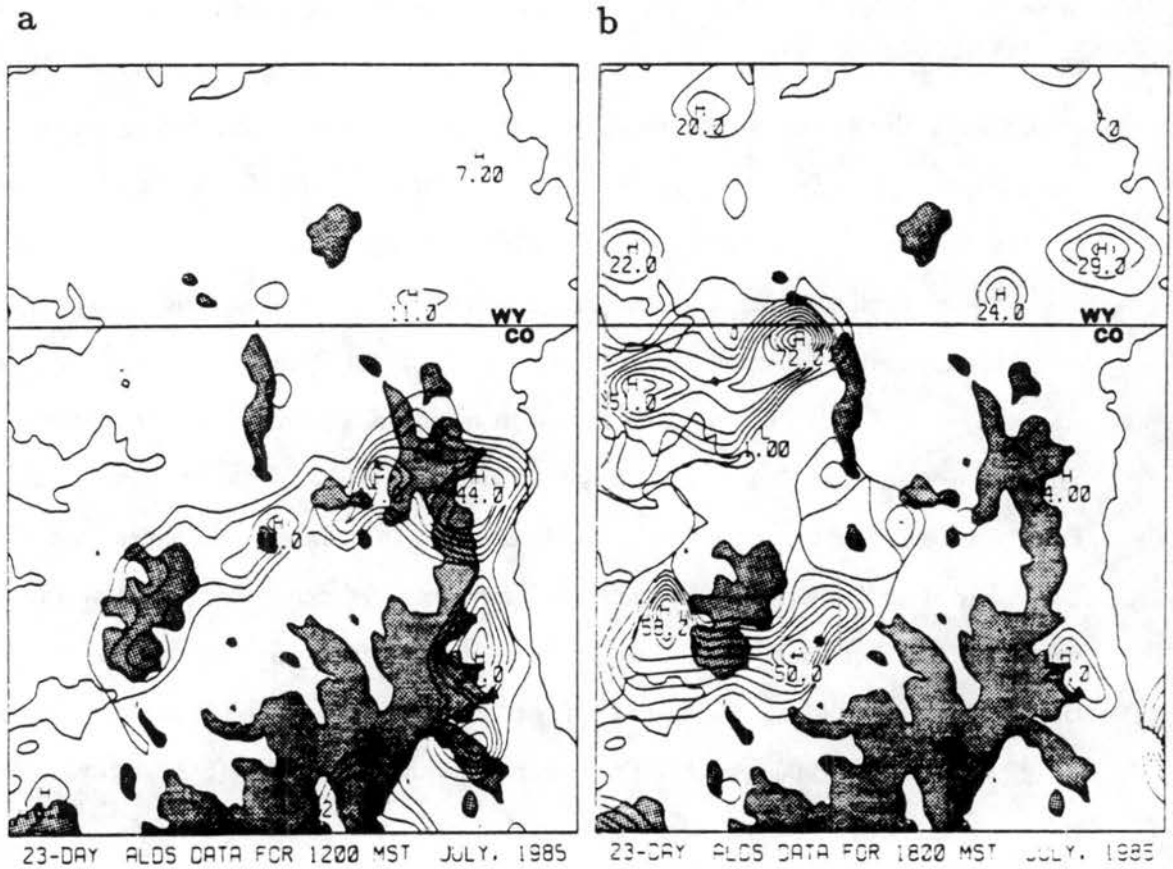

Figure 4.3: Contours of total lightning strikes in each 0.167° sector of latitude and longitude, for (a) 1200-1300 MST and (b) 1800-1900 MST 9-31 July 1985 for a portion of north-central Colorado and south-central Wyoming. Contouring begins at 10 strikes per 0.167°, with a 5 strike interval thereafter. Triangles denote the Mount Werner and Squaw Mountain stations. Topographic contours are 2000 and 3000 msl.

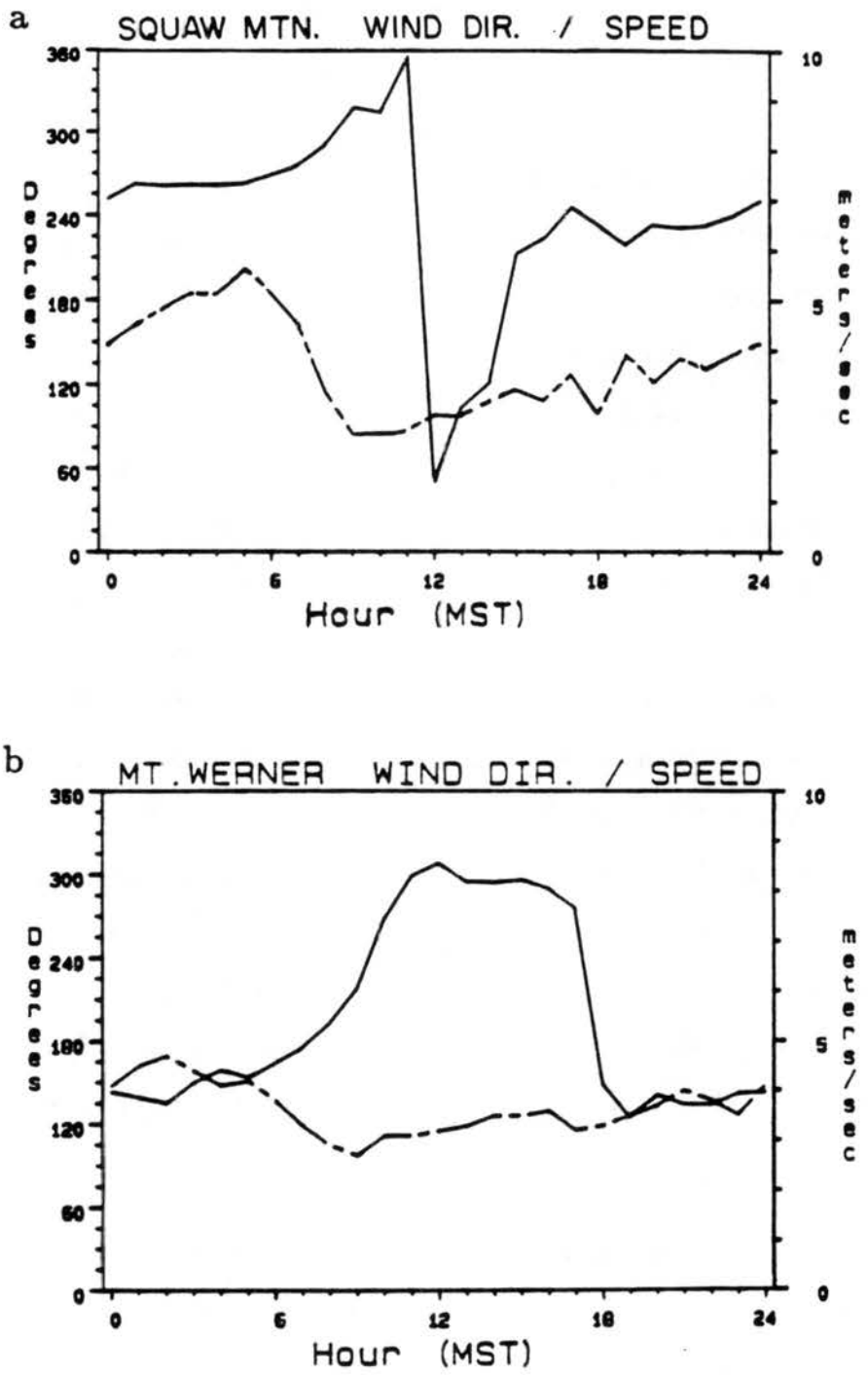

Figure 4.4: Hourly averaged wind direction (solid) and wind speed (dashed) at (a) Squaw Mountain and (b) Mount Werner for the period 9-31 July 1985.

at SQ has become well established, ALDS data indicates convective activity over the site (Fig. 4.3a), while the persistent effects of deep convective clouds at SQ can be seen in the severely reduced afternoon insolation, and the frequent afternoon precipitation. A return to more normal insolation values and a decrease in precipitation amounts at SQ by 1600 MST would appear to indicate a decrease in convective cloudiness, due either to dissipation, or advection of storms away from the vicinity of the station.

Averaged lightning strike data between 1800 and 1900 MST (Fig. 4.3b) confirms that active convective storms have moved away from the Front Range at this time, toward the plains in eastern Colorado (not shown) and westward toward the mountains and lower elevations of western Colorado. Associated with this movement in convective activity away from the high mountains is the tendency for an abrupt reversal in flow direction at MW, from the prevailing upslope west-northwest flow to southeasterly flow. The total solar radiation curve (Fig. 4.5b) reveals that nearly uninterrupted insolation occurs on the average at MW up to 1200 MST, with some minor cloud effects noted in the afternoon hours, much less than the thick afternoon cloudiness at SQ. Afternoon rainfall at MW is reflected in the precipitation maximum at 1500 MST, while a secondary maximum is found at 1800 MST, this occurring with the onset of the nocturnal wind regime. The diurnal averages at Vail Mtn. (VA; not shown) also reveal a tendency for frequent early evening precipitation, in agreement with the westward development of convective activity during the afternoon. From this analysis, we can hypothesize that the westward progression of storm development in the late afternoon toward the MW and VA stations is associated with the abrupt flow reversal and much later precipitation, which occurs at these western slope sites in July 1985.

4.2.2 Convection-induced outflow winds

By examining thermodynamic data from the mountaintop stations, the characteristics of the air mass along the western slope of the mountain barrier, before and after the passage of an easterly nocturnal wind surge, can be determined (Betts 1982; 1984). In particular, by observing a significant change in a conservative variable such as equivalent potential temperature, we can show that the surging air mass was probably produced through convective processes. This analysis has been previously done with data from the MW station for a

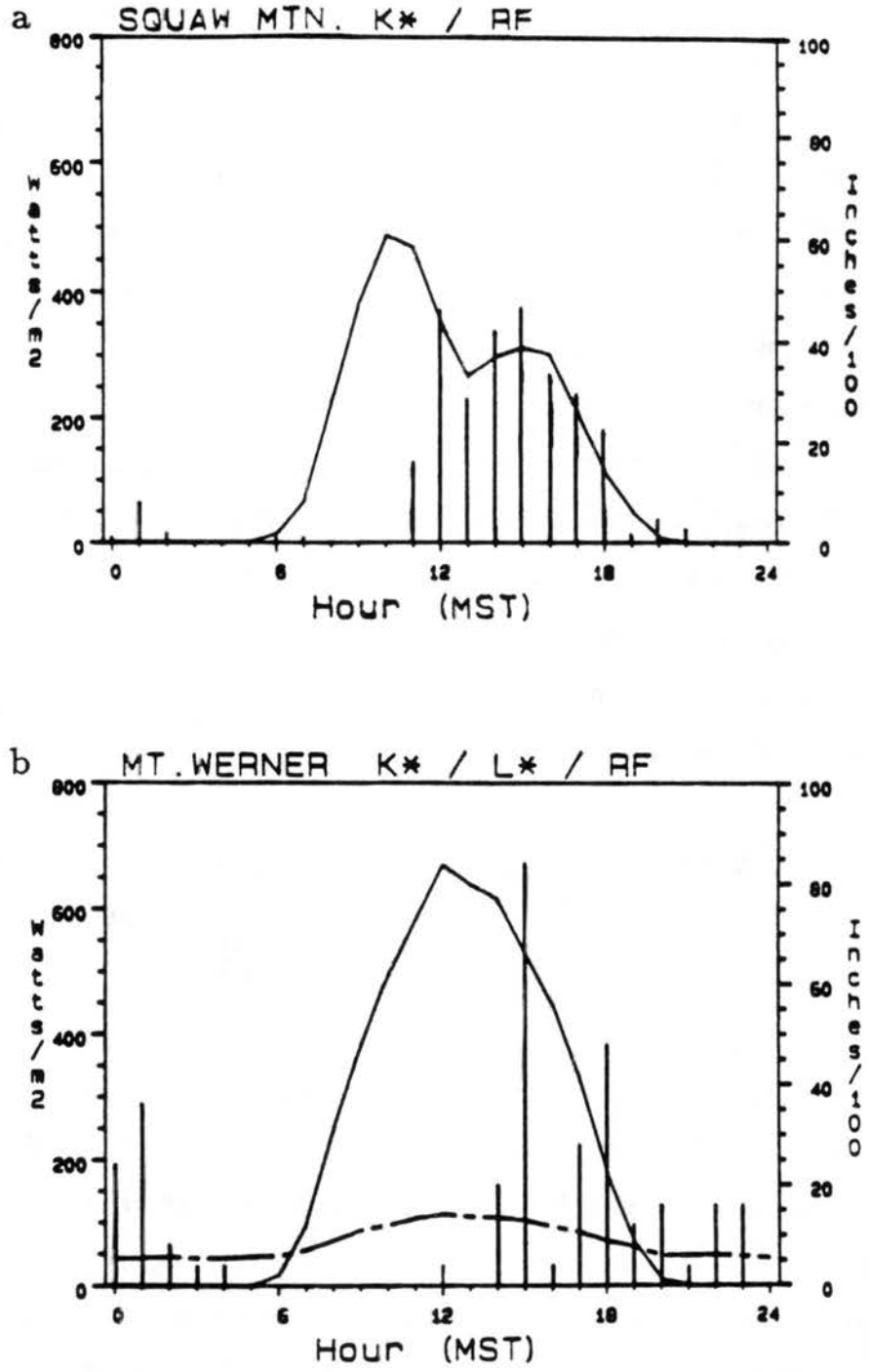

Figure 4.5: Hourly averaged total downward solar radiation and precipitation at (a) Squaw Mt. and (b) Mt. Werner for the period 9-31 July 1985. Dashed line in (b) is the total upward longwave radiation.

case on 13 August 1986 (Bossert *et al.* 1989), during moist monsoonal conditions similar to those which prevailed in July 1985.

For the present study, we examine in detail the wind and temperature changes which occurred on 27 July 1987, a day included in a 5-day time-series shown in chapter 5 (see Fig. 5.16). Satellite photos at 1431 and 1445 MST July 27 (Fig. 4.6) show that convective storms were prevalent over the intermountain west, due to strong moisture advection from the tropics on prevailing south-southwest flow. Over north-central Colorado at this time, convective anvil debris can be seen in an arc along the Front Range, indicating storm activity in a pattern similar to that depicted by ALDS data in July 1985 (Fig. 4.3a). In addition, a recent, more circular tower can be seen forming at 1431 MST over the southern portion of Middle Park, in close proximity to the ROMPEX-87 station network, especially the Williams Peak station (WL in Fig. 3.10).

To observe changes in the air mass residing over the ROMPEX-87 study region, an equivalent potential temperature (θ_e) was calculated, based upon the method described by Bolton (1980). Pressure data for this calculation were obtained from a station at Rabbit Ears Pass operated by the U.S. Geological Survey. The station is located midway between Mt. Werner and Whiteley Peak, and records meteorological data in 15-minute averages, the same averaging period used by the ROMPEX-87 stations. The pressure data were then interpolated to the various heights of the ROMPEX-87 stations using an integrated form of the hypsometric equation, assuming a standard atmosphere lapse rate. Given the small differences in height between the ROMPEX-87 stations and the Rabbit Ears station (at most 400 m) this method should not introduce significant errors into the calculated θ_e values.

In Fig. 4.7, the values of θ_e, wind direction, and wind speed are given at 15-minute averaged time intervals for the western slope ROMPEX stations (EM, WL, WP, MW in Fig. 3.10) for a 6-hour period of 27 July 1987. The time-series begins at 1215 MST, when strong thermal heating and moist lower tropospheric conditions produced high values of θ_e at all stations (upper panel). The extremely high θ_e values at WL and WP appear to be caused by a lack of wind motion (lower panel), which allows thermal eddies to effectively carry heat and water vapor from the moist ground up to the sampling level, while remaining insulated

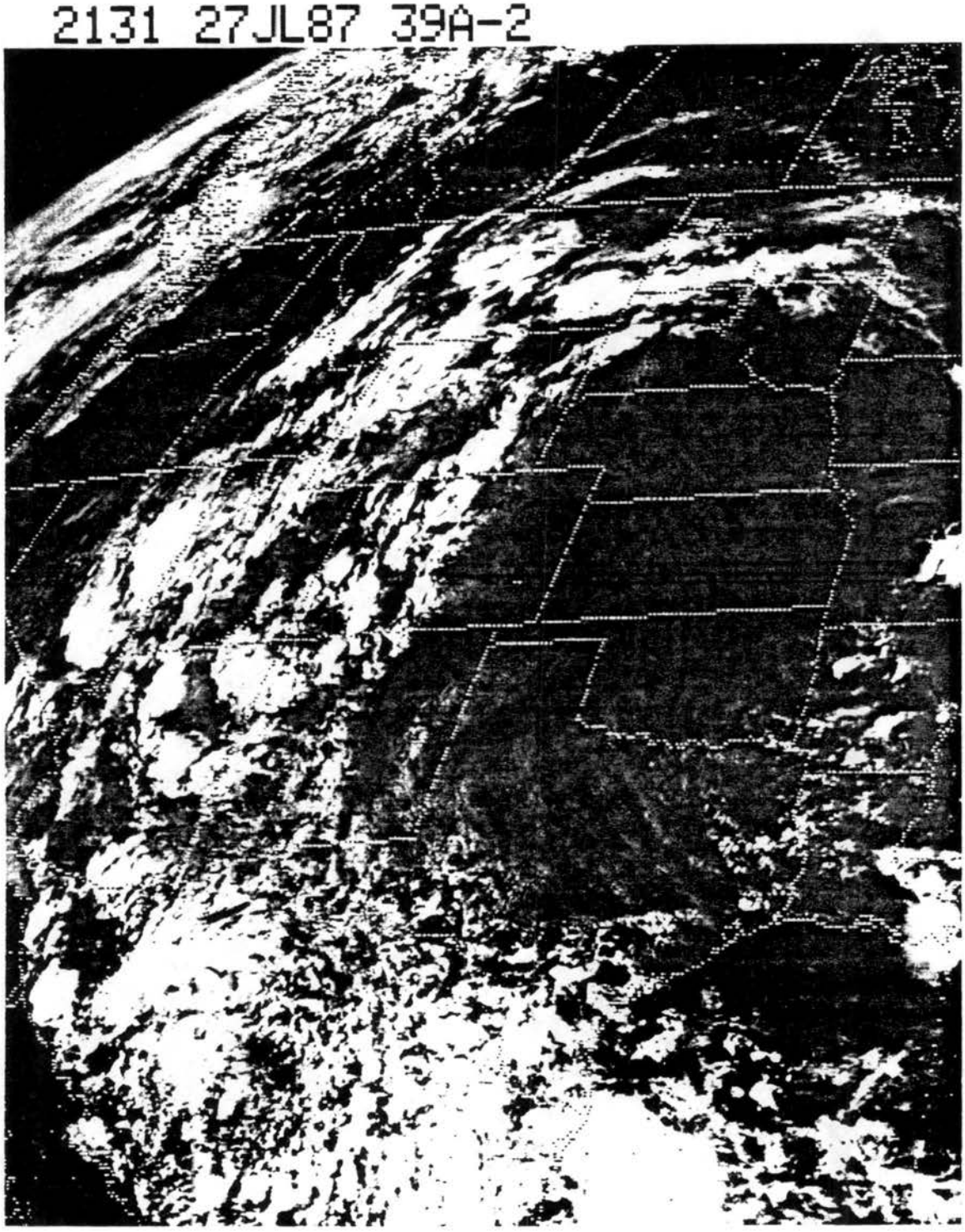

Figure 4.6: Visible satellite images over the western U.S. at (a) 1431 MST and (b) 1445 MST 27 July 1987.

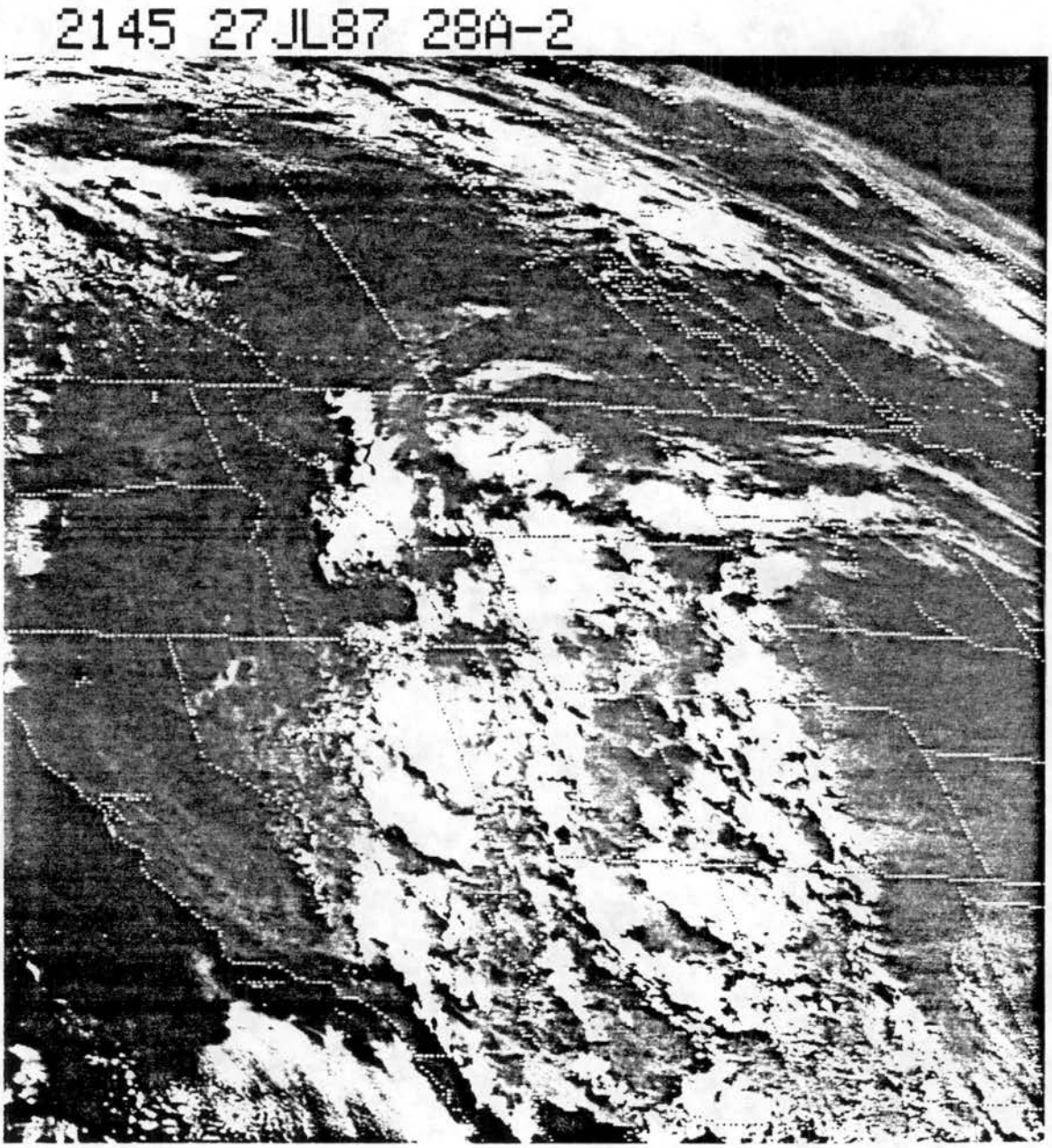

Figure 4.6: Continued.

from the cooler, drier air above the surface layer. Winds are from a westerly direction at all of the stations at this time (middle panel).

Cloud shading at the WL site between 1330 and 1345 MST suppresses the surface heating, reducing θ_e to a value in line with EM and MW, which experience fairly steady θ_e values, due in part to the higher wind speeds at these stations. The WP site also undergoes a similar reduction in θ_e by 1400 MST. Following the reduction in θ_e at WL, a wind shift to easterly flow occurs by 1400 MST and θ_e continues to decrease, dropping 11°C between 1345 and 1430 MST. At EM, located 32 km to the north-northeast of WL, a shift to easterly flow also occurs along with a comparable drop in θ_e beginning at 1400 MST. Wind speeds at WL and especially at EM increase substantially with the onset of this cold easterly flow. Thus, the thermodynamic structure of the air behind the wind shift is much different than the well-mixed daytime mountain boundary layer air which existed prior to the flow reversal. Without additional data, we can only surmise that the cold easterly flow was associated with outflow from storms in the vicinity, as seen in the satellite photos, but this would certainly be the most likely prospect.

At the WP station, located 50 km north-northwest of WL and 35 km northwest of EM, θ_e values dropped significantly between 1445 and 1500 MST, under conditions of westerly flow at 2-3 ms^{-1}. By 1530 MST, however, the wind direction began to shift toward a southeasterly direction. These southeasterly winds became very strong by 1600 MST, producing a 15-minute average velocity of 11.6 ms^{-1}. From 1530 to 1600 MST θ_e dropped an additional 5°C at WP, to 343°C, very close to the minimum value reached at WL over one hour earlier with the onset of the cold easterly flow. The air mass over the WP station warmed dramatically after the dissipation of the strong gust front-like winds, so that by 1645 MST θ_e was back to a pre-front value of 357°C. This suggests that a "sloshing" back of the well-mixed air occurred after the gust-front passage. A similar warming event, though less dramatic, occurred at the EM station one hour earlier at 1545 MST. At WP, however, this warming was brief, and the cold air returned by 1700 MST.

At the MW station, 25 km northwest of WP and 75 km northwest of WL, θ_e values remained very steady near 355°C all afternoon until 1630 MST when the wind shifted from very steady afternoon northwesterly flow to stronger southeasterly flow. As at the other

three stations, the southeasterly winds ushered in the cold air, which was reflected at MW by an 8°C drop in θ_e between 1630 and 1700 MST. The cold air and brisk southeasterly flow at MW remained through the end of the time-series at 1800 MST, while at the other three stations the winds began to veer toward a south-southwest direction by this time.

The case study presented above shows compelling evidence of a convectively-induced outflow current propagating through all of the ROMPEX-87 stations west of the Front Range barrier. Dramatic cooling was associated with a reversal of the winds from weak daytime west-northwest flow to stronger southeasterly flow. The current appeared first at the WL station and shortly thereafter at the EM station, implying a southwest-northeast orientation to the surge front. These two stations were closest to the large, circular convective tower, which appeared in the satellite photographs to be undergoing rapid development around 1400 MST. The current arrived approximately 90 minutes later at the WP station, indicating a propagation speed of ~ 7 ms^{-1}. Winds behind the current were very strong at the WP station (11.6 ms^{-1}), revealing a relative flow toward the head of the current. One hour after passing over the WP station, the current swept through the MW station, again showing a propagation speed of ~ 7 ms^{-1}.

From the evidence presented above, it appears that the diurnal convective cycle can play an important role in the initiation of the regional-scale outflow wind regime, particularly along the western slope of the mountain barrier. On days with strong convection, these outflow winds generally arrive with an abrupt shift from a daytime westerly inflow to southeasterly outflow direction and are associated with an air mass which has been modified from the in situ, well-mixed, air by convective storms located over the higher terrain. The decrease in θ_e within the post-surge air mass is due primarily to convective-scale downdrafts associated with the evaporation of precipitation into the subsaturated mountain boundary layer air mass (e.g. Newton 1950; Kamburova and Ludlam 1966; Betts 1976; Johnson 1976; Brown 1979; Knupp 1987). The cold, dense air produced by this process then flows northwestward past the ROMPEX-87 stations toward lower elevations.

While the importance of convective processes in affecting the regional-scale circulations, particularly over the western portion of the ROMPEX study region, has been established in this section, details of the mechanisms involved await further investigation. One serious

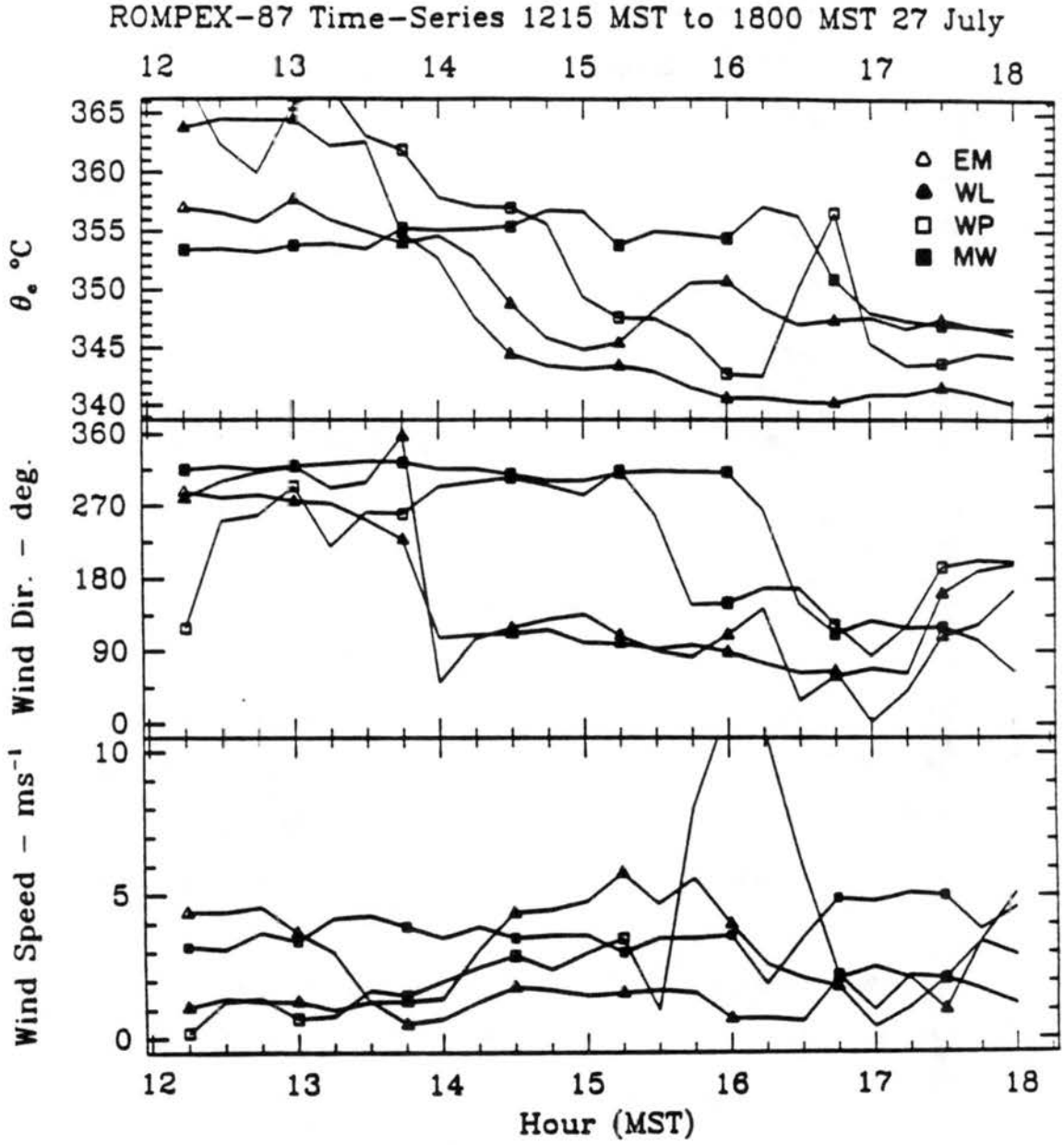

Figure 4.7: Time-series of θ_e, wind direction, and wind speed at Elk Mountain (EM), Williams Peak (WL), Whiteley Peak (WP), and Mt. Werner (MW) for 1215 to 1800 MST 27 July 1987.

limitation within this study involves the small-scale nature of convective processes over the mountains, despite the tendency for cells to form over widespread areas of the higher terrain. However, given the strong diurnal signature of the regional-scale circulation system under study, in all of our analyses to this point, convective forcing must be regarded as a second order influence in the generation of the observed flows, with thermal forcing of the elevated terrain being the primary driving component. In an effort to achieve a more thorough understanding of the basic elements driving the regional-scale flow evolution, further observational and numerical investigation will focus upon those circulations which evolve within a dry environment from thermal forcing.

4.3 Effects of Thermal Forcing at Mountaintop

To observe the development of regional-scale flows across the north-central Colorado mountain barrier without the complicating influences of intense convective storms or strong synoptic winds, the mountaintop observations were examined for clear sky conditions with weak upper-level flow, when thermal heating and cooling of the regional terrain would most strongly influence the resulting circulations. To acquire this data set, the ROMPEX data collected over the years of 1985, 1986, and 1987 were subjectively examined for lack of lightning strikes and radar echoes, weak upper level flow, low humidity, clear sky daytime insolation, and high, uninterrupted nocturnal outgoing infrared radiation values (available only at MW). From this analysis, 47 days were obtained for the MW and SQ stations. The wind data from these 47 days are presented as hodographs to highlight their oscillatory behavior within the diurnal cycle (Fig. 4.8 The primary feature of these hodographs is the out of phase relationship between the maximum u-component at the eastern slope station (SQ, Fig. 4.8a) and the western slope station (MW, Fig. 4.8b). In the afternoon hours, when strong northwesterly winds are found at MW, the winds at SQ are generally very light, while 12 hours later at night, the u-component reverses between the stations with southeasterly flow at MW and southwesterly flow at SQ.

Weak afternoon flow at SQ is caused by unsteadiness in the afternoon wind which tends to oscillate between a weak upslope and downslope component, due to the proximity of this station to the crest of the Front Range and, hence, the western edge of the daytime inflow

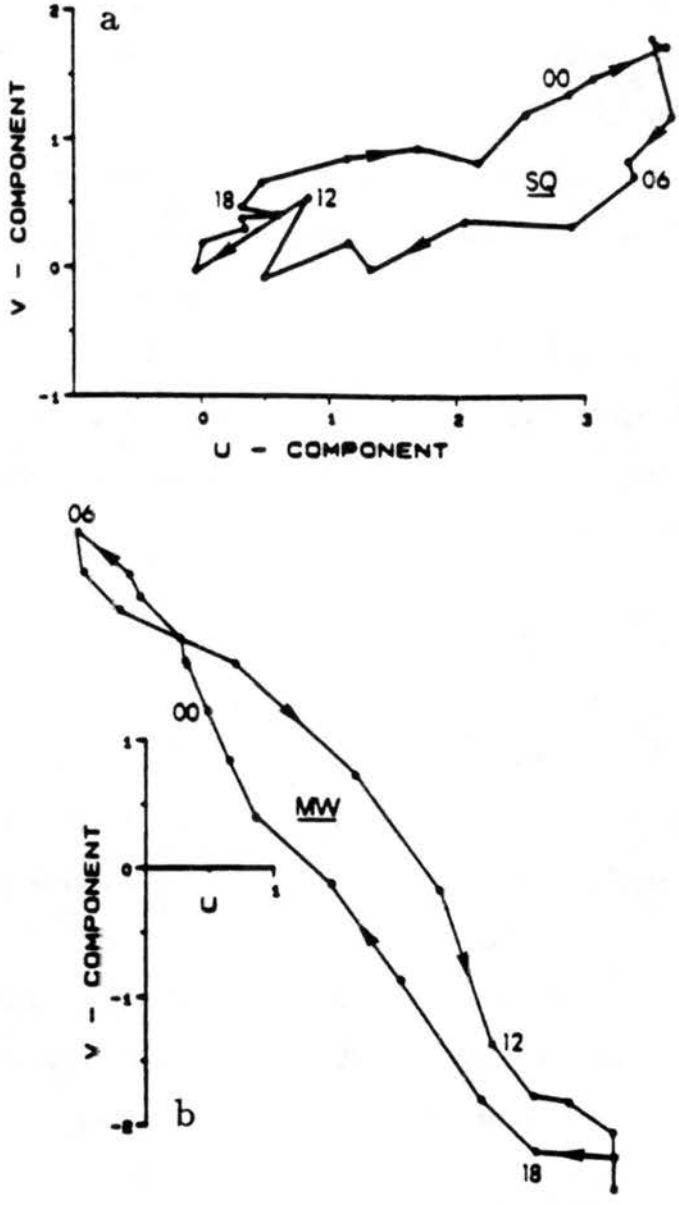

Figure 4.8: Averaged wind hodographs for 47 clear days at (a) Squaw Mountain (SQ) and (b) Mount Werner (MW). Labeled times are midnight (00), 0600 (06), 1200 (12) and 1800 (18) MST. Axes are horizontal wind component speeds in ms^{-1}.

solenoid. In addition, the downward transport of westerly momentum from aloft (Banta and Cotton 1981; Banta 1984), through a deep-mixed layer which evolves over this mountain region in summer, may contribute to this afternoon variability. Of further interest here is the prolonged transition time between diurnal inflow and outflow regimes at each station. The transition time between each quasi-steady regime at SQ and MW takes approximately seven hours (1900-0200 MST at SQ; 1800-0100 MST at MW) for daytime to nocturnal; and approximately five hours (0600-1100 MST at SQ; 0800-1300 MST at MW) from nocturnal to daytime flow. These hodographs demonstrate that thermal forcing alone produces the basic inflow/outflow pattern over the mountain barrier. However, the prolonged transition between daytime and nocturnal flow regimes, and generally weaker nocturnal flow than noted with convectively-modified outflow winds, suggests that the additional influence of convective forcing can significantly alter this fundamental regional-scale pattern, even affecting the longer-term averages (Fig. 4.4).

4.4 Vertical Structure of the Nocturnal Wind Regime

The previous sections of this chapter have emphasized the horizontal structure of diurnally oscillating flows observed at mountaintop. To gain additional insight into the nature of these circulation systems requires information on their vertical structure. While mesoscale wind systems are often observed below the surrounding mountaintop level of rawinsonde ascents from the Denver and Grand Junction stations, it is difficult to determine their relationship (if any) to circulations observed during the ROMPEX experiments over the higher elevations between these two stations. The only way to obtain useful measurements of the vertical structure of the nocturnal regional-scale wind regime is to release sondes at remote locations where the flows under investigation are known to exist. Such measurements have been obtained with the portable sounding system described in the previous chapter.

4.4.1 Nocturnal flow evolution at Mt. Werner

Using the portable Airsonde sounding system, six airsondes were launched from the top of Mt. Werner on 27 - 28 August 1986, recording the vertical wind and temperature structure through an entire nocturnal easterly wind event from onset to decay. The MW site

was chosen for its high probability of observing strong nocturnal outflow, and its mountaintop laboratory which served as a base station. Large-scale weather conditions during this particular episode were dominated by a high amplitude ridge moving into the central Rocky Mountain region with weakening upper level winds. The 70 kPa winds at Denver at 0000 UTC 28 August (1700 MST) were from the northeast at 3.5 ms^{-1}, unfortunately Grand Junction winds were unavailable. Due to the fairly dry conditions over Colorado associated with the ridge, only weak convection developed during the day, virtually eliminating the influence of moist convective processes on the resulting flow.

The first sounding was launched at 2100 MST, approximately 30 minutes after winds at the site shifted to a northeasterly direction. This sounding (Fig. 4.9a) shows the development of a strong low-level jet with a maximum speed of 9.0 ms^{-1} from the northeast 200 m above the mountaintop surface (AGL). This jet appears within a shallow stable layer of 450 meters depth. Above the jet lies a 1 km deep layer with very weak wind speeds ($\sim$ 2 ms^{-1}) from the northwest, within a remnant mixed layer which extends to 53 kPa. The shallow stable layer encompassing the low-level jet has a Brunt-Vaisala frequency $N = [g/\theta(d\theta/dz)]^{1/2}$ =0.0102 s^{-1}, and a Richardson number $R_i = N^2/(dU/dZ)^2$ of between 0.16 and 0.3 from near the surface to the jet level, depending upon the near surface wind speed and stability used. This R_i is very close to the critical value of 0.25, indicating that the flow is probably unstable, with significant turbulent mixing in the layer up to the jet level.

Despite the presence of turbulent mixing, the low-level flow remains steady over the next three hours, as revealed through surface observations and an additional sounding launched at 2300 MST (not shown). By 2400 MST (Fig. 4.9b), the low-level jet structure is still evident, with the jet maximum at 96 m AGL. At this time, however, the low-level winds have shifted to an east-southeast direction through a 700 m layer above the surface. Above this layer the flow shifts abruptly to southwesterly up to the 53 kPa level where another shift to northeast flow occurs. The temperature profile continues to show strong stability throughout the low-level jet layer, above which lies the remnant adiabatic layer, which is decreasing in depth.

Two additional soundings were taken over the course of the next five hours, during which time the low-level east-southeast flow over the mountaintop remained a persistent

feature (Fig. 4.9c), with jet speeds decreasing gradually through the period. West-southwest flow above the low-level jet begins to gradually mix down toward the low-level flow, so that by 0600 MST (Fig. 4.9d) the southeasterly flow is restricted to a very shallow layer near the surface, which is eventually mixed out by surface heating over a several hour transition period, after which the normal daytime northwesterly flow regime begins.

This set of soundings through a nocturnal wind event at the top of MW reveals that the outflow winds were a very low-level phenomenon, with the maximum winds in this case never more than 200 m AGL. However, the persistence of this low-level flow over a 10 hour time span, within a distinct stable layer detached from upper level winds, suggests that a continuous source for this flow must exist. From the gradual decrease in the depth and speed of the flow above mountaintop, we can infer that the source diminishes throughout the night. However, surface heating was required to actually dissipate the low-level flow. The time-series signature of this particular event (not shown) reveals it to have a time period, average wind direction, and average wind speed similar to many of the other nocturnal easterly wind events within the MW station data record (see Figs. 4.1, 4.2). In addition, wind data from the Buffalo Pass station on 27-28 August 1986 showed an onset time of the nocturnal regime nearly simultaneous to MW, and a similar northeast-southeast turning of the winds during the night. This implies that the 27-28 August nocturnal wind event also occurred at this station, 10 km to the north. This evidence suggests that the wind event was fairly widespread, indicative of a regional-scale outflow. Thus, we can speculate that other easterly nocturnal events along the western slope may possess a similar vertical structure.

4.4.2 Vertical structure during dry and moist conditions

Additional confirmation of a low-level jet-like structure to the nocturnal easterly flow observed at MW is shown in Fig. 4.10 for 2300 MST 1 October 1987. This easterly wind event was observed during very dry autumn conditions under a strong upper level ridge of high pressure. The sounding reveals a structure similar to that noted in the previous example, with an 8 ms^{-1} low-level jet 50 m above the surface of the mountaintop. The jet speed decreases dramatically over the next 50 m above the jet core, then maintains

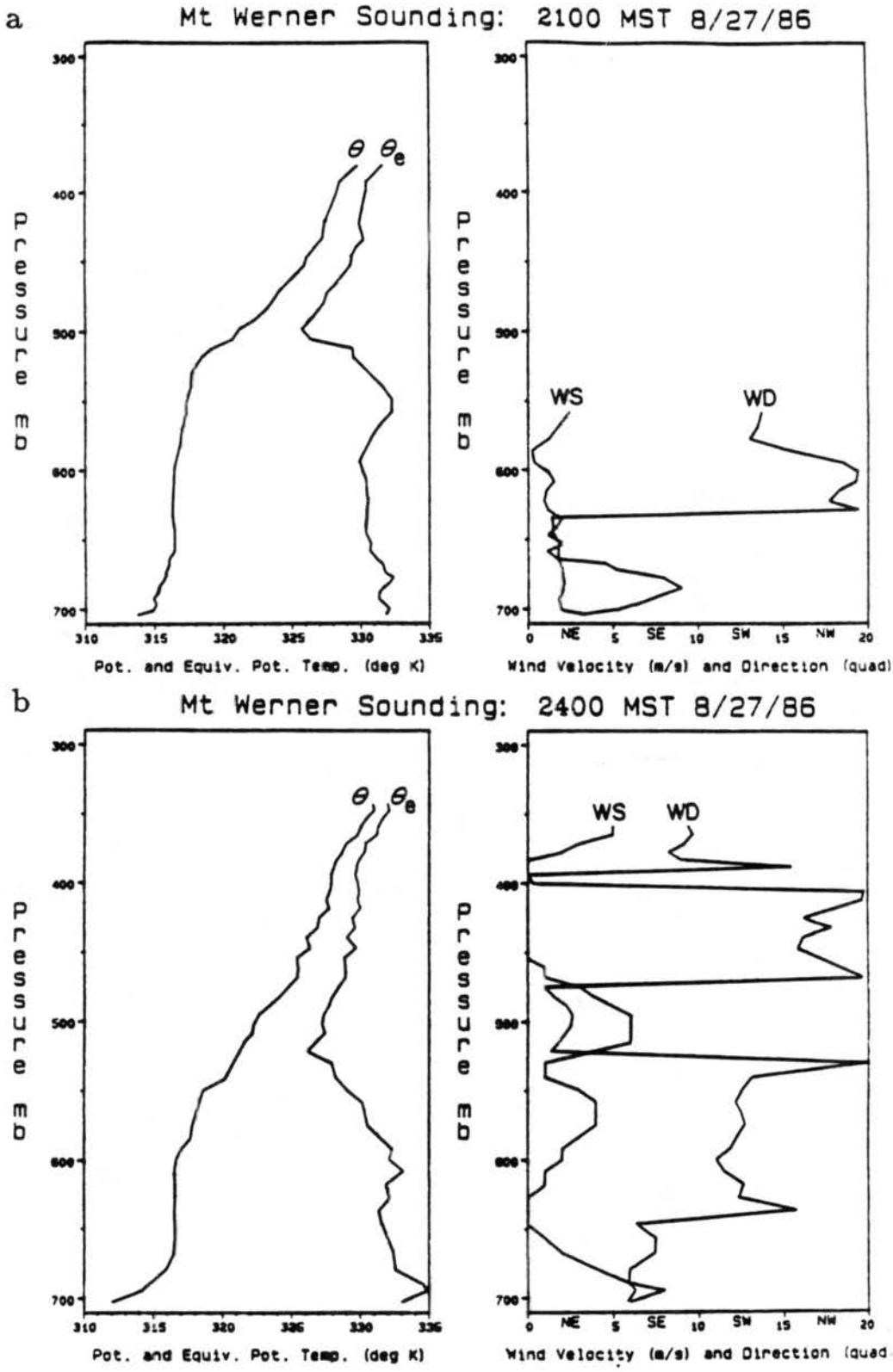

Figure 4.9: Vertical profile of θ, θ_e, wind speed, and wind direction at Mount Werner at (a) 2100 MST 27 Augsust 1986; (b) 2400 MST 27 August 1986; (c) 0300 MST 28 August 1986; (d) 0600 MST 28 August 1986.

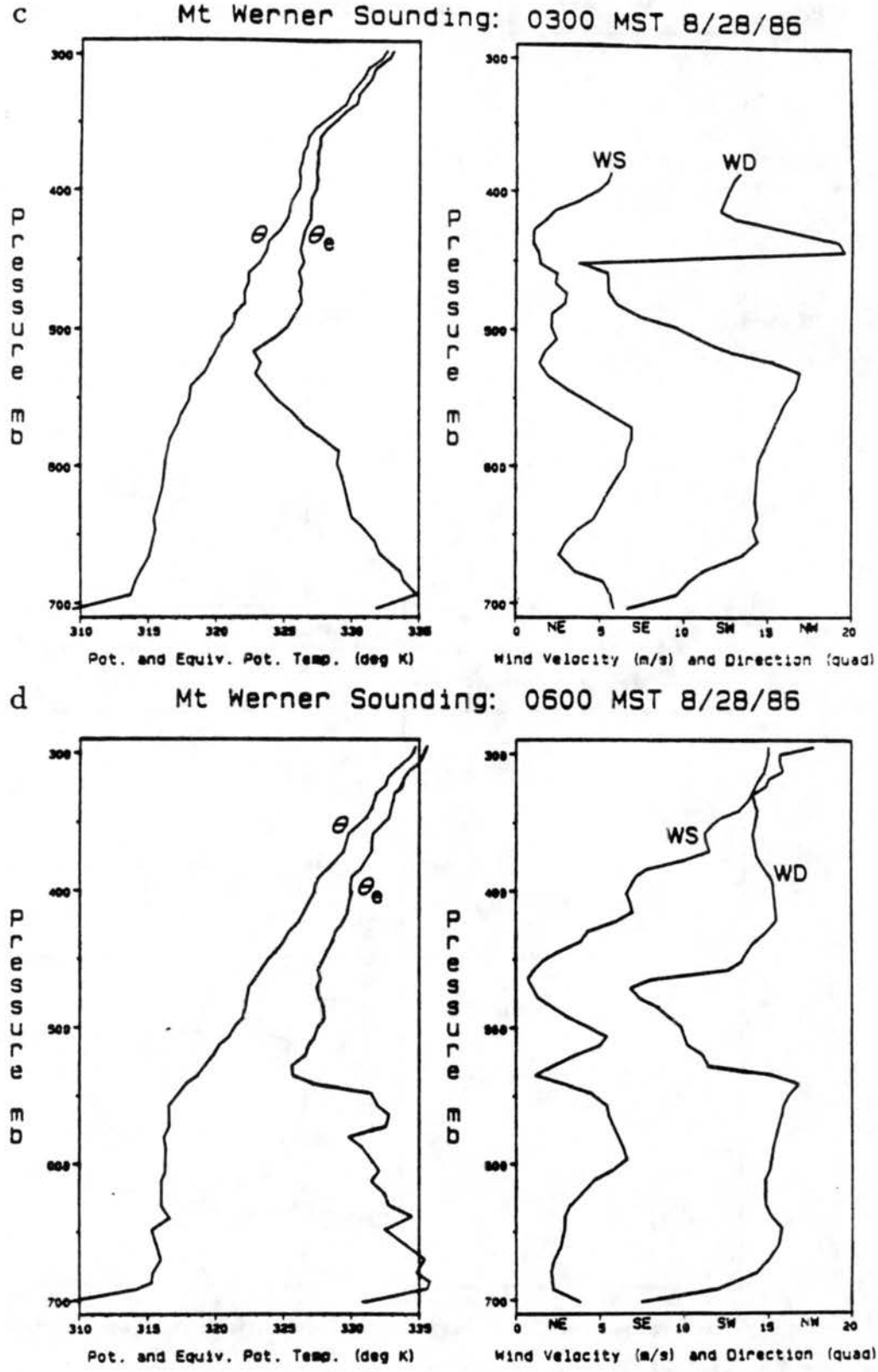

Figure 4.9: Continued.

fairly constant weak speeds near 3 ms^{-1} through a 200 m layer, before fading into ambient northwesterly flow. The thermal structure shows a complicated low-level stability consisting of a surface based inversion below a layer of weaker stability, within which the jet core is located. This low-level northeasterly jet was observed in a later sounding at 0000 MST 2 October (not shown) to rotate to a east-southeast direction with a similar shallow jet structure. Surface southeasterlies persisted until 0500 MST 2 October.

Several soundings have also been launched during nocturnal outflow wind events following strong convective activity. One such sounding, launched from the base of Mt. Werner near the town of Steamboat Springs at 2300 MST 22 August 1987, is shown in Fig. 4.11. This sounding shows the vertical structure through the valley atmosphere and above the surrounding peaks. The wind profile shows light and variable flow within the valley between 2010 and 2500 MSL. This layer is within the surface based inversion, noted by the distinct, very stable potential temperature profile. Above the surface inversion, southeasterly winds prevailed through a layer 1800 m deep, which has a nearly constant stable stratification of $0.3^{o}/100$ m, indicative of a homogeneous air mass. Southeasterly flow within this deep layer reaches a maximum speed of 8 ms^{-1} near ridgetop ($\sim$ 3150 MSL). Winds at MW had shifted abruptly from a northwesterly to southeasterly direction 6 hours before this sounding was launched (1700 MST), and were from the southeast at $\sim$ 6 ms^{-1} during the time of the sounding. This deep southeasterly layer stands in contrast to the previous soundings which show the nocturnal outflow winds to be confined to a shallow layer over the mountaintop. This gives some indication that the outflow layer may be significantly deeper in conditions with strong convective forcing.

4.5 Flow Climatology

Throughout this chapter reference has been made to the persistent nature of the diurnally reversing flow regime observed across the Colorado mountain barrier. Monthly diurnal wind averages taken at MW and SQ over four summer months during four different years (Fig. 4.12) reveal this regional-scale circulation system to be the climatological average summertime flow at these mountaintop sites. While significant month-to-month deviations

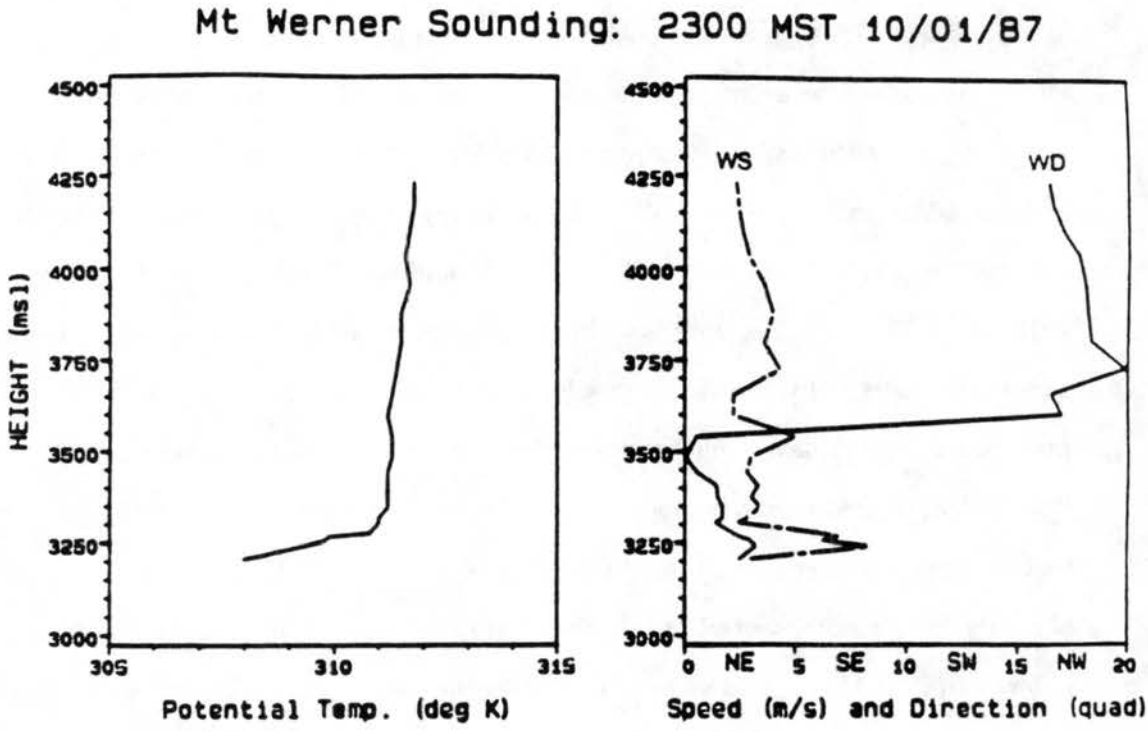

Figure 4.10: Vertical profile of θ, wind speed, and wind direction at Mount Werner on 2300 MST 1 October 1987.

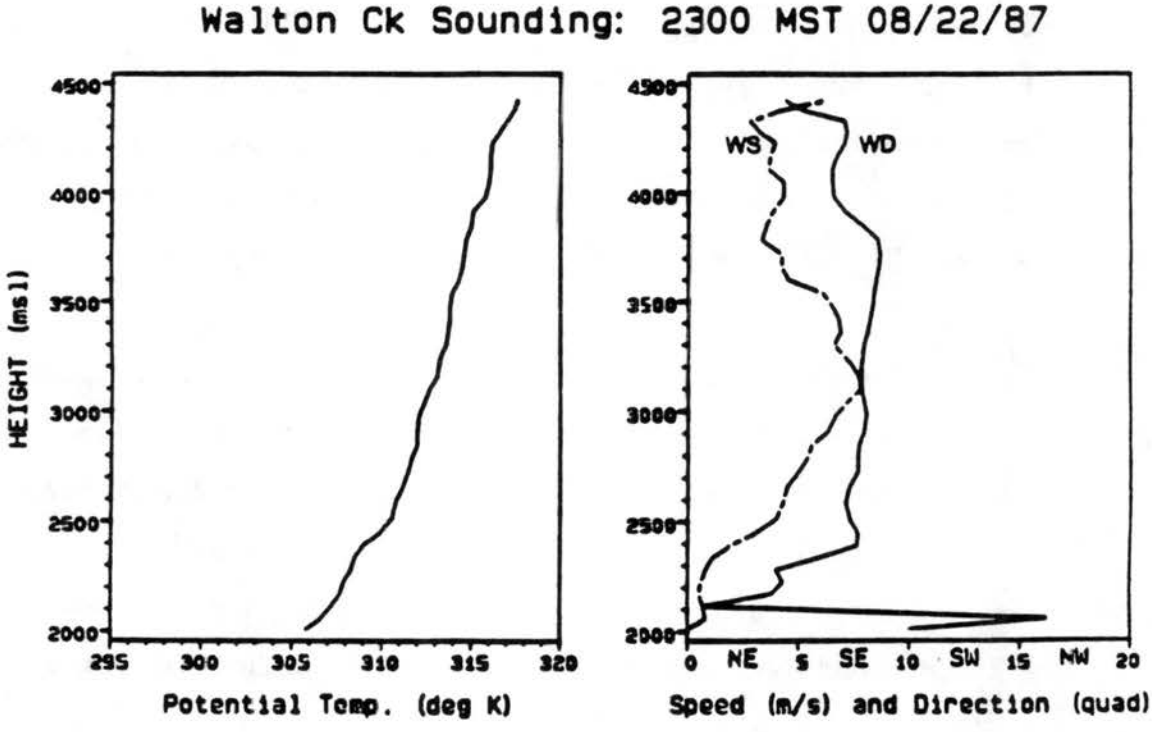

Figure 4.11: Vertical profile of θ, wind speed, and wind direction at Walton Creek on 2300 MST 22 August 1987.

exist in the transitional phases, in all months two dominant wind regimes occur at both stations.

At MW (Fig. 4.12a upper panel), steady daytime west-northwest upslope flow prevails from late morning until late afternoon/early evening when a transition period to south-easterly downslope flow occurs. The onset time and length of this transition period varies between the different months, beginning as early as 1700 MST (August 1986), but always occurring by 1900 MST (approximately local sunset), and lasting between 1 hour (July 1985) and 3 hours (August 1986), revealing the variation in onset time between individual days of the month. Steady nocturnal southeasterly flow follows the early evening transition at MW, lasting between 5 and 7 hours, after which a more gradual transition begins with a veering of the wind vector over a 6-8 hour period towards the northwesterly daytime inflow circulation.

The SQ station (Fig. 4.12a lower panel) also reveals a dominant diurnal circulation pattern, consisting of steady nighttime southwest-westerly downslope flow, which veers towards northerly flow following the onset of morning heating, and towards an easterly upslope direction by noon in all months except August 1986, when the averaged wind vector remains from a northwesterly direction during the early afternoon. In all other months, the wind vector continues its clockwise rotation in the early afternoon, showing a 3-4 hour period during which the flow has an upslope component. By late afternoon the winds quickly veer towards a westerly direction again, signaling the onset of the nocturnal downslope wind regime which persists at the station for an average of 12 hours.

Wind speed is also similar between the four months at each station (Fig. 4.12b). Both stations show a wind speed minimum during the morning transition period, after which a gradual increase in wind speed is noted throughout the afternoon inflow regime. Following a minor lull during the late afternoon/early evening flow transition, both stations begin a significant increase towards a maximum averaged speed near 5 ms^{-1} within the nocturnal downslope flow regime. The fairly light average wind speeds at both stations throughout the diurnal cycle demonstrates the lack of strong synoptic pressure gradients during the summer months, allowing the diurnal heating and cooling cycle, with superimposed effects from moist convective processes, to control the mountaintop wind climatology.

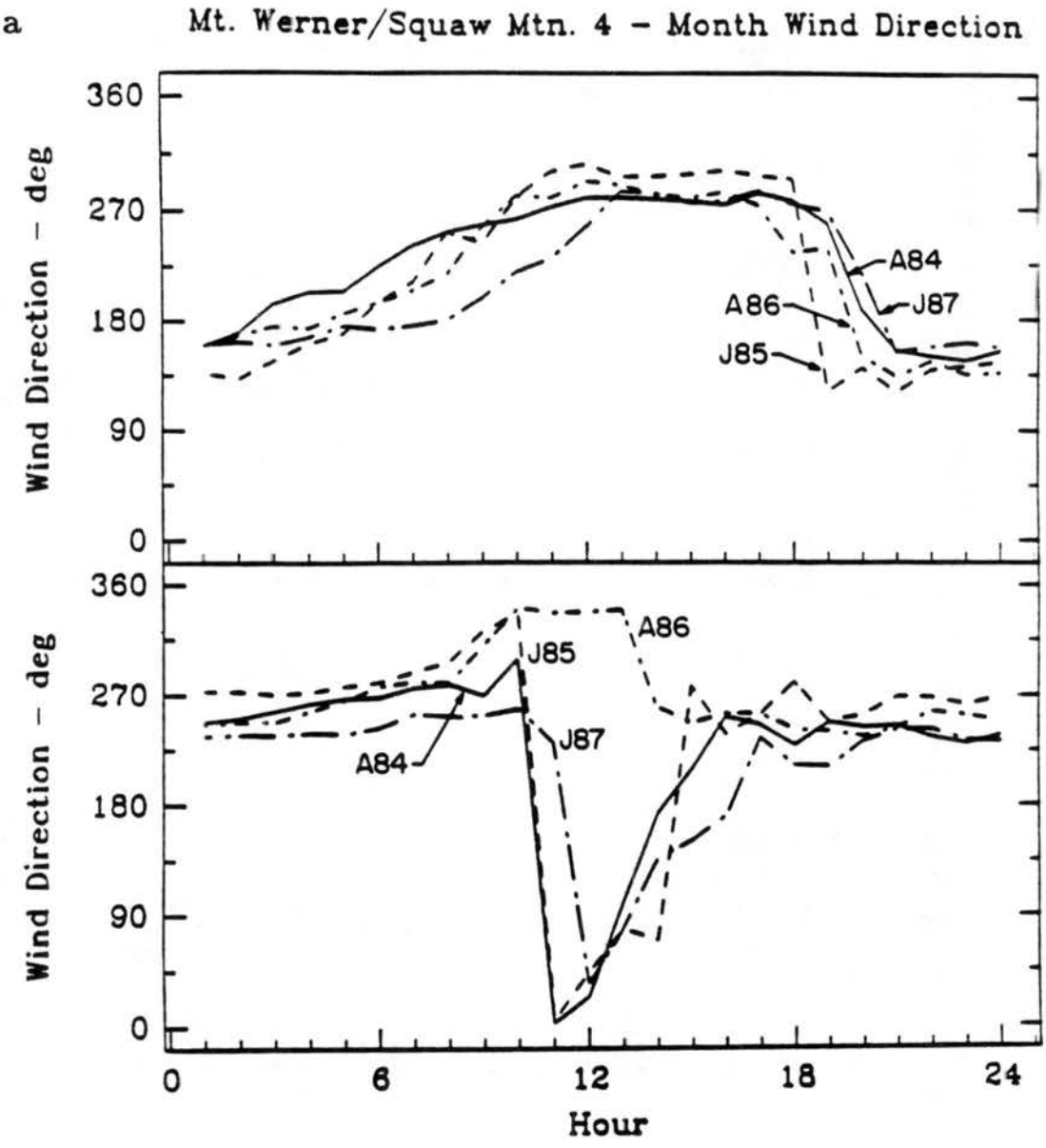

Figure 4.12: Hourly averages of (a) wind direction and (b) wind speed at Mount Werner and Squaw Mountain for the months of August 1984, July 1985, August 1986, July 1987.

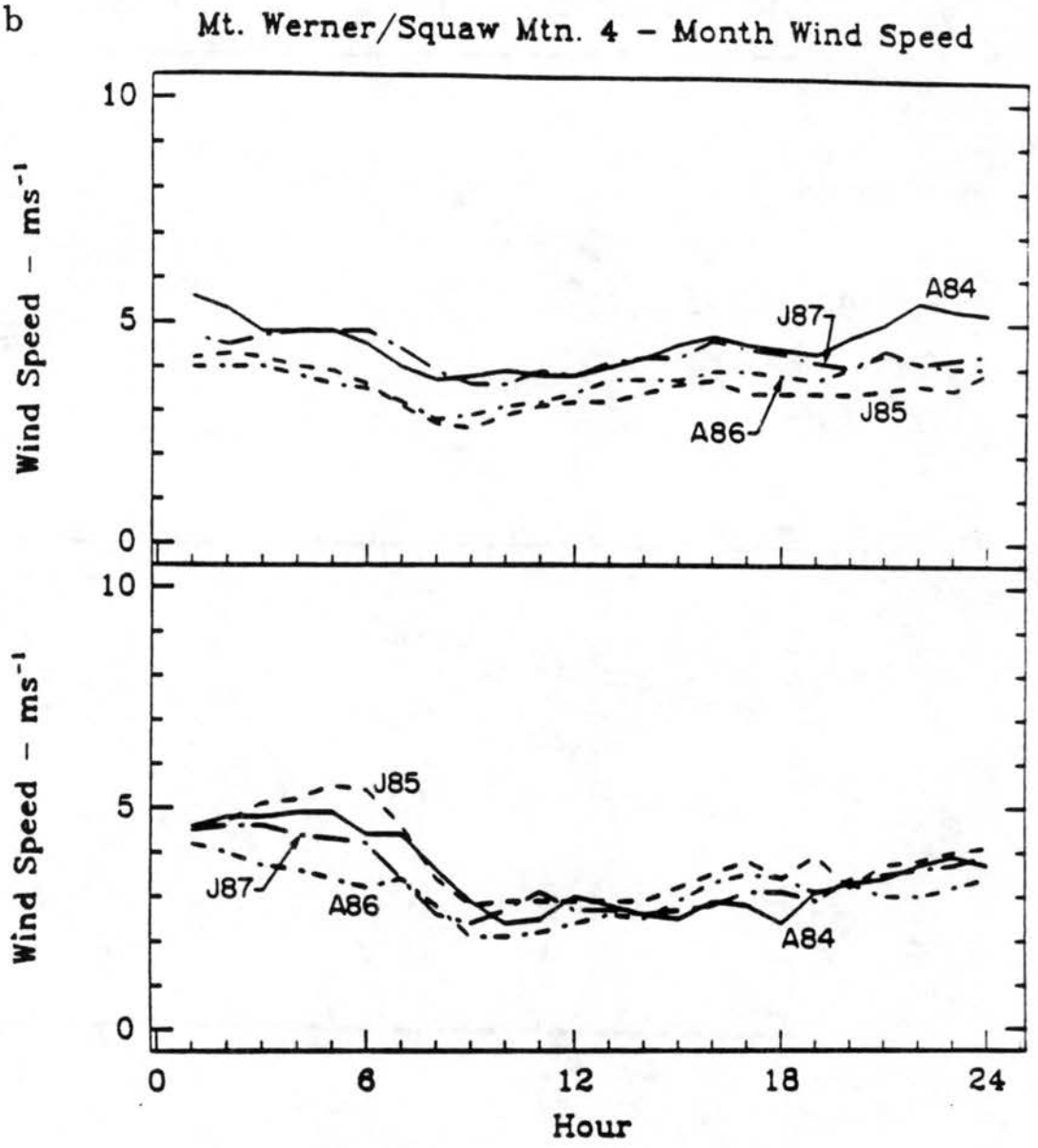

Figure 4.12: Continued.

Chapter 5

NUMERICAL SIMULATION OF REGIONAL-SCALE WINDS

In the previous chapter, observational data were presented which describe summertime wind circulations at mountaintop. These circulation systems were regarded as regional-scale flows, due to their coherent signature on meso-β to meso-α scales over the complex terrain of the Colorado mountains. Although many characteristics of these flows were elucidated from the observed data, further details cannot be resolved by the widespread but sparsely-spaced observing network. To gain insight into the physical processes driving the observed mountaintop flows requires additional resources. For this purpose, a numerical model has been incorporated into the study. The simulations will examine only the dry circulations, leaving the effects of clouds and precipitation on regional-scale flows for future research. Provided the model can realistically simulate the observed flows, the gridded output of the various fields will allow an investigation of regional-scale circulations with much higher resolution than the observations alone can provide. In addition, through various sensitivity experiments, we can attempt to isolate the important physical processes producing the observed flows. In the following section, a description of the CSU-RAMS mesoscale model is presented. An idealized, three-dimensional simulation is then analyzed, after which two-dimensional sensitivity experiments are examined.

5.1 Model Description

The CSU-RAMS mesoscale model is a highly flexible modeling system, capable of simulating a wide variety of mesoscale phenomena. This primitive equation model has evolved from the merger of a hydrostatic mesoscale model (Mahrer and Pielke 1977a), and a nonhydrostatic explicit cloud model (Tripoli and Cotton 1980). The basic structure of the model is described in Tripoli and Cotton (1982), Cotton *et al.* (1982), Tremback *et al.*

(1985), and Tripoli (1986). More recent model developments are described in Tremback *et al.* (1986), Cotton *et al.* (1988), Flatau *et al.* (1989), and Tremback (1990). Three model configurations are used in this study. All three feature a terrain-following vertical coordinate system (Clark 1977) and a non-hydrostatic form of the basic model equations. At the lower boundary, surface layer temperature and moisture fluxes are determined from the surface energy balance, which includes both longwave and shortwave radiative fluxes, latent and sensible heat fluxes, and heat conduction from the soil with an 11 level soil temperature model (Tremback and Kessler 1985). The parameterization of short- and longwave radiation (Chen and Cotton 1983) considers absorption, scattering, transmission, and emission from both clear and cloudy atmospheric layers. The simulations described here include moisture for its effect upon radiation, otherwise it is essentially a passive tracer within the model, with no condensation allowed to occur. Surface fluxes are based upon the parameterization of Louis (1979), which uses Monin-Obukhov similarity theory to describe the constant flux layer. Turbulence is parameterized using a Smagorinsky-type eddy viscosity including a Richardson number dependence. Boundary conditions, initial conditions, and grid sizes are specific to each of the three types of simulations to be shown and these will be discussed in later sections of this, and the following chapter.

5.1.1 Grid nesting

A two-way interactive grid nesting scheme following Clark and Farley (1984) is employed in all of the simulations. Grid nesting allows one to focus higher spatial and temporal resolution on desired regions within the model domain with greater computational efficiency. With one-way nesting the fine grid has no effect on the coarse grid model, because the fine grid uses only the coarse grid boundary conditions and feeds no information back to the coarse grid. With two-way interaction, the fine grid model results are averaged and fed back to the coarse grid model, which improves the boundary conditions for the fine grid model and changes the coarse grid model solutions. Two-way interactive grid nesting has been found to produce improved numerical solutions over one-way nesting (Phillips and Shukla 1973; Clark and Farley 1984).

In this study, grid nesting permits a high resolution simulation over the complex terrain of the central Rocky Mountains. Without grid nesting, an extremely large model domain would be required to adequately resolve important topography features. With grid nesting it is possible to retain a high resolution model, and still maintain coarser grids that encompass a region large enough to resolve important synoptic-scale and regional-scale information. In addition, higher resolution topography data can be incorporated into each finer model grid, which provides an increasingly realistic representation of the terrain forcing. Thermal forcing over realistic model topography is a critical component of this investigation.

5.1.2 Silhouette topography

In an effort to enhance the topographic representation within the CSU-RAMS, a silhouette averaging scheme was developed. In the real atmosphere, the flow must either go around or over a given mountain barrier. With long unbroken mountain chains, such as the Sierra Nevada or the Rocky Mountains, the flow will be forced over the mountain barrier. Thus, it is important to maintain the effective height of the barrier for accurate simulation of the flow response due to these effects. This problem has been recognized by several modeling groups, resulting in the development of various "silhouette" or "envelope" topography averaging schemes. For example, Wallace *et al.* (1983) found that an envelope averaging scheme in the ECMWF operational model reduced long-range forecast errors over mountainous terrain. Mesinger *et al.* (1988) used a silhouette type scheme to successfully simulate secondary storm development southeast of the Appalachians, which neither the National Meteorological Center's Limited Fine Mesh (LFM) nor the Nested Grid Model (NGM) were able to produce.

There are several important features of a silhouette averaging scheme which are different from regular topography averaging: 1) The preservation of barrier height is accomplished by adding mass to the actual topography. Regular averaging preserves mass at the expense of the maximum topography height. 2) In filtering the topography, many schemes, such as Fourier or pointwise, lower barrier heights while accomplishing the necessary smoothing. The silhouette averaging scheme achieves this smoothing while preserving the effective barrier height.

The silhouette averaging algorithm within the RAMS code provides for regular topography averaging and any permutation in between regular and silhouette averaging by use of a weighting factor. In addition, any desired amount of topography smoothing may be accomplished. This topographic averaging technique has been incorporated into this numerical investigation, primarily to improve the representation of the high mountains and their slopes which encompass much of the domain of interest over Colorado.

5.2 Thermal Forcing over the Central Rocky Mountains

In this section we examine the effects of terrain heating over the three-dimensional topography of the central Rocky Mountains, under conditions of zero ambient flow. This affords a realistic simulation of thermally-induced regional-scale flows, without additional complications from external forcing. This simulation will provide a "control" run for comparisons with an actual case day simulation in the following chapter. Important flow features revealed in this experiment will be further studied in the following section through two-dimensional simulations. Thus, a detailed discussion of the important processes forcing regional-scale circulations over the central Rocky Mountains is delayed until then.

5.2.1 Model initialization

The simulation described here is three-dimensional and uses two grids; a coarse grid with 28 km horizontal resolution, and a fine grid spacing of 7 km. Each grid includes topography data derived with a silhouette averaging scheme, at the given horizontal resolution. Figure 5.1 shows the geographical location of the topography used. The coarse grid (Fig. 5.1a) has 42 points in the x-direction and 34 in the y-direction, spanning 1148 km in the west-east direction from western Utah to western Kansas, and 924 km in the south-north direction from northern New Mexico to central Wyoming. The fine grid (Fig. 5.1b) consists of 58 points in the x-direction, spanning 400 km across the Colorado Rocky Mountain barrier, and 54 points in the y-direction, extending 370 km from southern Colorado to extreme southern Wyoming. The topographic representation over the fine grid resolves the major mountain ridges and valleys of the north-central Colorado region. A stretched vertical grid spacing is employed, which varies the vertical resolution from 100 m

near the surface to 500 m at 3.5 km and above. The model has 42 vertical levels, with the top at 17.15 km. Radiative lateral boundary conditions are employed following Klemp and Wilhelmson (1978a,b). The upper boundary condition consists of a Rayleigh friction layer through the top 10 vertical grid points below a rigid lid.

The model simulation uses a horizontally-homogeneous temperature initialization, based upon rawinsondes taken in summer at Grand Junction, Colorado during dry anticyclonic conditions. To isolate the wind field response resulting from terrain heating, the simulation is initialized with zero ambient flow. While not completely realistic, the initial state approximates atmospheric conditions that could be expected with a stagnant ridge of high pressure over the Rocky Mountain region. During these periods, weak upper-level flow occurs and atmospheric conditions are slowly varying, making horizontal homogeneity over the region an acceptable initial state. Figure 5.2 shows the initial sounding. The sounding exhibits decreasing stratification from the surface to 5 km. Above 5 km, the potential temperature shows a fairly constant stratification of $3 - 4°C$/km. The model run was started at 1200 UTC (0500 Mountain Standard Time (MST)) and a 24-hour diurnal cycle was simulated.

5.2.2 The daytime response to surface heating

The model simulation begins before sunrise and during this time surface cooling and weak downslope flows evolve. The onset of heating by 0700 MST quickly erodes the downslope winds and by 0900 MST upslope flows begin within a developing mixed layer over the terrain slopes, as shown in Fig. 5.3 for a cross-section at y = 59.5 km through the nested grid. After 7 hours of simulation time (1200 MST), thermal forcing from the surface creates a deep, well-mixed boundary layer (Fig. 5.4a). The turbulent heat transfer from the surface is controlled by the surface energy balance equation

$$Q^* = H_L + H_S + H_G \tag{5.1}$$

where Q^* is the net radiation, H_L the latent heat flux, H_S the sensible heat flux, and H_G the heat flux from the soil. In the simulation, sensible heat values of 320 to 400 Wm^{-2}

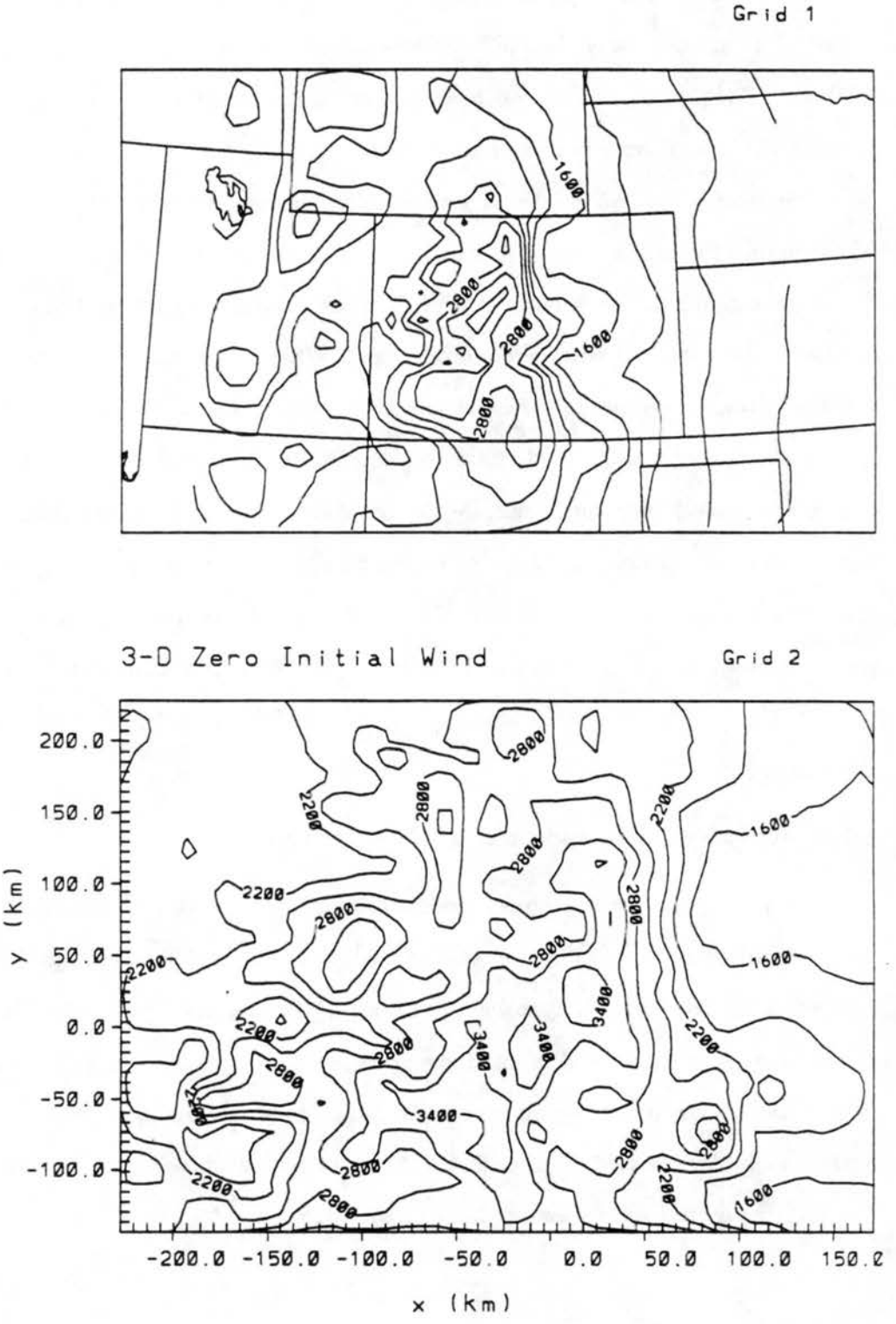

Figure 5.1: Topographic representations on Grids 1 and 2 for 3-D zero ambient flow case. Contour interval is 300 m.

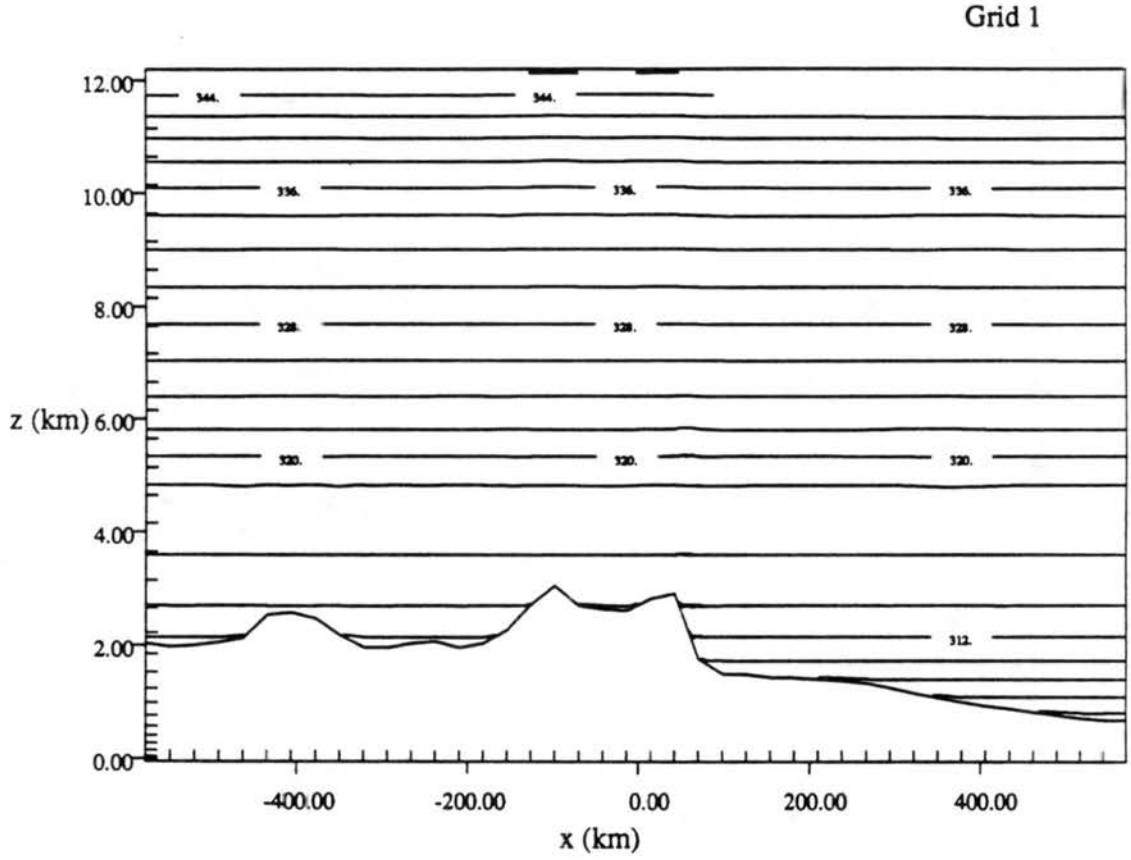

Figure 5.2: Initial potential temperature profile over the coarse grid topography. Contour interval is 2°C.

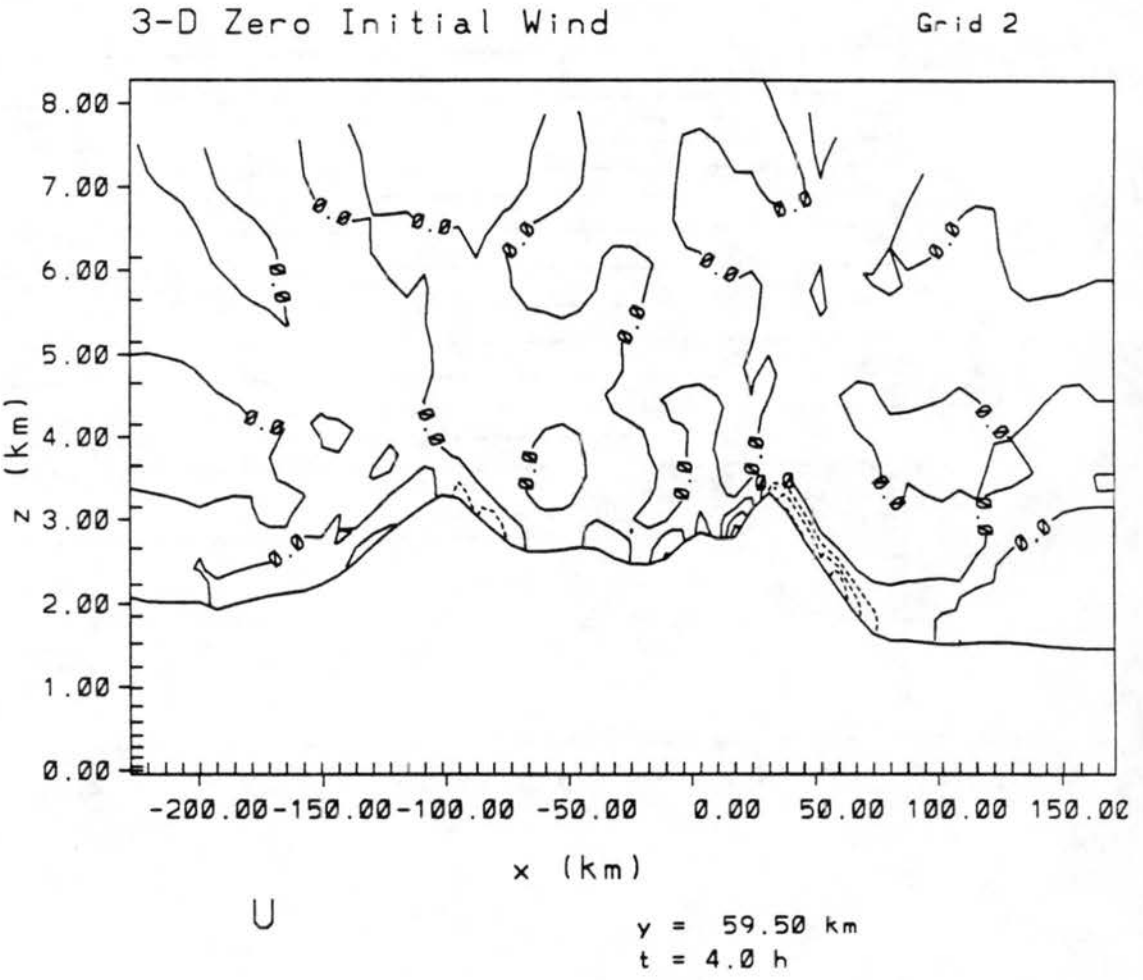

Figure 5.3: Simulated u-component wind profile after 4 hours. Contour interval is 1 ms^{-1}.

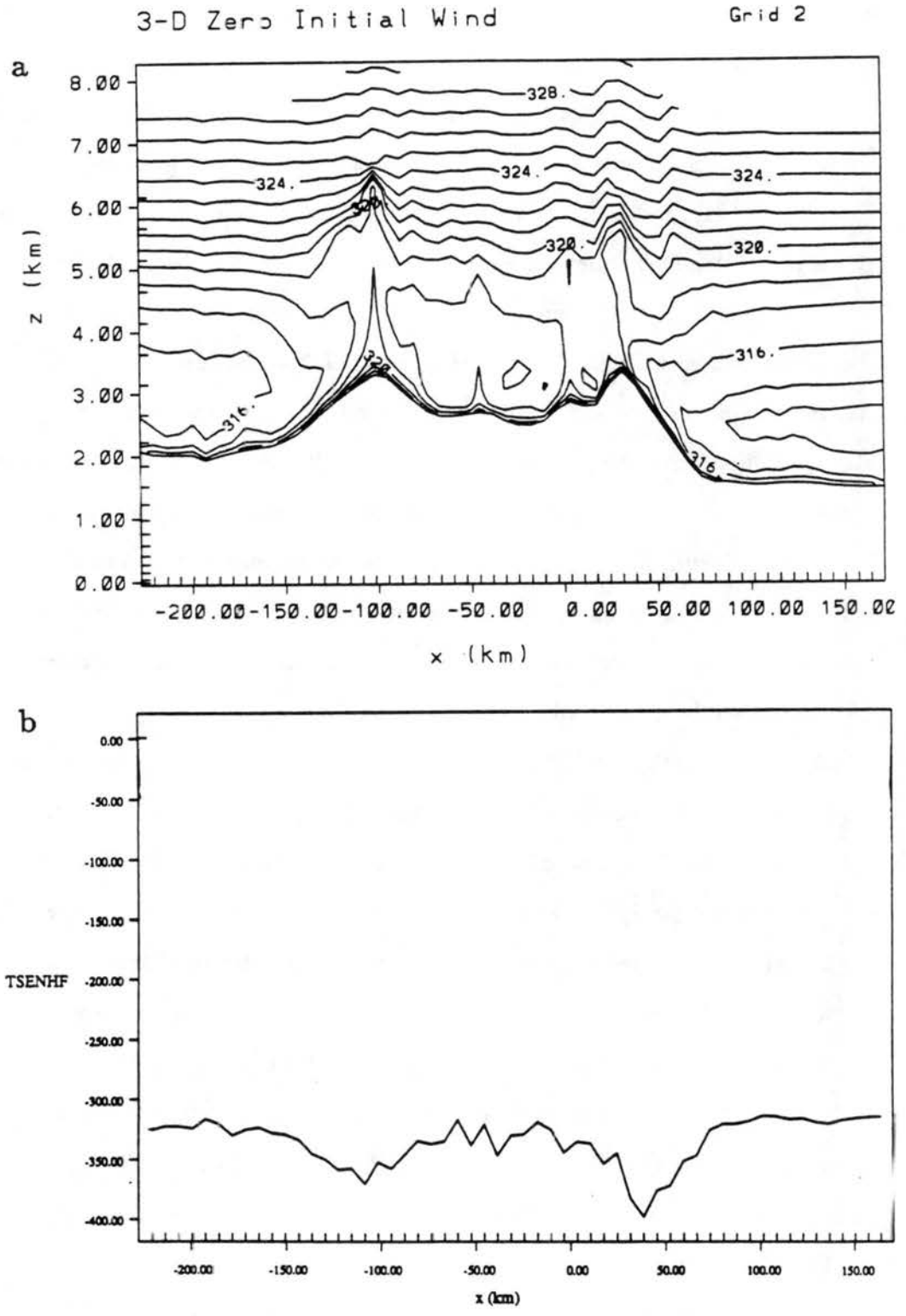

Figure 5.4: (a) Potential temperature profile in °C and (b) surface sensible heat flux in Wm^{-2} on Grid 2 after 7 hours of simulation time. Contour interval is 1°C. Mount Werner (MW) and Squaw Mountain (SQ) stations indicated.

are found across the fine grid domain at 1200 MST (Fig. 5.4b), with the highest values occurring along the east slope of the Front Range.

Latent fluxes (not shown) are much more variable across the fine grid, but are generally an order of magnitude weaker than the sensible fluxes. This gives Bowen Ratio values, $\beta = H_S/H_L \sim 10$, indicative of very dry conditions. Such conditions would be expected with a large, stagnant anticyclone over the region, of which this simulation is representative. Surface energy balance data from the ROMPEX experiments at several mountaintop sites are presented in Fig. 5.5a-c for the period of 23-31 August 1985. The figure shows that sensible fluxes typically dominate the latent fluxes by an order of magnitude in the afternoon, supporting the simulated results. In reality, the surface fluxes would be very inhomogeneous over this complex terrain region, due to variations in soil types and vegetation (Segal *et al.* 1989). However, in this simulation, no parameterization of vegetation exists, and the soil moisture is initialized throughout the 0.5 m depth of the soil model at 35% of its saturation value. Variations in soil moisture and their impact on the thermally-induced circulations will be considered in a later section.

Over the coarse grid at 1200 MST (Fig. 5.6), horizontal "inflow" toward the mountains is quite evident. The coarse grid uses averaged fine grid values over the region where the fine grid exists on the coarse grid. Thus, the topography and motion fields in the fine grid region look significantly noisier than the lower resolution values on the coarse grid. Since the fine grid covers the region of interest to this study, we will focus upon this area for further analysis of the regional circulations.

A plan view over a section of the fine grid at 278.8 m above the terrain surface at 1200 MST (Fig. 5.7a) shows that upslope flows are pronounced along the eastern slopes of the Front Range, near x = 50 km, and over the Park Range at x = -50 km, y = 100 to 150 km. The large, oval-shaped mountain region around x = -100 km, y = 50 km, known as the Flat Tops, also shows strong upslope flow development on all sides. A cross-section of the u-component winds at y = 59.5 km through the model domain (Fig. 5.7b), shows the vertical structure of the thermally-induced flows. The upslope circulations over the Flat Tops at x = -100 km and the Front Range at x = 30 km are over 1 km deep at this time. Maximum speeds include an easterly component of -12 ms^{-1} over the top of

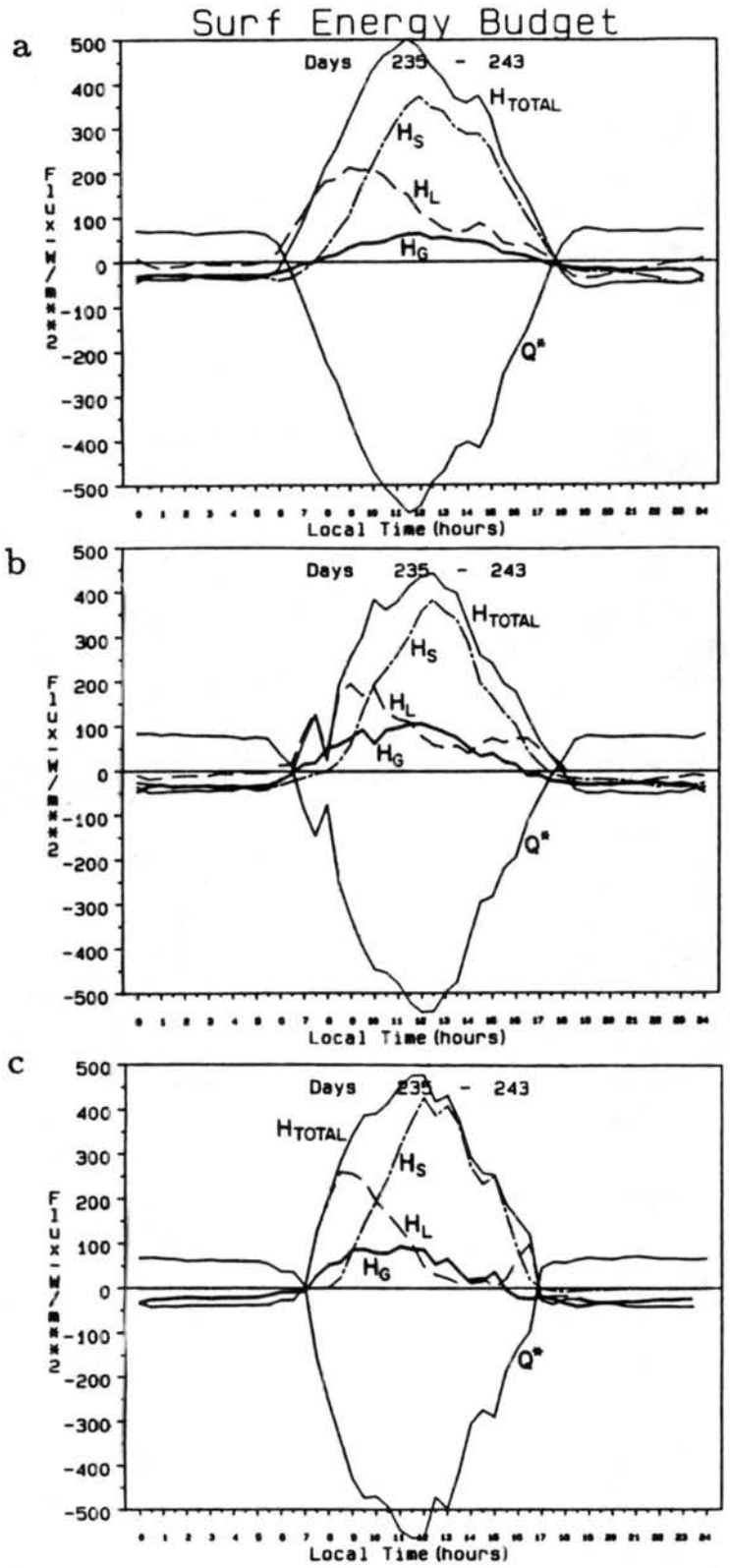

Figure 5.5: Surface energy budget data for (a) Mount Werner (b) Flat Tops and (c) Crested Butte (See text for description of terms).

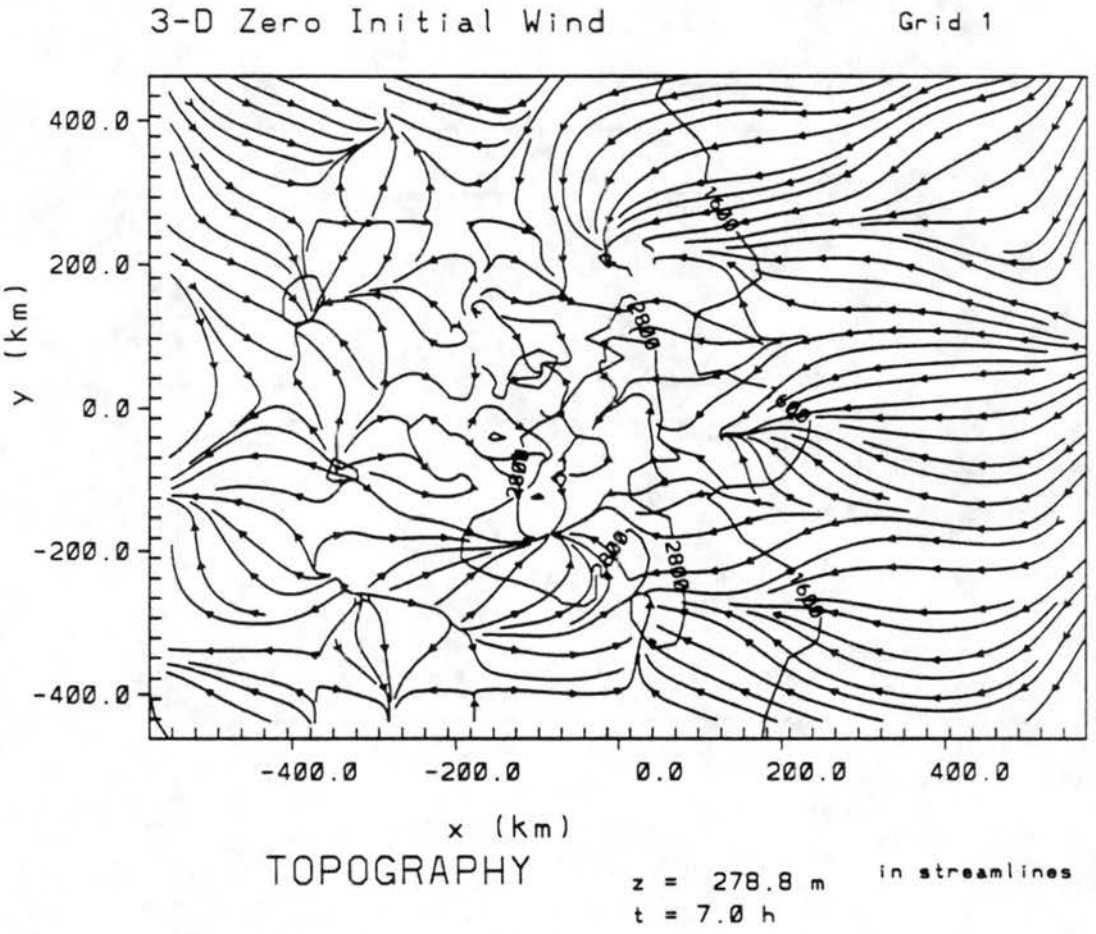

Figure 5.6: Flow streamlines at 278.8 m above the surface on Grid 1 after 7 hours of simulation time.

the Front Range, with a maximum westerly component of 11 ms^{-1} at the western base of the Front Range. Smaller slopes within the inter-mountain region also show evidence of weaker and shallower slope circulations. Over both the Front and Flat Tops Ranges, the slope circulations are the low-level component of a much deeper mountain-plain solenoid. This solenoid penetrates to 3 km above ground level (AGL), with well-developed, divergent, return circulations evident above the upslope flows. Strong ascending motion is associated with the vertical branch of these mountain-plain solenoids (Fig. 5.7c), up to 2.4 ms^{-1} over the Flat Tops. The simulated mountain-plains circulation system closely resembles observational and theoretical descriptions of mesoscale thermally-induced solenoids given by Burger and Ekhart (1937), Defant (1951), Orville (1968), Dirks (1969), Tyson and Preston-Whyte (1972), Simpson *et al.* (1977), Barry (1981), and Atkinson (1981), among others.

5.2.3 Afternoon flow characteristics

By 1400 MST, the circulations over the slopes reach their maximum intensity, after which they undergo a decay phase covering the next several hours toward sunset. Since the decay of the upslope circulations is of particular importance in understanding the transition between daytime upslope and nocturnal downslope, this period will be described next in more detail.

For this analysis, we focus on the convergent upslope circulation which developed over the Front Range, as shown in Fig. 5.7. Again, a horizontal cross-section through y = 59.5 km is used, however, only the region from x = -24.5 km to x = + 87.5 km is shown to present a clearer picture of the flow evolution. The atmospheric structure over the Front Range at 1400 MST is shown in Fig. 5.8. The easterly upslope flow (Fig. 5.8a) is more than 1000 m deep over the barrier crest, extending well out onto the surrounding plains and reaching a maximum speed in excess of -14 ms^{-1} approximately 200 m above the barrier. Curiously, the east slope solenoid now extends west of the Front Range crest by 7 km, invading the opposing westerly upslope flow which prevailed there at 1200 MST (see Fig. 5.7a) and creating strong low-level convergence west of the barrier crest.

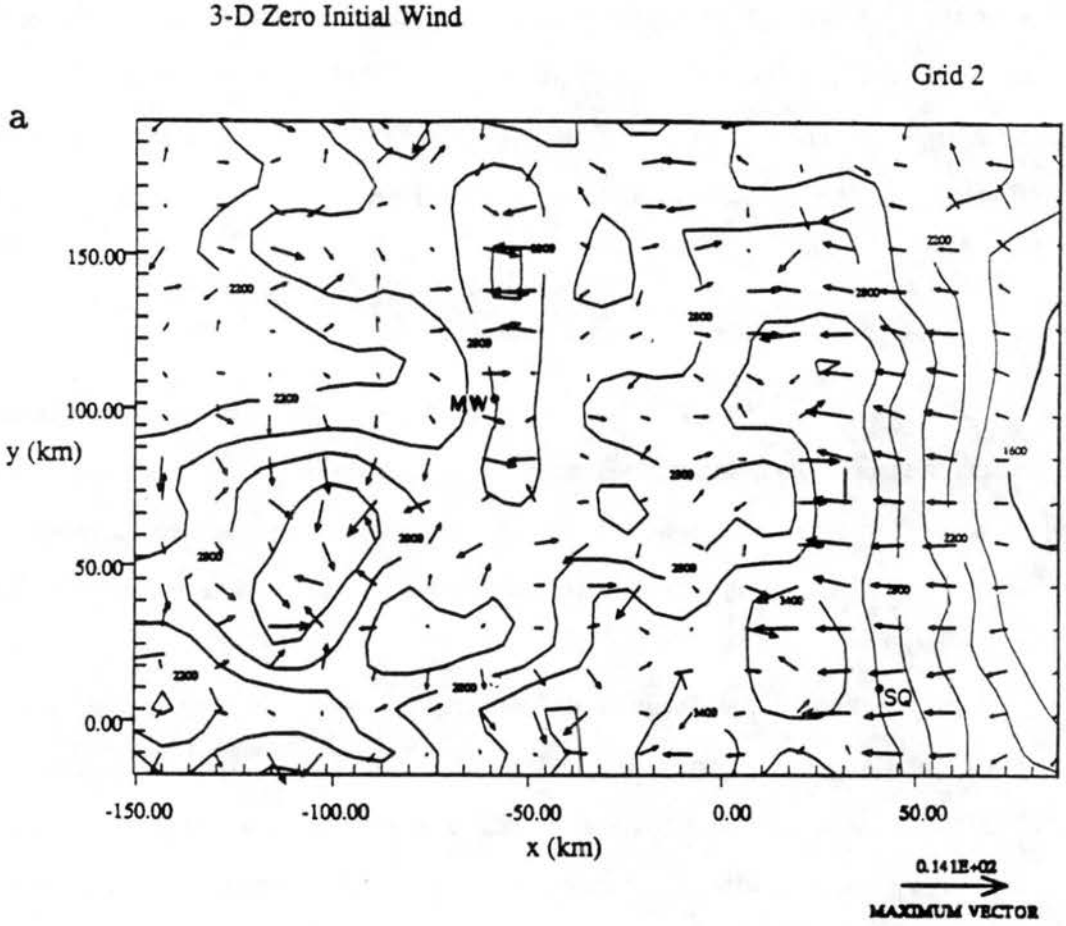

Figure 5.7: Simulated (a) flow streamlines at 278.8 m above the surface, with the Mount Werner (MW) and Squaw Mountain (SQ) stations indicated; (b) u-component velocity with 1 ms^{-1} contour interval, and (c) w-component velocity with 0.2 ms^{-1} contour interval on Grid 2 after 7 hours.

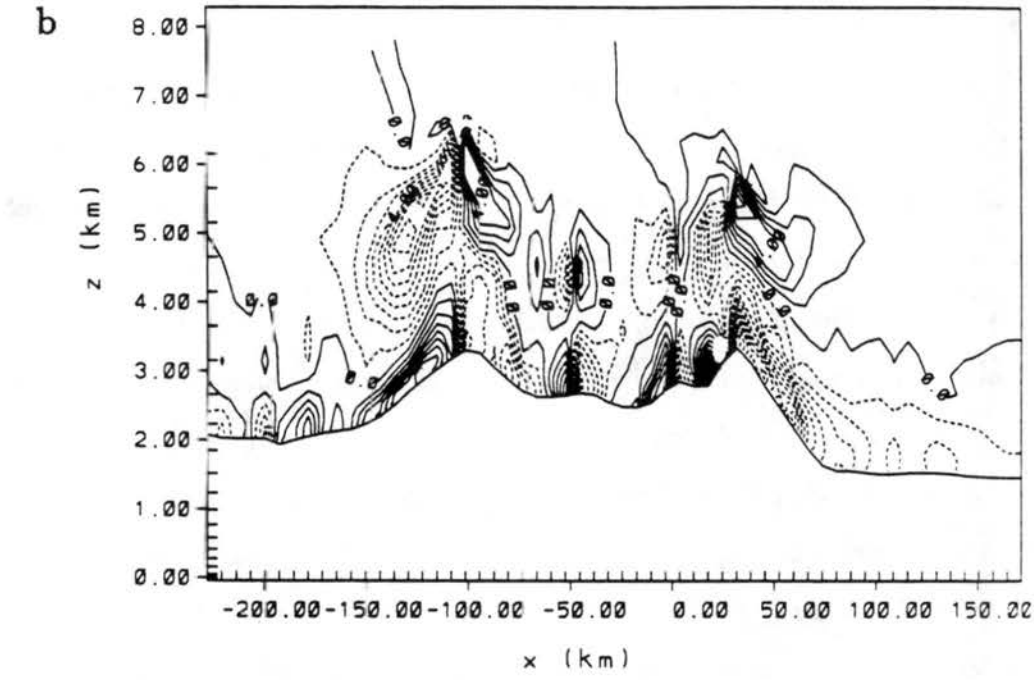

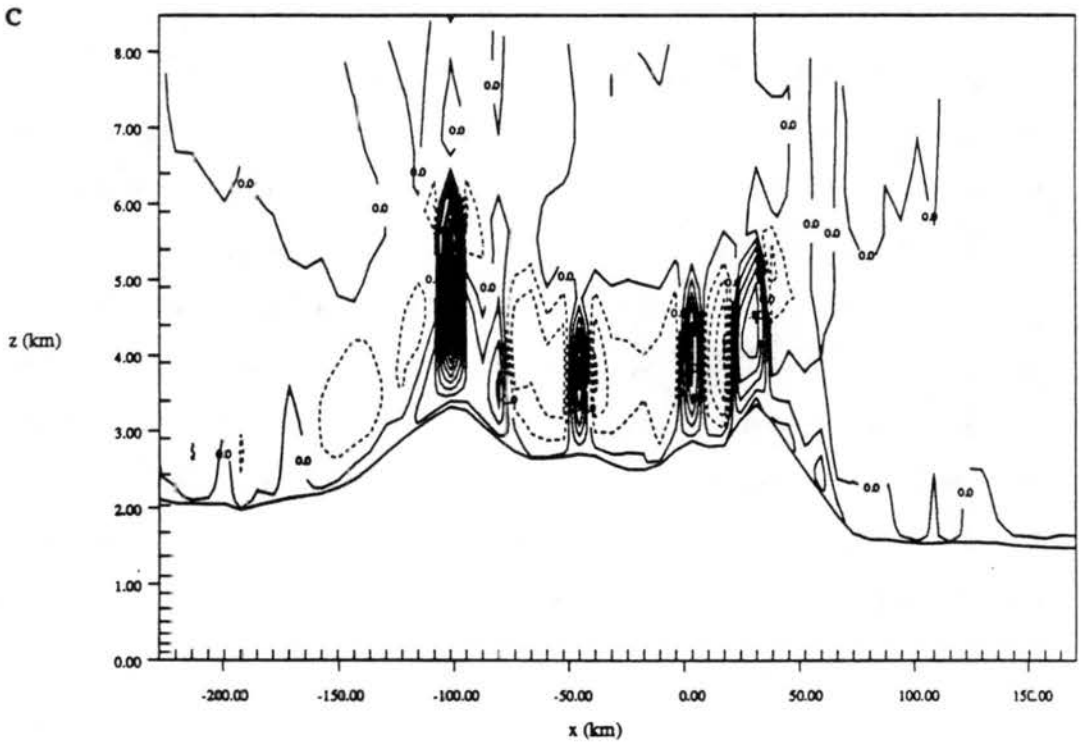

Figure 5.7: Continued.

Ascending motion is found throughout the low-level easterly upslope circulation along the Front Range (Fig. 5.8b), induced by superadiabatic lapse rates that exist within the boundary layer (Fig. 5.8c), from the intense surface heating. This surface heating produces lower pressure near the mountain surface relative to air parcels located in the unheated air some horizontal distance away (Fig. 5.8d). The resulting horizontal pressure gradient force toward the slope constrains the rising parcels to reside within the upslope layer, where they are advected up the slope. Eventually these parcels are ejected from the upslope layer through the vertical branch of the mountain-plains solenoid and carried downstream within the westerly return circulation located near the top of the mixed layer.

A belt of high pressure is evident at the top of the boundary layer over the domain (Fig. 5.8d), which develops to compensate for relative low pressure near the surface, driven by thermal heating. Relative high pressure just west of the barrier crest is due to the vertical mass flux associated with the ascending branch of the mountain-plains circulation. Compensating subsidence currents are found to the east and west of the ascending branch of the circulation, producing adiabatic warming and relatively low pressure on each side of the ascending branch. The divergent flow at the top of the ascending branch compensates for the strong convergent flow within the low-levels, redistributing the accumulated mass and completing the thermally-driven solenoid between mountain and plain.

The three-dimensional aspects of the circulation can be seen in the v-component velocity (Fig. 5.8e) which reveals that weak southerly flow has developed along the eastern slope near the crest of the Front Range, in response primarily to Coriolis turning of the parcels within the mountain-plains circulation system. Similarly, weak northerly flow appears with the low-level westerly upslope current west of the Front Range. This low level cyclonic circulation tendency is matched near the top of the boundary layer by compensating anticyclonic flow and is similar to the circulation discussed by Tripoli and Cotton (1989a,b).

Over the following two hours (1600 MST), the Front Range mountain-plains solenoid continues to advance westward an additional 28 km (Fig. 5.9a), which gives a slow rate of advance of 3.9 ms^{-1}. This flow behavior is a very intriguing and highly unexpected result. With this westward movement, the -14.2 ms^{-1} easterly flow has eliminated the

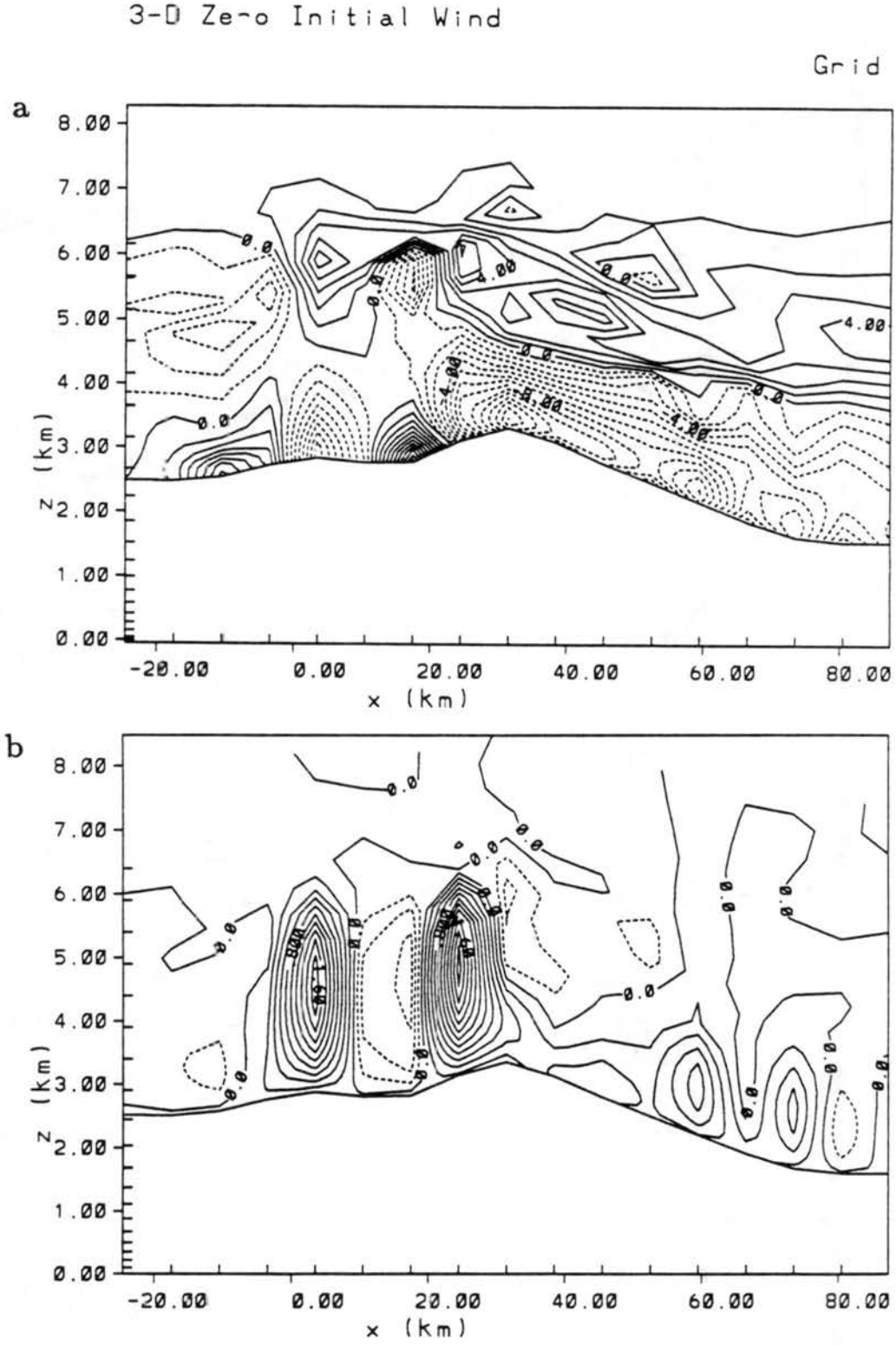

Figure 5.8: Vertical profiles of (a) u-component with 1.0 ms^{-1} contour interval, (b) w-component with 0.2 ms^{-1} contour interval, (c) potential temperature with 0.5°C contour interval, (d) perturbation pressure with 0.1 kPa contour interval, and (e) v-component with 1.0 ms^{-1} contour interval, on Grid 2 after 9 hours of simulation time.

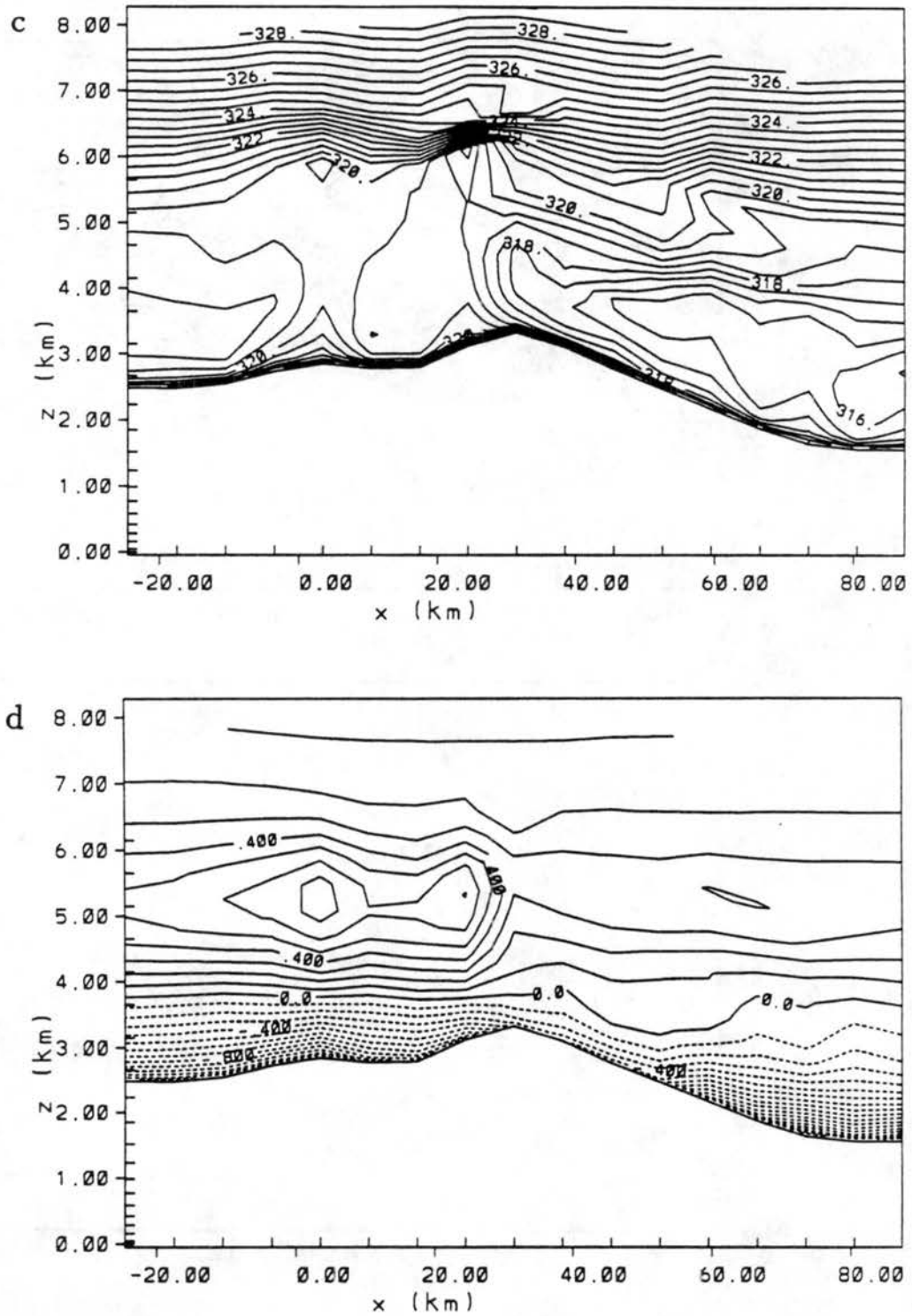

Figure 5.8: Continued.

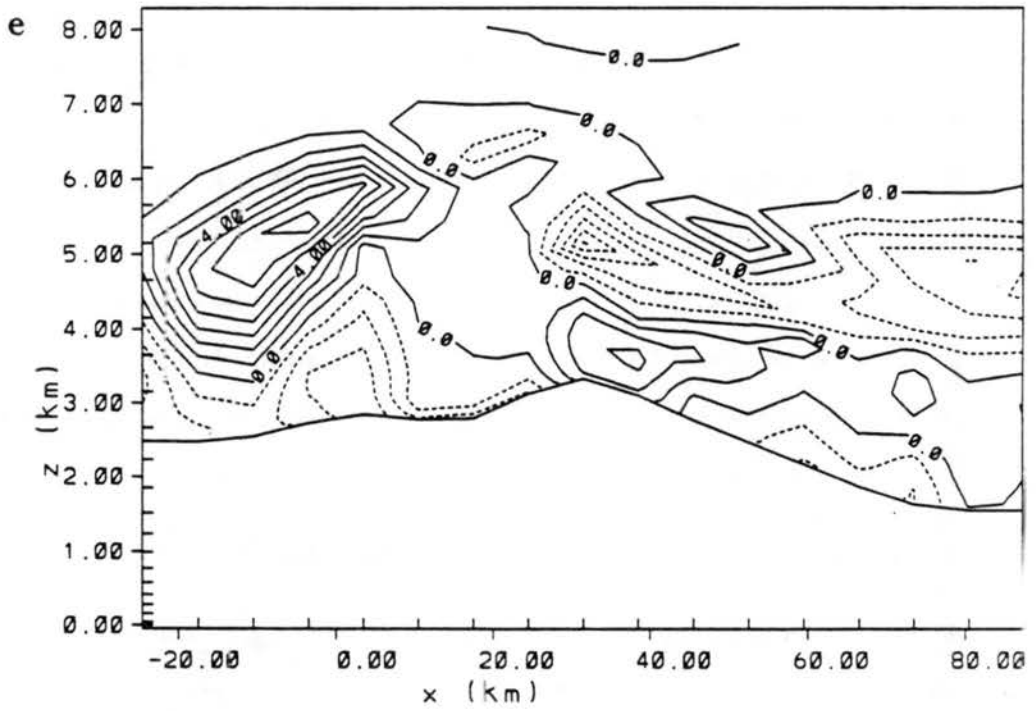

Figure 5.8: Continued.

opposing westerly upslope which was apparent in Fig. 5.8a. Coriolis turning of the flow trapped within the low-level branch of the solenoidal circulation has further increased the v-component velocity, producing southerly winds up to 6.1 ms^{-1} 500 m above the barrier crest (Fig. 5.9b). The vertical branch of the solenoidal circulation is now located at x = -3.5 km (Fig. 5.9c). The ascending branch is similar in magnitude to that shown two hours earlier, while an extensive region of subsidence is now located over the western slope of the Front Range, associated with descending motion as easterly flow surges over the barrier crest and down the western slope. Ascending motion is still evident within the remnant upslope circulation along the eastern slope.

The potential temperature field at 1600 MST (Fig. 5.9d) shows that cooler air from the eastern slope is surging over the Front Range crest. This cooler air mass is well-mixed up to a height of 500 m above the barrier crest, and is capped by a very stable layer associated with prolonged subsidence warming within the return circulation of the mountain-plains solenoid. Adiabatic cooling of the eastern slope air, which has ascended over 2 km from the plains, is forced over the barrier and induces a strong horizontal pressure gradient (Fig. 5.9e). Relatively high pressure therefore resides east of the barrier crest and lower pressure west of the crest within the warmer air of the elevated intermountain region.

5.2.4 The cessation of heating and nocturnal flow evolution

Over the course of the late afternoon, surface heating decreases as insolation values steeply decline toward sunset. The deep daytime mountain-plains circulation over the Front Range collapses with the lack of surface forcing, transforming into a more shallow easterly current which continues to propagate westward into the nocturnal period. The analyses in this section follow this transforming flow from its origins over the Front Range into its nocturnal phase over the western slope.

While in the previous section we examined the regional-scale flow structure via two-dimensional cross-sections, these circulations are three-dimensional in nature, extending over a widespread portion of northern Colorado. This is demonstrated with a plan view of the region at 1800 MST (Fig. 5.10), which shows the winds at 278.8 m, with the east slope flow surging westward across the inter-mountain region. Strong east to southeast winds are

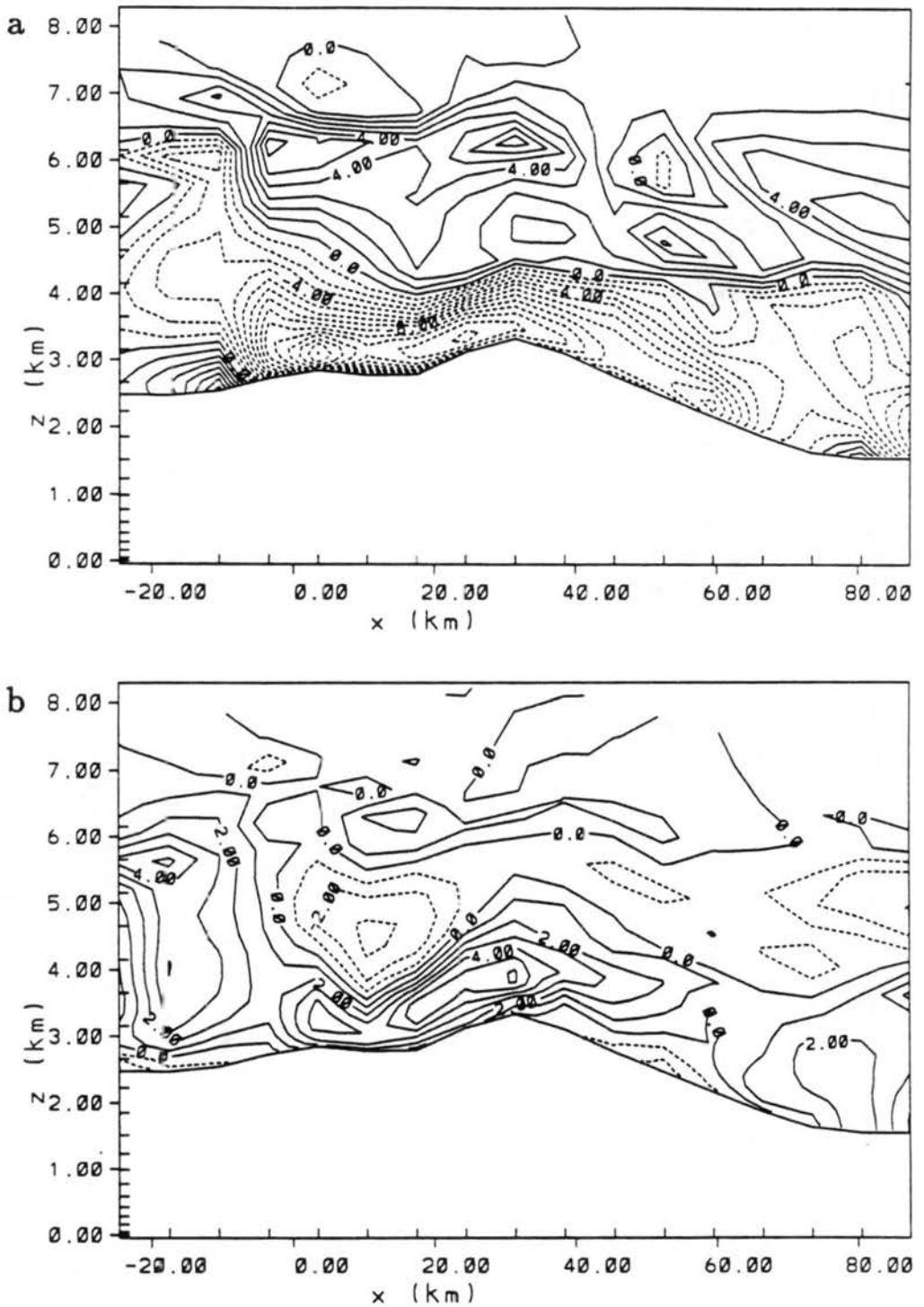

Figure 5.9: As in Fig. 5.8 only for (a) u-component, (b) v-component, (c) w-component, (d) potential temperature, (e) perturbation pressure after 11 hours of simulation time.

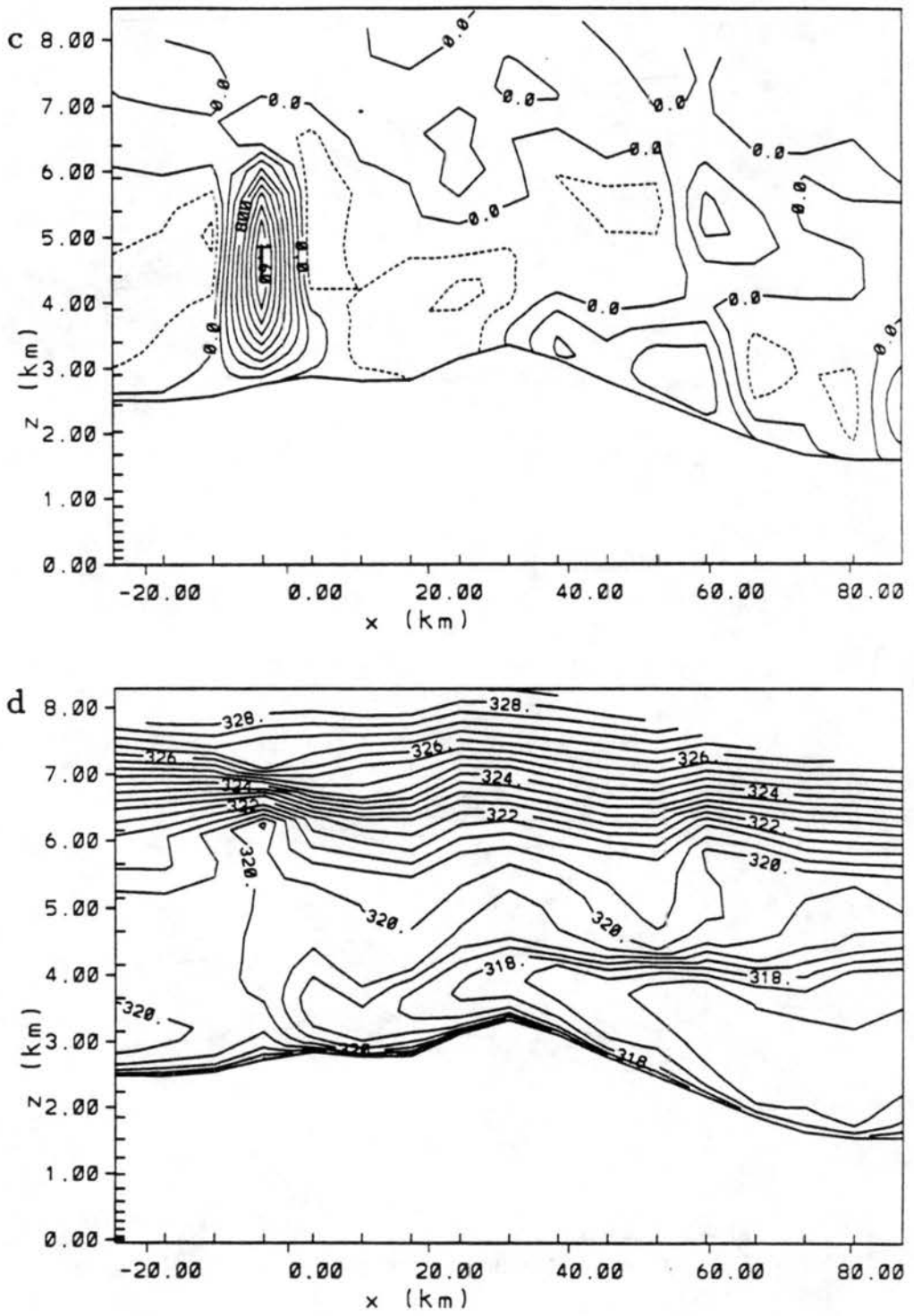

Figure 5.9: Continued.

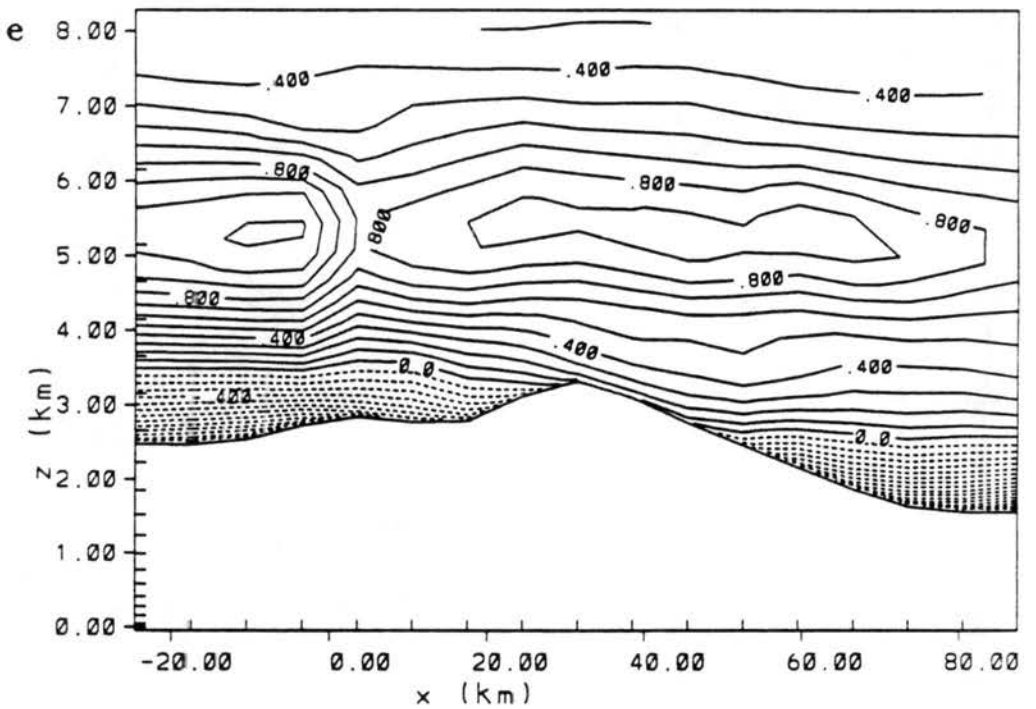

Figure 5.9: Continued.

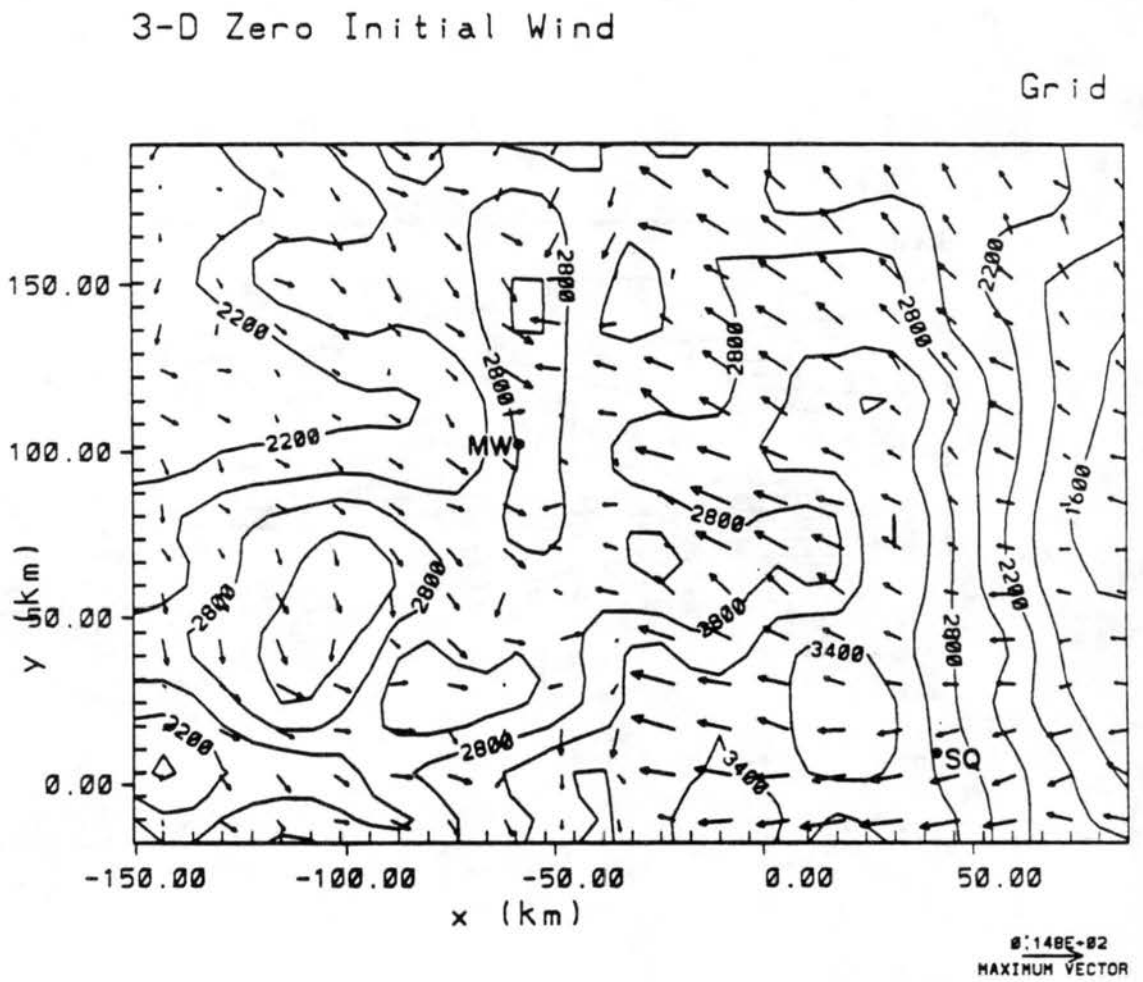

Figure 5.10: Wind vectors at 278.8 m above the surface on Grid 2 after 13 hours of simulation time. Mount Werner (MW) and Squaw Mountain (SQ) stations indicated.

apparent over the high mountain terrain between x = 0 and x = -50 km, signifying the core of the surging flow. In contrast, winds over the low basins within the inter-mountain region at x = -35 km and y = 70 km and y = 150 km are weak and variable. Over the western mountains and plains generally northwesterly flow prevails, characteristic of the continuing daytime wind circulation in this region.

With the onset of surface cooling by 1800 MST, the decaying solenoidal circulation begins to advance rapidly westward (Fig. 5.11), as denoted by the 320°C isentrope. By this time the circulation has collapsed into a shallow ($\sim$ 500 m) current which invades the well-mixed air within the intermountain region. A similar cool current, though weaker, can be seen moving eastward down the eastern slope of the Flat Tops.

Over the next two hours, the low-level easterly flow from the Front Range continues its westward propagation within the intermountain region as a coherent shallow density current-like feature, so that by 2000 MST the leading edge of the current has propagated 80 - 90 km west of the Front Range crest (Fig. 5.12). The flow within the current rotates towards a southeasterly direction in response to Coriolis turning. Northwesterly flow still predominates over the western slope of the intermountain region. This plot approximately corresponds to nightfall over the domain, and consequently the upslope flows are diminishing rapidly, as can be seen, for example, over the eastern slope of the Front Range. The highest flow speed of 17.3 ms^{-1} is located within the southeasterlies near x = -50 km, y = 30 km indicating an acceleration of the flow as it propagates down the western slope.

An x-z cross-section through y = + 108.5 km provides an additional perspective on the circulation across the high terrain at 2000 MST (Fig. 5.13). This cross-section slices through the Yampa River Valley in western Colorado, the Park Range at the latitude of the Mt. Werner ROMPEX station (MW in Fig. 3.10), the northern edge of the Rabbit Ears Range, and finally over the Front Range and eastern slope. The figure shows that by this time the low-level current has propagated the length of the inter-mountain region through this cross-section and is now surging down the slope of the Park Range into the Yampa River valley. Over the inter-mountain region, the core of the flow is shallow at $\sim$500 m, but reaches depths of 1300 m over the crests of the Front and Park Ranges. The easterly flow behind the surge steadily increases in velocity down the gradual slope of the

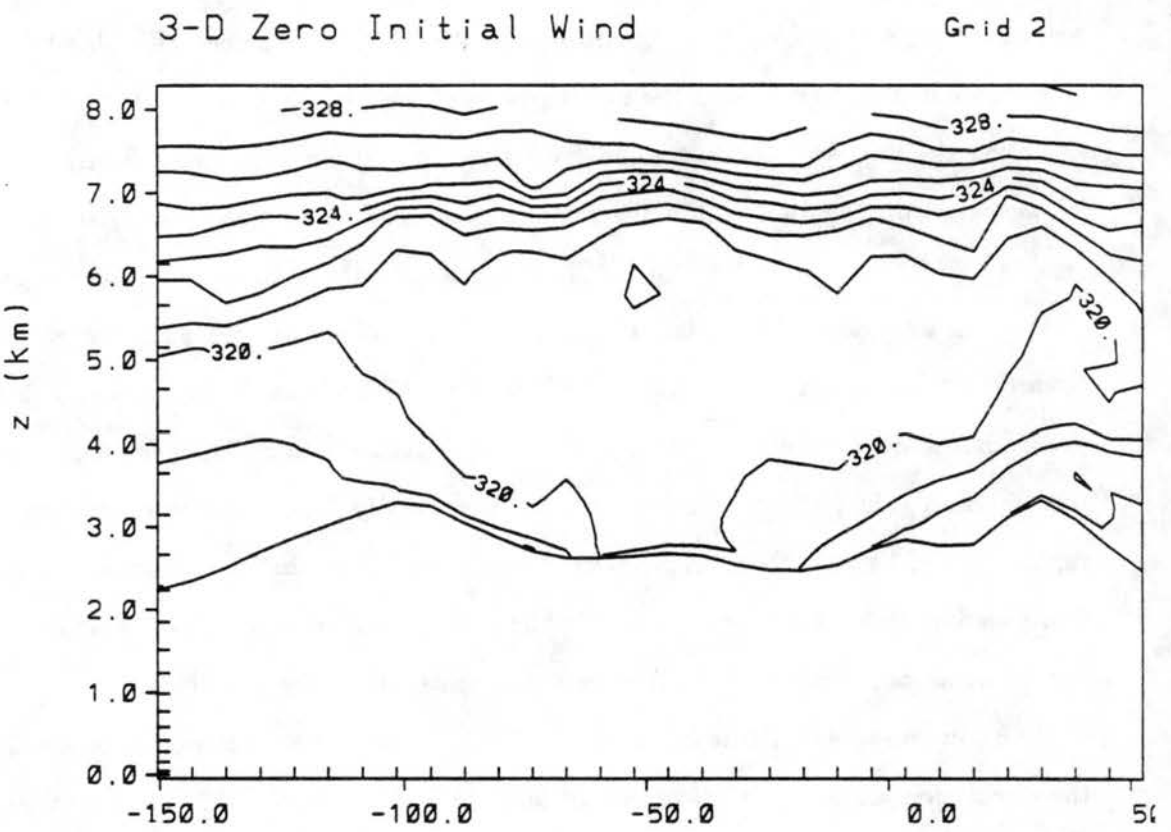

Figure 5.11: Vertical profile of potential temperature on Grid 2 after 13 hours of simulation time.

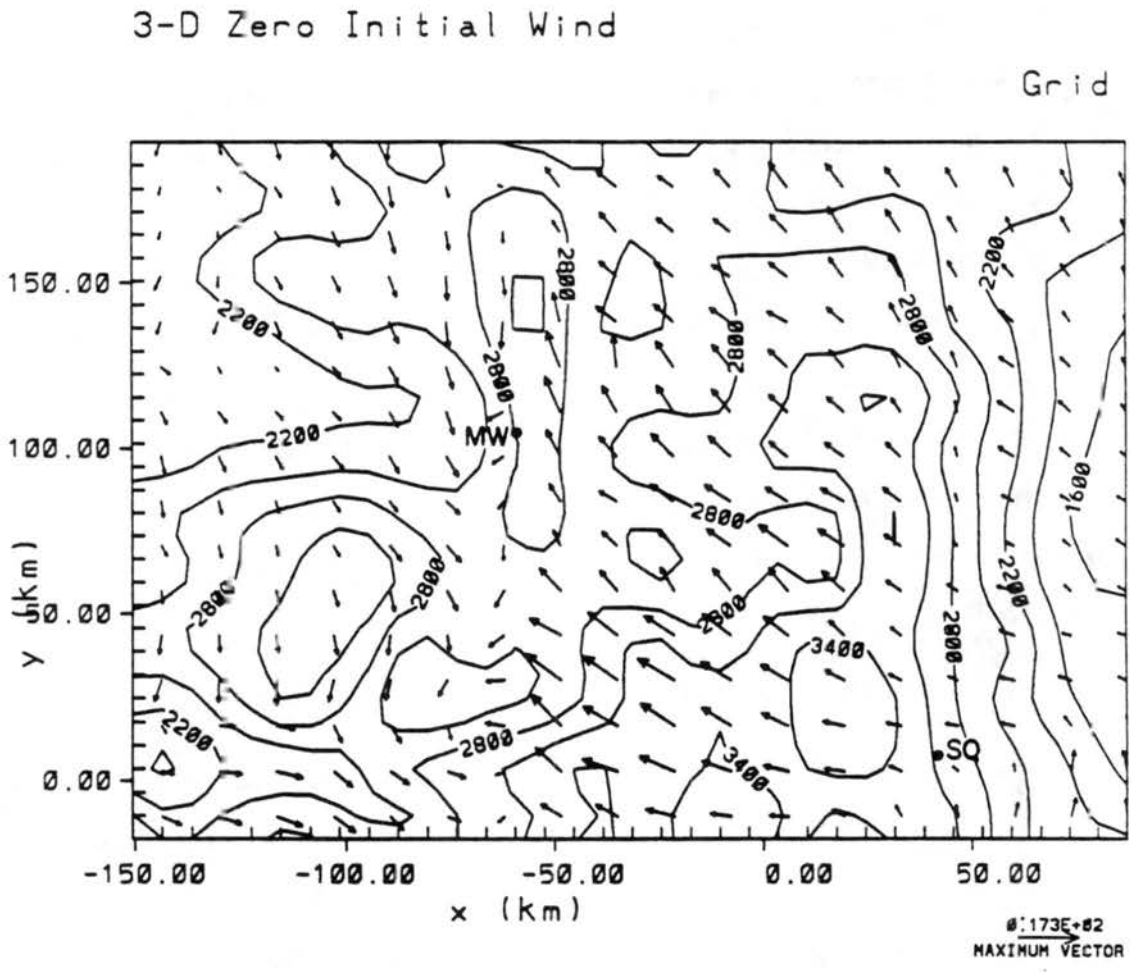

Figure 5.12: Wind vectors at 278.8 m above the surface on Grid 2 after 15 hours of simulation time. Mount Werner (MW) and Squaw Mountain (SQ) stations indicated.

inter-mountain ranges, having a maximum speed of -9.1 ms^{-1} along the western base of the Front Range (x = 10 km) and over the crest of the Park Range (x = 50 km). An equally strong southerly wind component accompanies these easterly winds. Meanwhile, the easterly flow is weakening over the Front Range, especially along the eastern slope, where the onset of surface cooling has produced weak westerly downslope flows.

After the current propagates down the western mountain slope, it continues on as an isolated disturbance detached from the main current. This perturbation is visible at 2200 MST within the developing stable layer near the surface at x = -122.5 km (Fig. 5.14). The westward propagation of this feature creates a surge effect in the shallow downvalley winds which have developed over the Yampa Valley by this time. Over the mountain area, the southeasterly flow continues to be strong, but is becoming increasingly shallow. Over the east slope of the Front Range, strong downslope southwesterly flows are now evident.

The nocturnal easterly flow initiated by the Front Range mountain-plains circulation continues to affect the intermountain region throughout the night, but generally decreases in depth, and becomes quasi-steady from a southerly direction (Fig. 5.15). Shallow downslope flows are also evident over most of the intervening slopes and ridges, and are particularly strong over the eastern slope of the Front Range. This general scenario continues until the end of the simulation at 0500 MST.

5.2.5 Comparison with observations

In this section, we compare the previous three-dimensional simulation results with wind direction time-series from seven high altitude stations included in the ROMPEX-87 experiment data set (see Fig. 3.10), for the period 24 - 28 July 1987 (Fig. 5.16). The upper portion of Fig. 5.16a shows the interdiurnal wind cycles at two east slope stations, Squaw Mountain (SQ) and Rollinsville (RO). In the middle figure are two stations bordering Middle Park, Elk Mtn. (EM) and Williams Peak (WL). Finally, in the bottom panel we have three northwestern stations, Whiteley Peak (WP), Mt. Werner (MW), and Buffalo Pass (BP). While intra-diurnal variability is fairly strong within the wind direction cycles, especially at those stations located west of the Front Range, the figure shows that the seven stations are also subject to significant wind variations operating on a diurnal time-scale.

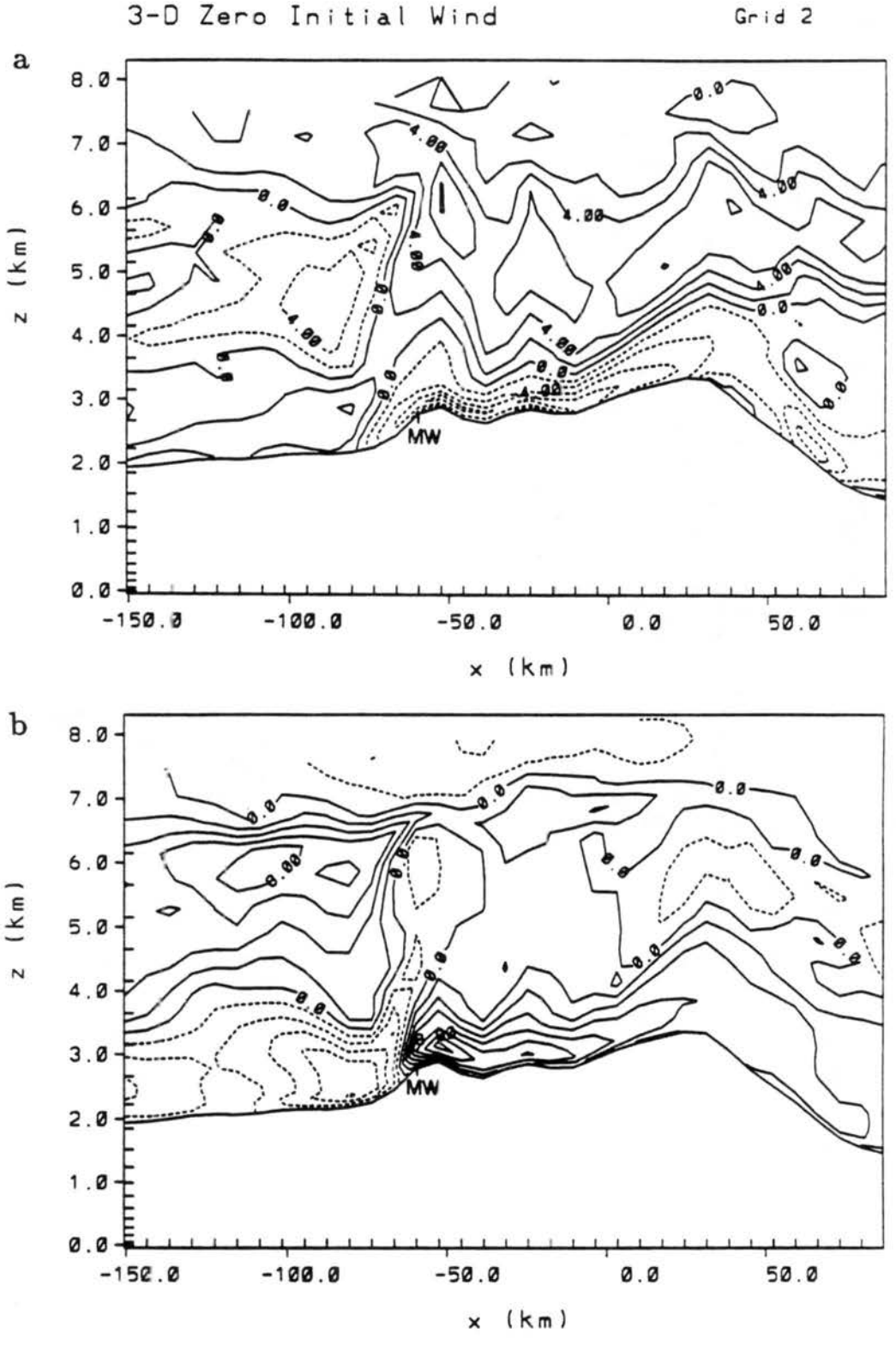

Figure 5.13: As in Fig. 5.8 only for (a) u-component, (b) v-component, and (c) potential temperature after 15 hours of simulation time. Location of the Mount Werner (MW) station is indicated.

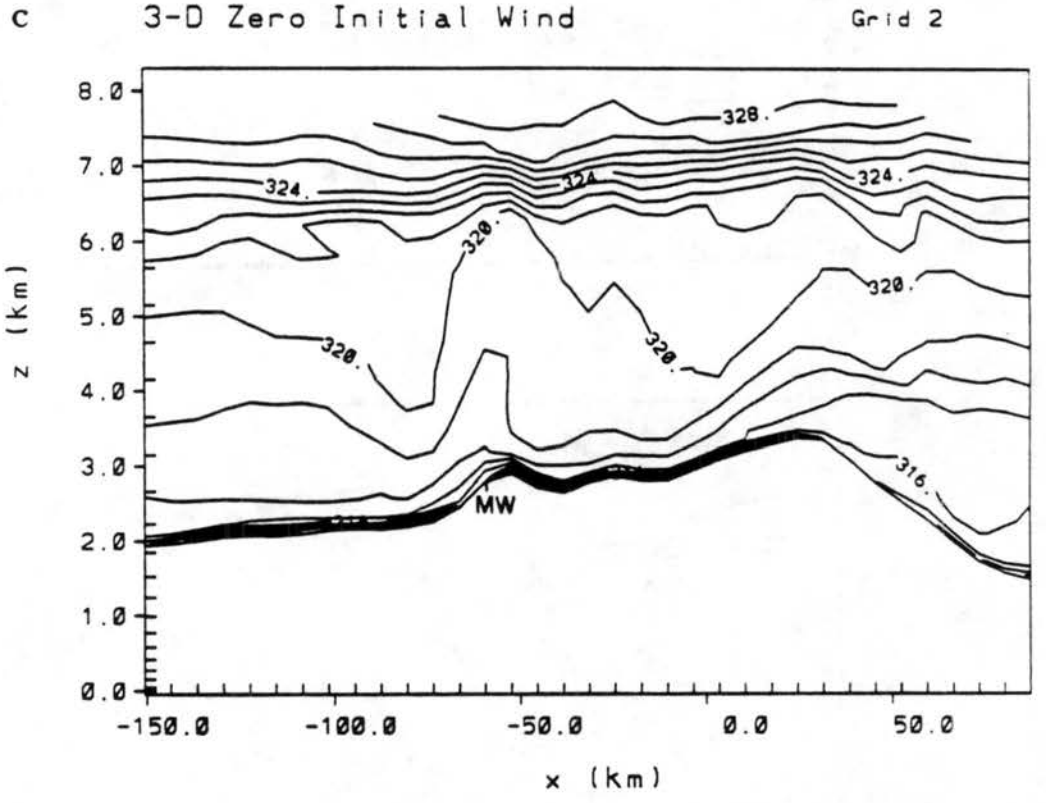

Figure 5.13: Continued.

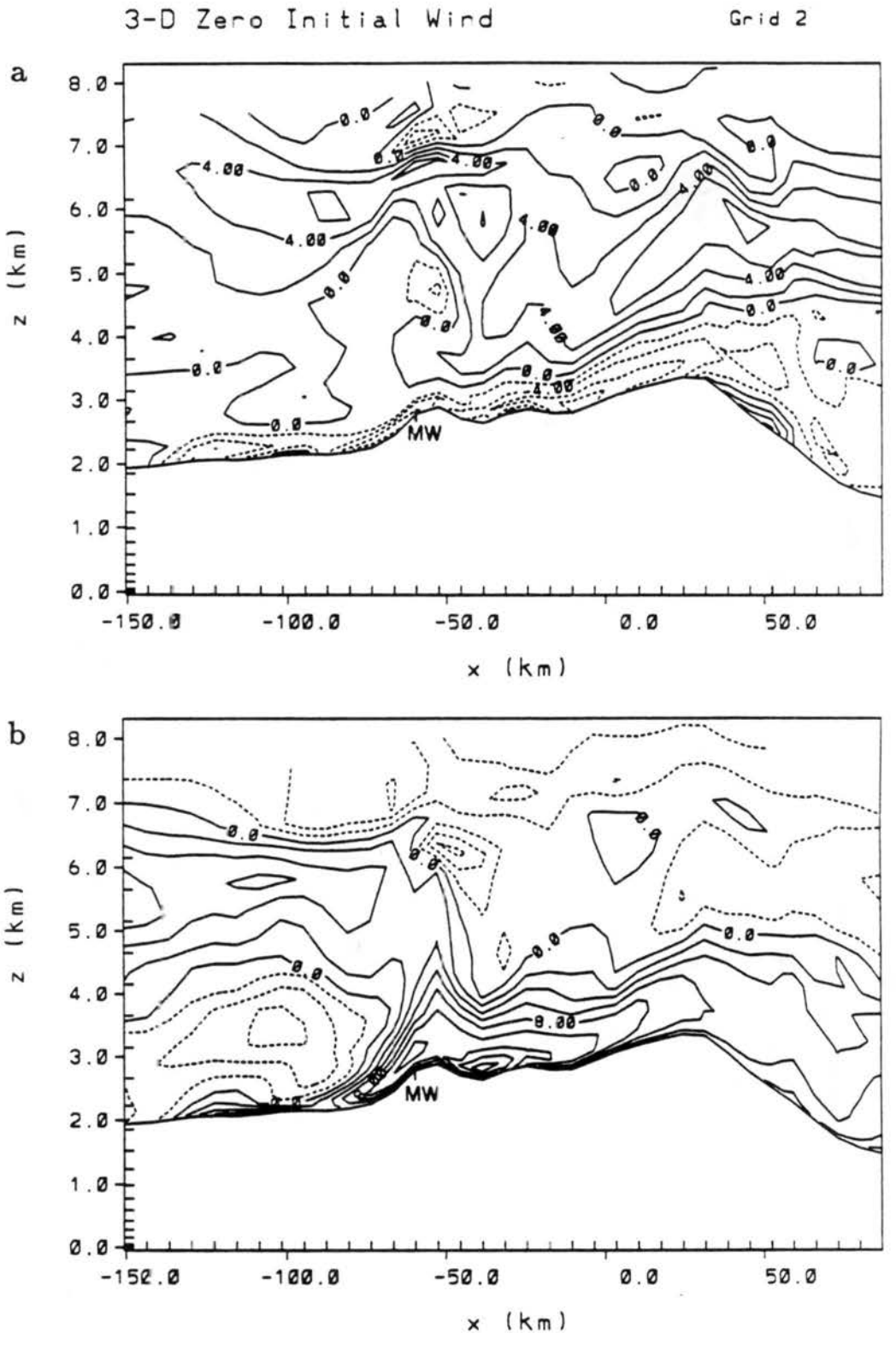

Figure 5.14: As in Fig. 5.8 only for (a) u-component, and (b) v-component after 17 hours of simulation time. Location of the Mount Werner (MW) station is indicated.

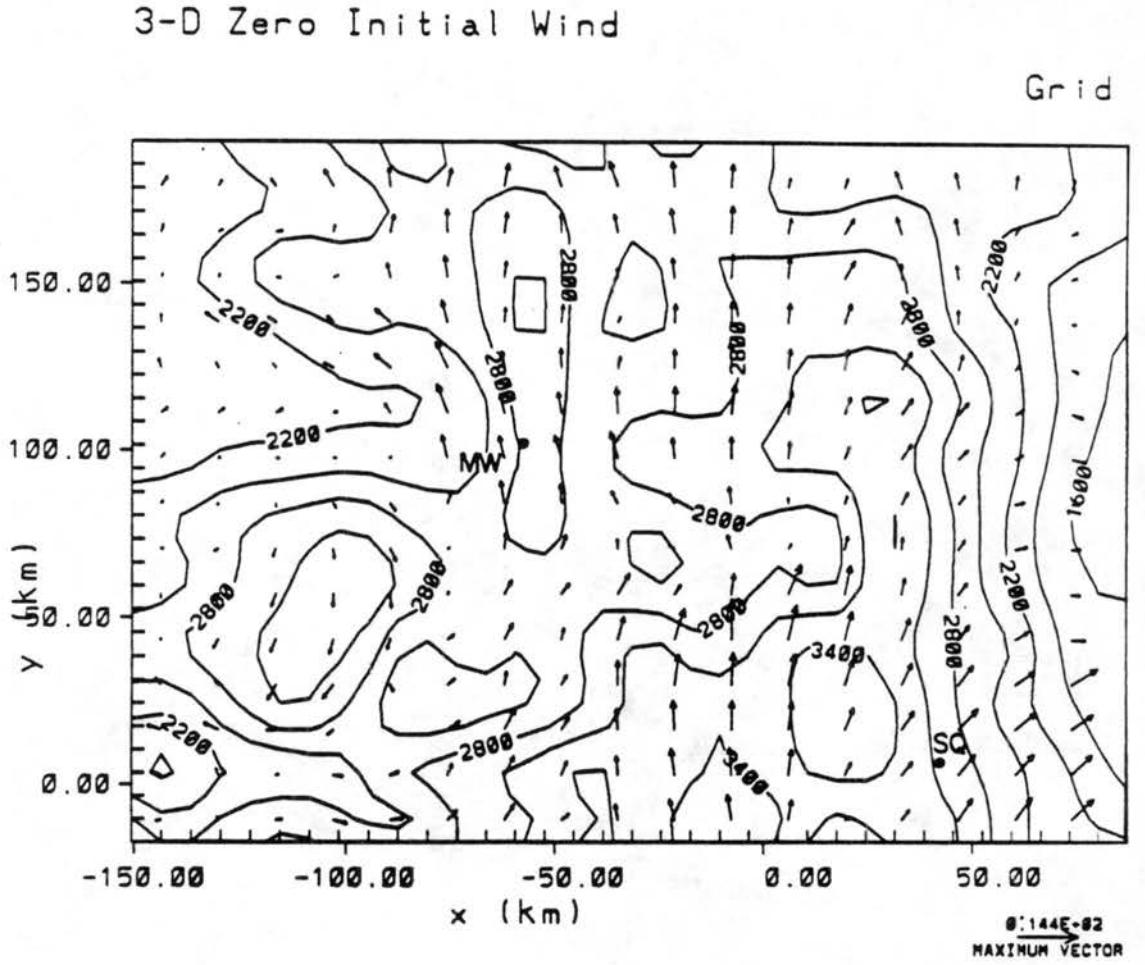

Figure 5.15: Wind vectors at 278.8 m above the surface on Grid 2 after 21 hours of simulation time. Location of the Mount Werner (MW) station is indicated.

The diurnal wind signal here shows substantial coherence between stations located within each particular geographic region, implying the existence of a large mesoscale circulation phenomenon producing these diurnal flow oscillations.

Of particular interest here is the onset time of the shift in wind direction from a westerly to easterly component flow between station groups across the mountain barrier. This is shown by the solid line drawn through each day of Fig. 5.16a. This flow transition occurs initially at the east slope stations. West of the Front Range, the two stations located on the periphery of Middle Park show a westerly to easterly wind shift in the early to late afternoon on each of the five days in the time-series, always lagging the east slope stations by several hours. At the last three stations, farther to the north and west of Middle Park, the westerly to easterly transition occurs 2-6 hours later than at the Middle Park stations, appearing generally near dusk or shortly thereafter.

Wind speeds at the 7 stations during the 5-day July 1987 period (Fig. 5.16b) show that the onset time of the southeasterly-southerly flow at each station group appears as a progressive phenomenon which begins initially at the east slope stations, and is delayed at the westernmost stations until late afternoon/early evening, when an abrupt flow reversal to strong southeast flow occurs at all three stations on several of the days within the time-series. These three westernmost stations have the strongest winds overall, especially WP and MW. The high speeds are nearly always associated with southeasterly nocturnal winds, a characteristic also observed at MW in August 1984 and July 1985.

The observed shifting of the winds at mountaintop from a westerly to easterly direction across the central Rocky Mountain barrier agrees remarkably well with the previous three-dimensional simulation. In the simulation, the eastern slope winds shift to easterly upslope flow in mid-morning, while the western slope stations respond to thermal heating of the regional terrain with a daytime westerly wind component (see Fig. 5.7a). With the westward propagation of the Front Range mountain-plains circulation in the afternoon, the winds on the western slope of the Front Range were simulated to experience a shift from westerly to east-southeast flow (Fig. 5.9a). The timing of this event is nearly coincident with the westerly to easterly wind shift at the two Middle Park stations of EM and WL during the observed period. Further, with the evening propagation of the shallow easterly current

across the intermountain region in the simulation, an abrupt arrival time at 2000 MST occurs at the MW station as shown in Fig. 5.13. In each of the five days shown in Fig. 5.16, the observed onset time of easterly winds was within several hours of 2000 MST. In addition, the observed wind speeds during the five day period also agree in some respects to the simulated wind fields. In particular, the strong nocturnal southeasterly winds at the three westernmost stations agree well with the simulated low level southeasterly jet seen at the mountaintop level in Fig. 5.13.

Supporting evidence for the westward propagating nocturnal easterly current phenomenon can also be found in the consistent 8 - 10 hour lag in the westerly to easterly flow transition between the east slope and west slope stations shown in Fig. 4.2 with ROMPEX-85 data. Also, the vertical soundings of a highly stratified 400 m low-level easterly jet over the top of Mt. Werner, shown in Fig. 4.9, agree remarkably well with the depth and thermal structure of the simulated cold current over Mt. Werner (Fig. 5.13). These comparisons between the idealized three-dimensional simulation and the actual ROMPEX observations imply that the model is providing a realistic depiction of the regional-scale flow regimes through the diurnal period.

The foregoing three-dimensional experiment has shown that the primary mechanism involved in the diurnal transition of the mountaintop winds over the western slope is the over-barrier propagation of the Front Range mountain-plains solenoid in late afternoon. The subsequent collapse of this deep solenoidal circulation into a shallow density current, which propagates swiftly westward over the peaktops, appears to be the primary mechanism controlling the onset of strong nocturnal outflow winds from an easterly direction observed to occur at mountaintop along the western slope of the mountain barrier. In the following section, we will use a two-dimensional version of the CSU-RAMS model to further investigate the salient features of the regional-scale flow evolution surrounding this propagation mechanism.

5.3 Two-Dimensional Sensitivity Experiments

The goal of this section is to examine the conditions under which deep mountain-plains circulation systems develop and evolve into westward propagating density currents, and

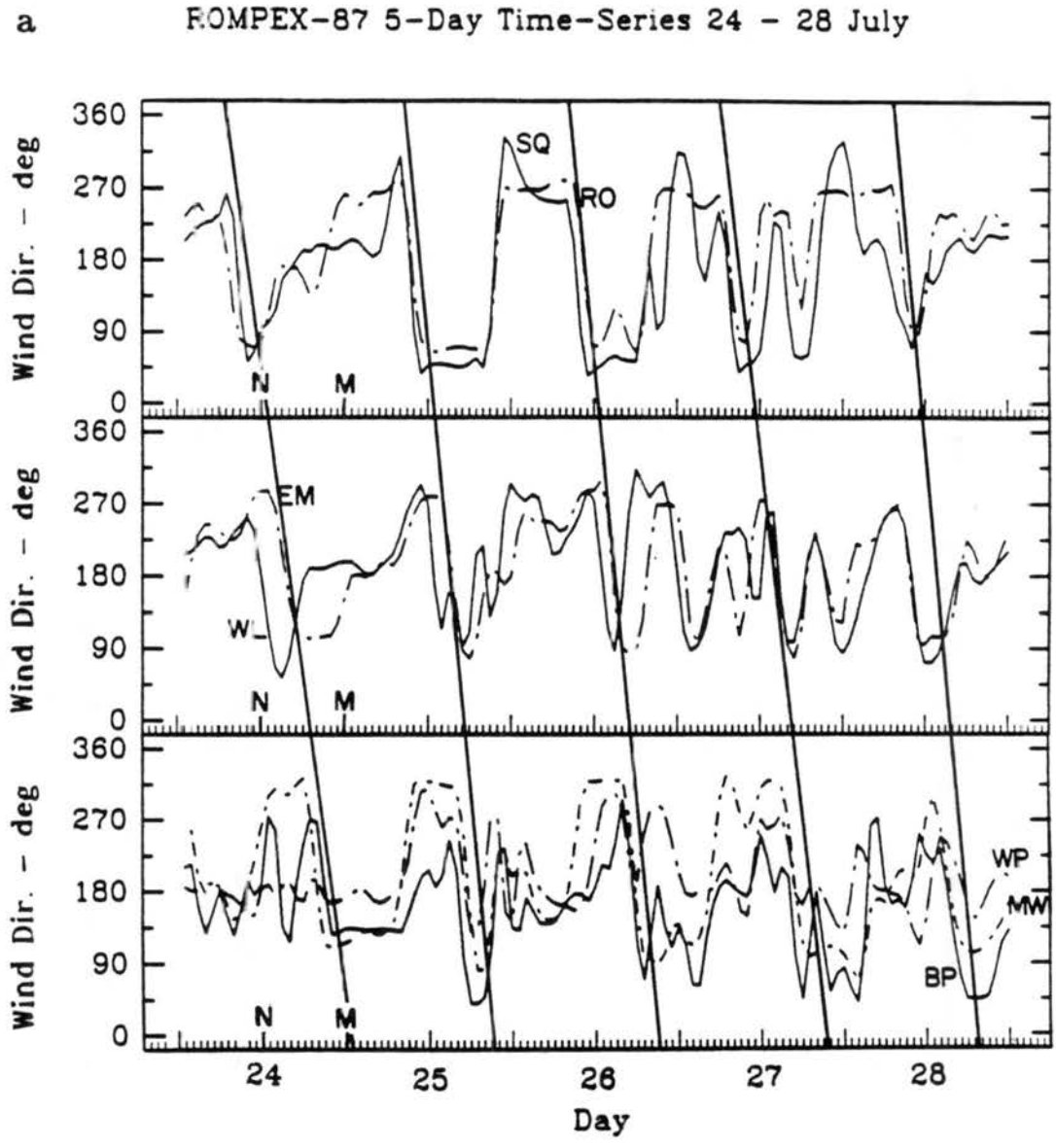

Figure 5.16: Time-series of (a) wind direction and (b) wind speed at 7 ROMPEX-87 stations for 24-28 July 1987. (See Fig. 3.10 for station location).

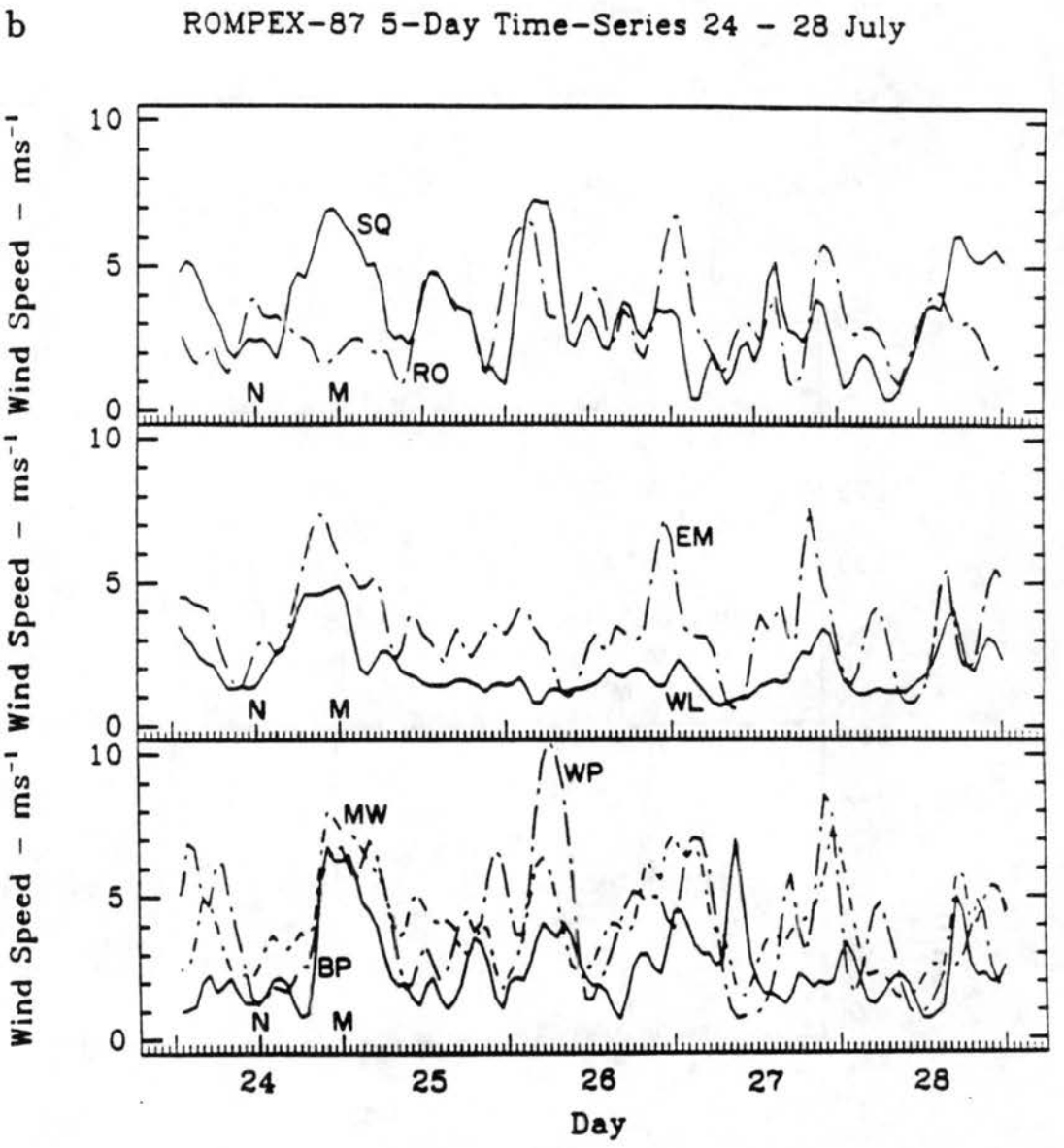

Figure 5.16: Continued.

illuminate the primary controls upon this development. To accomplish this task, several forcing mechanisms are investigated which are likely to have an influence on the development of the thermally-induced mountain-plains circulation, with a nested, two-dimensional version of the RAMS model. These simulations use two grids, with 32 km and 8 km horizontal resolution. All other numerical and initialization aspects are as described in section 5.1 and 5.2.1. The experiments are summarized below.

5.3.1 Simulations with idealized topography

In this section, a set of experiments are designed to investigate the specific role that topographic forcing across the central Rocky Mountain barrier plays in the development of the easterly density current. The approach used is to build simplified topography models and analyze the resulting thermally-driven flows. By varying the height of the plateau in the western portion of the simulation domain we can demonstrate the role of elevated terrain heating in generating inhomogeneous thermally-forced circulations. The following experiments use the same initial conditions as the previous three-dimensional simulation, with zero initial flow and a thermodynamic sounding as shown in Fig. 5.2.

The three idealized topography configurations used in this study are shown in Fig. 5.17, after 6 hours of simulation time (1100 MST). The first simulation, called the "mountain" experiment, has symmetric slopes which rise 2000 m over a 64000 m horizontal distance (3.1% slope) from a flat plain at 1500 m elevation to a 3500 m mountaintop. The second simulation has a 1000 m slope rise over 64000 m in the west from a 2500 m "low plateau" and a 2000 m slope rise in the east, identical to the previous experiment. This terrain configuration is similar to the actual topography across Colorado at 40°N, where the intermountain basin region of Middle Park resides at an average elevation of 2500 m AGL. The third experiment features a "high plateau" at 3500 m to the west of the 2000 m high slope. This terrain configuration crudely resembles the actual topographic situation in Colorado to the north and south of Middle Park (see Fig. 5.13), where high mountain ranges present a fairly unbroken chain to the regional-scale flow across the intermountain region.

Heating of the slopes in the "mountain" experiment generates a very symmetric upslope circulation (Fig. 5.17a), with some slight differences due to the variable solar azimuth angle

included in the model radiation parameterization. This upslope circulation is similar to that simulated by Mahrer and Pielke (1977b) over a 900 m mountain. A simplified theoretical discussion of the buoyancy generated by heating of the slopes is provided by Atkinson (1981). This buoyancy forcing is easily recognized in the equations for u- and w-component momentum over a slope (Mahrt 1982)

$$du'/dt + fv' = -\frac{1}{\rho_o}\frac{\partial p'}{\partial x} + g\frac{\theta'}{\theta_o}sin\alpha - \frac{\overline{\partial u'w'}}{\partial z} \tag{5.2}$$

$$dw'/dt = -\frac{1}{\rho_o}\frac{\partial p}{\partial z} + g\frac{\theta'}{\theta_o}cos\alpha \tag{5.3}$$

where $d/dt = \frac{\partial}{\partial t} + \frac{\partial}{\partial x} + \frac{\partial}{\partial y} + \frac{\partial}{\partial z}$, α is the slope angle, and all other terms have their usual meaning. From these equations, it is obvious that slope heating signified by θ' will generate buoyancy effects through the $g\theta'/\theta_o sin\alpha$ and $g\theta'/\theta_o cos\alpha$ terms, causing accelerations to occur in both the x and z directions. With positive θ', an acceleration will occur toward and up the slope.

At this early stage in the daily heating cycle, the circulation over the low plateau (Fig. 5.17b) is also very symmetrical about the mountain crest, with the horizontal and vertical circulations closely resembling the symmetric mountain experiment. The third experiment with the high plateau (Fig. 5.17c) has a very asymmetric flow, with a stronger easterly upslope circulation than in the other two experiments, which peaks at the top of the slope. A similar result was obtained by Ye *et al.* (1987, their Fig. 8), who show the flow maximum at the top of the plateau to be a symptom of steep slopes (slope angle α=2.3 in their case, α=3.1 here). A weak opposing westerly circulation is apparent to the west, which is forced by the low-level pressure gradient associated with the heated, ascending column of air one grid point west of the top of the slope.

After 12 hours of simulation time (1700 MST), the diurnal heating cycle and the upslope circulations have both peaked and are beginning to decline in amplitude. The upslope circulations remain fairly strong, however, and are very symmetric about the mountain experiment topography (Fig. 5.18a), reaching peak velocities of 8 ms^{-1} in the u-component and 4.2 ms^{-1} in the v-component. Distinct asymmetries in the upslope flow arise in other two experiments, in accordance with their underlying topography variations. Thus, in

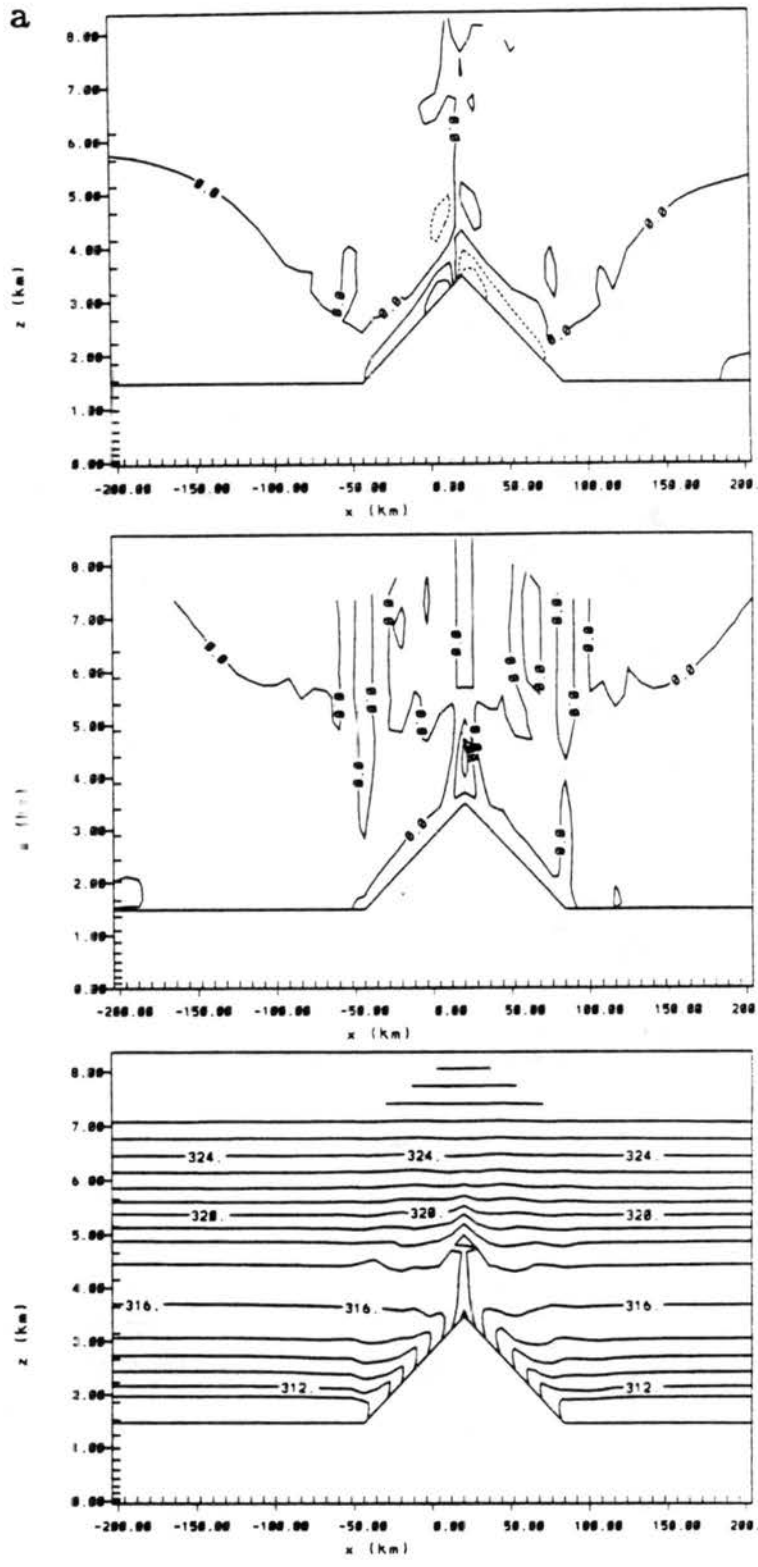

Figure 5.17: Vertical profiles of the u (2.0 ms^{-1} contour interval) and w (0.2 ms^{-1} contour interval) wind components, and potential temperature (1.0°C contour interval) after 6 hours of simulation time for (a) the "mountain" experiment; (b) the "low plateau" experiment; and (c) the "high plateau" experiment.

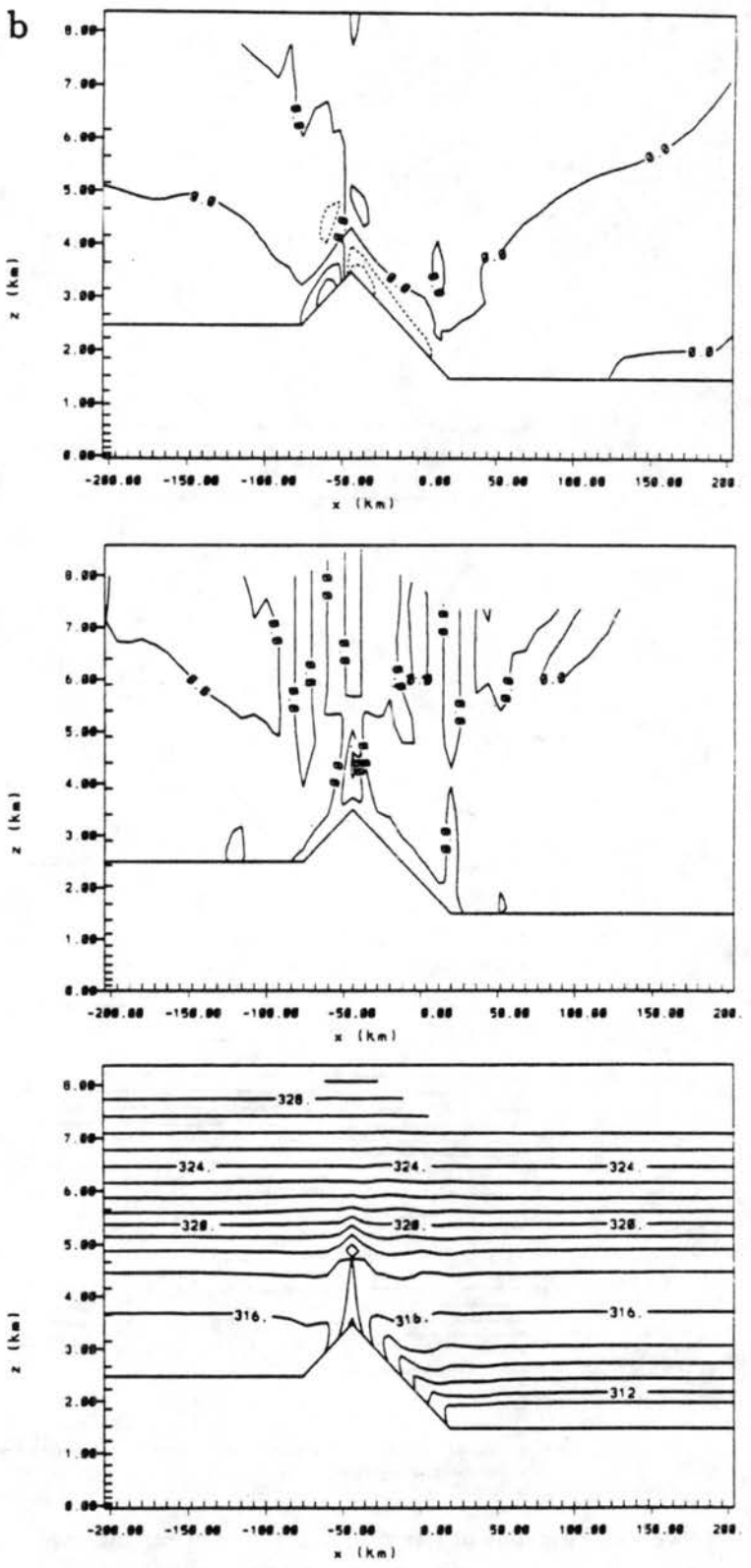

Figure 5.17: Continued.

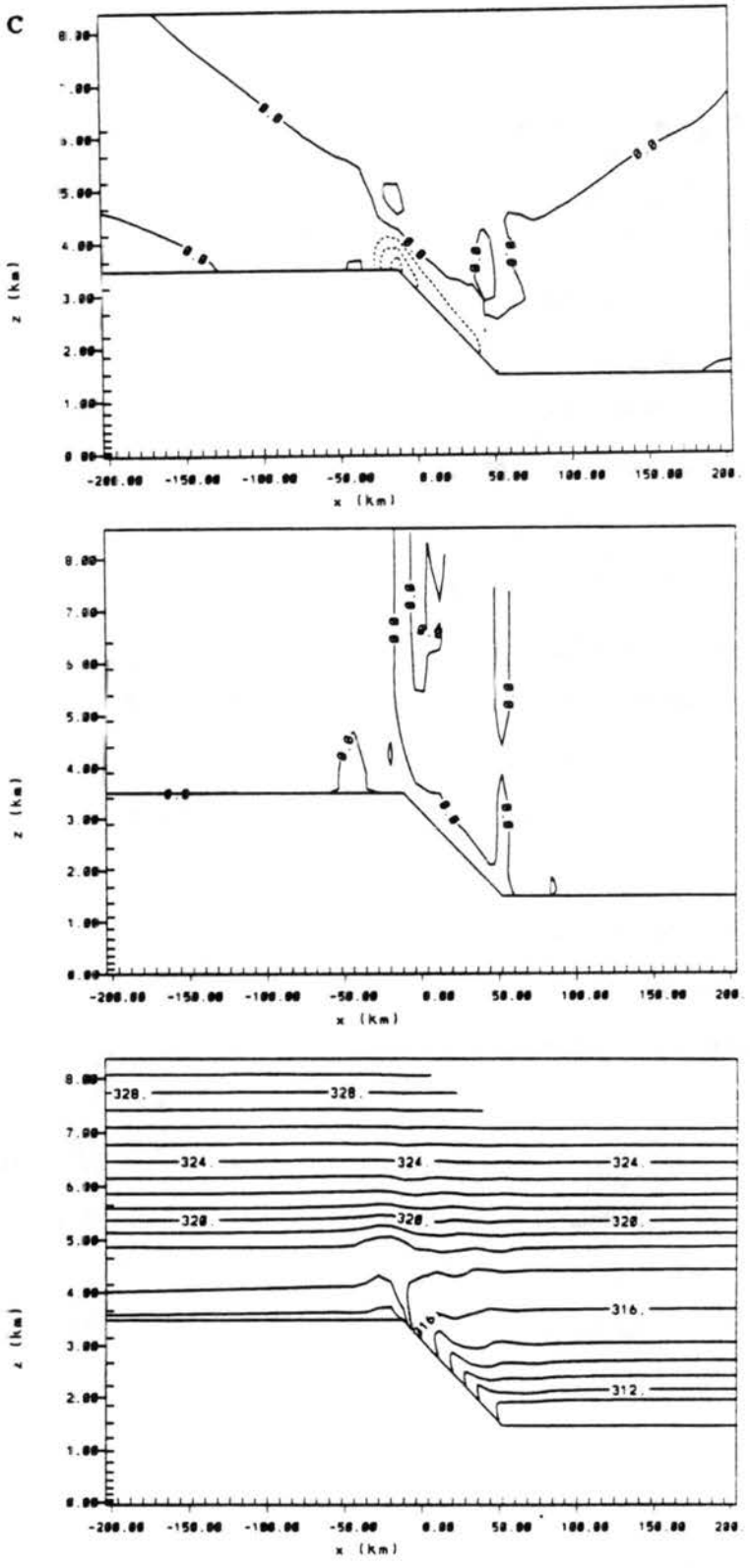

Figure 5.17: Continued.

the experiment with the low western plateau, the easterly upslope flow has now begun to overpower the westerly flow up the shorter western slope. Though the westerly flow remains of equal strength to the easterlies, Coriolis turning of the easterly flow has resulted in stronger southerly winds than the northerlies along the western slope.

The low plateau experiment (Fig. 5.18b) illustrates that the primary forcing mechanism for the propagation of the easterly flow over the crest of the barrier is the thermal gradient which develops along the eastern slope due to the differences in heating between the elevated plateau and the lower eastern plain. Air over the elevated plateau, initially at the same potential temperature as the air over the plain at an equivalent height, heats disproportionately during the diurnal heating cycle due to the less dense air mass over the plateau, and the less stratified air layer between 3 and 5 km AGL in the initial sounding. A deep, warm boundary layer is produced over the plateau by penetrating thermals which arise from convergent flow over the plateau driving large recirculating eddies.

In the high plateau experiment (Fig. 5.18c), the plateau boundary layer mixes to deep levels (over 6 km), reaching potential temperature values of 326 °K, while the boundary layer over the lower plains to the east of the slope remains at a depth slightly lower than the top of the slope, as in the other experiments, and at a much cooler temperature. Surface temperatures over the high plateau are 5 °C greater than in the low plateau experiment. This dramatic heating effect induces an intense thermal gradient to evolve between this elevated plateau region and the unheated, stratified air located just east of the plateau edge. The strong pressure gradient force associated with this thermal difference drives a powerful, cool southeasterly flow onto the plateau, with speeds nearly twice those in the low plateau experiment. The circulation system associated with this penetrating southeasterly current covers 200 km in horizontal distance at this time (1700 MST), and is opposed by weak eddy circulations which arise in response to the strong plateau heating. Turbulent mixing at the interface and continuing heat input into the current actually slows the rate of advance of the colder air during the day (Toth 1987).

A plateau experiment with very similar dimensions and results was simulated by Mannouji (1982), although his initial temperature profile was more stable. Mannouji claimed that two different types of circulation systems evolve over this high plateau topography,

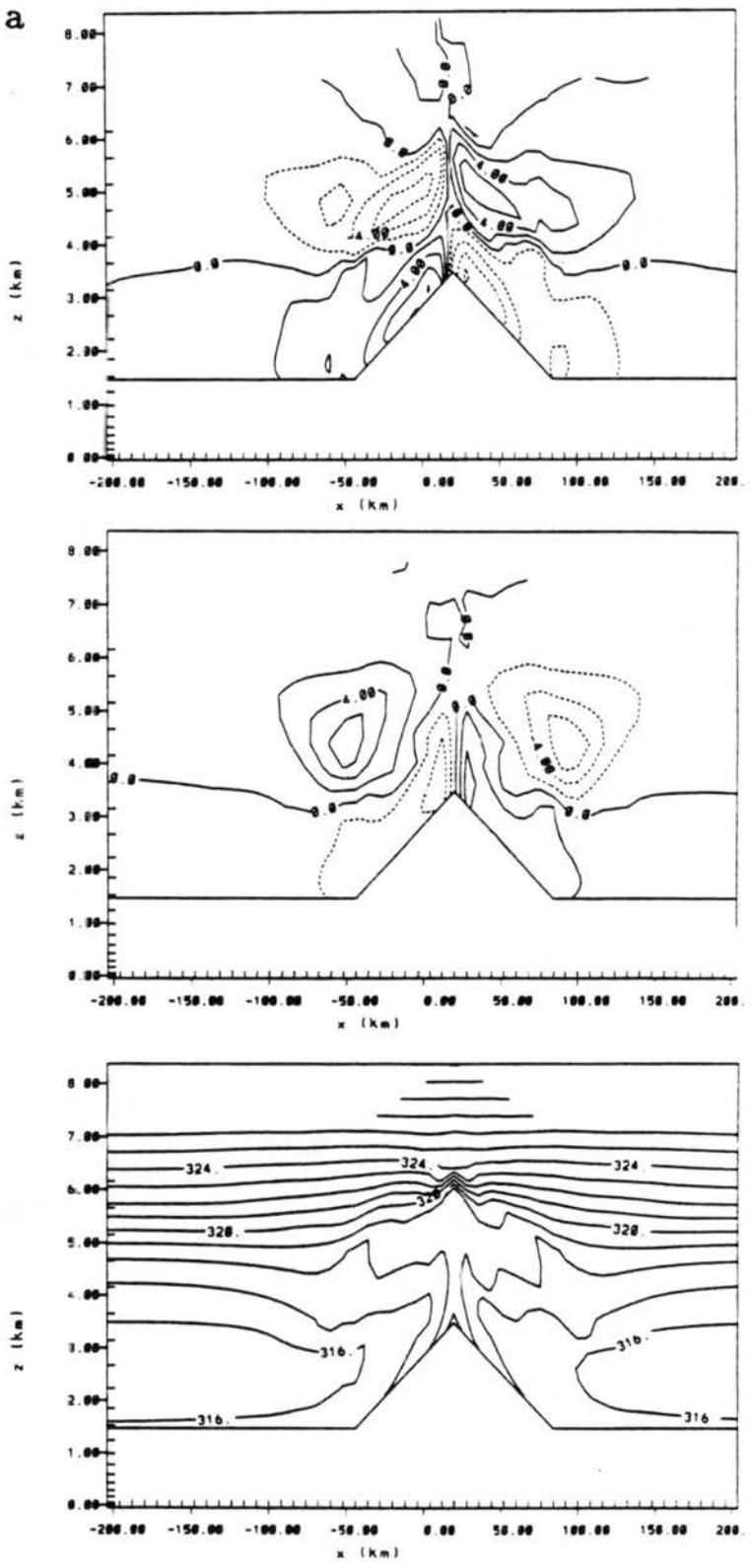

Figure 5.18: As in Fig. 5.17, but after 12 hours of simulation time.

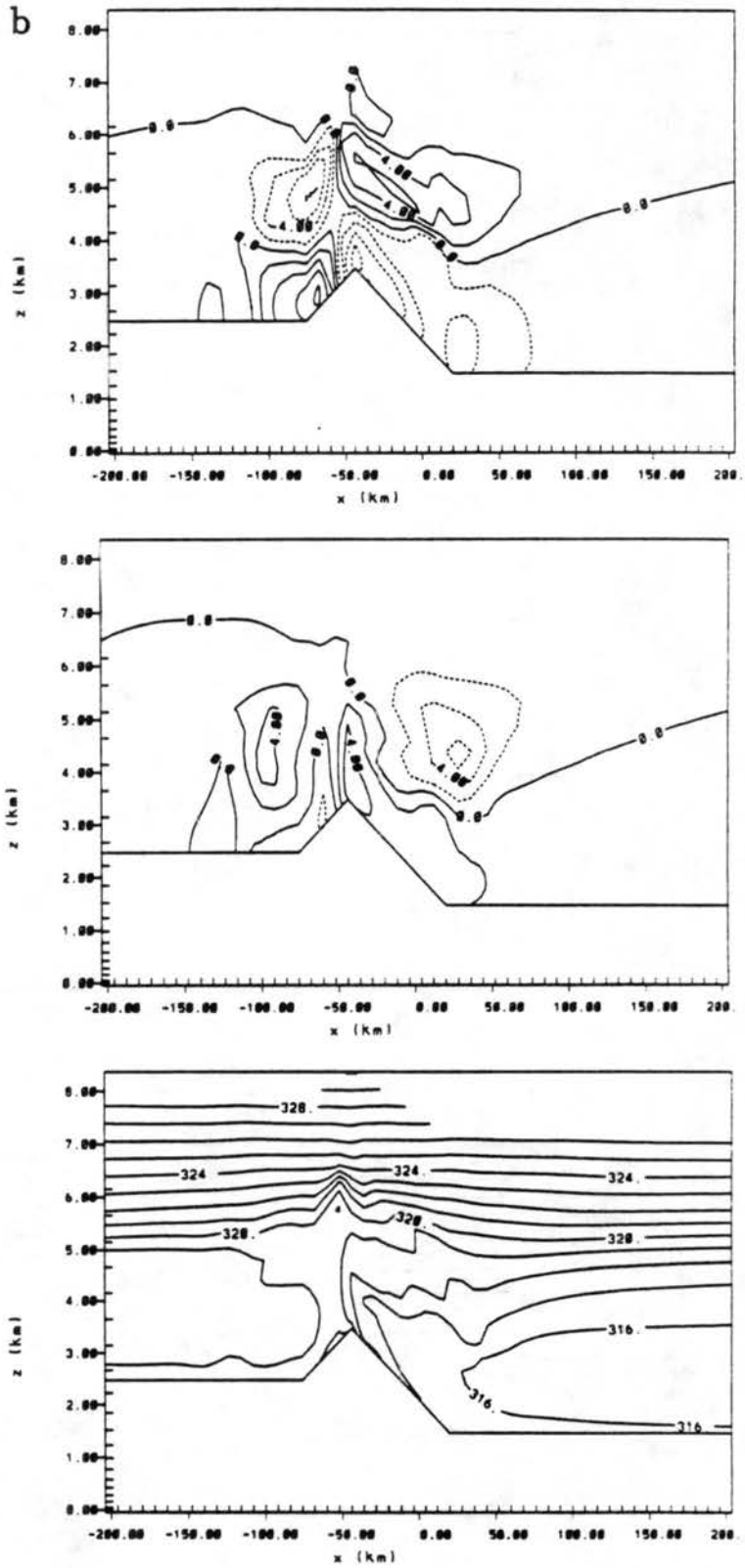

Figure 5.18: Continued.

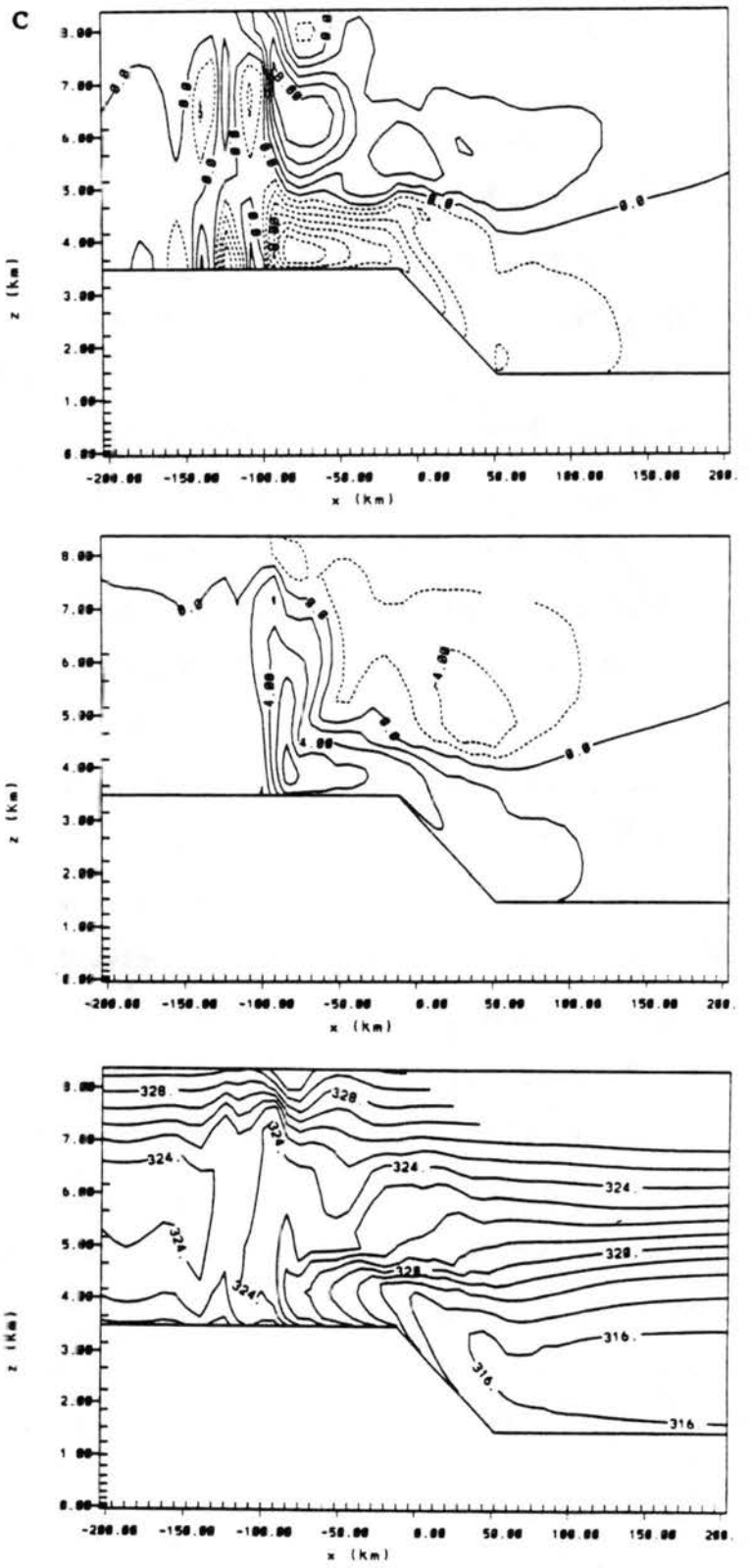

Figure 5.18: Continued.

a regional-scale (~100 km) system forced by the plateau-plain temperature gradient, and a more locally driven circulation system of smaller dimensions over the slope itself. His findings are corroborated in this experiment, although at this particular time the slope and plateau circulations appear to be acting in concert.

The nocturnal phase of the thermally-forced circulations in the three experiments is revealed in Fig. 5.19 after 18 hours of model simulation time (2300 MST). Whereas twelve hours earlier the mountain simulation showed a very symmetric upslope pattern in response to the heating, it now shows a symmetric, shallow, downslope circulation in response to diurnal cooling over the slope. The v-component reveals that a remnant cyclonic circulation persists just above the mountain slopes, a low-level geostrophic response to the diurnal heating cycle, while near the 5 km level a strong anticyclone exists.

A similar downslope flow has also developed along the eastern slope of both the low and high plateau experiments, thus revealing the primary source of this flow to be local cooling of the slope, confirming Mannouji's hypothesis. However, in both of these plateau experiments the region to the west of the eastern slope has a very different flow evolution, as a result of the regional-scale plateau to plain asymmetry in thermal forcing. In the low plateau experiment, this thermal gradient forces the westward propagation of the easterly upslope current over the crest of the mountain barrier and down the western slope, importing cooler air from the eastern slope over 64 km into the plateau region. In the high plateau experiment the head of the current has propagated 300 km west of the plateau edge, beyond the plot window. Nocturnal cooling and the subsequent stabilization of the surface layer promote this rapid propagation (Toth 1987). Thus, a transformation occurs in the evening within the low-level circulation, which now displays the characteristic signature of a density current, with an elevated head, relative flow of colder air toward the front of the current, ascending motion at the head of the current, and subsident motion behind the current head. These features, though somewhat poorly resolved in the simulation, are consistent with the observations, and laboratory and numerical models of density (or gravity) flows (e.g. Charba 1974; Goff, 1976; Simpson 1969; Simpson and Britter 1980; Mitchell and Hovermale 1977; Droegemeier and Wilhelmson, 1987).

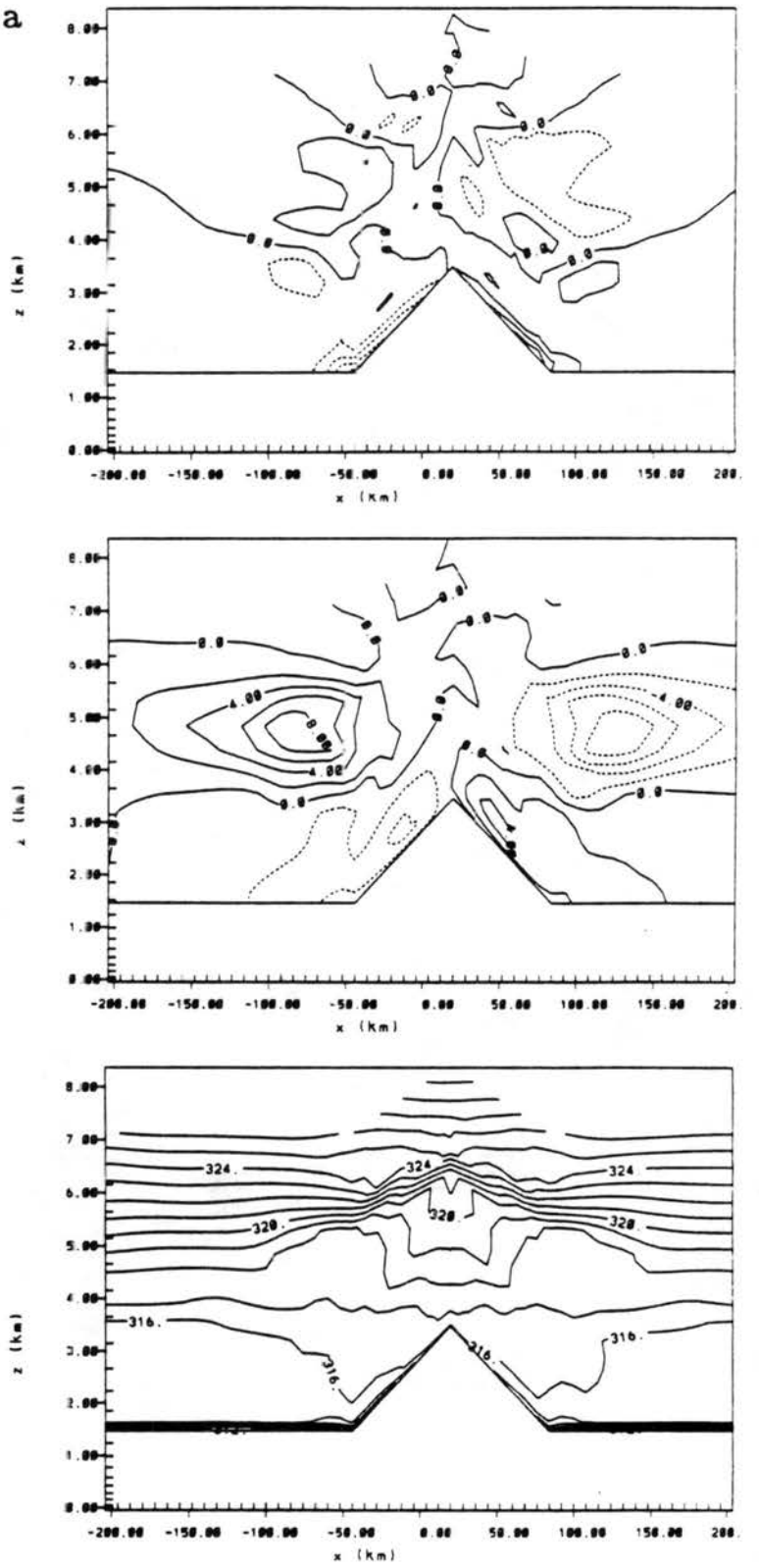

Figure 5.19: As in Fig. 5.17, but after 18 hours of simulation time.

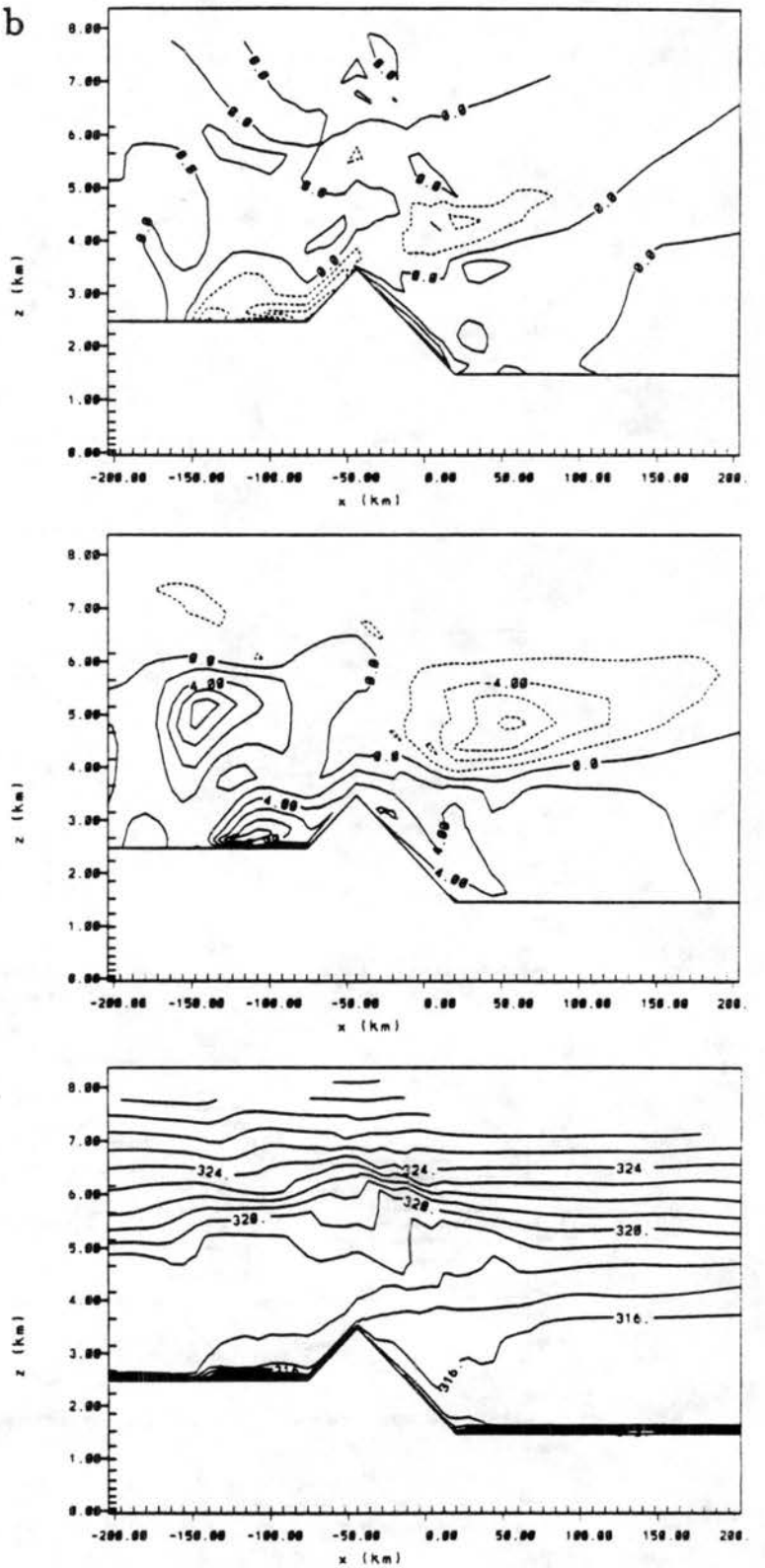

Figure 5.19: Continued.

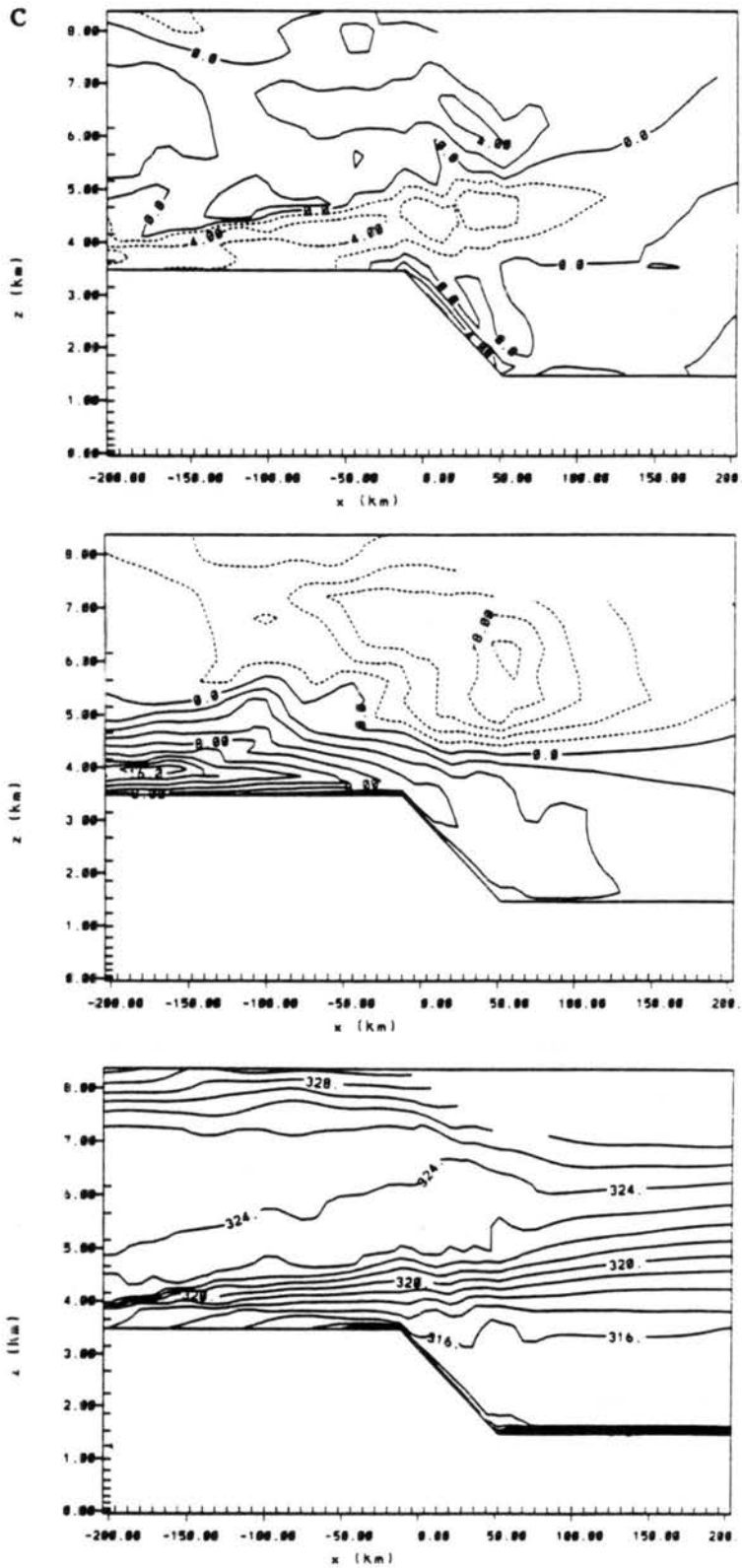

Figure 5.19: Continued.

Southerly flow is found behind the current head and is particularly strong in the high plateau experiment, nearly three times the speed of the easterly flow. The cold advection within the current has largely eliminated the low level temperature gradient so prevalent during the daytime heating phase of the circulation. The current continuously decreases in depth with its westward propagation as it outruns its source, leaving behind a tilted isentropic structure between colder, denser air over the plains and less dense, warmer air over the high plateau. The geostrophic response to this thermal structure induces strong southerly flow which maximizes in the low-levels over the plateau behind the decaying density current. These southerly winds persist throughout the night, while the ageostrophic density current decays away along with the easterly flow over the plateau.

5.3.2 Effects of Coriolis forcing

Without the influence of the Coriolis force upon the evolving circulation system, the response to the thermal imbalance generated between the the high plateau and the lower eastern plains is to increase the ageostrophic u-component. This follows directly from a simplified version of the u-momentum equation

$$du'/dt = -\frac{1}{\rho}\frac{\partial p'}{\partial x} = -R\frac{\partial T'}{\partial x} \tag{5.4}$$

where d/dt is defined as in (3). Clearly, neglecting f causes the u-component to accelerate in an attempt to balance a given horizontal temperature difference and associated pressure gradient force. This effect is only slightly apparent after 12 hours of simulation time, as shown in Fig. 5.20a. Here, an increase in westward propagation by 8 km and a 2 ms^{-1} stronger easterly flow compensates for the lack of Coriolis turning in the simulation. By 18 hours, however, the differences are dramatic (Fig. 5.20b), with the no Coriolis experiment maintaining u-component winds which are over 8 ms^{-1} stronger than the experiment with Coriolis influence. In the no Coriolis experiment, the head of the current propagates much farther westward, advecting cold air from the eastern slope onto the plateau surface, leading to a less tilted isentropic structure than in the experiment with Coriolis influence.

This experiment demonstrates that the Coriolis acceleration has an important influence on the nocturnal development of the density current. Without Coriolis effects, the

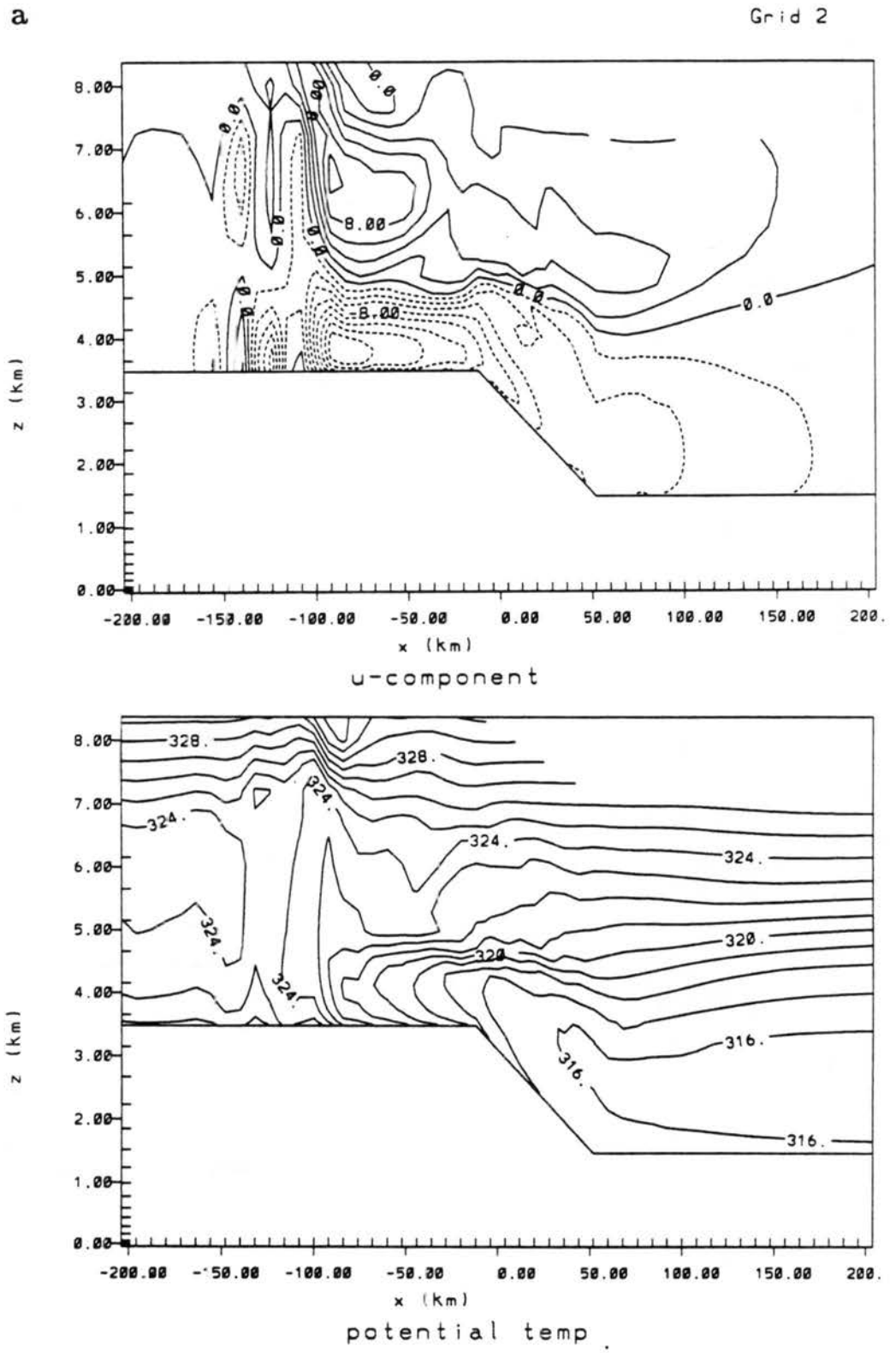

Figure 5.20: Vertical profiles of the u wind component (2.0 ms^{-1} contour interval) and potential temperature (1.0°C contour interval) for the "high plateau" experiment with no Coriolis forcing after (a) 12 hours of simulation time and (b) 18 hours of simulation time.

b

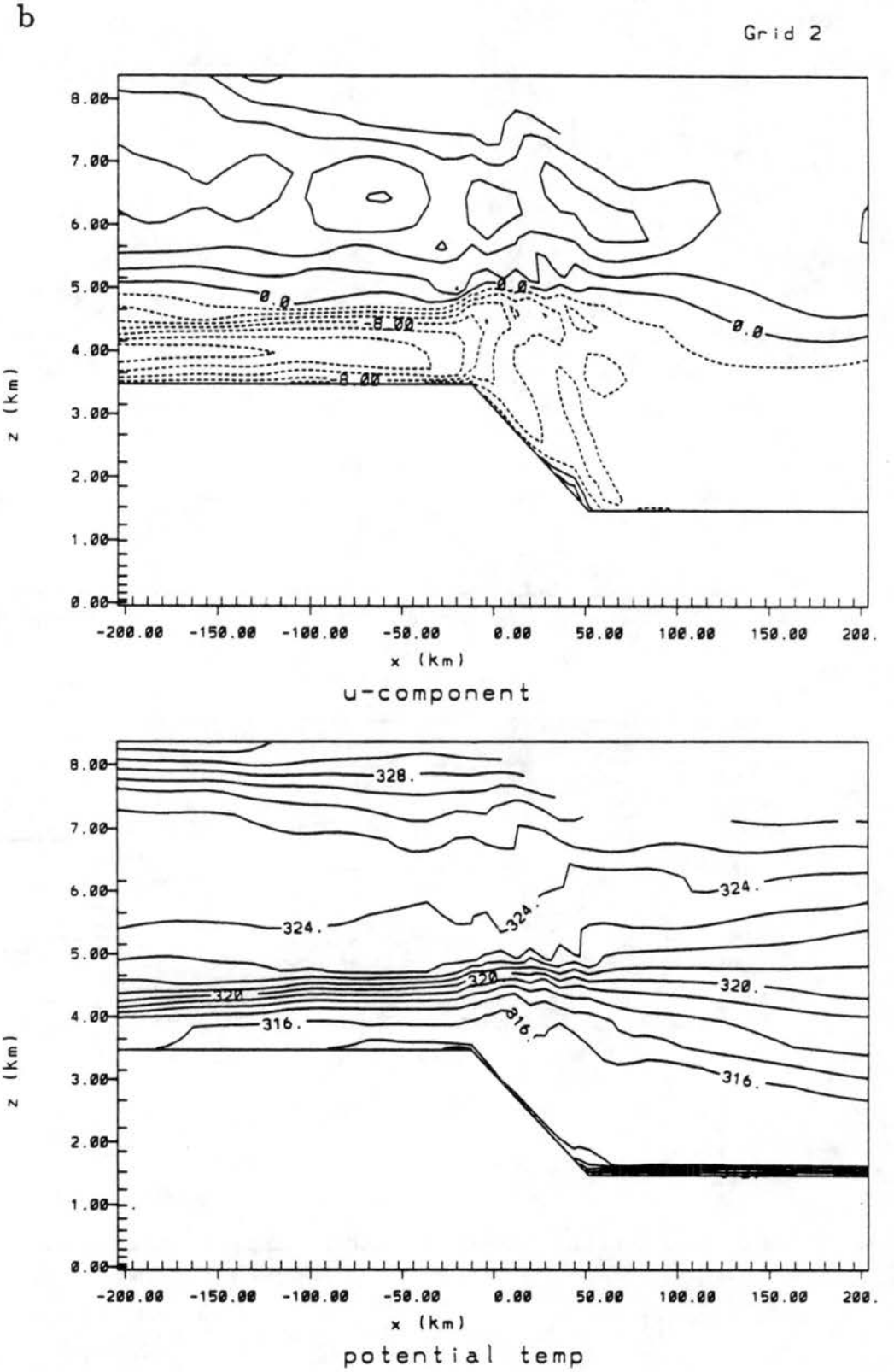

Figure 5.20: Continued.

ageostrophic flow acceleration provides the only means of achieving thermal equilibrium over the plateau. With Coriolis influence, the u-component flow and density current depth and speed all decrease during the night as the v-component increases, in accordance with a shift in the adjustment process from an unbalanced gravity wave response to a balanced geostrophic response. Thus, a strong low-level southerly flow develops during the night over the plateau, while an associated northerly current evolves at 6 km AGL at the eastern edge of the slope, in response to the deep well-mixed air mass still in place over the plateau, whose increased thickness produces isentropes at this level with a tilt opposite to that in the low-levels.

5.3.3 Effects of westerly shear

The influence of westerly shear on the propagation of the easterly density current over the high plateau topography is now examined. The initial shear profile chosen for this experiment includes easterly flow of -3 ms^{-1} at the base of the plains, which weakens with height to surface westerlies over the high plateau of 1 ms^{-1}. Above the plateau surface, the westerly shear increases to 10 ms^{-1} at 6 km AGL and to 19 ms^{-1} at 12 km AGL. The effect of the shear on the westward propagation of the current at 12 hours across the high plateau is apparent in Fig. 5.21a, where we find that the shear has intensified the baroclinicity of the current through the process of differential temperature advection, while inhibiting its upstream propagation by 32 km, as compared with the zero ambient flow case (see Fig. 5.18c). Due to the initial low-level easterlies, the v-component velocity is much stronger at this time, while the u-component is similar in speed to the zero ambient experiment.

The westward propagation of the current continues to be inhibited by the westerly shear into the night, while constant advection of warmer air over the density current produces a shallow wedge of cold air over the plateau, with an intense inversion delineating the vertical boundary between the two air masses (Fig. 5.21b). Within this wedge of cold air only weak easterly flow is found, but strong southerly flow occurs throughout the current, with a jet of 18 ms^{-1} near the top of the inversion. Above the density current, lies a deep layer of warm, mixed air which has been advected far downstream by the strong westerly flow.

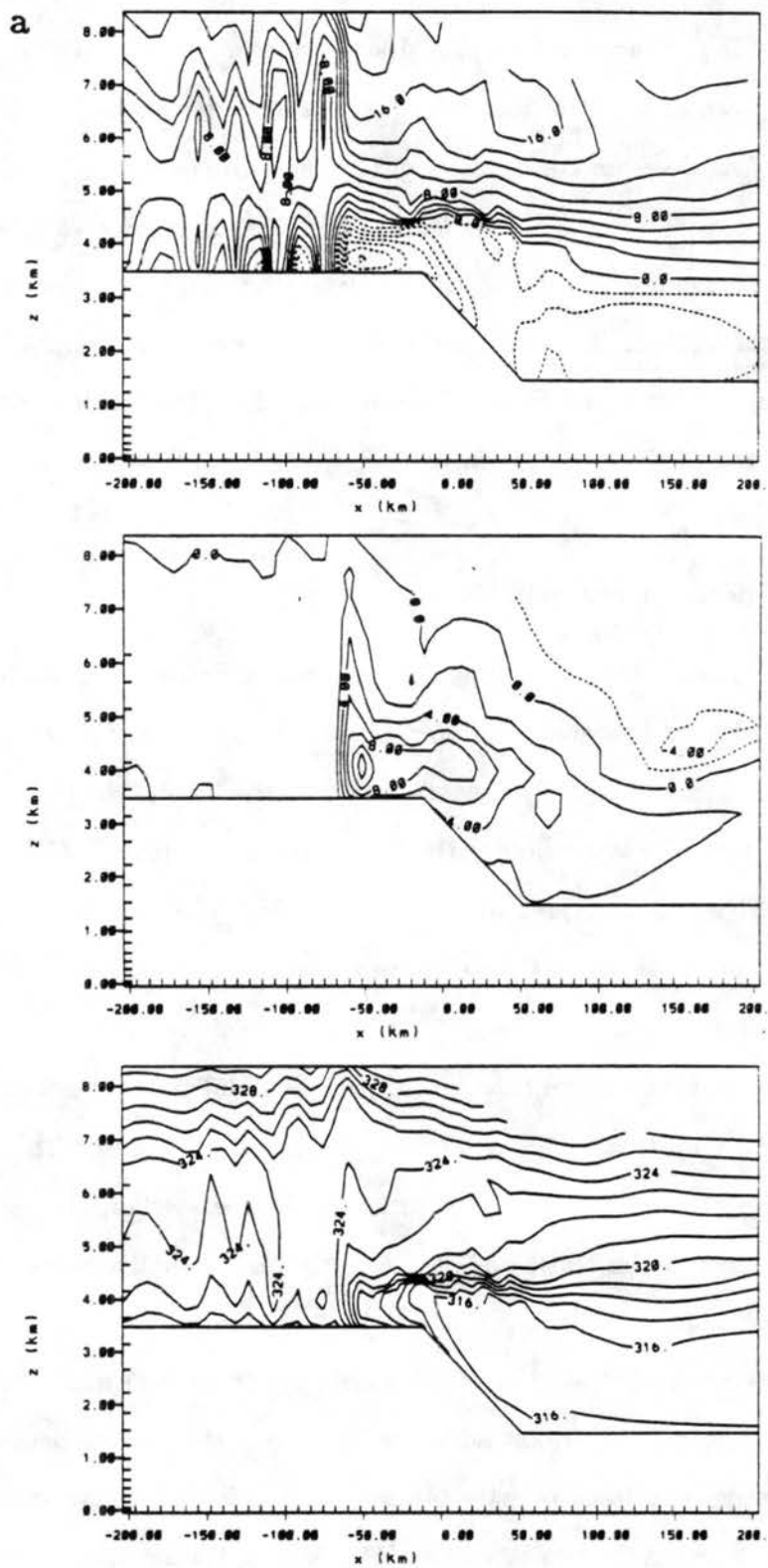

Figure 5.21: Vertical profiles of the u wind component (2.0 ms^{-1} contour interval), v wind component (2.0 ms^{-1} contour interval), and potential temperature (1.0°C contour interval) for the "high plateau" experiment with westerly shear after (a) 12 hours of simulation time and (b) 18 hours of simulation time.

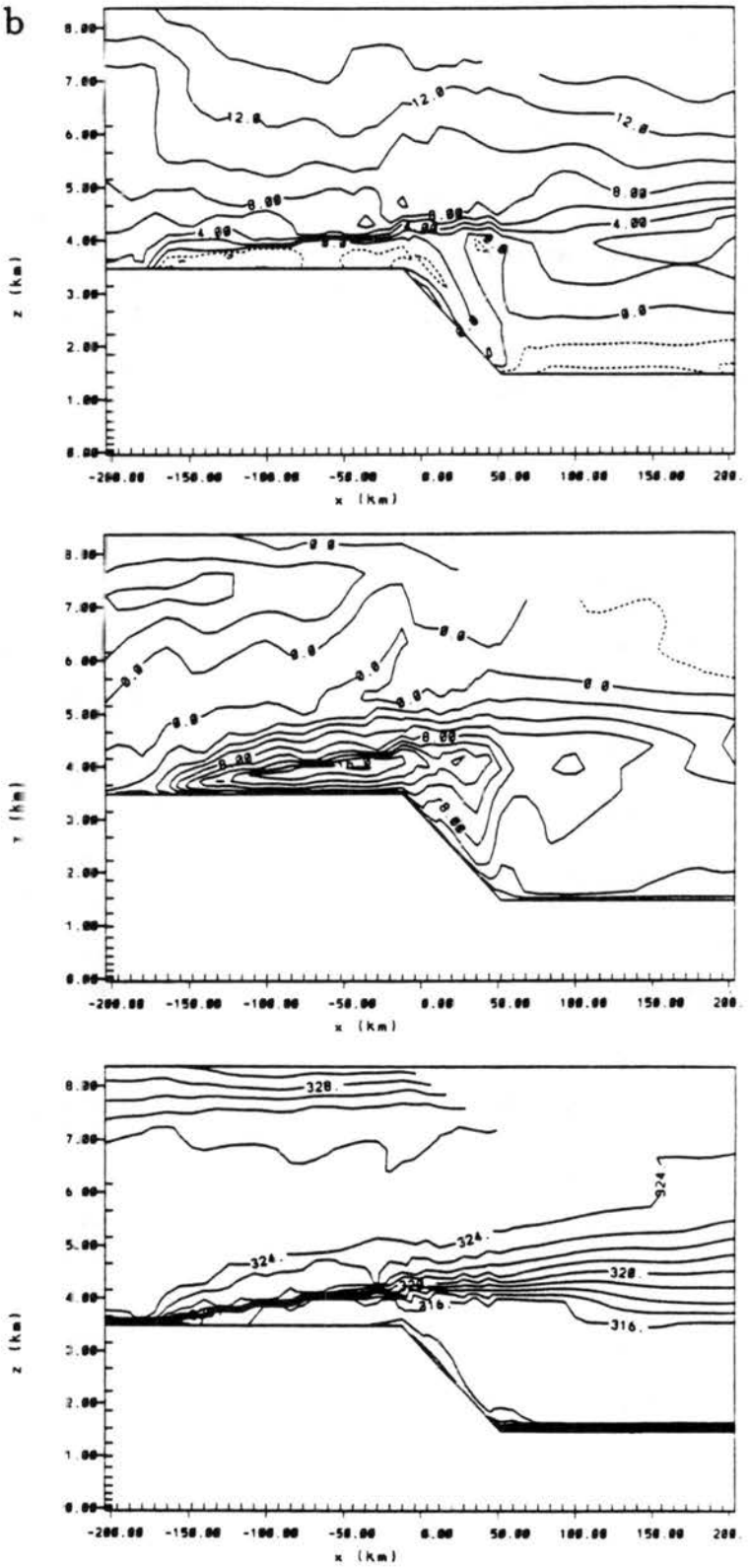

Figure 5.21: Continued.

This experiment demonstrates the robust nature of the easterly density current which can evolve from the mountain-plains solenoid into a strong, deeply penetrating circulation system, despite the retarding effects of westerly shear. The primary differences between the density current in this sheared experiment and the simulation with zero initial winds is the decreased total westward propagation, shallower depth of the current, and the stronger thermal boundary that develops between the contrasting air masses.

5.3.4 Effects of ambient wind speed and direction

In this section, we examine the effect of varying wind speed and direction upon the development of the intermountain density current over more realistic topography, through a cross-section at 40°N. Since numerous simulations were necessary to investigate these effects, the data will be presented for several runs within the same category, and at only one time, 16 hours into the simulation (2100 MST). All of the simulations shown in this section use the same initial potential temperature sounding, presented in Fig. 5.2.

In Fig. 5.22a, we compare the u-component velocity at 155 m AGL for three different experiments with initial easterly flow which is constant with height. Also included for comparison is a simulation with zero initial wind. The figure shows that the primary impact of initial easterly winds upon the density current evolution is to increase the propagation speed, so that the head of the current is located farther westward with increasing easterly flow speed. The increase in propagation speed is due in part to the greater depth of the current with increasing easterly wind speed (not shown), and also from earlier cold advection which occurs as the mean easterly flow forces unheated ambient air over the crest of the Front Range barrier. This effect tends to intensify the temperature contrast between the evolving density current and the heated air over the intermountain basin. Both of these effects will increase the phase velocity of the density current as shown in the relationship

$$c = k[gh(\Delta\overline{\theta}/\theta_o)]^{1/2} \tag{5.5}$$

where c is the propagation speed of the density current, k is an empirically determined Froude number, g is gravity, h is the depth of the current, $\Delta\overline{\theta}$ is the potential temperature

contrast across the interface or over the current depth h, and θ_o is the mean potential temperature.

Several features common to all four simulations are worthy of mention here. In all cases, the flow speed is greater 8 km behind the current head, indicating relative flow toward the current interface, a characteristic feature of density currents (Charba 1974; Mitchell and Hovermale 1977). An acceleration of the easterly flow behind the current head is apparent along the western slopes of both the Flat Tops and Front Ranges, as the negative buoyancy of the current provides an additional accelerating force.

Simulations run with an initial westerly wind profile are presented along with the zero ambient flow case in Fig. 5.22b. Of interest here is the very similar flow behavior at 16 hours of simulation time between the zero ambient and 1 ms^{-1} westerly initial flow cases. The difference in the amount of westward propagation at this time appears to be primarily due to the retarding effect of the initial westerlies, much the same as the initial easterlies enhanced the westward propagation of the easterly current. Of further interest are the 3 ms^{-1} and 6 ms^{-1} westerly flow cases. In the former case, a very weak easterly density current is found just at the crest of the Front Range at this time, while a westerly jet is apparent near x = -50 km. This westerly jet is formed in a manner similar to the easterly current, propagating as a density current forced by the collapse of the mountain-plains solenoid along the western slope of the Flat Tops Range. Thus, in this case the easterly density current is barely able to form in the dominant westerly flow regime.

In the 6 ms^{-1} westerly flow case, the westerly jet through the intermountain basin forms early in the day (much like the preceding -6 ms^{-1} easterly wind case) from the advection of colder air from west of the Flat Tops Range, and proceeds eastward, surging through the intermountain basin, and over the crest of the Front Range, creating a mountain wave-like disturbance in the lee. This strong westerly jet suppresses the development of the easterly upslope circulation, which is shallow and confined to the lower eastern slope during the day, with a remnant circulation at this time located along the base of the mountain barrier. The suppressed development of the Front Range mountain-plains solenoid with strong westerly ambient flow could be associated with the downward mixing of westerly momentum observed by Banta (1984) over the South Park. Observations from the ROMPEX experiments also

show a lack of diurnally varying flow during conditions with strong westerly or northwesterly upper-level flow.

5.3.5 Effects of stratification

To examine the effects of variable lower tropospheric stratification on the thermally-forced regional-scale circulations, three experiments were run over a realistic cross-section of topography at 40°N through the Colorado Rocky Mountains. All of these experiments are initialized with zero ambient flow to isolate the effects of the differing stabilities. The first experiment features a neutral stratification up to 4.9 km AGL. The second run uses the realistic summer sounding shown in Fig. 5.2. The third experiment is at the opposite extreme from the first, having an isothermal atmosphere up to 4.9 km AGL. Above 4.9 km, the stratification is the same between all three experiments, based upon the realistic sounding.

The potential temperature and u-component wind fields for the three experiments after 8 hours of simulation time (1300 MST) are presented in Fig. 5.23. The potential temperature field in the neutral case (Fig. 5.23a), which had an initial temperature of 317.5°K below 4.9 km, now shows a superadiabatic lapse rate near the surface from strong surface heating. The warmest temperatures are located near the crests of the mountain barriers. Despite the initially neutral environment, a strong horizontal temperature gradient has again developed along the eastern slope of the Front Range. A similar potential temperature structure has developed in the simulation with a realistic sounding, with even stronger horizontal temperature gradients over the mountain slopes, due to the the initial stratification. The isothermal experiment, on the other hand, shows very suppressed boundary layer development, especially along the eastern slope of the Front Range, as a result of the intensely stable air mass.

The u-component velocity fields for the three experiments (Fig. 5.23b) reveal strong upslope circulations and associated mid-tropospheric return flows characteristic of a well-developed mountain-plains circulation in both the neutral and realistic simulations. The neutral case has somewhat weaker flows along the western slopes due to the lack of concentrated horizontal temperature gradients. These gradients are generally stronger in the

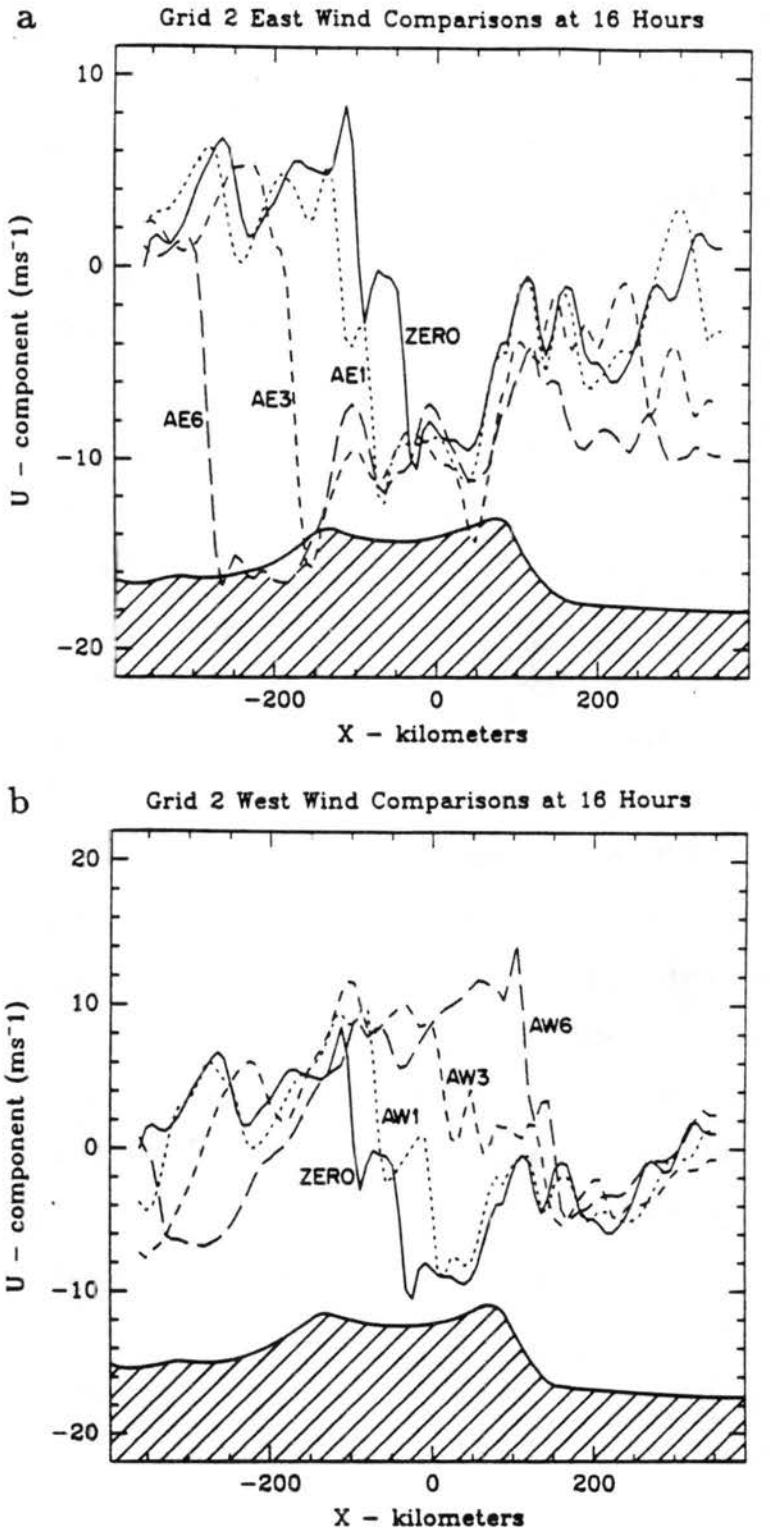

Figure 5.22: Simulated u-component velocity at 155 m above the terrain surface for experiments with (a) initial easterly winds, where ZERO=0 ms^{-1}, AE1=-1 ms^{-1}, AE3=-3 ms^{-1}, and AE6=-6 ms^{-1}; and (b) initial westerly winds, where ZERO=0 ms^{-1}, AW1=+1 ms^{-1}, AW3=+3 ms^{-1}, and AW6=+6 ms^{-1}; after 16 hours of simulation time.

realistic case due to the initial stratification. Strong damping within the isothermal atmosphere produces much weaker and shallower circulations.

After 16 hours of simulation time (2100 MST), the mountain-plains solenoids over the barrier crests have collapsed in all cases (Fig. 5.24a), with radiationally cooled air near the surface. The induced horizontal temperature gradients within the density currents are a function of the initial stratification, as seen in the neutral case which exhibits the weakest gradient, while a very strong thermal contrast exists in the isothermal experiment. This baroclinicity produces the density currents which propagate from each major slope of the mountain barrier toward the center of the intermountain region (Fig. 5.24b). The figure shows that the distance these currents have propagated after 16 hours of simulation time is related to the strength of the temperature gradient at the current interface, as predicted by the phase velocity equation (5). Thus, in the neutral case the density current is the weakest of the three experiments, and is located much farther east than in the other two cases which feature stronger temperature contrasts across the interface. Some of the effects of the temperature contrast are counterbalanced by the depth of the current, which decreases with increasing atmospheric stability. Current depth is directly related to the strength of the mountain-plains solenoid which initiates the current. These solenoids are more vigorous in a less stable environment.

Of further interest is the stronger flow and farther horizontal distance covered by the easterly density current, relative to the eastward propagating current initiated by the Flat Tops Range mountain-plains solenoid. This contrast can be attributed to the longer and steeper slope along the Front Range, which develops greater baroclinicity above the eastern slope with daytime heating, as opposed to the more gradual slope west of the Flat Tops Range. This effect is much more dramatic in three dimensions, since the Front Range presents a long north-south barrier with a steep slope along much of its distance, while the Flat Tops is actually an oval shaped range surrounded by numerous valleys and other small mountain ranges, which comprise the extremely complex topography of western Colorado. The resulting flows over this extremely complex topography tend to be weaker and much more variable than along the Front Range.

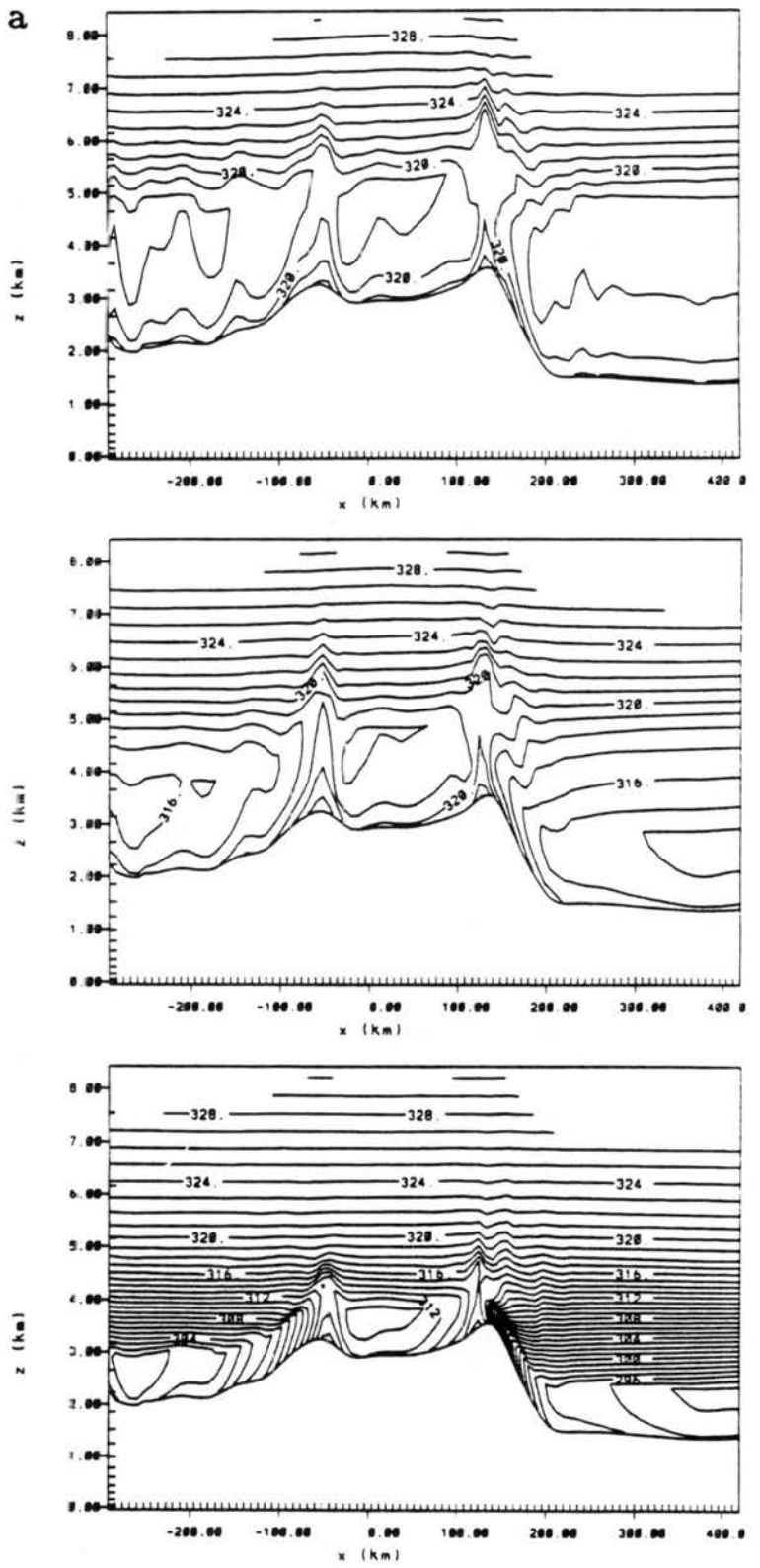

Figure 5.23: Vertical profile of (a) potential temperature and (b) u-component wind after 8 hours of simulation time for three experiments with neutral (upper), realistic (middle), and isothermal (lower) initial stratification.

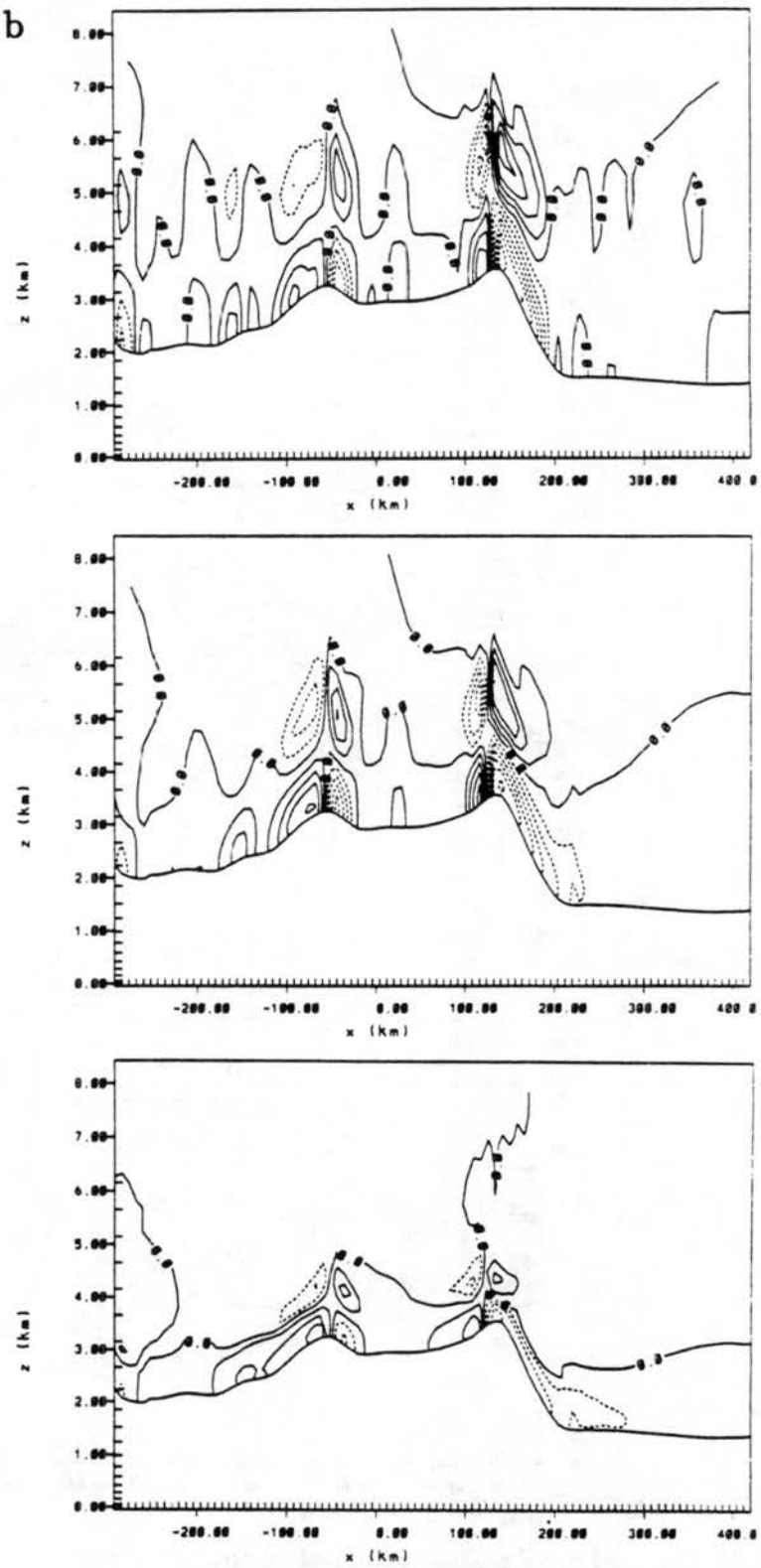

Figure 5.23: Continued.

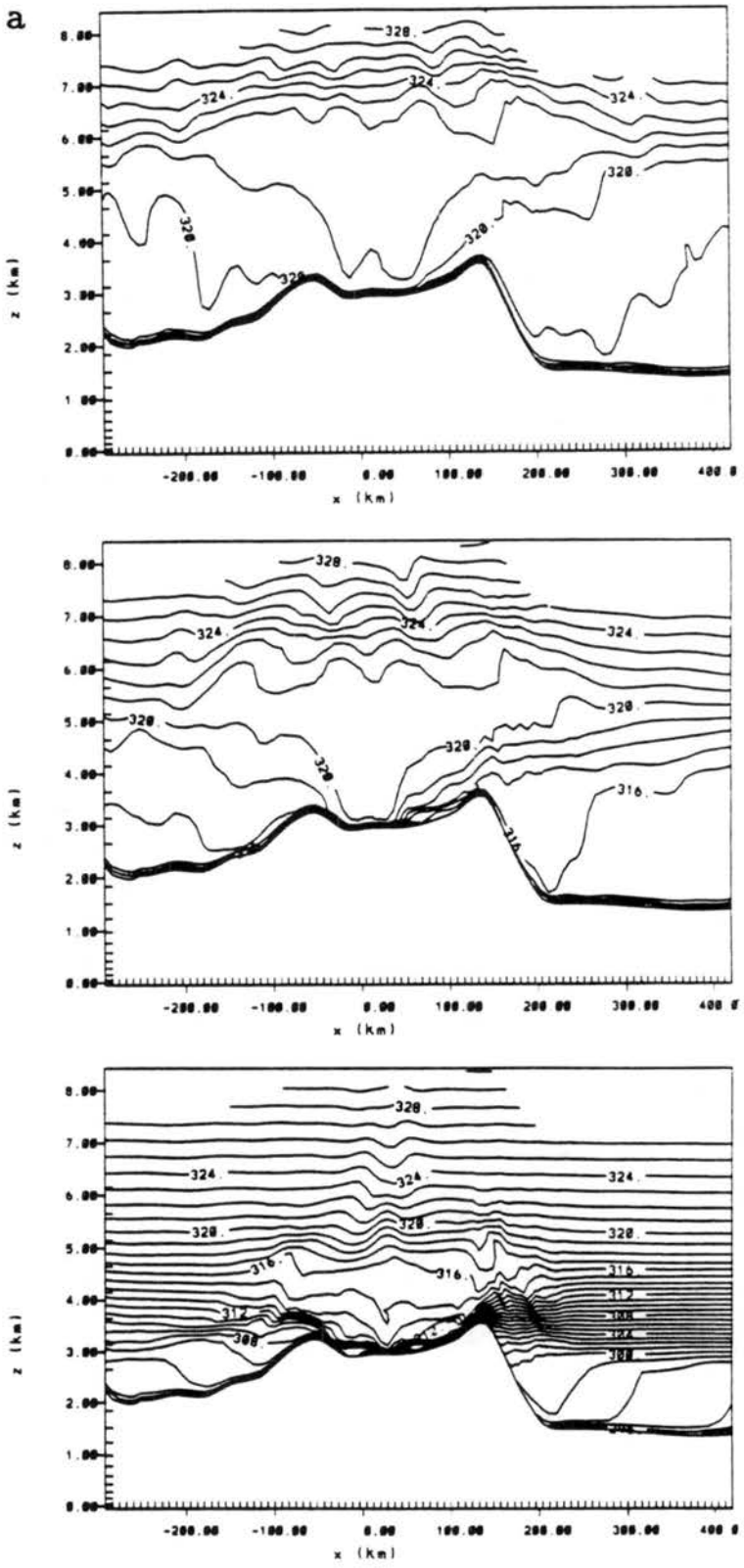

Figure 5.24: As in Fig 5.23, but after 16 hours of simulation time for three experiments with neutral (upper), realistic (middle), and isothermal (lower) initial stratification.

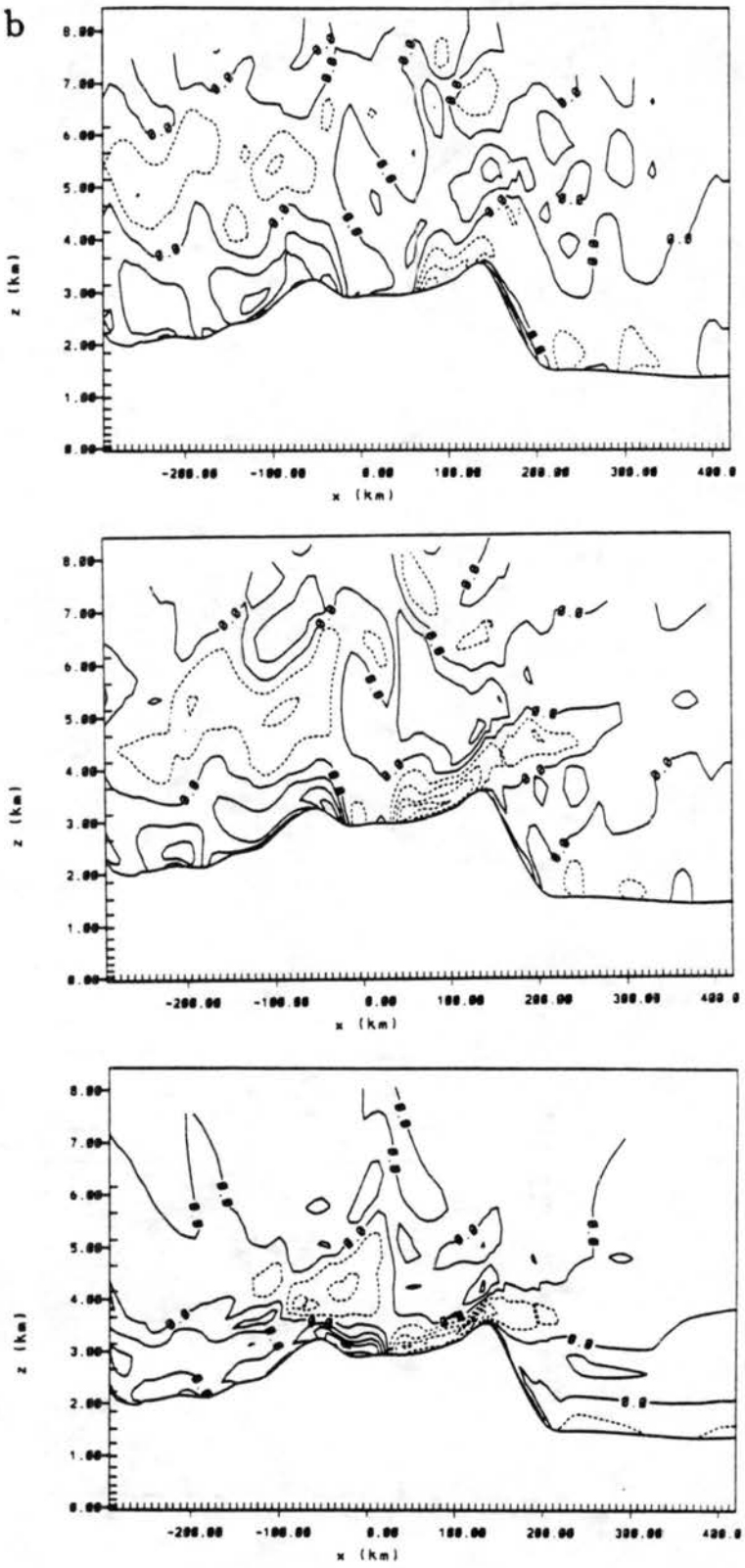

Figure 5.24: Continued.

From this set of experiments, we can deduce that with virtually any configuration of lower tropospheric stratification, intense summer heating of the elevated terrain will result in the development of a mountain-plains solenoid over the crest of the barrier which transforms with the cessation of the diurnal heating cycle into a density current. The initial stratification will determine to some extent the depth and strength of the solencidal circulation, and the depth, strength, and speed of the resulting density current.

5.3.6 Effects of variable ground wetness

Three experiments are conducted over realistic topography in this section, each having different initial soil moisture properties. The purpose of these simulations is to isolate the effect of regional-scale variations in precipitation, and hence soil moisture, on the associated thermally-induced circulation systems. The three simulations shown here include one with dry soil (w_{soil}= 0.15; 15% of capacity) east of the Front Range and wet soil (w_{soil}=0.85) over the intermountain basin and western Colorado. This type of soil moisture variation might be expected with monsoon surges in July or August, which bring moisture from the south or southwest producing strong convective storms and ample precipitation over the mountains and lower elevations of western Colorado, while providing little rainfall over the eastern slope of the Colorado Rocky Mountains and eastern plains. The second simulation features dry soil over western Colorado, with wet soil over eastern Colorado and the eastern slope of the Front Range. This scenario might be expected after a heavy upslope precipitation event over eastern Colorado. In the third experiment, the high terrain of the Rocky Mountains was kept moist, while the eastern and western slopes and lower elevation plains remained dry. This type of condition might prevail early in the summer, when runoff from snowmelt keeps the high mountain peaks and valleys wet, while the lower slopes and plains dry out from intense insolation. All of the simulations are initialized with a realistic summer sounding and zero ambient flow.

The primary effect of increased soil moisture is to partition more of the net radiation into latent as opposed to sensible heating. The can be seen by expanding the terms for H_S and H_L in (1)

$$H_S = \rho C_p C_d u (T_s - T_a) \tag{5.6}$$

$$H_L = \rho L C_d (q_s - q_a) \tag{5.7}$$

where ρ is the air density, C_p is the heat capacity of air at constant pressure, C_d is the drag coefficient, u is the near surface wind speed, T_s is the surface temperature, T_a is the air temperature at, say 10 m, L is the latent heat of vaporization, q_s is the surface mixing ratio, and q_a is the mixing ratio at 10 m. Over wet soil areas q_s will be greatly increased and T_s reduced. The potential temperature for the three simulations after 8 hours of simulation time (1300 MST; Fig. 5.25a) shows the influence of the wet soil region, through a decrease in the slope heating (H_S) and subsequently the depth of the mixed layer over the wet region, while H_L and hence the low level moisture (Fig. 5.25) are increased. The magnitude of the upslope velocity is much reduced over the wet region (Fig. 5.25) in accordance with the lack of sensible heating of the slope. Thus, in the first case where eastern Colorado is dry, we find a strong upslope circulation over the crest of the Front Range, while over the Flat Tops Range the boundary layer becomes very moist, with suppressed solenoid development. Predictably, the situation reverses when the region west of the Front Range is dry. However, in this case the upslope circulation along the eastern slope of the Front Range still maintains fairly strong velocities of over 6 ms^{-1}, which advects copious amounts of moisture up the slope. In the third experiment, boundary layer development over the intermountain region is suppressed, while the circulations over both the eastern and western slopes are strong.

In the evening (2100 MST), the circulations which evolve are vastly different between the three soil moisture variation experiments (Fig. 5.26). With dry conditions along the eastern slope, a deep boundary layer results over the Front Range barrier crest and along the eastern slopes and plains. Over the moist intermountain region and the western slope, boundary layer development is suppressed. This situation reduces the baroclinicity between the eastern slope and the intermountain basin, resulting in a weak, shallow density current which is overshadowed by a stronger westerly density current from the western slope, bringing substantial low-level moisture into the intermountain region. When the west is dry and the eastern slope moist, however, an intense thermal gradient develops along and above the eastern slope of the Front Range, which forces a strong density current into the intermountain basin, shown here to have propagated the length of the basin to the base of the Flat

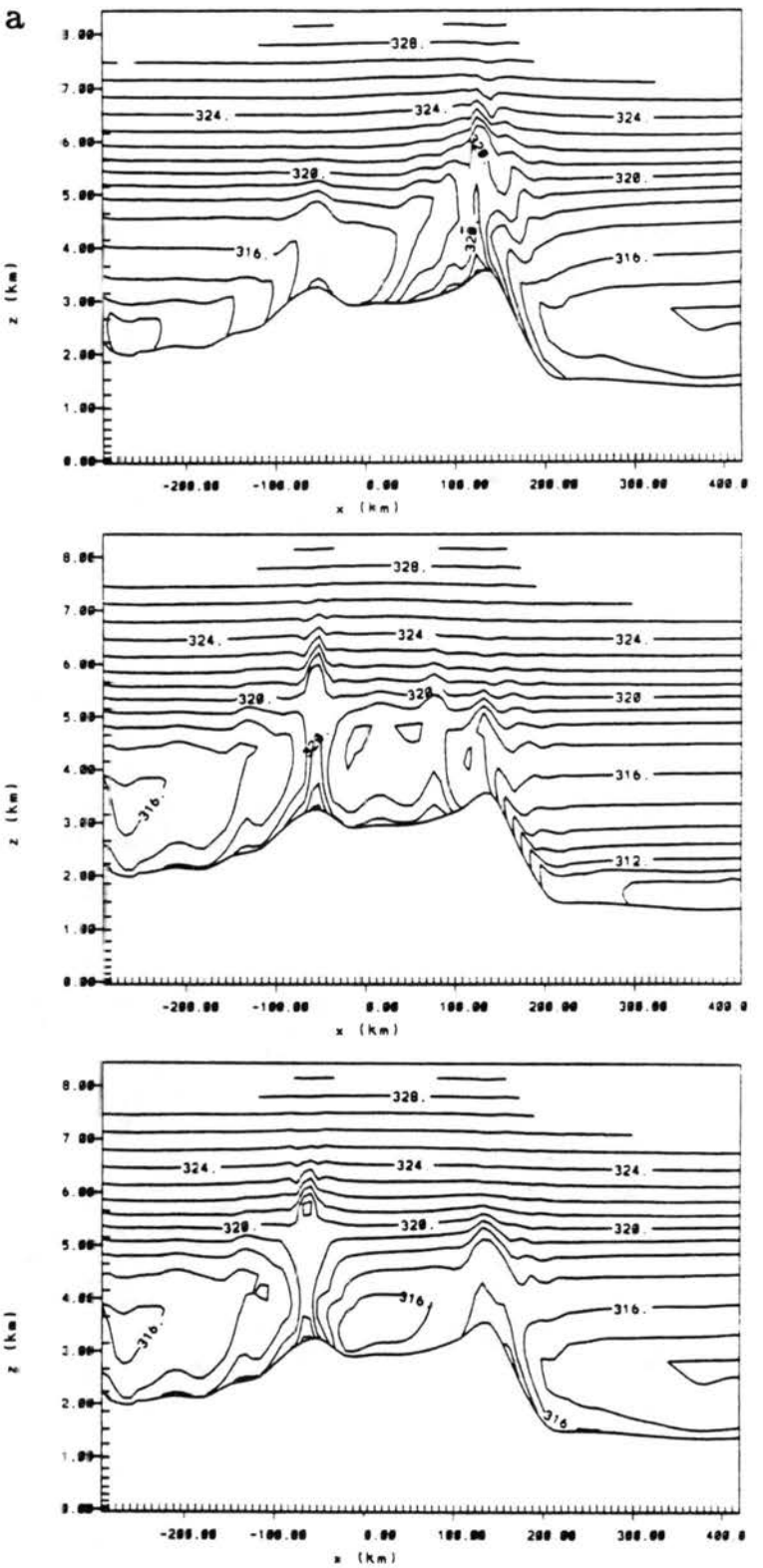

Figure 5.25: Vertical profile of (a) potential temperature (b) total mixing ratio and (c) u-component wind after 8 hours of simulation time for dry east (upper), dry west (middle), and dry lower terrain (lower) initial soil moisture (See text for further details.)

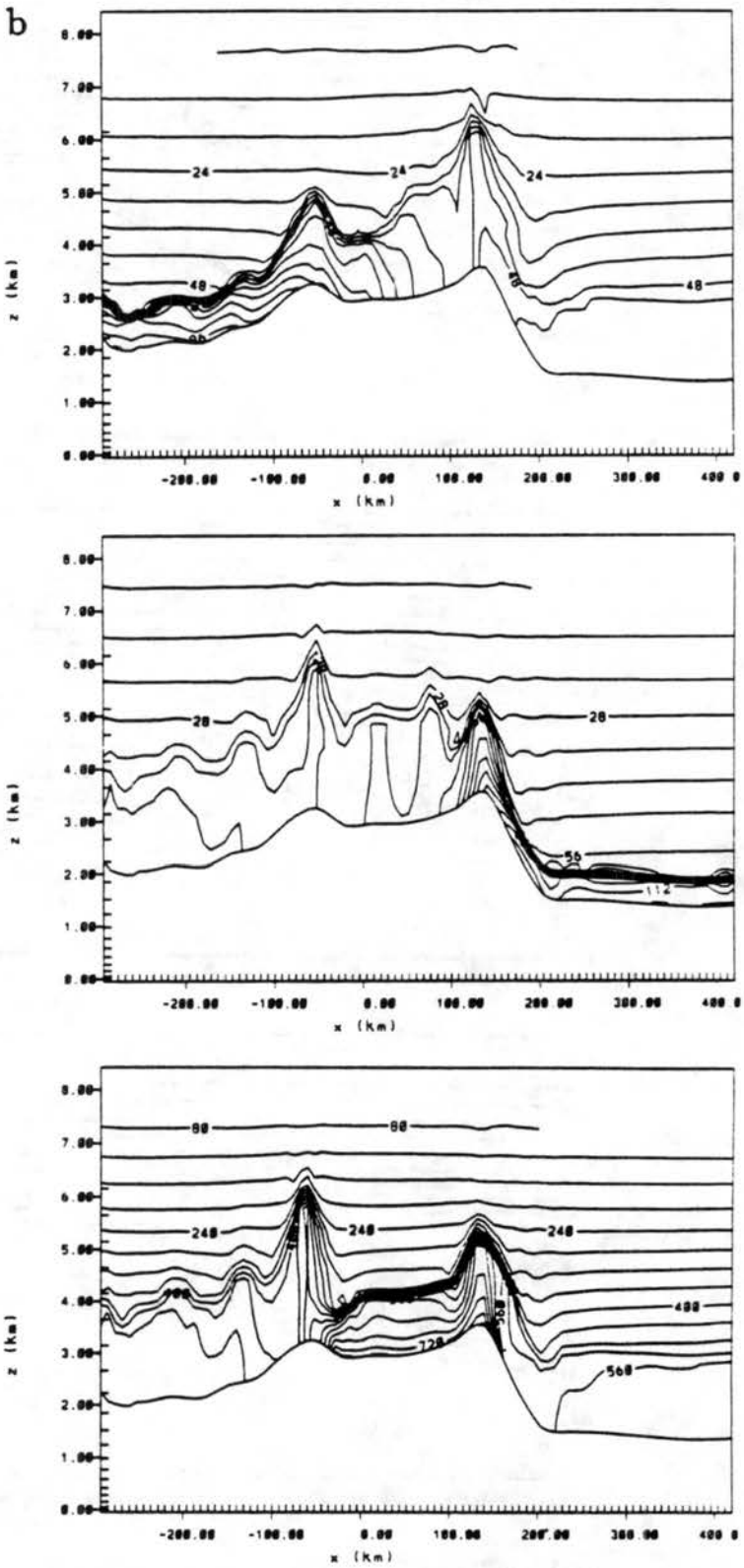

Figure 5.25: Continued.

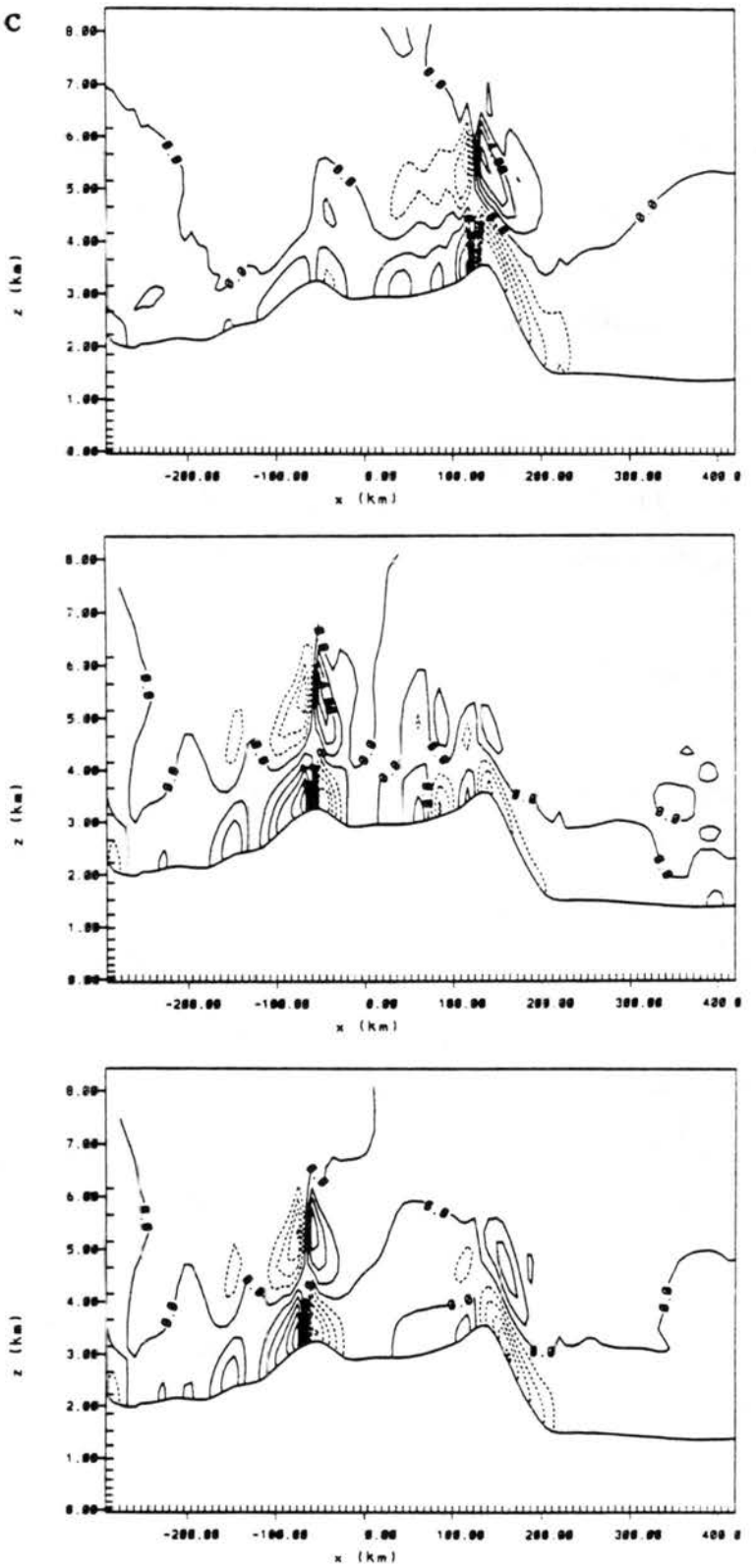

Figure 5.25: Continued.

Tops Range. Behind the head of this density current, southeasterly winds of up to 16 ms^{-1} are found several hundred meters above the surface.

The results shown above are similar to those of Ookouchi *et al.* (1984) who simulated a strong low-level current over flat terrain, which propagates over 100 km from wet (cooler) toward dry (warmer) ground between 1600 and 2400 MST, and evolves an 8 ms^{-1} southerly flow from Coriolis influence. In the present simulation, the current advects an air mass of eastern slope origins westward over the intermountain region. This current contains enough low-level moisture to potentially initiate convection in a region favorable for deep growth, given the mixed layer depth of 6 km msl. In the third experiment with moist high terrain and dry low terrain, we find a peculiar flow structure has evolved. Deep mixing along both slopes and the suppression of the mixed layer depth over the high intermountain region has led to a reversed thermal structure with cooler air over the intermountain region and warmer air along the eastern and western slopes. One symptom of this thermal structure is the westward propagation over the Flat Tops Range of a cool southeasterly density current.

Of course, these idealized experiments can explain only bits and pieces of a very complex situation, and on any given day many of these mechanisms may be superimposed in varying ways to produce a nonlinear circulation response which does not resemble any of the simulations shown herein. However, these idealized runs provide some basis through which we can attempt to understand what controls the formation of the regional-scale wind regimes over the Colorado mountains, and provide a background for interpreting the results of a case day simulation using actual data to initialize the model. This simulation is presented in the next chapter.

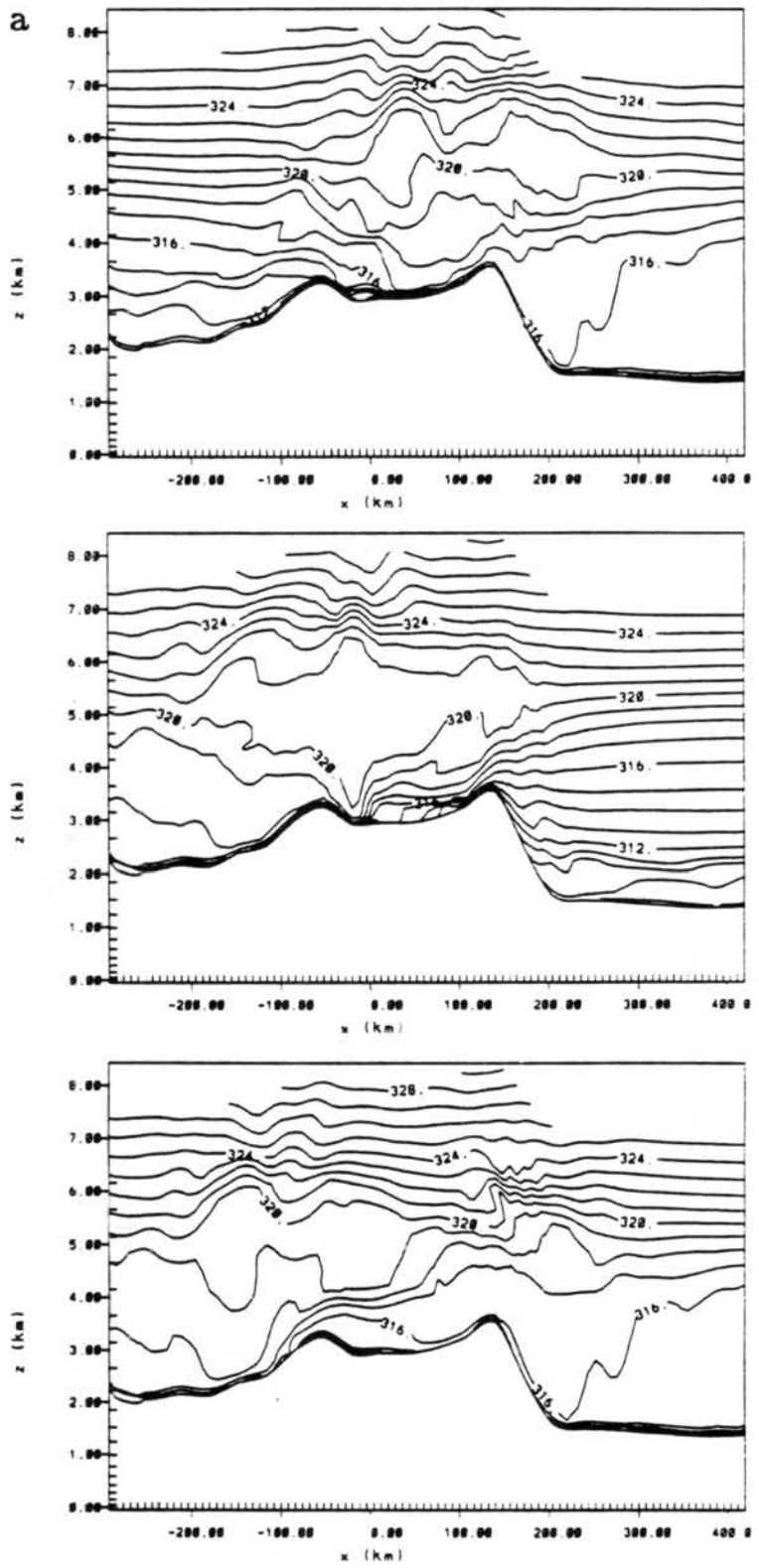

Figure 5.26: As in Fig 5.25, but after 16 hours of simulation time for dry east (upper), dry west (middle), and dry lower terrain (lower) initial soil moisture.

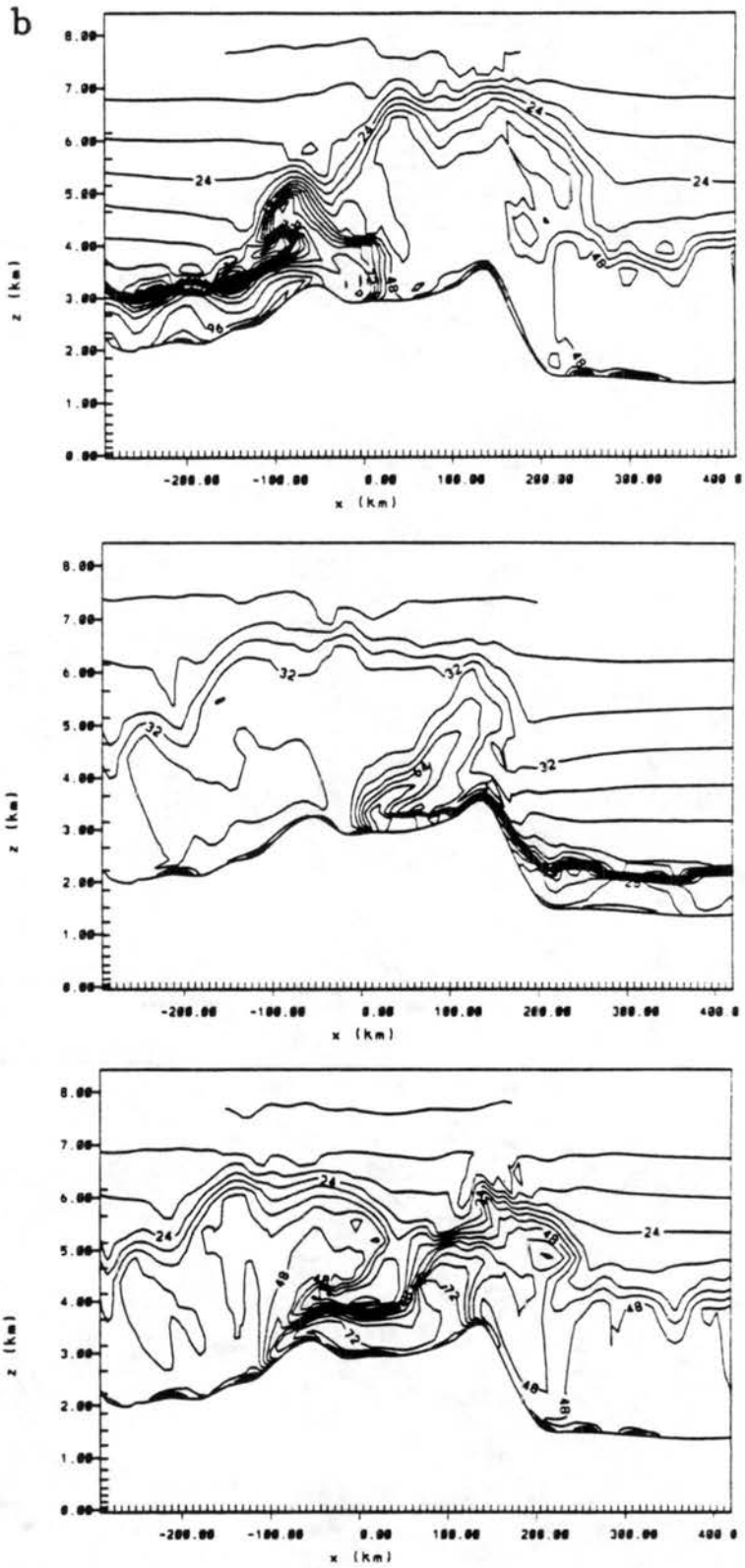

Figure 5.26: Continued.

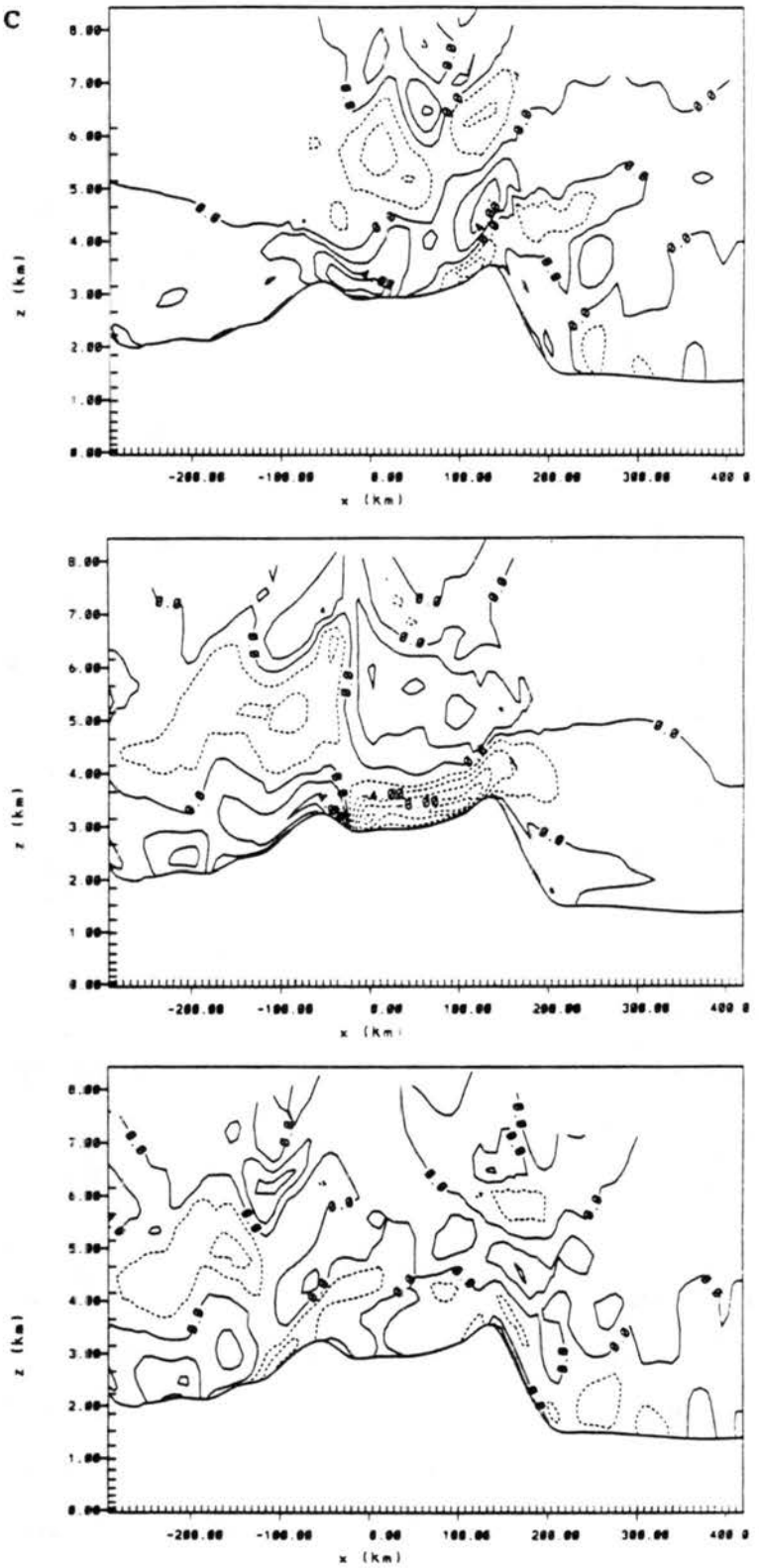

Figure 5.26: Continued.

Chapter 6

CASE STUDY

In an effort to further understand the development of the regional-scale circulation systems described in detail in the previous chapters, a case study day has been selected for initializing numerical simulations. The case day chosen for study is 26 - 27 August 1985. Although this particular day is not a "classic" example of strong southeasterly nocturnal winds over the western slope, it is perhaps the best day, with regards to the number of stations involved in the ROMPEX-85 network, to demonstrate the inflow/outflow pattern characteristic of a strong, regional-scale circulation system over the Colorado mountains. During this case day, a strong ridge of high pressure produced very warm temperatures and relatively low moisture over the Colorado Rocky Mountains. The prevailing dry conditions eliminates effects from strong thunderstorms, allowing an examination of the mesoscale flow response to surface thermal forcing in the presence of weak synoptic flow. Several figures describing the large- and regional-scale conditions which prevailed during this period are presented below.

6.1 Large-Scale Observations

A broad ridge appears at 50 kPa over the western United States at 1200 UTC on 26 August (Fig. 6.1a), which is centered over the Four Corners region, with a deep trough over the Midwest centered over Lake Michigan. Winds over the intermountain west are fairly light (5-15 ms^{-1}), but much stronger over the Midwest and Atlantic seaboard. Weak pressure gradients and generally light and variable winds are found at the surface over the western U.S., in association with the strong upper level ridge. A trailing surface front, associated with a strong low pressure system in central Canada, can be found moving southeastward through Montana.

On the following day, at 1200 UTC 27 August (Fig. 6.1b), the center of the ridge over the western U.S. has moved 200 km to the southeast. The ridge axis has moved through Colorado over this 24-hour period, as noted by the shift from northwest (Fig. 6.1a) to southwest flow at the two rawinsonde stations over the state. Off of the west coast a strengthening trough is moving onshore, enhancing southwesterly flow over the western U.S. The deep trough and closed low over the Midwest has weakened significantly at this time, and is lifting out over New England. The surface chart shows that the trailing front, previously located over Montana, has moved further southward into Wyoming, but appears to be weak and poorly analyzed in this region.

Maximum and minimum temperatures and precipitation which occurred on 26 August are given in Fig. 6.2. In association with the broad upper level ridge, temperatures at the surface stations over the intermountain west were very warm, as much as 9°C above normal at Denver. The precipitation map shows only spotty showers over the southwestern U.S. with no rain recorded at any first-order stations in Colorado. As a further confirmation of the hot, dry conditions which prevailed on 26 August 1985 over Colorado, a cursory examination of the Climatological Data for Colorado revealed this to be one of the warmest summer days over the mountains, with many high altitude stations recording their warmest temperature of the month. In addition, light precipitation was recorded at only 4 stations out of 213 reporting, showing this day to be quite dry.

6.2 Regional-Scale Conditions

6.2.1 Rawinsonde data

The vertical structure over Colorado on 26 August is given in Fig. 6.3 at 1200 UTC for both Denver (DEN) and Grand Junction (GJT), and at 0000 UTC 27 August for GJT. No sounding was available for DEN at 0000 UTC 27 August. The potential temperature at 1200 UTC (Fig. 6.3a) shows a very similar structure between the two stations through the entire sounding. A strong low-level inversion gives way, near the surrounding mountain barrier height ($\sim$ 3200 m), to a weakly stable atmosphere which persists to 8000 m at DEN. The GJT sounding shows an unstable layer between 5000 and 6000 MSL, which appears to be caused by a temperature reading at the 5940 m level (50 kPa) that is too cold, although

a

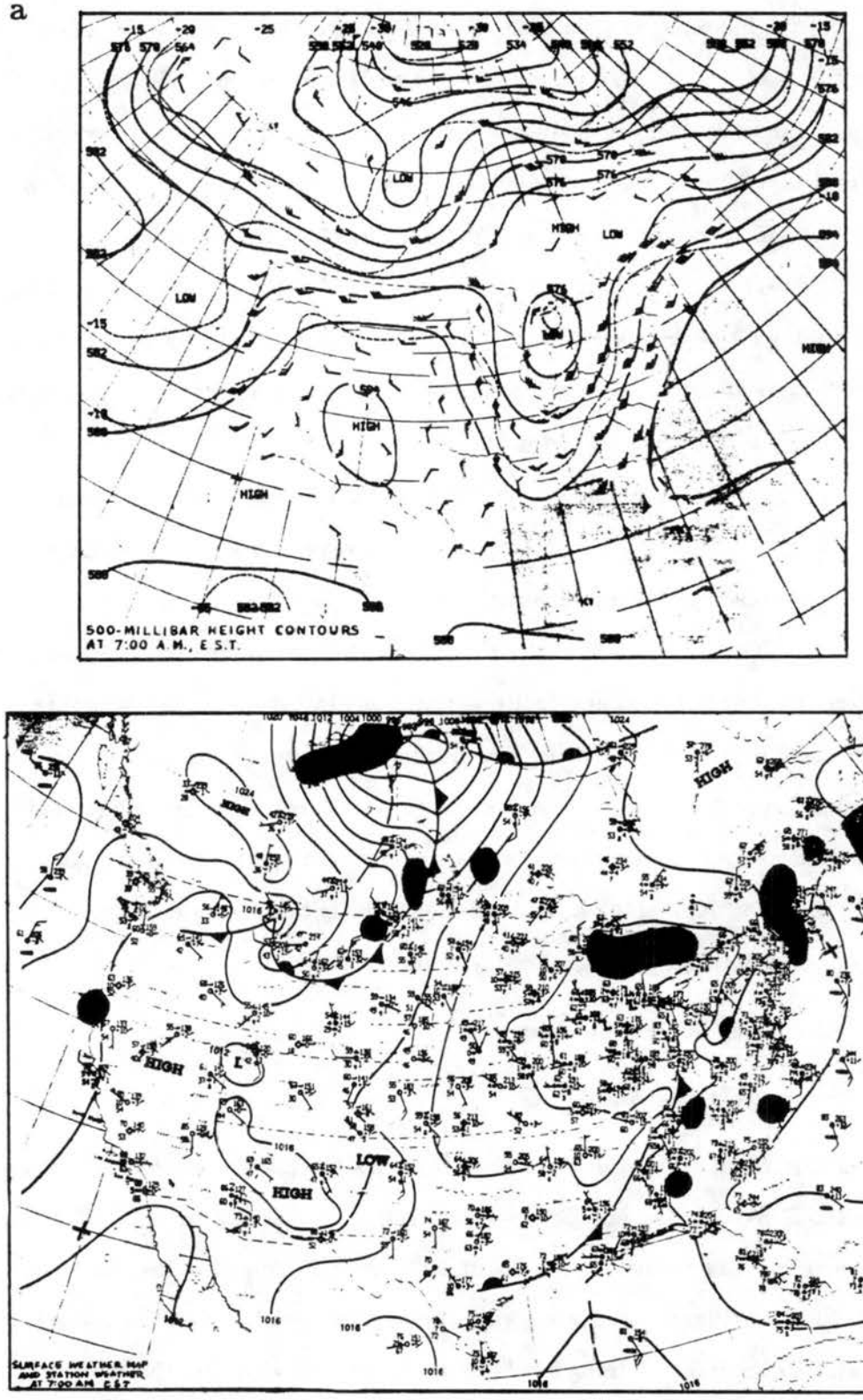

Figure 6.1: Geopotential heights at 50 kPa (upper) and surface pressure (lower) for (a) 1200 UTC (0500 MST) 26 August 1985 and (b) 1200 UTC (0500 MST) 27 August 1985.

b

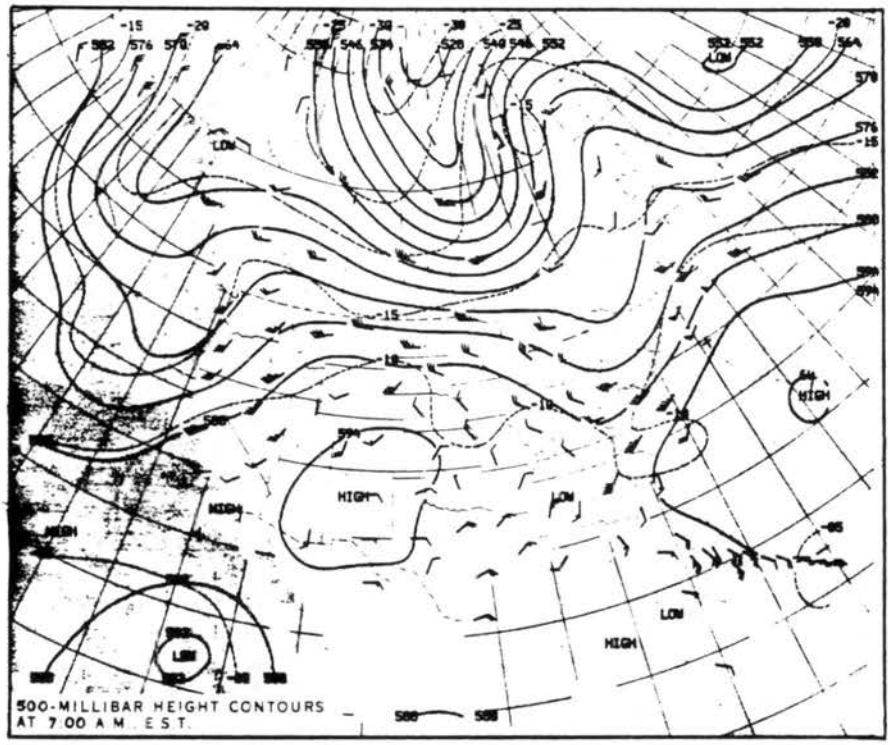

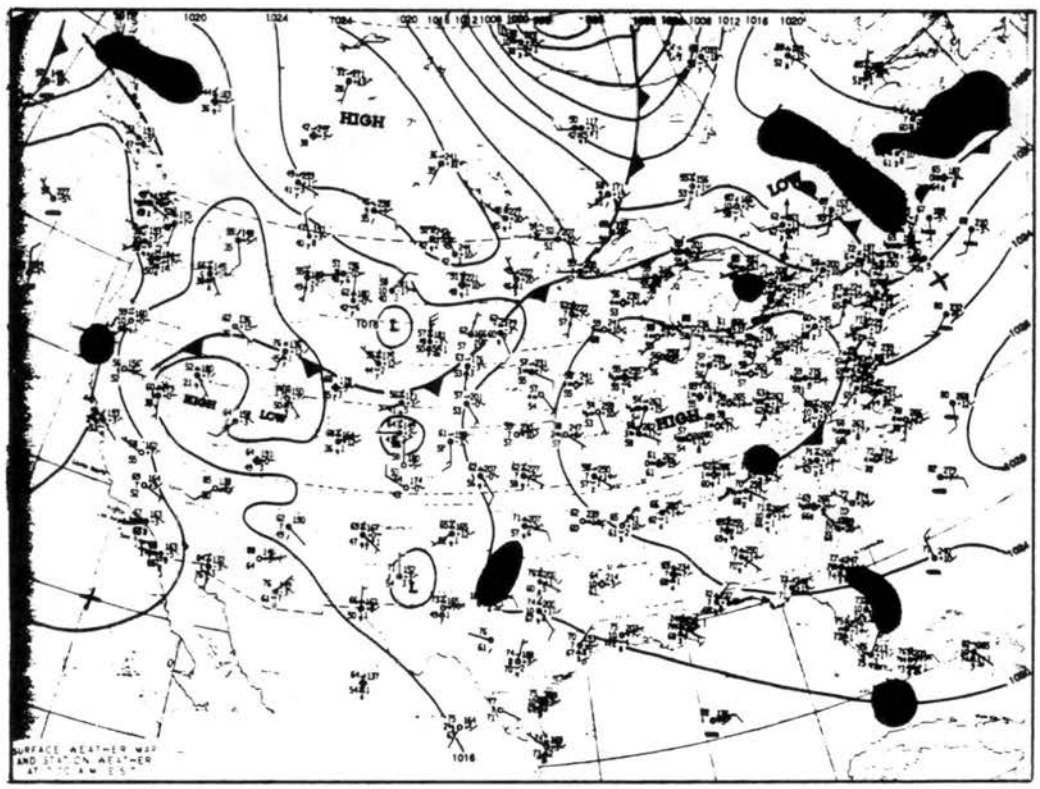

Figure 6.1: Continued.

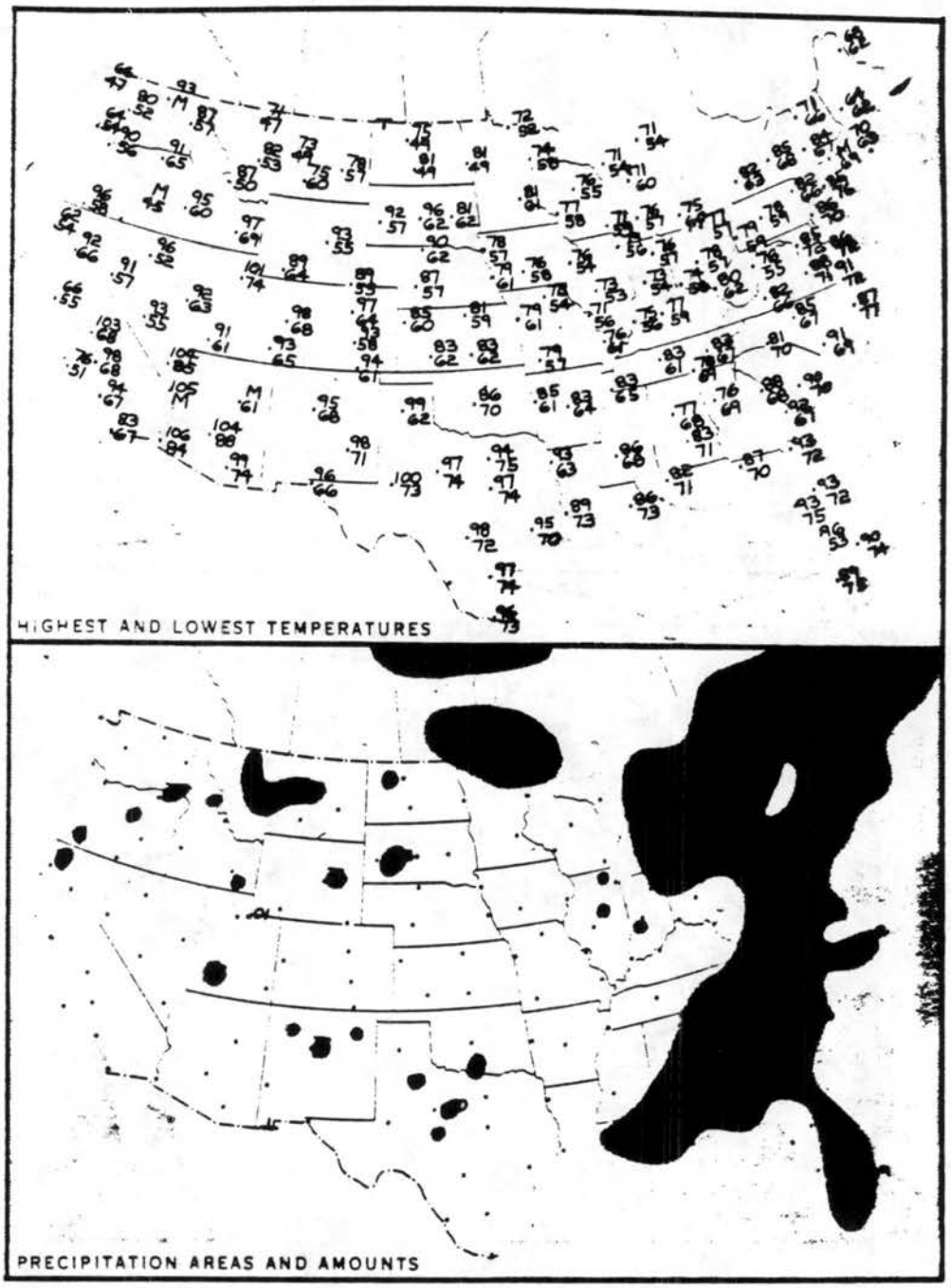

Figure 6.2: Highest and lowest temperatures (upper) and precipitation areas and amounts (lower) over the continental U.S. for 26 August 1985

it passed all data quality checks. Twelve hours later, the 0000 UTC sounding at GJT shows the development of a mixed layer to 5000 MSL, 3500 m above the surface. Above the surrounding mountain level ($\sim$ 3200 m) conditions are largely unchanged from the morning sounding, indicative of fairly stagnant conditions which prevailed under the broad upper level ridge.

The winds at 1200 UTC 26 August (Fig. 6.3b) also show a very similar vertical structure between DEN and GJT, with mesoscale wind systems apparent below 3200 m at each station. These low-level winds generally have speeds of 3-4 ms^{-1}, although a jet of 5.5 ms^{-1} is noticeable at the top of the southeasterly wind layer within the surface based inversion at GJT. A transition to northwesterly flow occurs near the top of the inversion in both soundings, which back toward a westerly direction in the upper troposphere. Wind speeds remain fairly light, at less than 10 ms^{-1} up to the 9000 msl level ($\sim$ 33 kPa). The winds become even weaker in the 0000 UTC GJT sounding with speeds less than 5 ms^{-1} up to 7600 msl, above which stronger westerly flow prevails. Wind direction at 0000 UTC backs from near-surface northwest to southwest flow at 5000 m.

6.2.2 Mountaintop flow structure

Strong thermal heating and the lack of upper level forcing on 26 August 1985 allowed the formation of mesoscale flows over the ROMPEX network, as shown in Fig. 6.4 with averaged daytime and nocturnal wind data. The daytime winds (Fig. 6.4a) show easterly component upslope flow at all of the high mountain stations along the Front Range. Westerly flow prevails at stations west of this mountain barrier. The nocturnal winds over the station network (Fig. 6.4b) show a shift to southwesterly winds at many stations, including those along the Front Range. This wind shift from northwest to southwest flow is consistent with the upper level winds at GJT (Fig. 6.3). However, several stations west of the Front Range in the northern portion of the network (FT, MW, and VA) experience nocturnal winds from a southeast to south direction, while the CB and MP stations show northeasterly flow. This wind direction shift between the daytime and nocturnal wind regimes, particularly noticeable in the northern portion of the network, reveals the characteristic inflow/outflow signature associated with the thermally-forced, regional-scale wind regime discussed extensively in Chapter 4.

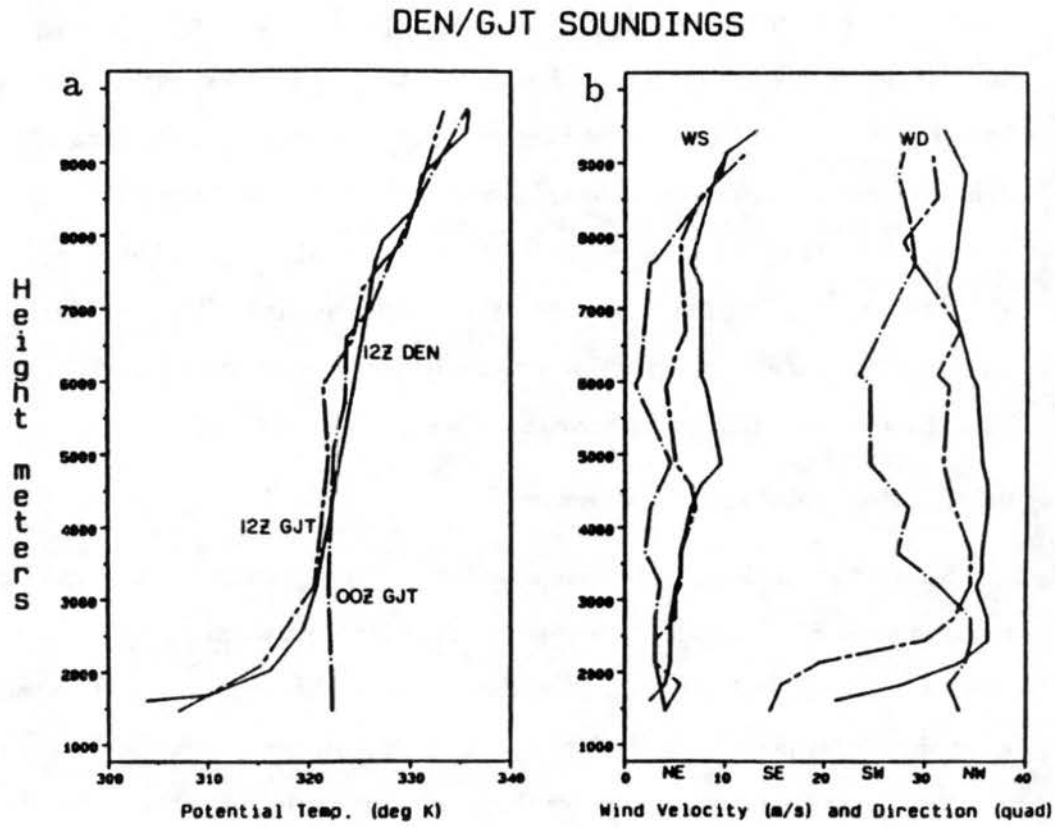

Figure 6.3: Vertical profiles of (a) θ, and (b) wind speed and wind direction at Denver (DEN) and Grand Junction (GJT) for 1200 UTC (0500 MST) 26 August 1985 and 0000 UTC (1700 MST) 27 August 1985.

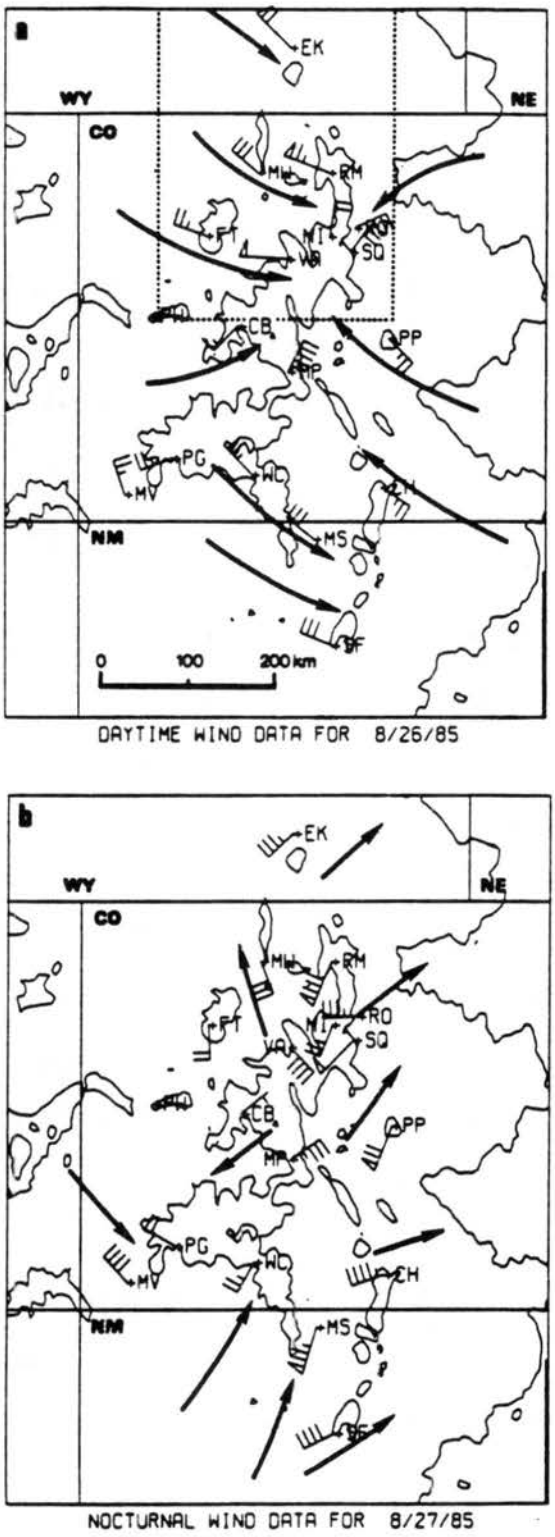

Figure 6.4: Averaged resultant winds over the ROMPEX-85 station network for (a) 1200-1500 MST 26 August 1985, and (b) 0000-0300 MST 27 August 1985. Barb represents 1 ms^{-1} wind speed, flag represents 5 ms^{-1}. Topographic contours are 1500 and 3000 msl.

6.2.3 Mountaintop station time-series

Additional insight into this case study day can be gained through an examination of the wind direction and wind speed time-series of stations located across the northern portion of the ROMPEX network. These time-series span the 24-hour period beginning at 0600 MST (1300 UTC) 26 August and ending at 0500 MST (1200 MST) 27 August. At the two east slope stations of SQ and RO (Fig. 6.5a top), strong westerly flow is evident as heating begins. This downslope wind reaches a maximum of 8.2 ms^{-1} at SQ at 0900 MST (Fig. 6.5b top), after which the wind vector veers at both stations to a more northerly direction in response to thermal forcing of the eastern slope. The wind response to the heating becomes progressively more easterly at SQ and RO during the afternoon, with fairly weak flow speeds between 2-3 ms^{-1}. A gradual veering toward southwesterly flow occurs throughout the late afternoon and early evening, with a slight increase in wind speed. At both stations the winds return to a steady southwest-west direction with stronger flow speeds after midnight on 27 August, completing the diurnal cycle.

To the west of the east slope stations lie three stations at the crest of the Front Range barrier, EK, RM, and MI (see Fig. 6.4). The MI station undergoes a diurnal flow cycle very similar to that of the east slope sites of SQ and RO (Fig. 6.5a middle). The two other stations have strong northwesterly flow until late afternoon (1800 MST), when the wind at RM shifts to southeasterly flow with speeds near 5 ms^{-1} (Fig. 6.5b middle). A similar shift to northeasterly flow occurs at EK at 1900 MST and continues for 3 hours with speeds of 3-4 ms^{-1} before returning to northwesterly flow.

At the four stations located west of the Front Range, westerly upslope flow in the afternoon hours yields to flow with an easterly component in the early evening hours (Fig. 6.5a bottom). This wind shift occurs initially at the FT station (1900 MST). At 2000 MST, the VA and BP stations undergo abrupt flow reversals to northeasterly flow, while at the MW site the wind shifts briefly to a southerly direction at 2300 MST, but then oscillates for several hours before shifting again to steady southeasterly flow at 0100 MST 27 August. This oscillatory wind behavior also occurs for several hours after the initial wind shift at BP and FT, as well. Only the VA station maintains steady southeasterly flow throughout the

nocturnal period, although MW and BP regain steady southeasterly winds during the last several hours of the time-series. Flow speeds (Fig. 6.5b bottom) are fairly light throughout this diurnal cycle at all of the western slope stations except VA, which has relatively strong afternoon westerly flow near 5 ms^{-1} and equally strong southeasterly nocturnal flow.

6.3 Case Day Simulation

The purpose of this simulation is to attempt to simulate the conditions which existed over the north-central Colorado region on an actual day during the ROMPEX-85 experiment on 26 August 1985. If the model is capable of adequately simulating the observed mesoscale conditions, then our confidence in its ability to realistically represent the physics of the flow will be greatly enhanced. However, it is important to keep in mind that the model is still only a crude representation of the actual, very complex topographic situation which exists over the north-central Colorado region and especially over the larger grids which encompass most of the continental United States. The analysis here will concentrate on examining the general features of the simulated flow fields as they compare to the observed situation.

6.3.1 Model initialization

The case day simulation is three-dimensional and uses a latitude-longitude grid configuration with three grids; the coarsest having a 1.0° spacing in latitude and a 1.3° spacing in longitude. This spacing provides an approximately equal latitude/longitude dimension of $\sim$ 111 km at 40°N, i.e. over the region of interest. The next coarsest grid incorporates a 4:1 nesting ratio, which gives an approximate 28 km horizontal resolution at 40°N. The third grid is again at a 4:1 nest ratio from the second grid, providing an approximate grid spacing of 7 km on this finest resolution nest. As in previous simulations, each grid includes topography data, derived with a silhouette averaging scheme, at the given horizontal resolution. The topography used and geographical location of the coarsest grid is shown in Fig. 6.6a, along with the simulated near surface winds. The second and third grids are the same as those used in the previous three-dimensional simulation with zero ambient wind, and are shown in Fig. 5.1. The coarse grid has 30 grid points in the x-direction and 30 in the y-direction, thus it spans $\sim$ 3190 km in the west-east direction at 40°N from 200 km

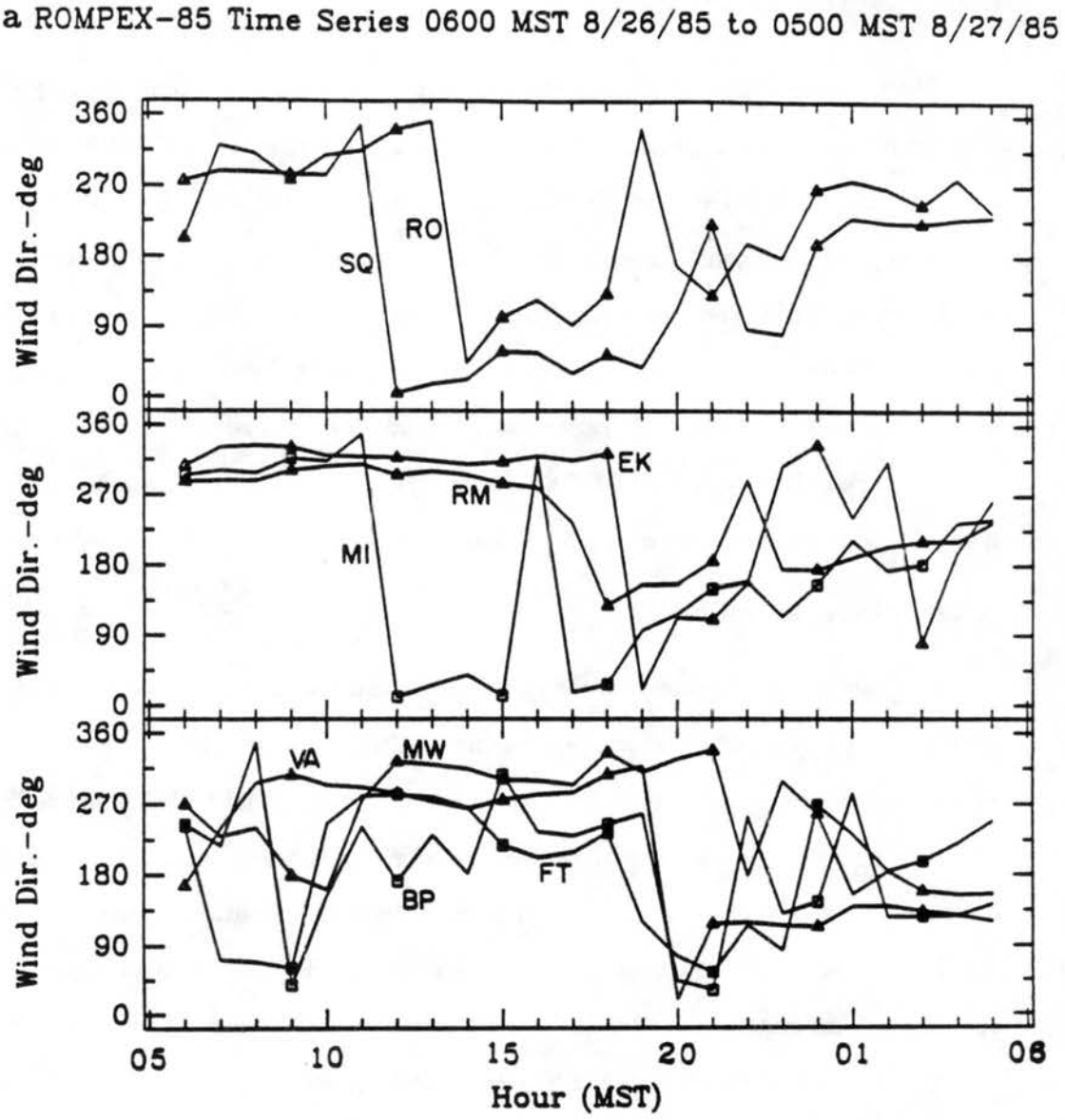

Figure 6.5: Time-series of (a) wind direction and (b) wind speed for selected ROMPEX-85 stations from 0600 MST 26 August 1985 to 0500 MST 27 August 1985.

b ROMPEX-85 Time Series 0600 MST 8/26/85 to 0500 MST 8/27/85

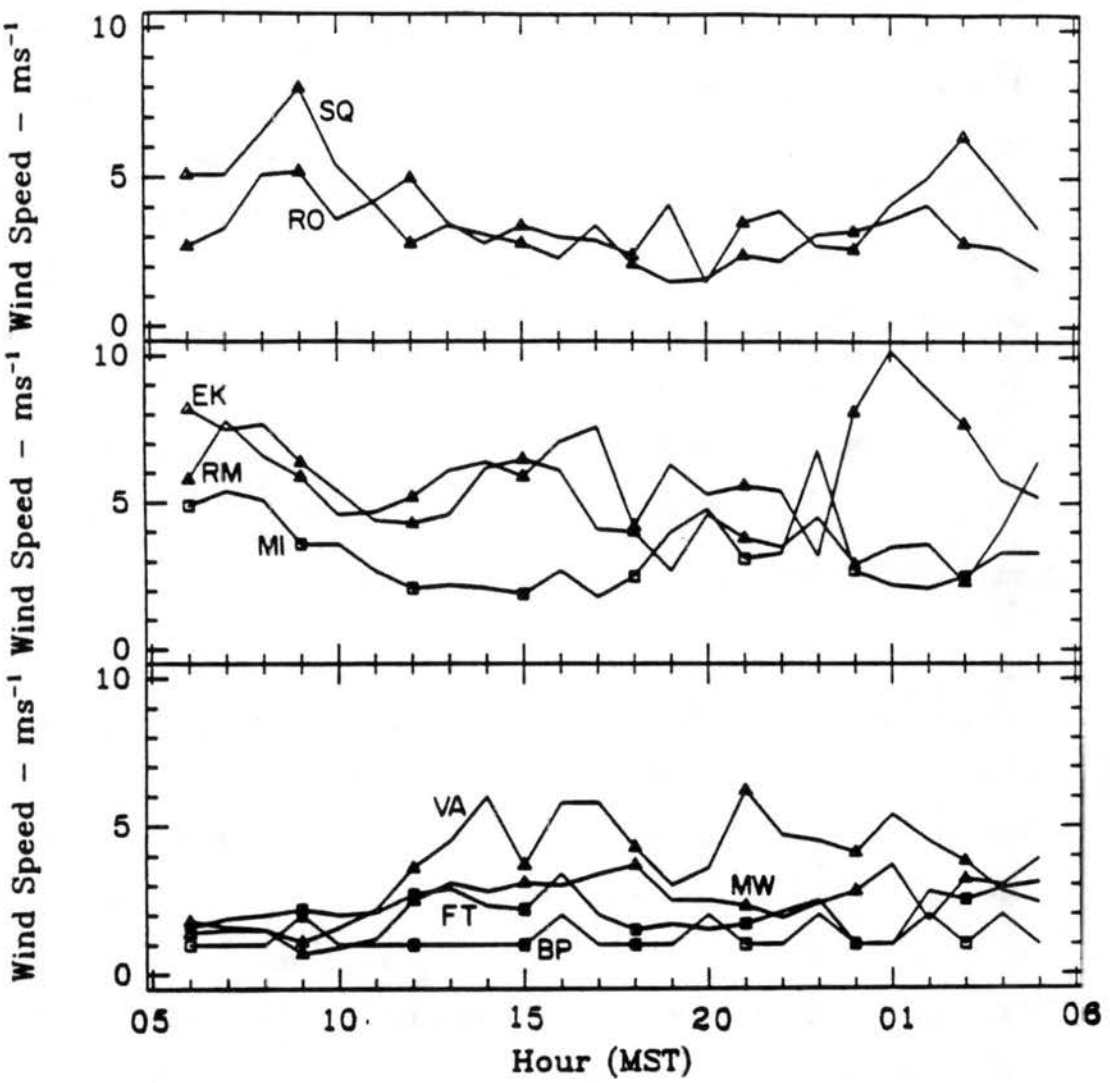

Figure 6.5: Continued.

west of the Pacific Coast in California (125°W) to central Indiana (86°W). In the north-south direction, the coarse grid extends 3190 km from central Mexico at 24°N to central Canada at 53°N. The two nested grid boundaries, along with the vertical grid spacing and number of levels are as described in section 5.2.1. Radiative lateral boundary conditions are employed following Klemp and Wilhelmson (1978a,b).

The model simulation is initialized via an objective analysis scheme, following Barnes (1973), which is assimilated from the National Meteorological Center (NMC) 2.5° gridded data and standard rawinsonde and surface data observations, onto the coarse model grid. The nested grids are then initialized by interpolation from the coarse grid. For this case study, the model is initialized with data from 0000 UTC 26 August 1985. The simulation begins at this time, and is then run until 1200 UTC 26 August 1985, during which time simulated radiational cooling over the complex model terrain produces low-level stratification which is more realistic than would be possible from standard initialization techniques. The boundary values are nudged via a linear interpolation throughout the 12-hour simulation towards the objectively analyzed data at 1200 UTC 26 August 1985.

6.3.2 Model initial fields

Of interest for this case study is the 24-hour diurnal period beginning at 1200 UTC 26 August 1985. The simulated initial state at 1200 UTC 26 August 1985 is shown in Fig. 6.6. The simulated upper-level flow is depicted in Fig. 6.6a at z = 5.65 km above the terrain surface. Although this is not a constant height surface, the presence of a well-defined upper-level ridge is clearly shown, centered over the Four Corners region of the southwestern United States. The location of this anticyclone, the jet stream across the U. S./Canada border, and the strong northerly flow over the midwestern U.S. are all in reasonable agreement with the 50 kPa height field shown in Fig. 6.1a for the same time. The near surface streamlines (Fig. 6.6b) and potential temperature field (Fig. 6.6c) on the coarse grid reveal the presence of a frontal system moving across the upper Midwest, with northerly flow behind the system over eastern Montana. This strong front is associated with a baroclinic wave embedded within the strong upper level flow across the U.S./Canada border, as seen in Fig. 6.1a. The model appears to be somewhat fast with the movement

of this frontal system, showing its location to be $\sim$ 200 km east and south of its position in the analysis. The low-level anticyclonic circulation over eastern Kansas and Oklahoma agrees well with the observations, as does the cyclonic flow near the Great Lakes.

Over the central Rocky Mountains westerly flow is simulated, with lee troughing along the Front Range, which is also evident in the surface analysis. The potential temperature field over the coarse grid domain (Fig. 6.6c) shows warmer air over the elevated plateau of the intermountain west. The near-surface mixing ratio (Fig. 6.6d) reveals that conditions are fairly dry over much of the western U.S. with a strong moisture gradient along the Colorado Front Range. Moist conditions prevail throughout the southern portion of the model domain, with very high values off of Baja California associated with a hurricane.

A look at the near surface wind field with the increasing resolution provided by the finer grids is shown in Fig. 6.7. While primarily westerly flow over Colorado is resolved on the coarse grid (Fig. 6.6b), the second grid (Fig. 6.7a) shows that much of the low-level flow goes around the Colorado mountain massif on the western slope, while weak flow prevails in the South Platte and Arkansas River valleys. The highest resolution is provided by the third grid (Fig. 6.7b) which shows even more structure to the low-level flow within the complex terrain of the central Rocky Mountains. Very strong downslope flow is simulated over the Colorado Front Range on the third grid, with a maximum of 19.4 ms^{-1} at this 278.8 m level. These winds appear to be excessive, although data from the ROMPEX surface network for this day (Fig. 6.5) do show brisk winds of 5-8 ms^{-1} from a west to northwest direction at stations along and at the top of the Front Range (SQ, RO, EK, RM, MI).

6.3.3 Simulated daytime circulations

To study in more detail the evolution of the regional-scale flow throughout the diurnal cycle from 0500 MST 26 August to 0500 MST 27 August 1985, plan views are presented of the highest resolution grid for both the near surface vector wind and streamline fields. These plots will serve to illustrate the flow development, as well as provide a comparison for actual observations. Plan view figures will be supplemented with vertical cross-sections of the model domain at appropriate time intervals to observe the various phases of the regional-scale flow evolution on this particular case day.

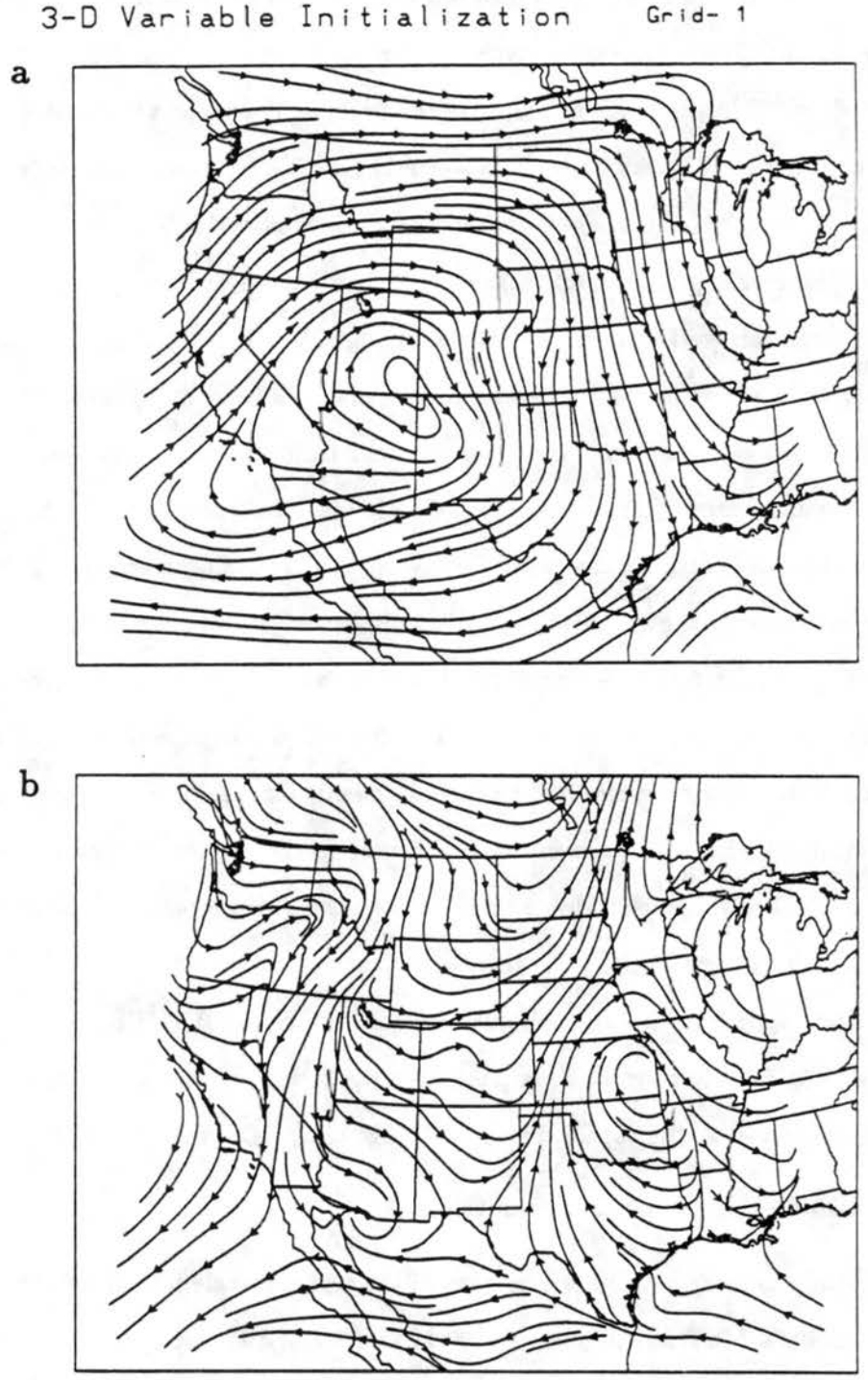

Figure 6.6: Case study day initial (a) streamlines at 5.65, and (b) streamlines at 0.28 km, (c) potential temperature every 2°C at 0.28 km, and (d) total mixing ratio (x 10^5 every 0.001 g/kg at 0.28 km above the surface on Grid 1 at 1200 UTC (0500 MST) 26 August 1985.

c

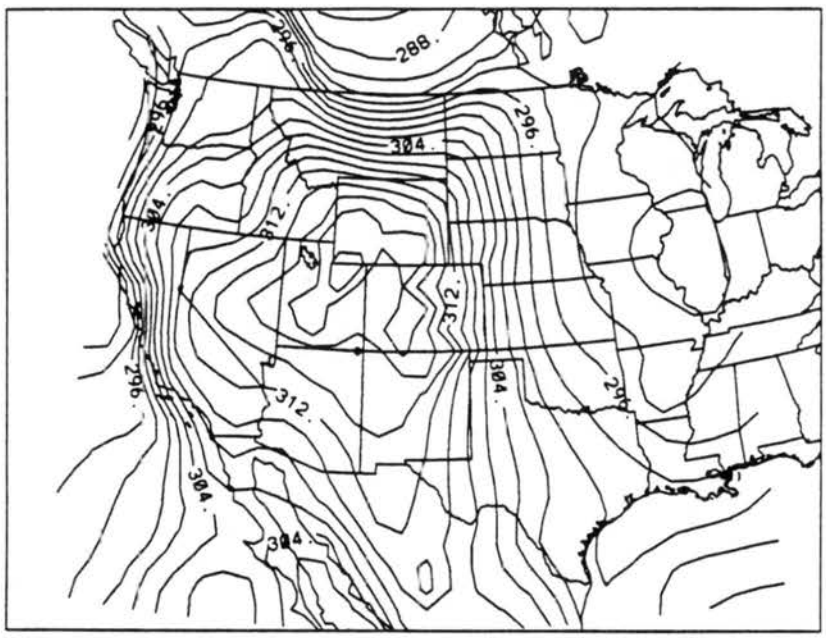

d

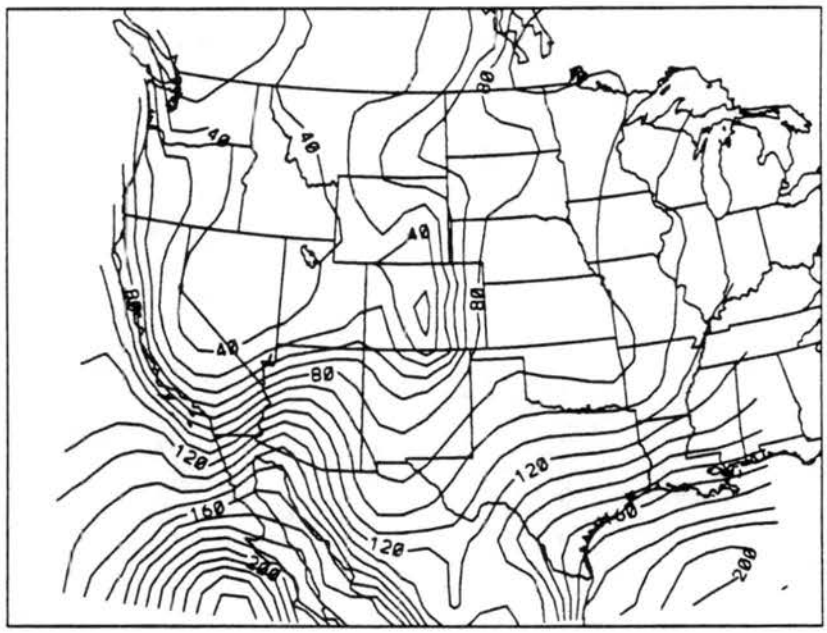

Figure 6.6: Continued.

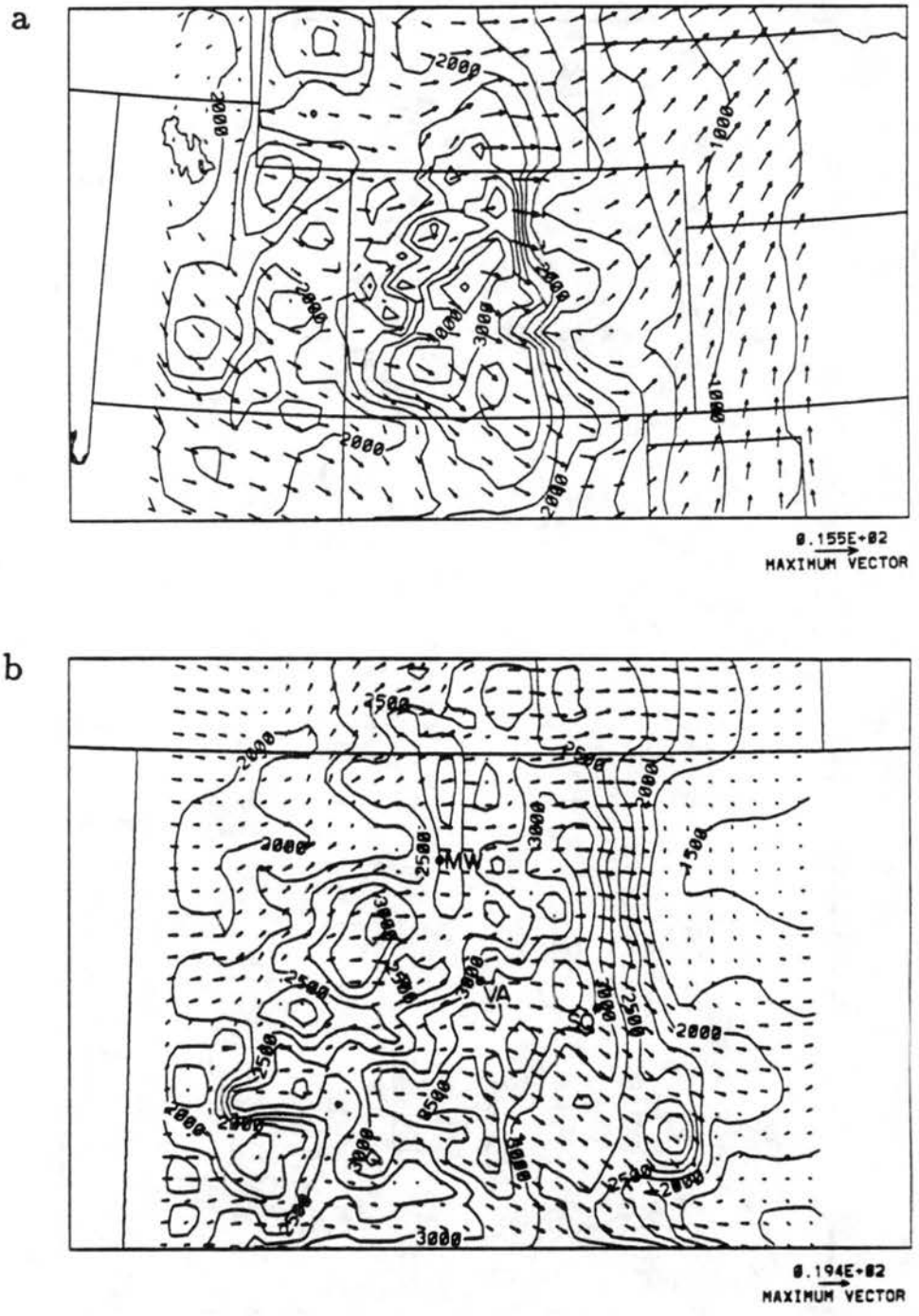

Figure 6.7: Wind vectors on (a) Grid 2 and (b) Grid 3 at 0.28 km above the surface for 1200 UTC (0500 MST) 26 August 1985. Locations of the Mount Werner (MW), Vail Mountain (VA), and Squaw Mountain (SQ) stations indicated for reference.

The near surface flow after four hours of simulation time is shown in Fig. 6.8a. The figure shows primarily westerly flow over the north-central Colorado mountain region, with an anticyclonic turning of the winds over the high mountain barrier, and troughing in the lee of the barrier. The low-level flow is especially strong over the eastern slope of the Front Range. Stable northwesterly flow over the Front Range generates a mountain wave disturbance and strong downslope flow. This mechanism is still apparent at 0900 MST, well after the onset of daytime insolation (Fig. 6.9). However, by this time the wave feature is gradually being dissipated by the development of easterly upslope flow within a shallow heated boundary layer along the slope surface (Fig. 6.9b). The convergence of low-level flow towards the mid-slope heat maximum is apparent in the 0900 MST streamline plot all along the northern Front Range. (Fig. 6.8b). Other regions located west of the Front Range, show only a slight veering of the wind towards an upslope direction by 0900 MST.

Thus far, the simulated flow field resembles the mountaintop surface observations fairly well (see Figs. 6.5a, b), with all stations along the east slope and at the crest of the Front Range maintaining strong west-northwest flow through the early morning hours, which decrease in speed along the barrier crest during the late morning, while stations over the west slope show much weaker velocities in both the simulation and the observations, with the southwesterly wind direction at MW and west-northwest flow at VA in good agreement.

The plan views four hours later, at 1300 MST (Fig. 6.10), reveal the intensification of the eastern slope upslope circulation, the progression of the convergence line associated with this circulation up to the crest of the Front Range, and the dramatic decrease in the strong westerly flow over the Front Range during this late morning/early afternoon period. The upslope circulation is the low-level branch of a deep mountain-plains circulation which is prevalent along the entire north-south extent of the Colorado Front Range, both in the simulation and in the ROMPEX observations (see Fig. 6.4). The observed late morning rotation of the wind vector at the two east slope stations of RO and SQ from westerly to northwesterly and then to a northeasterly direction by 1300 MST agrees well with the simulated streamline field which shows a wind rotation in a similar fashion as the upslope flow progresses steadily westward towards the barrier crest.

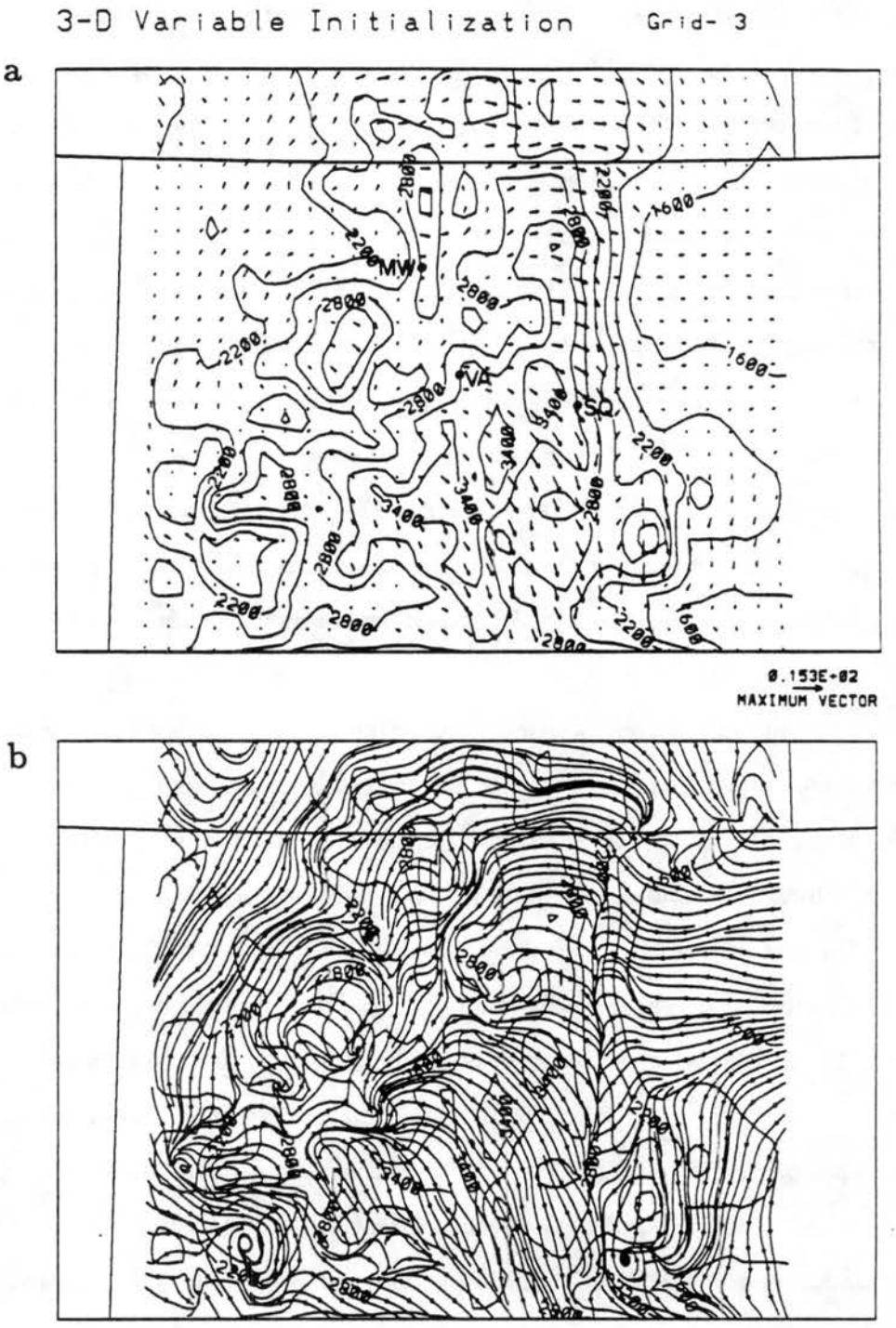

Figure 6.8: Case study (a) wind vectors and (b) streamlines on Grid 3 at 0.28 km above the surface for 1600 UTC (0900 MST) 26 August 1985. Locations of the Mount Werner (MW), Vail Mountain (VA), and Squaw Mountain (SQ) stations indicated for reference in (a).

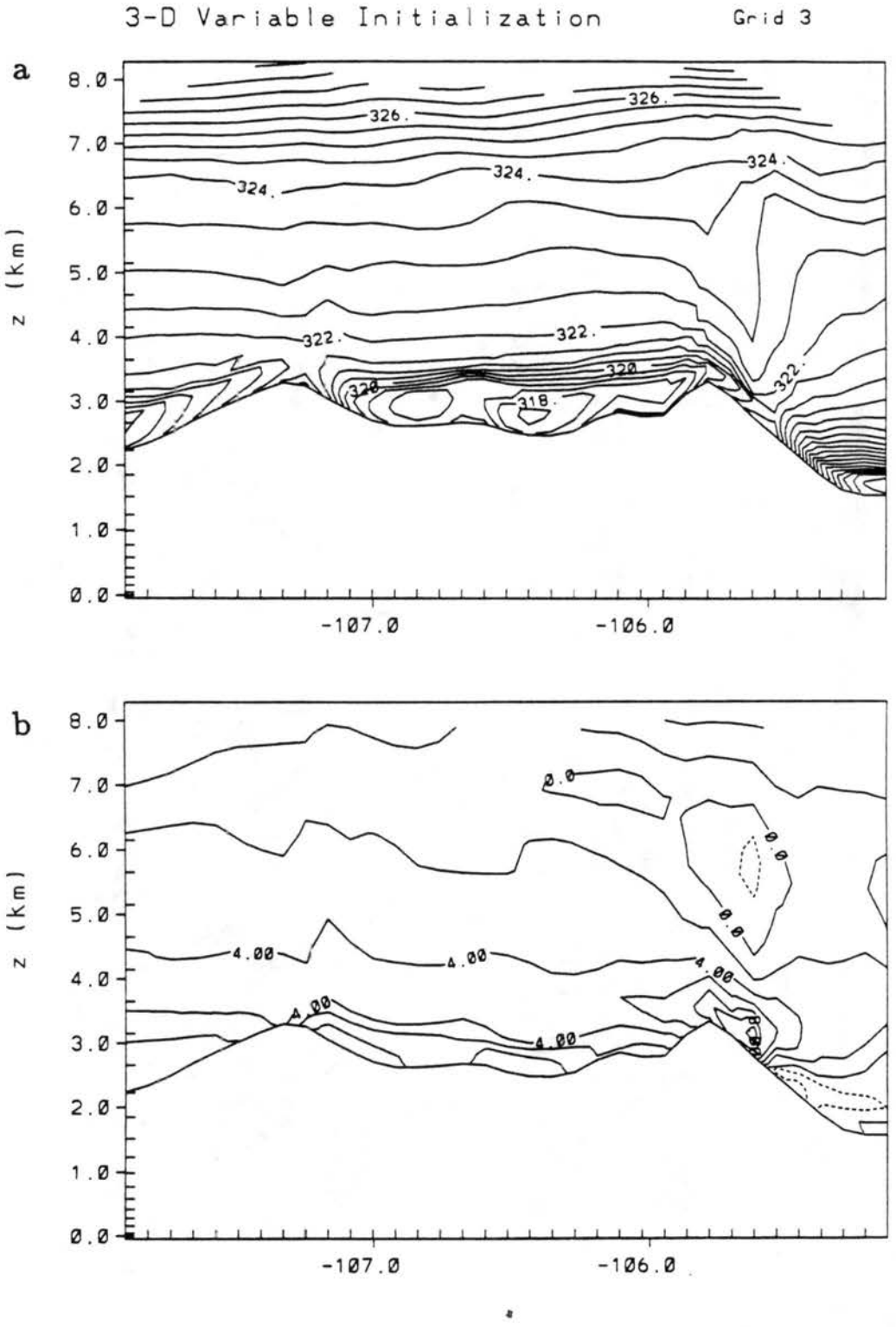

Figure 6.9: Case study (a) potential temperature and (b) u-component wind velocity profiles on Grid 3 at 40.0°N for 1600 UTC (0900 MST) 26 August 1985.

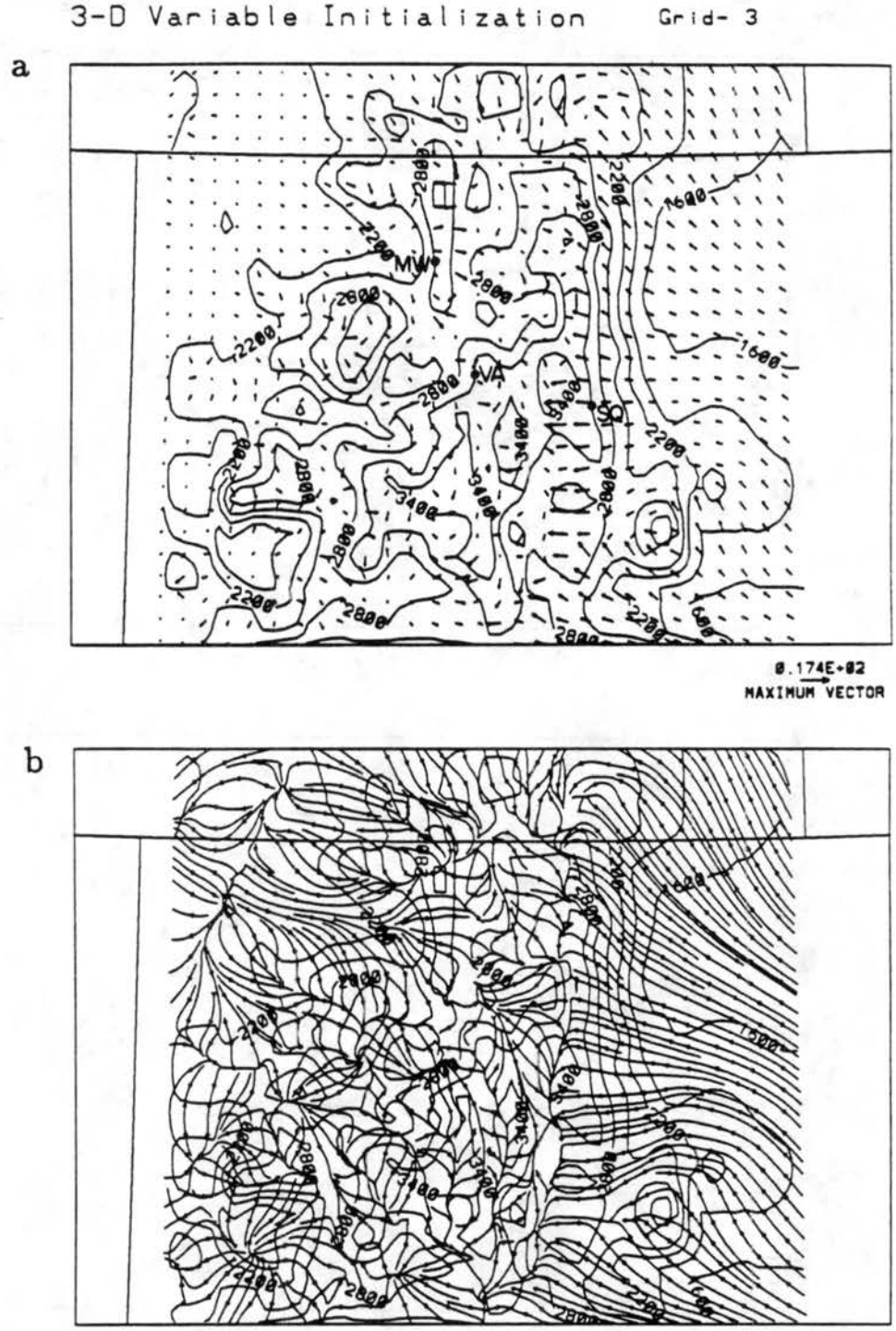

Figure 6.10: Case study (a) wind vectors and (b) streamlines on Grid 3 at 0.28 km above the surface for 2000 UTC (1300 MST) 26 August 1985. Locations of the Mount Werner (MW), Vail Mountain (VA), and Squaw Mountain (SQ) stations indicated for reference in (a).

The time of arrival of the upslope at the SQ and MI stations is fairly well simulated, as easterly winds pass these stations between 1100 and 1200 MST. However, at RO, lower in altitude than either SQ or MI, the easterlies were observed to arrive much later at 1400 MST. Local influences surely play a role in these arrival times. As was noted in Chapter 4, SQ nearly always leads RO in upslope onset time, despite being 750 m higher. The fact that SQ is located on the southern ridge of Clear Creek Canyon, while MI is at its head, is significant. This deep, narrow valley, unresolved in the simulation, should produce its own upvalley circulation, augmenting the penetration of the general mountain-plains circulation towards the barrier crest in its vicinity. The RO station, on the other hand, is located on the general slope of the Front Range and does not receive this additional mesoscale forcing. While here speculative, these types of local influences undoubtedly play a substantial role in determining the local wind climate of a particular site, but are very difficult to determine accurately in practice, and generally unresolvable in all but the most detailed of numerical models.

West of the Front Range, convergent upslope flow can be found over most of the prominent intermountain ranges within the simulation domain by 1300 MST, with divergent near-surface flow over the larger valleys and intermountain basins. Concurrent with this divergent flow pattern out of the large valleys the simulated wind vector at MW rotates from weak westerly to stronger northwesterly flow, similar to observations. The VA station is simulated to be in a region of westerly flow, as observed, while the FT site is simulated in a region of steady northwesterly flow, whereas the observations show westerly.

A vertical cross-section of the model domain through 40.0°N at 1300 MST provides another perspective upon the thermally-induced circulations (Fig. 6.11). By this time the 1.5 km deep easterly upslope circulation along the Front Range has eliminated the strong westerly flow from the previous morning, as evidenced by the -12.3 ms^{-1} u-component winds near the top of the Front Range barrier (Fig. 6.11a). Strong upslope flow is also evident over the Flat Tops Range in western Colorado from a westerly direction. Northerly winds, characteristic of the upper level flow, are still evident over much of the intermountain basin above the surface (Fig. 6.11b). The ascending branch of the Front Range mountain-plains solenoid is clearly evident in the w-component (Fig. 6.11c), while a broad region of

strong ascending motion over the Flat Tops Range is associated with an east-west running convergence zone, clearly seen in the streamline plan view for this time (Fig. 6.10b), through which this particular cross-section slices. Air from near the surface is entrained within these strong ascending currents and carried to nearly 8 km over the Flat Tops Range. (Fig. 6.11d). While this was a fairly dry day, with only on the order of 4 gkg^{-1} of water vapor available near the surface, ascent to this level would have resulted in a 2-3 km deep cumulus cloud, although such a process was not included in the simulation. The potential temperature field (Fig. 6.11e) shows that a very deep boundary layer exists in the vicinity of the ascending circulations, while over the rest of the domain boundary layer depths are on the order of 1.5 km. As seen in the three-dimensional simulation with zero ambient flow, baroclinic zones exist along each principal slope of the mountain barrier, with that along the east slope of the Front Range particularly pronounced.

The general lower tropospheric regional-scale flow pattern at 1300 MST looks quite similar to the afternoon circulation in the previous three-dimensional simulation, which featured a quiescent ambient state. This demonstrates the influence of thermal forcing over this complex topography region in controlling the wind patterns on a diurnal time-scale, particularly given the very different initial states between these two simulations.

6.3.4 Large-scale influences

By comparing the 1200 UTC 26 August 1985 simulated fields on the various grids (Fig. 6.6) with similar fields at 0000 UTC 27 August 1985 (1700 MST), we can begin to understand the role of terrain heating on wind circulations of meso- to synoptic-scale proportions. While flow away from the high topography of the intermountain west (the Western Plateau) was evident in the near surface wind field at 1200 UTC (Fig. 6.6b), a similar figure at 0000 UTC (Fig. 6.12a) shows that the low-level winds over much of the intermountain region have shifted to a direction into the Western Plateau, with convergent flow over most of the embedded high mountain areas. This type of large-scale, diurnally-reversing outflow/inflow pattern has been diagnosed in a climatological study by Reiter and Tang (1984) who attributed this effect to heating of the elevated Western Plateau area on a diurnal temporal scale. In this simulation, this wind shift response is especially prominent

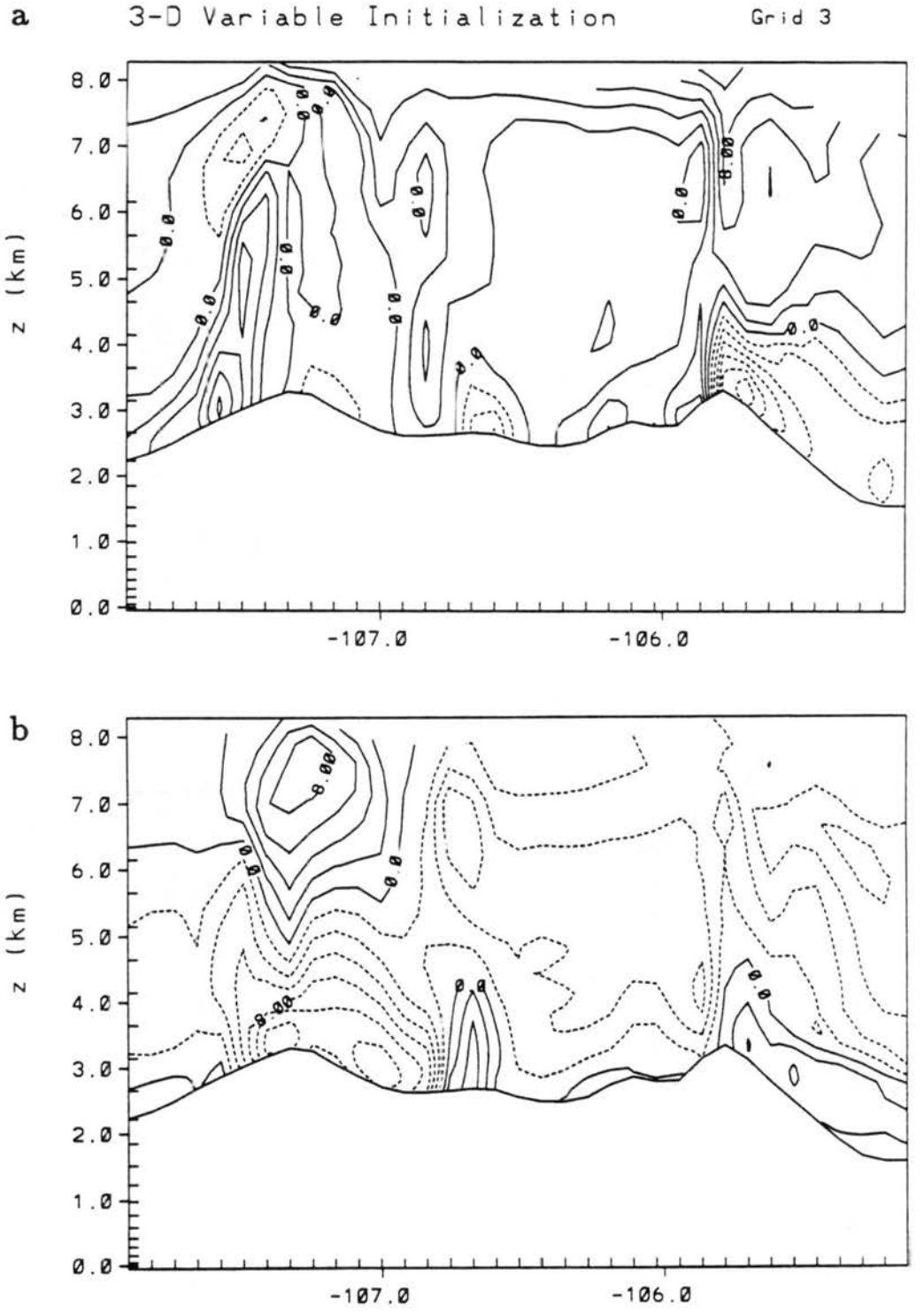

Figure 6.11: Vertical profiles of (a) u-component every 2 ms^{-1} (b) v-component every 2 ms^{-1} (c) w-component every 0.2 ms^{-1} (d) total mixing ratio (x 10^6) every .0002 g/kg and (e) potential temperature every 2°C on Grid 3 at 40.0°N for 2000 UTC (1300 MST) 26 August 1985.

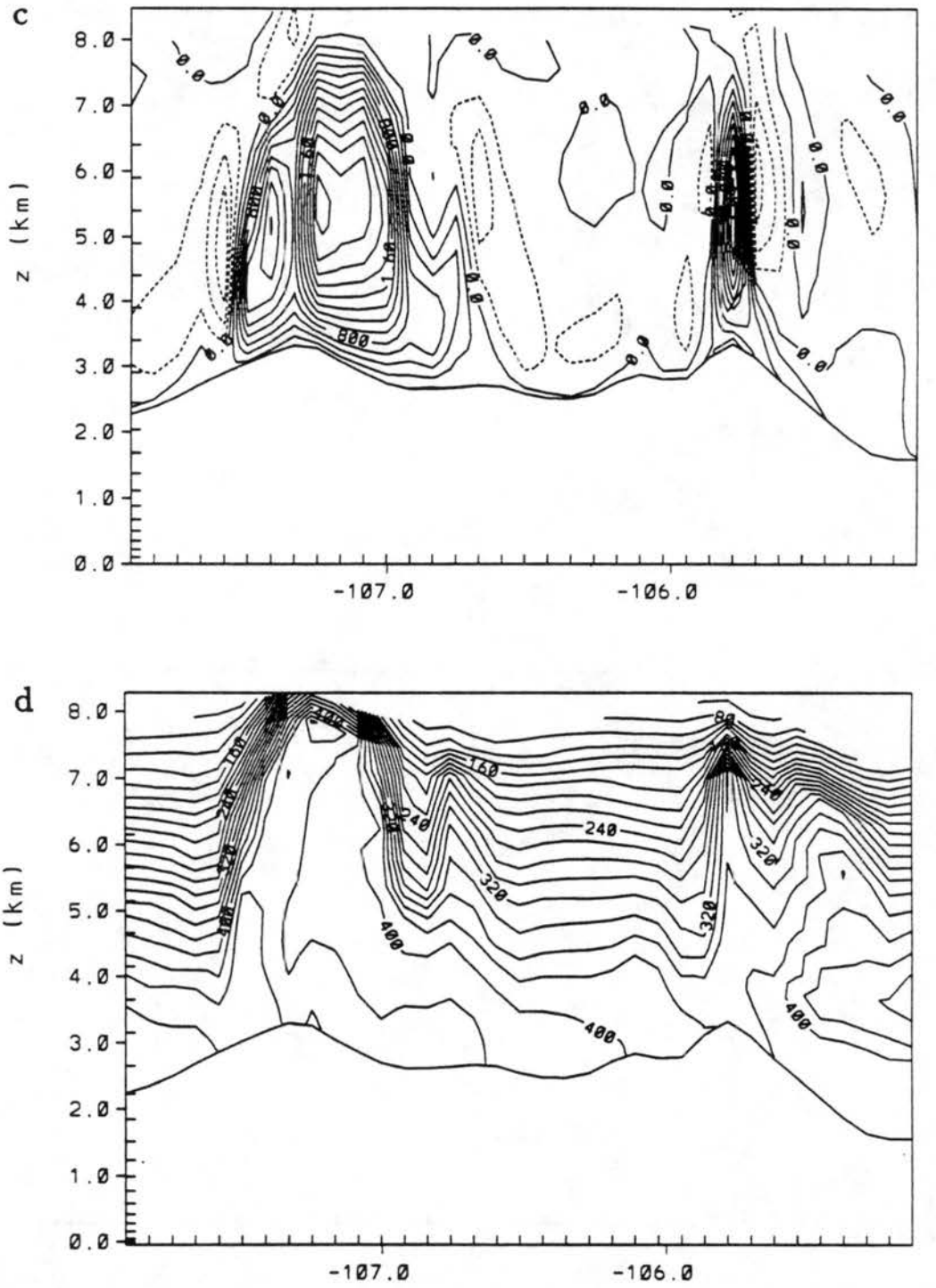

Figure 6.11: Continued.

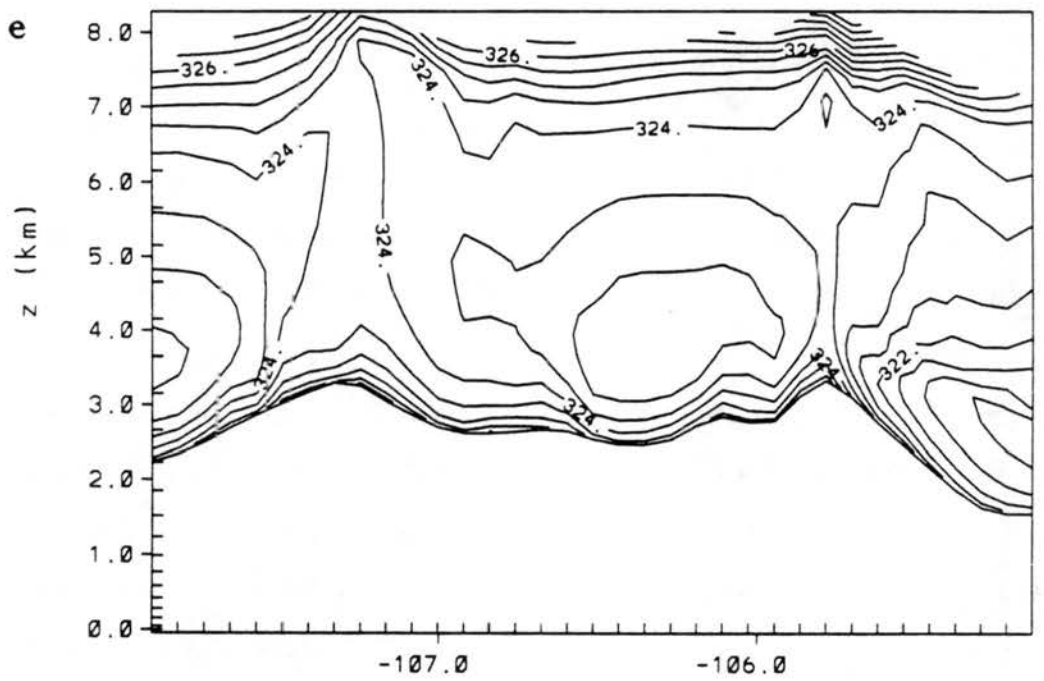

Figure 6.11: Continued.

over the Great Plains east of the Rocky Mountain barrier, where low-level early morning south-southwest flow shifts to afternoon southeasterly flow.

A look at the meso-α scale wind field over Colorado and surrounding areas at 0000 UTC is provided by the second grid (Fig. 6.12b), which shows that the low-level southeasterly flow has penetrated to the Continental Divide by this time along the mountain barrier in Colorado. The third grid provides the most detailed look at the regional-scale flow field over the Colorado mountains (Fig. 6.12c), showing that strong southeasterly flow has invaded the upper Arkansas River Valley in central Colorado, while somewhat weaker upslope winds from an easterly direction are found over the Front Range. Thus, the large-scale inflow response to heating of the Western Plateau appears to be superimposed here on the the regional-scale upslope flows driven by heating of the mountain-plain slope. This combination has been particularly successful in focusing strong southeast-south flow within the upper Arkansas Valley region west of Pikes Peak by 0000 UTC 27 August 1985.

Observed conditions at the ROMPEX stations (see Figs. 6.5a, b) remain relatively steady during this afternoon period in agreement with the simulated winds. Northeast to east winds of 3-4 ms^{-1} are observed at the east slope stations (SQ and RO) and on the barrier crest at MI. The two other barrier crest stations, RM and EK, both experience steady west-northwest flow at 5-6 ms^{-1}, although at RM the flow begins to rotate towards a southwesterly direction by 1700 MST. The west slope stations (VA, FT, MW, BP) all maintain winds from a primarily westerly direction with speeds of 2-5 ms^{-1} during this period.

The simulated afternoon winds are generally in good agreement with the observed winds from a directional standpoint, however, they tend to be significantly stronger. It should be kept in mind that the simulated winds shown are at 50 m above the surface, and the observed winds are from 3 m. Observations of upslope wind profiles show that the wind can increase dramatically to a maximum within 100 m of the surface (Defant 1951). In addition, the model surface is a very coarse representation of the actual terrain, which has many unresolvable topography, roughness, and vegetation variations that are not included in this simulation with 7 km horizontal resolution. Thus, the model simulation is very smoothed as compared to nature, allowing the simulated winds to flow relatively

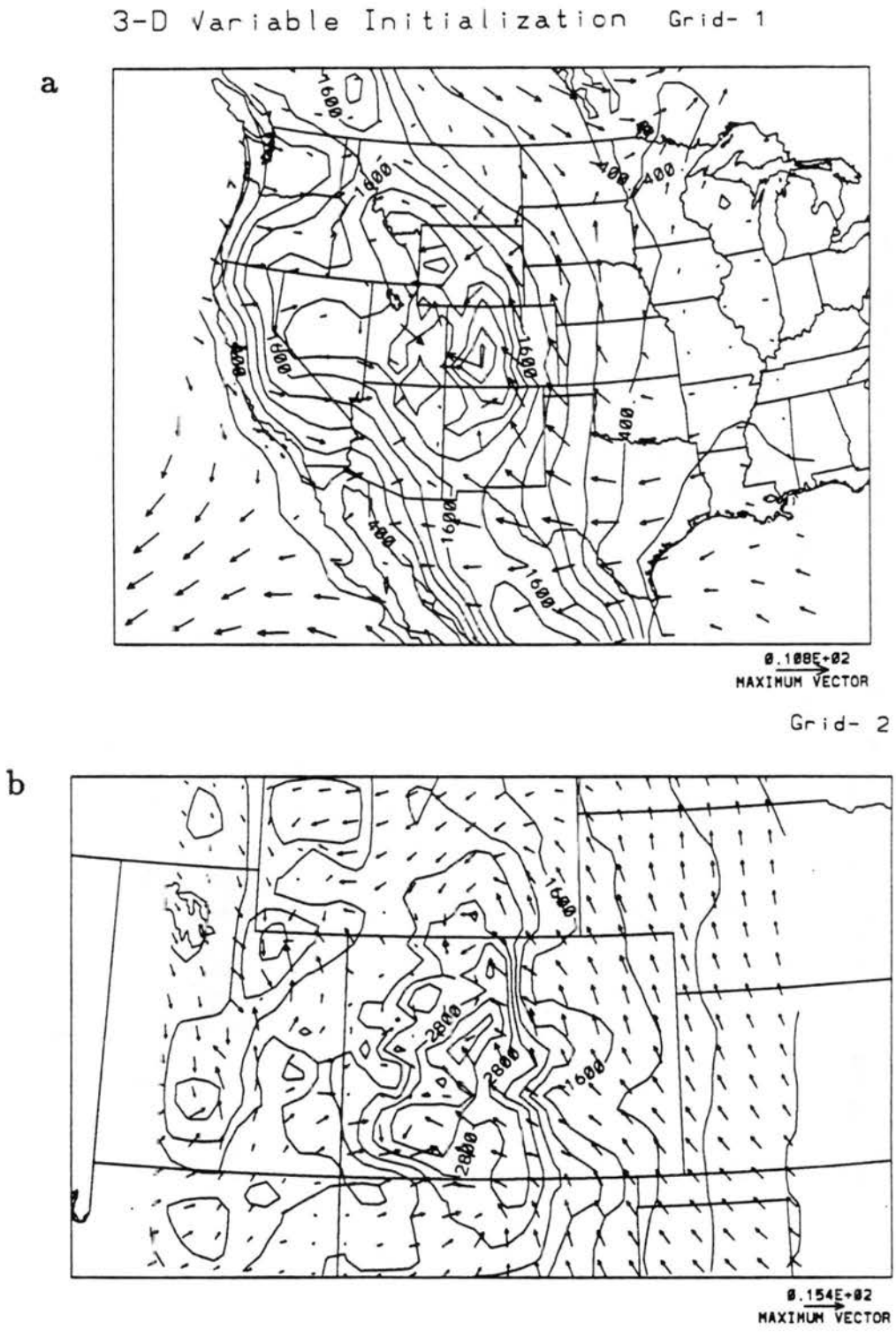

Figure 6.12: Wind vectors on (a) Grid 1, (b) Grid 2, and (c) Grid 3 at 0.28 km above the surface for 0000 UTC (1700 MST) 27 August 1985. Locations of the Mount Werner (MW), Vail Mountain (VA), and Squaw Mountain (SQ) stations indicated for reference in (a).

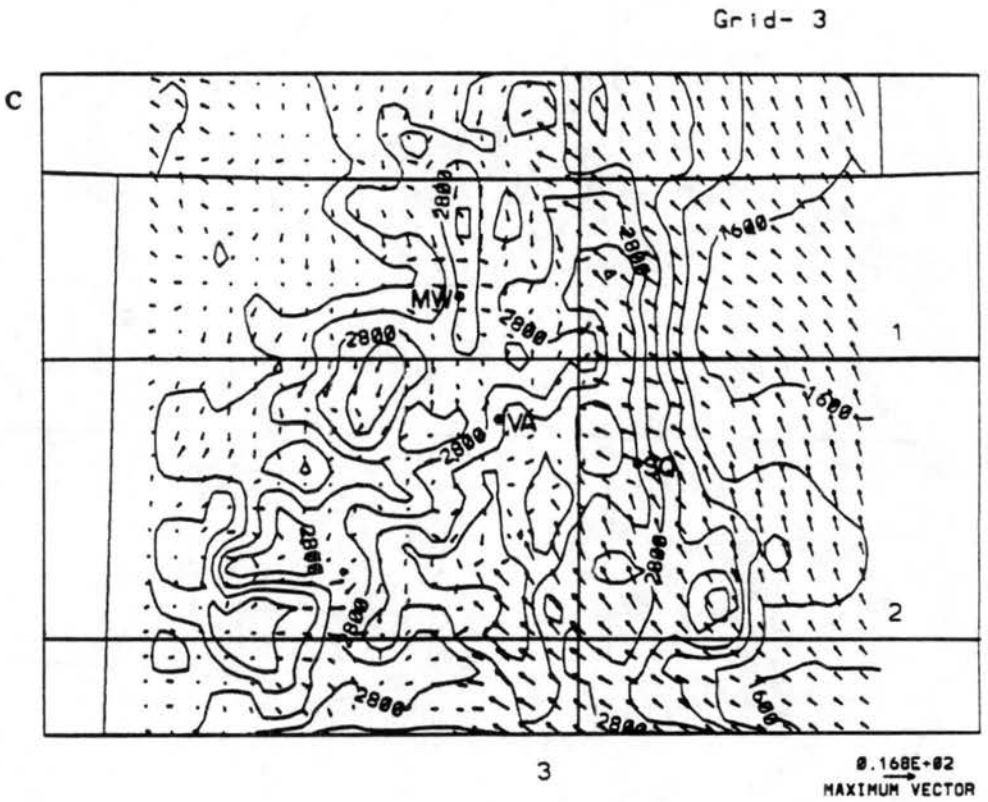

Figure 6.12: Continued.

unobstructed and attain greater velocities than actually observed near the surface. The simulated flow could have been reduced by increasing the roughness parameter (C_D) from its present value of 0.004, however, little experimental data exists upon which to base such a change.

6.3.5 Simulated transition phase

Several vertical cross-sections, illustrate the structure of the wind and temperature fields associated with the various regional-scale wind regimes that have evolved by 0000 UTC (1700 MST). The first, an x-z slice through the Front Range westward to the Flat Tops Range (Fig. 6.13a-d) (labeled "1." in Fig. 6.12c), is similar in many respects to the idealized simulations shown in the previous chapter, with a baroclinic zone evident just west of the crest of the Front Range, associated with the transitional phase of the Front Range mountain-plains solenoid. The solenoid moves westward over the crest of the barrier, as in the previous three-dimensional run with no initial flow, although here it occurs two hours later. This delay is due primarily to the morning suppression of upslope flow in the present case from strong low-level downslope winds. To the west of the baroclinic zone, a very deep, well-mixed boundary layer is present in this simulation over the intermountain region, extending to over 7 km. A diffuse thermal gradient is also present along the eastern slope of the Flat Tops Range.

Farther south, a cross-section within the strong southeasterly winds of the upper Arkansas Valley (Fig. 6.14a-d) (labeled "2." in Fig. 6.12c) reveals that a dramatic differential exists between the deep, well-mixed air mass over the western portion of the simulation domain, and the air which originated over the eastern slope of the mountain barrier and the Great Plains. This cross-section closely resembles the idealized "high plateau" simulation described in section 5.3.1. The deep inland penetration of the cooler east slope air mass has been driven by strong temperature advection within the low-level southeasterly flow. Such a process did not occur in the three-dimensional, zero initial flow simulation, and is thus associated with the synoptic-scale wind and temperature pattern on this particular case study day.

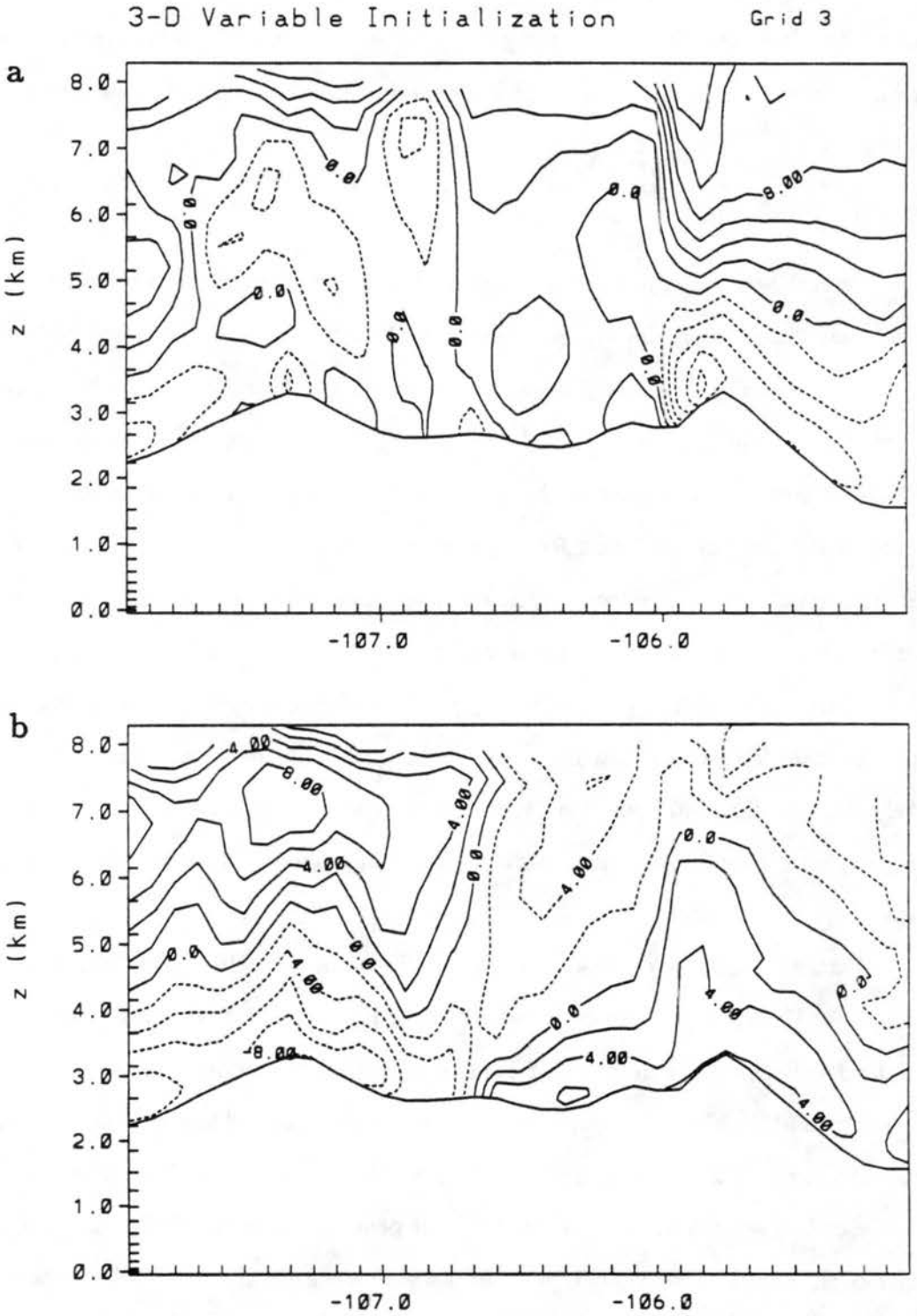

Figure 6.13: Vertical profiles of (a) u-component every 2 ms^{-1} (b) v-component every 2 ms^{-1} (c) w-component every 0.2 ms^{-1} (d) potential temperature every 0.5°C on Grid 3 at 40.0°N for 0000 UTC (1700 MST) 27 August 1985.

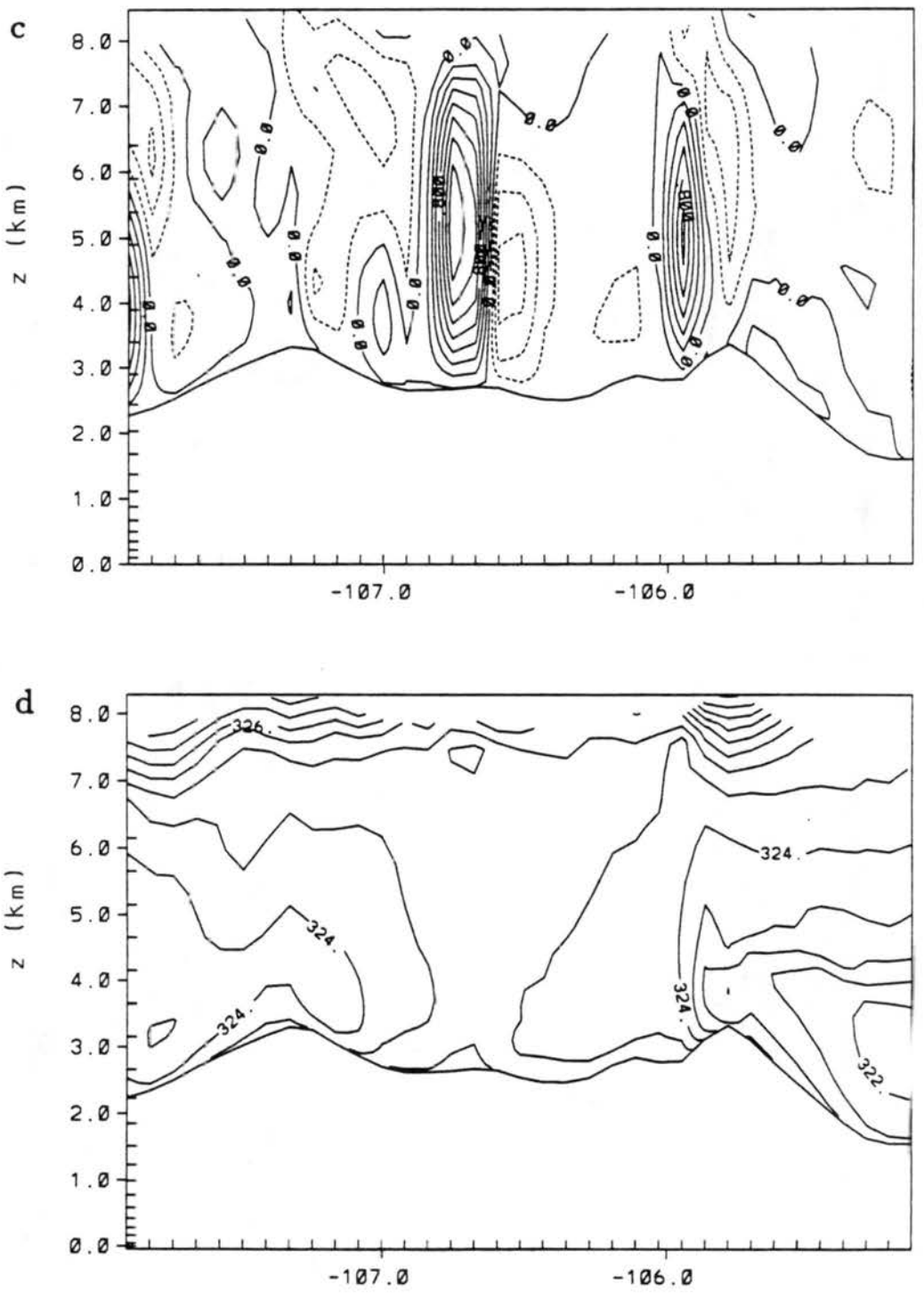

Figure 6.13: Continued.

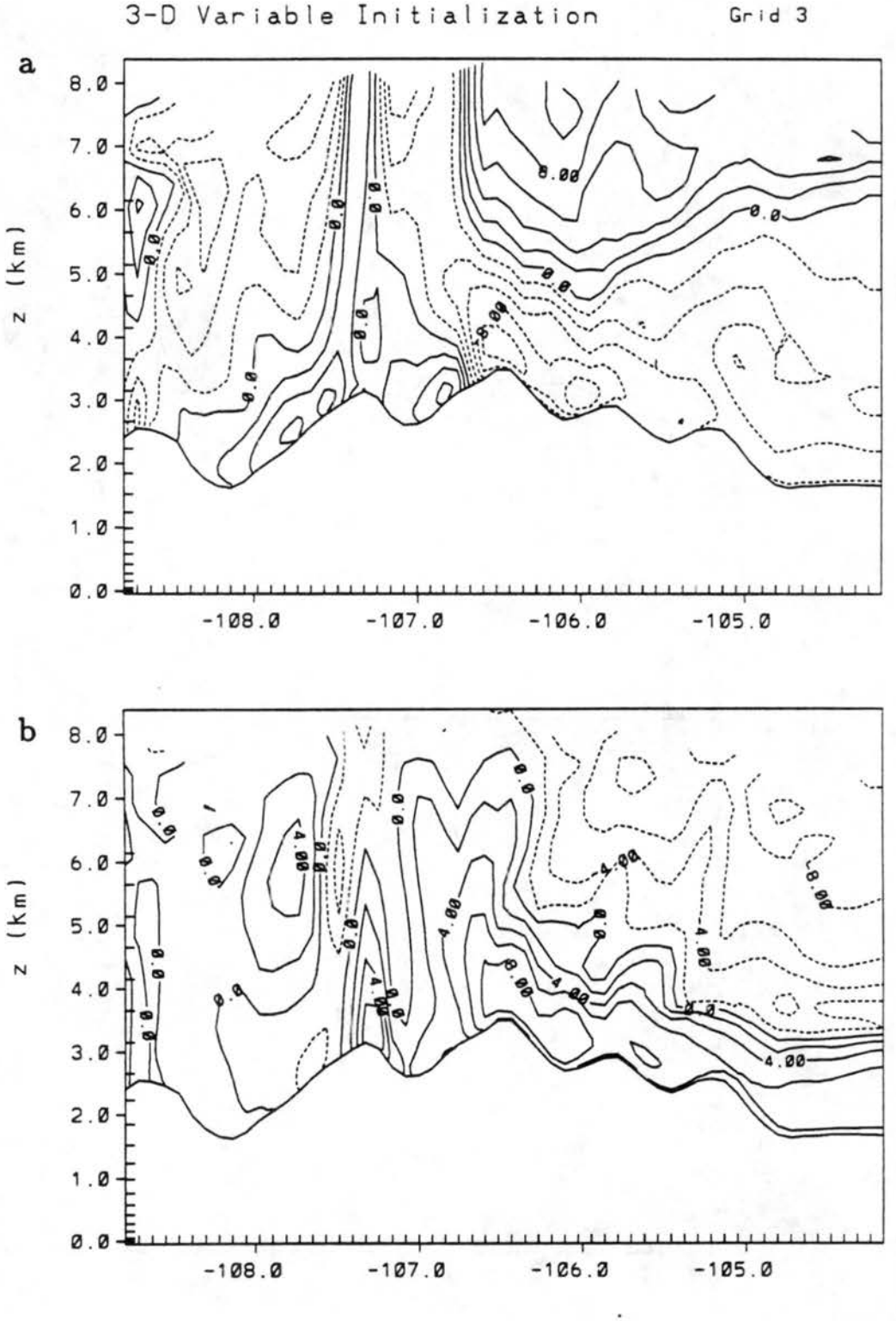

Figure 6.14: As in Fig 6.13, but for a west-east cross-section on Grid 3 at 38.7°N.

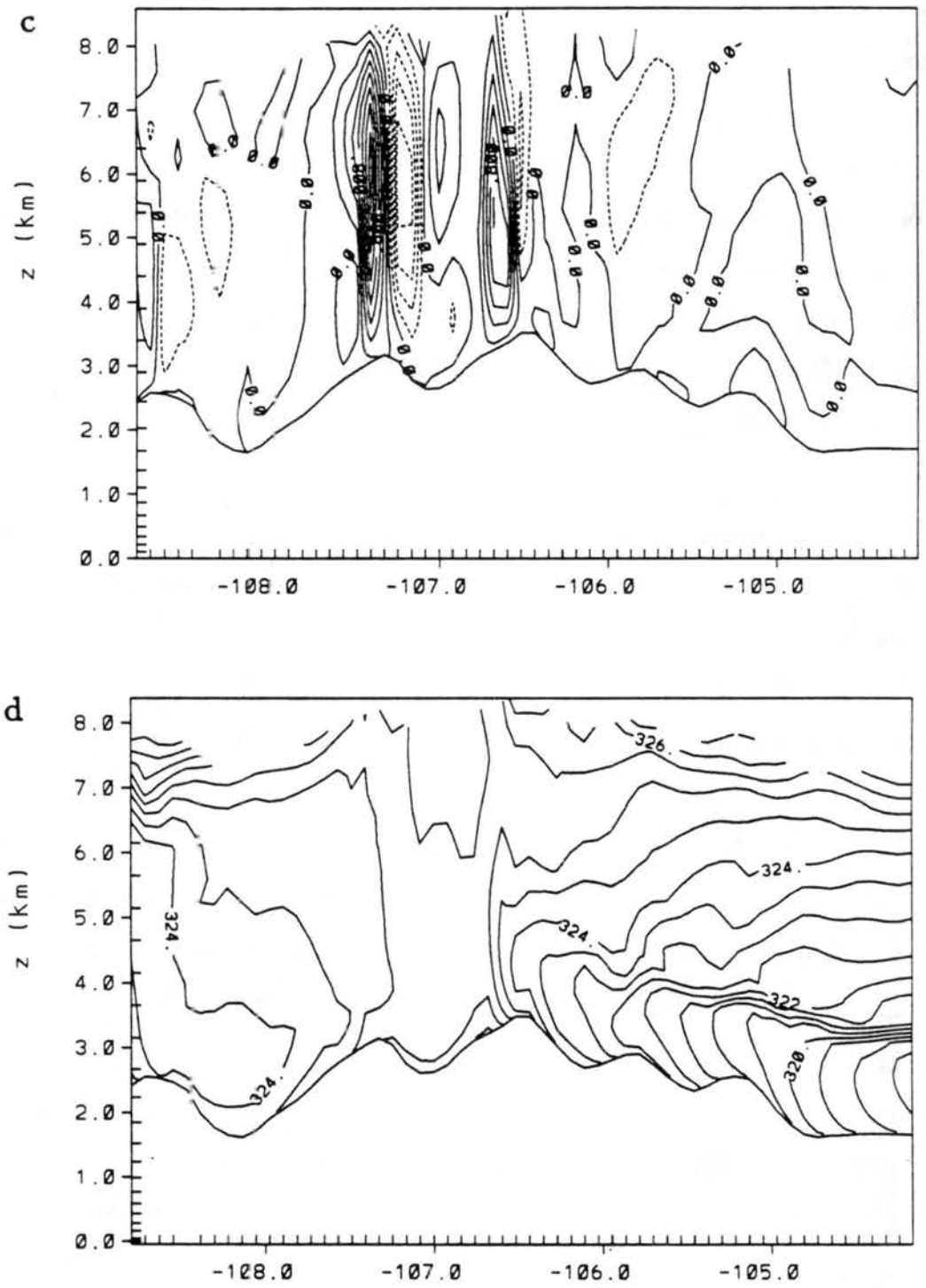

Figure 6.14: Continued.

A y-z (south-north) cross-section (Fig. 6.15) (labeled "3." in Fig. 6.12c) demonstrates the truly three-dimensional behavior of the regional-scale flows over the simulation domain which are unique to this case study. To the south, we see that a south-north temperature gradient exists between the cooler southeasterly flow, and the warmer air located within the large intermountain basin of Middle Park, shown in Fig. 6.13. To the north, a similar cool, southeasterly flow is also apparent. Both of these flows have advected cooler air from the eastern slope westward to the north and south of the steep Front Range barrier. A remnant of the deep, well-mixed intermountain boundary layer air remains over the Middle Park area, which is surrounded by high topography to the south and east, and hence, is protected from these intrusive cold currents much later in the day than other regions as far east.

The late afternoon/early evening westward advection of potentially-cooler air from the eastern side of mountain barrier to the western side is documented in Fig. 6.16, which shows the near-surface potential temperature field superimposed with the vector winds for the period 1700 - 2100 MST. Visible in these plots is a clearly delineated "front" along the length of the mountain barrier between the air masses over the eastern and western slopes at 1700 MST (Fig. 6.16a). Also apparent are stronger easterly winds behind the front, continuously reinforcing the cold air at the head of the current. This cold advection advances the front farther west (Fig. 6.16b) over the next hour, where it undercuts the turbulent, very homogeneous air mass over the western slope of the Colorado mountains. The onset of surface cooling by 1900 MST (Fig. 6.16c) begins to produce some inhomogeneity in the western slope air mass at this 50 m level, however the thermal gradient along the advancing front can be seen to further intensify. The influence of the Coriolis force is particularly evident in the southeast portion of the simulation domain, where the winds have undergone a gradual rotation from southeasterly (see Fig. 6.15a) to a more southerly direction. With the onset of significant surface cooling by 2000 MST, the surface front advances more quickly westward across the high mountain topography (Fig. 6.16d), and continues to intensify, particularly within the central portion of the simulation domain. By 2100 MST (Fig. 6.16e), enough near surface cooling has occurred to obscure the front near

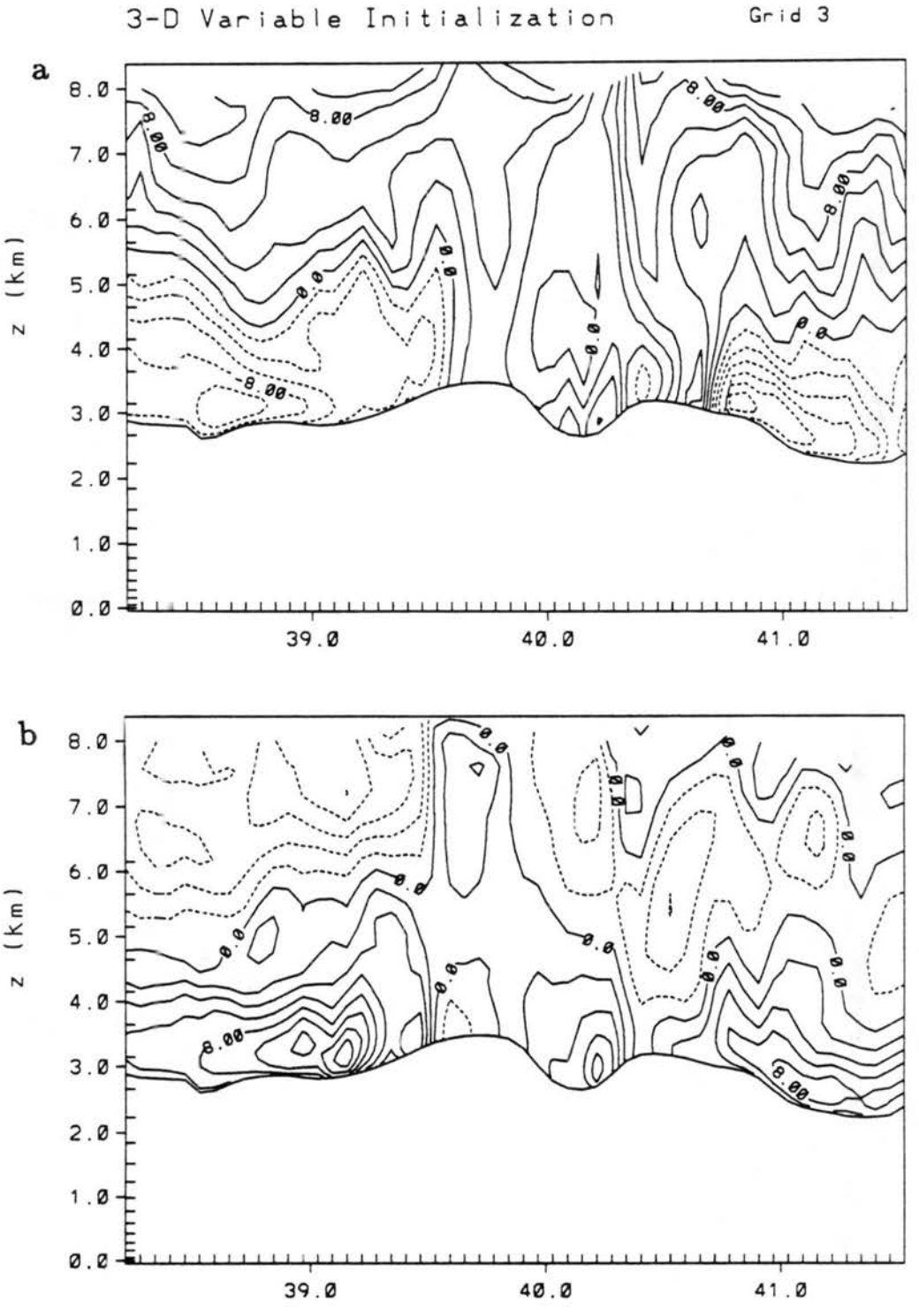

Figure 6.15: As in Fig 6.13, but for a south-north cross-section on Grid 3 at -106.0°W.

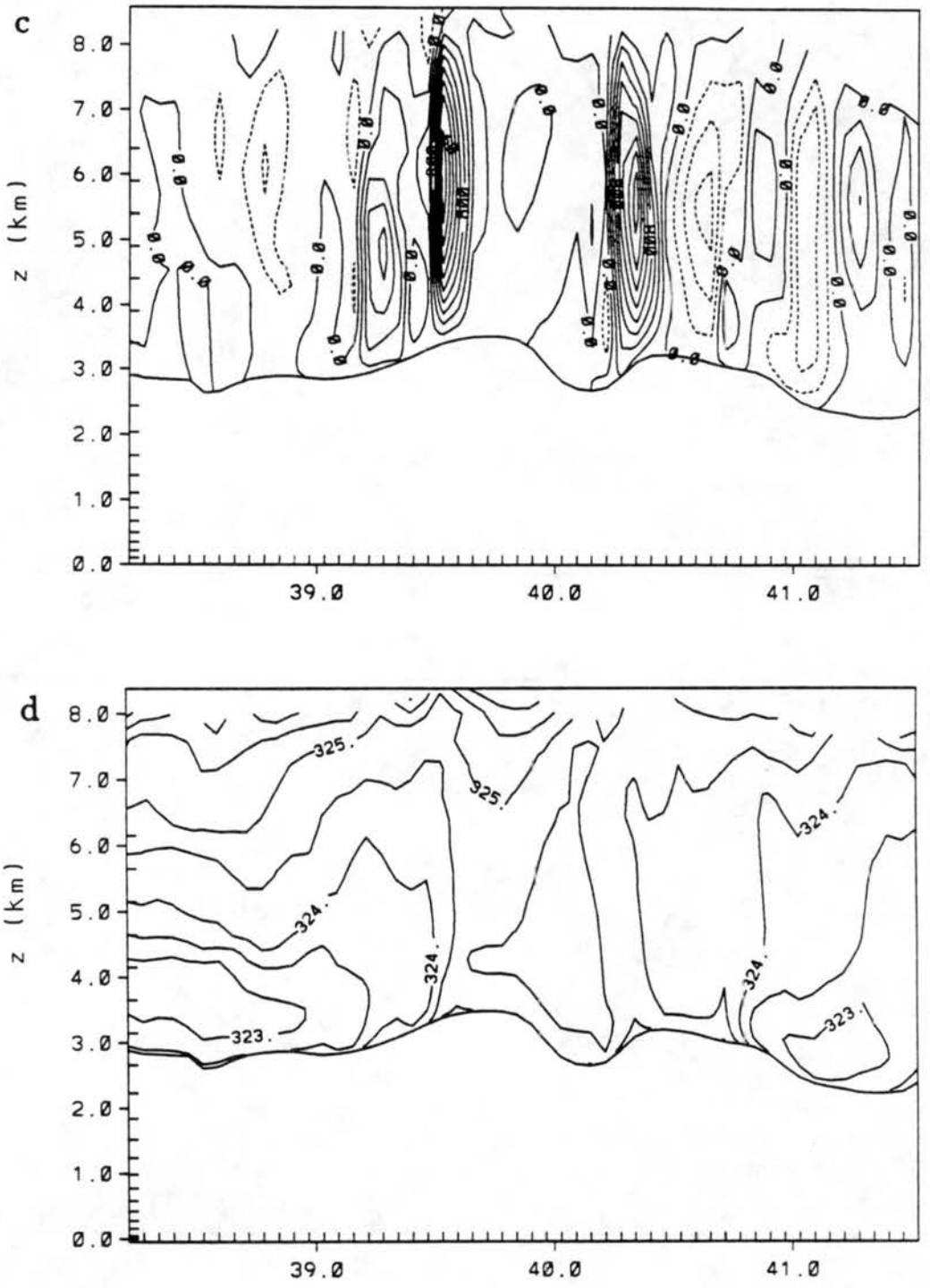

Figure 6.15: Continued.

the surface, however, it is still visible between the Flat Tops Range and the Park Range southeast of the MW station and is particularly evident in the wind field.

Over this four hour period the low-level eastern slope currents are simulated to propagate 80 - 100 km in a northwestward direction, giving a propagation speed of $\sim$ 7 ms^{-1}. Using appropriate values for the parameters in the gravity (density) current speed formula (see eq. 5 in chapter 5) we find that the simulated current speed is within the calculated range of 7-9 ms^{-1}. Thus, the potentially-cooler eastern upslope flows propagate across the barrier crests in the late afternoon as density currents. The increase in propagation speed of the current with the onset of surface cooling is proportional to the increasing temperature gradient across the current.

Two cross-sections of the wind and temperature fields are shown in Fig. 6.17a-d and Fig. 6.18a-d, which define the vertical structure of the density current at 2000 MST. The x-z section is taken through the high mountain terrain in central Colorado, where the front associated with the density current was especially well-defined (see Fig. 6.16d). The potential temperature field shows that the depth of the cold air is nearly 1 km over the high terrain, with a highly stratified low-level air mass to the east of the current head and well-mixed conditions above the surface to the west. The horizontal wind components show the very strong southeast-southerly air flow within the stable air just east of the current head, while the vertical wind component shows that ascending motion of 1 ms^{-1} is associated with the westward propagation of the current. The northward penetration of the dominant southerly density current flow from the upper Arkansas Valley can be seen in Fig. 6.18 as it invades the Middle Park region at 40°N at 2000 MST with very strong low-level southeasterly winds behind the front. Obviously, this low-level feature, occurring in a very stable air mass within 500-1000 m of the peaktops is exactly the same density current phenomenon described in the previous idealized simulations, only in this case study the primary surge of this eastern slope density flow comes from the south, while in the previous three-dimensional zero ambient flow simulation the surge came directly over the Front Range. This suggests that favorable ambient flow conditions, in this case strong low-level southeasterly winds from the Great Plains, can enhance the thermally-induced upslope flows over a particular region.

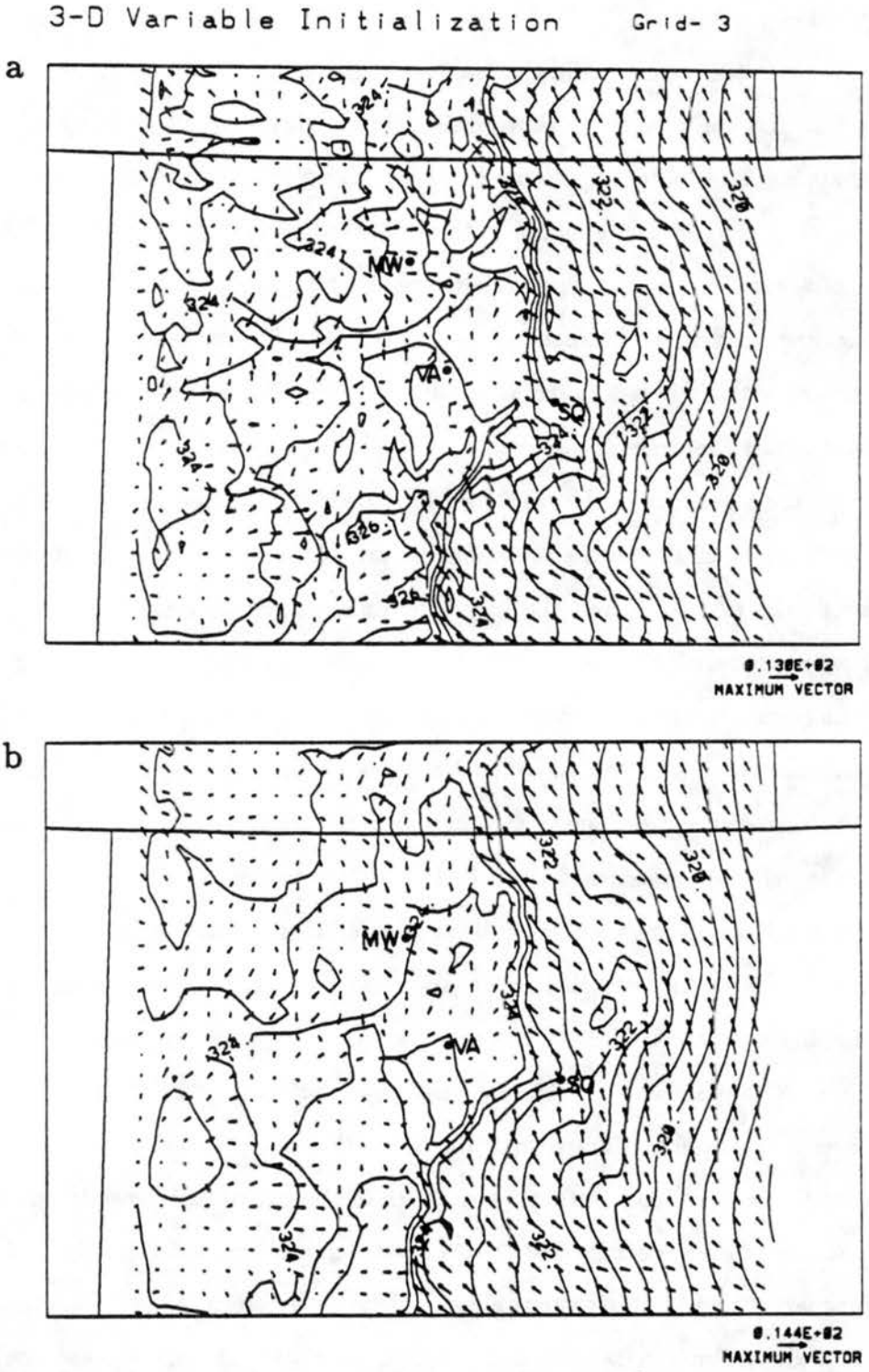

Figure 6.16: Simulated vector winds and potential temperatures every 0.5°C at 50 m above the surface for (a) 1700 MST (b) 1800 MST (c) 1900 MST (d) 2000 MST and (e) 2100 MST 26 August 1985. Locations of the Mount Werner (MW), Vail Mountain (VA), and Squaw Mountain (SQ) stations indicated for reference.

c

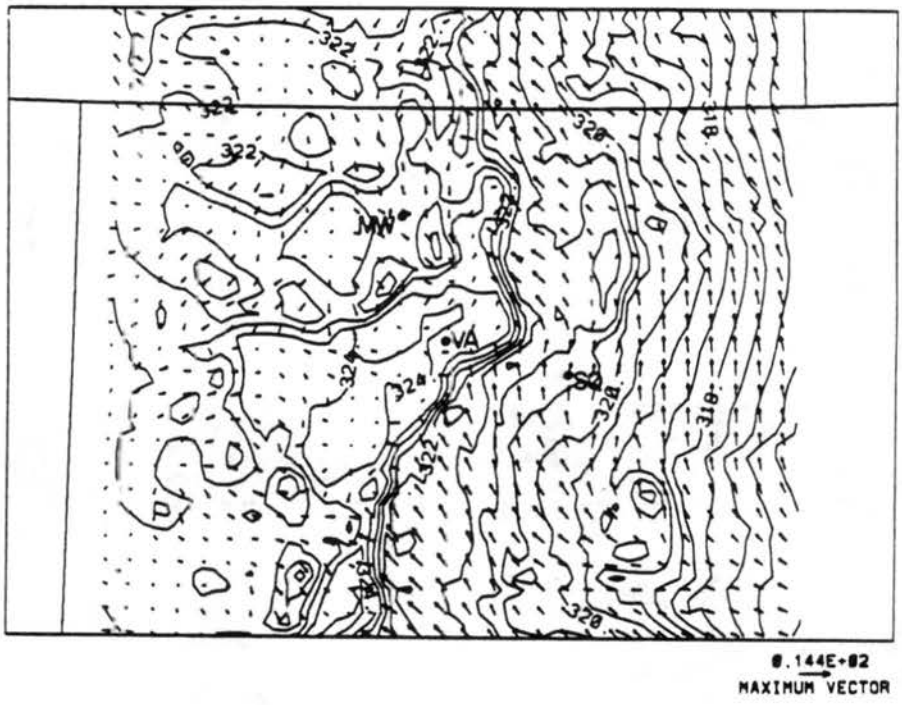

d

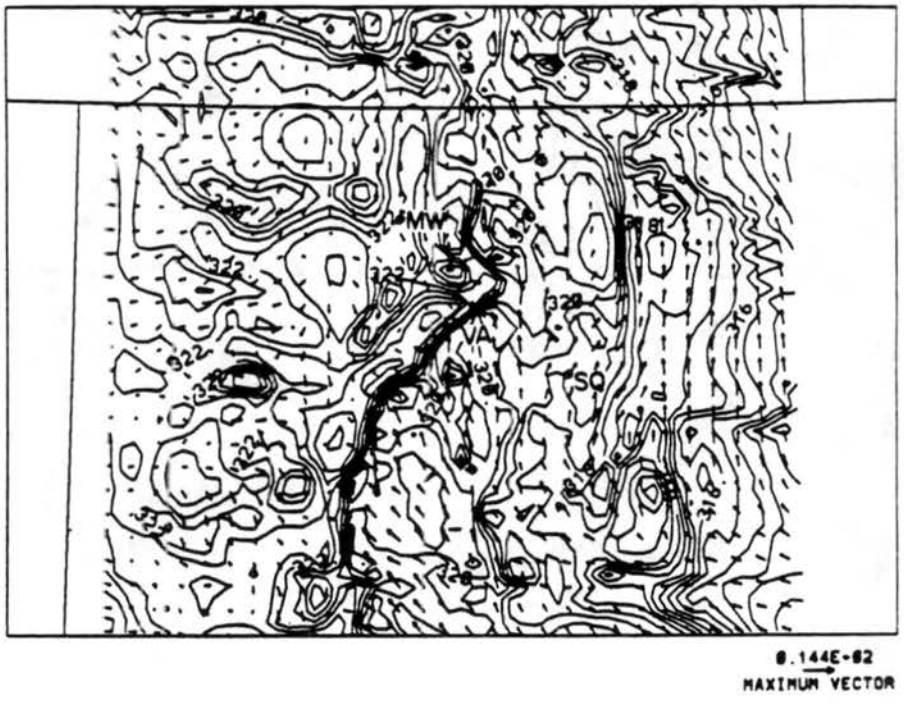

Figure 6.16: Continued.

e

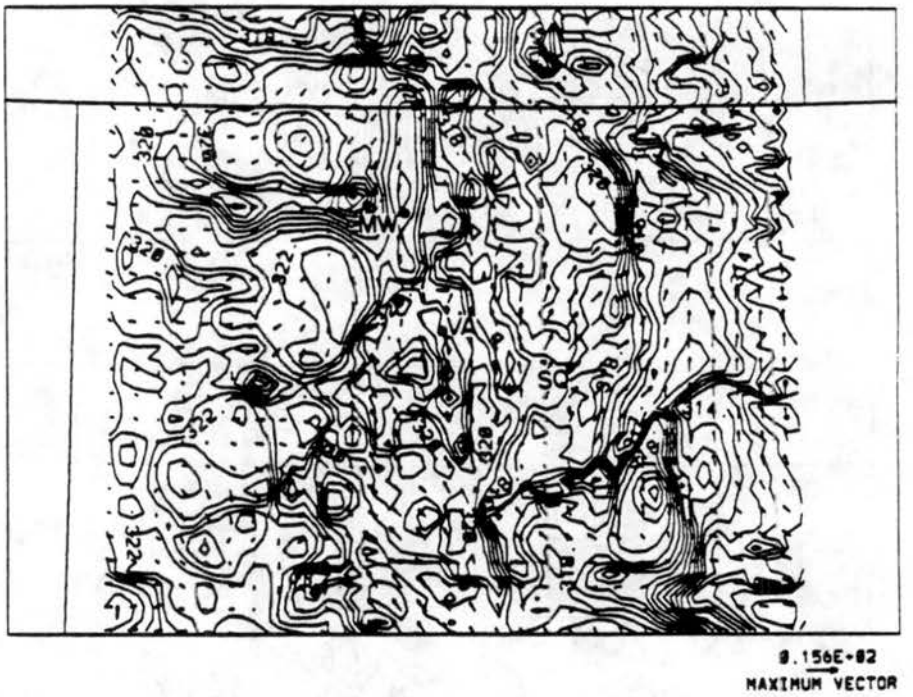

Figure 6.16: Continued.

6.3.6 Simulated nocturnal circulations

The simulated regional-scale flow evolution suggests that during this four hour period (1800 - 2100 MST) a transition occurs from a daytime inflow phase into a nocturnal outflow phase of the circulation. This transition is driven by the propagation of the strong eastern slope mountain-plains solenoid over the barrier crest, and by the onset of radiational cooling, which begins by 1900 MST. The westward propagation of the solenoid is well reflected in the observed data by the rotation of the wind vector at the barrier crest stations (RM, EK, MI) from a westerly to easterly direction during this period. The surface cooling allows the rapid propagation of the potentially-cooler flows generated over the eastern slope into the western slope region as intrusive density currents. Thus, we see the very strong southerly flow generated in the upper Arkansas Valley propagate rapidly northward between 1800 and 1900 MST, converging with the southeasterly flow from over the Front Range, creating a low-level vortical pattern in the flow over Middle Park (see Fig. 6.16c). In addition, this cool southerly current begins to flow down the eastern slope of the Front Range, inducing strong south-southwest flow in phase with the nocturnal downslope wind regime initiated by radiational cooling. This downslope pattern strengthens and becomes increasingly from a southwesterly direction by 2100 MST (see Fig. 6.16e). This abrupt shift to westerly flow over the eastern slope of the Front Range is not found in the observed winds at both the RO and SQ stations, which show only a gradual trend toward southwesterly downslope flow, which appears in earnest by 2400 MST.

West of the Front Range barrier, the cooler southeasterly flow continues its westward propagation, particularly in the northern sections of the simulation domain where it collides with the northwesterly flow generated during the daytime heating cycle over western Colorado. The northwest sector of the simulation domain remains largely unaffected by the invading eastern slope currents throughout this early evening time period, although radiational cooling begins to turn the flow from a northwesterly to northeasterly direction.

The southerly surge from the Arkansas Valley, depicted in Fig. 6.17, is supported by the observations at VA where the wind shifts between 1900 and 2100 MST from northwest to east-southeast, with a corresponding increase in wind speed. This wind shift initiates

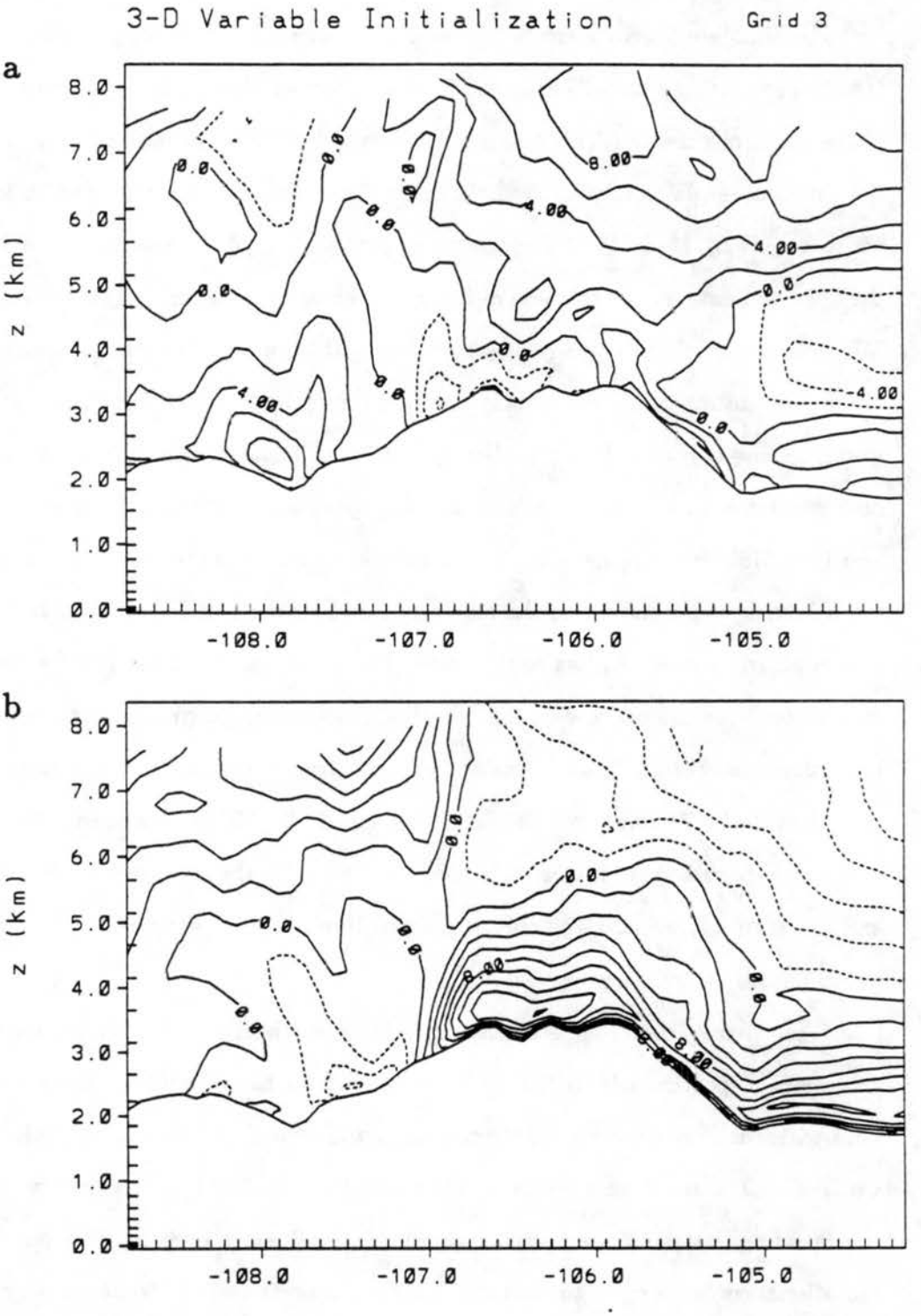

Figure 6.17: Vertical profiles of (a) u-component every 2 ms^{-1} (b) v-component every 2 ms^{-1} (c) w-component every 0.2 ms^{-1} (d) potential temperature every 0.5°C for a west-east cross-section on Grid 3 at 39.5°N for 0300 UTC (2000 MST) 27 August 1985.

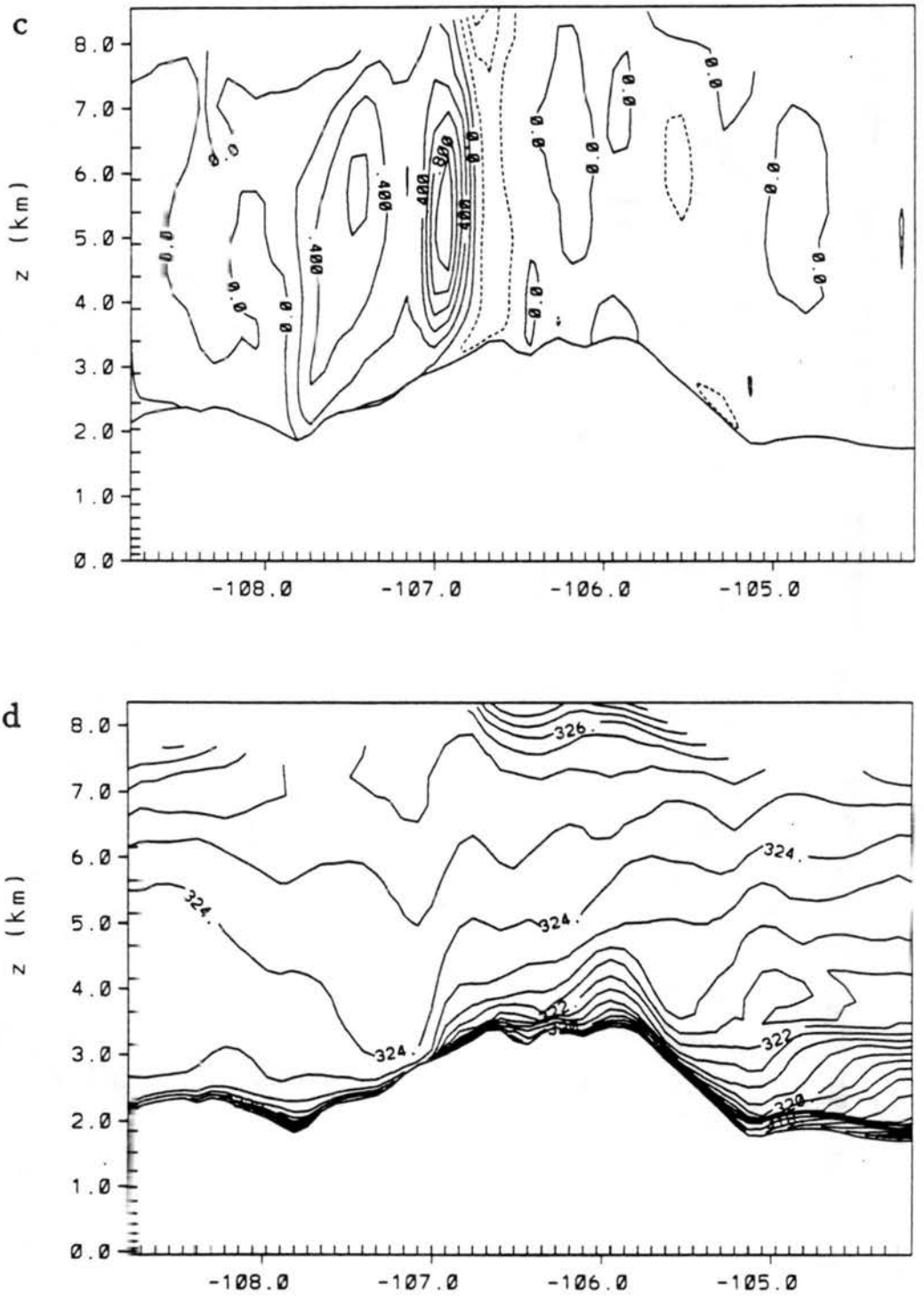

Figure 6.17: Continued.

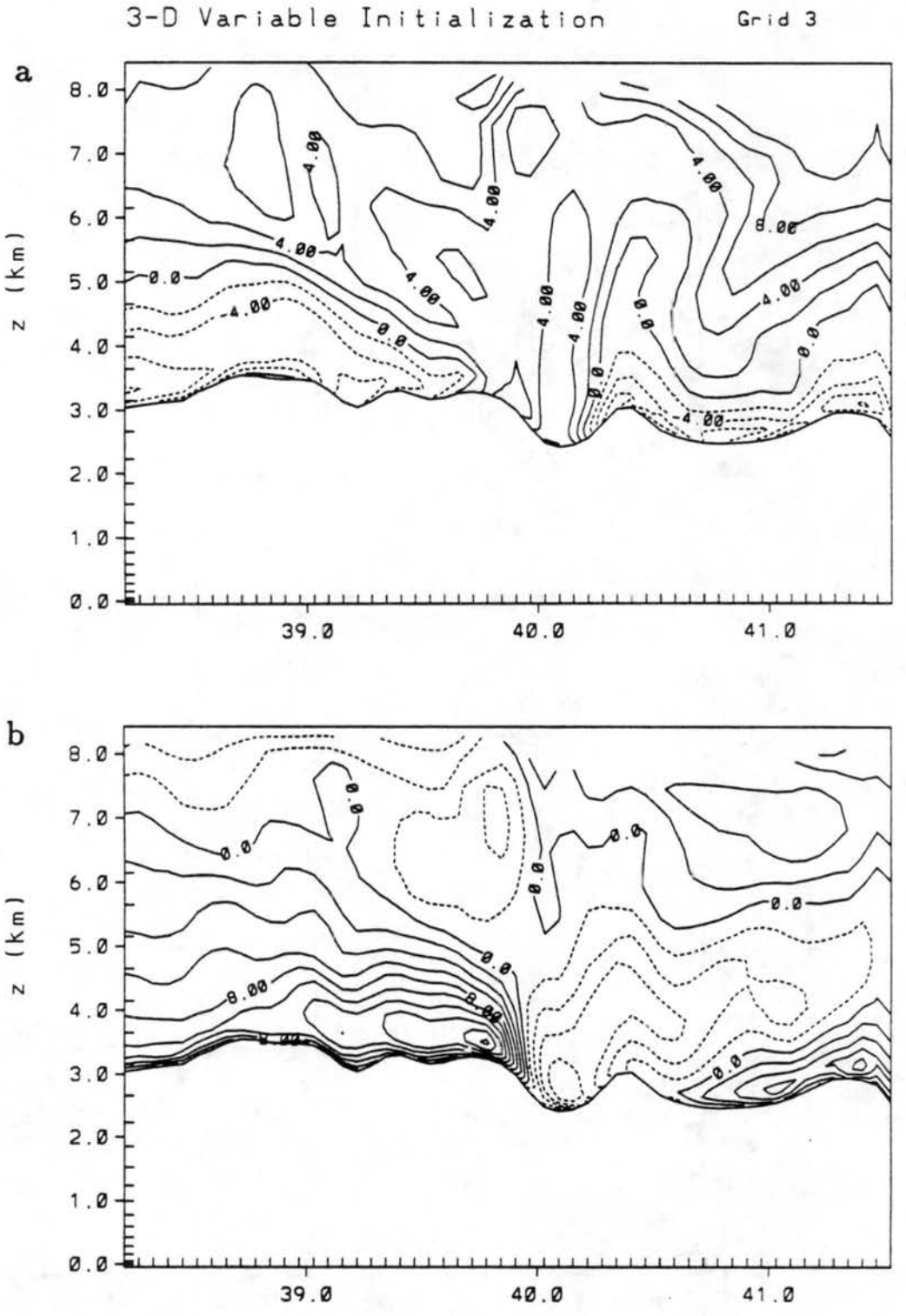

Figure 6.18: Vertical profiles of (a) u-component every 2 ms^{-1} (b) v-component every 2 ms^{-1} (c) w-component every 0.2 ms^{-1} (d) potential temperature every 0.5°C for a south-north cross-section on Grid 3 at -106.4°N for 0300 UTC (2000 MST) 27 August 1985.

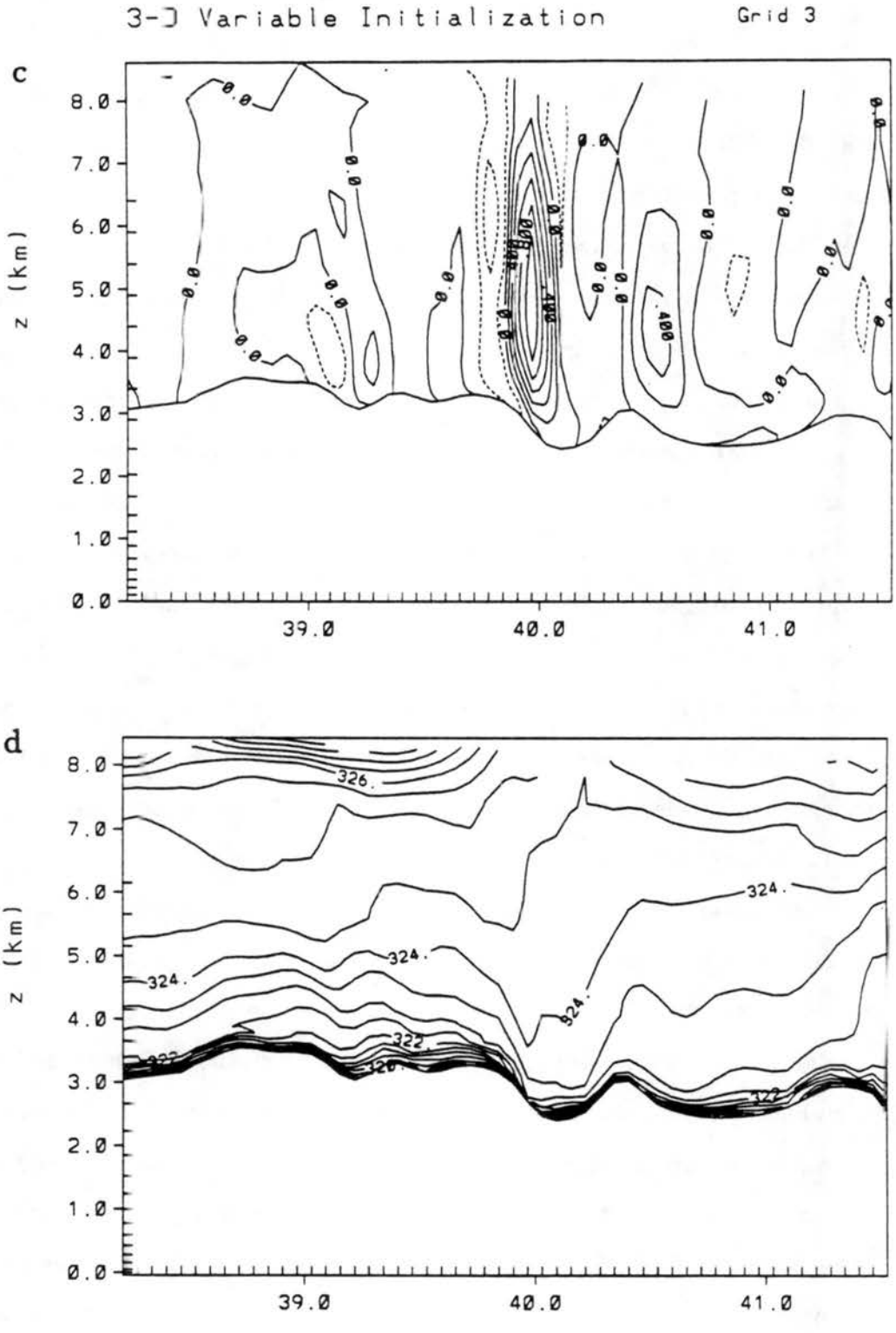

Figure 6.18: Continued.

a steady nocturnal outflow wind regime at this station. A similar west to east wind shift occurs at 2000 MST at BP, which is perhaps a result of the Front Range easterly surge impinging upon the Park Range as suggested in the simulation. However, it is possible that both this shift and the more gradual one at the FT station are driven by more local-scale processes, especially given the observed weak wind speeds.

The wind at the westernmost station, MW, is the last to shift from the daytime northwesterly flow regime to the nocturnal regime with flow from the south-southeast. Initially this occurs at 2200 MST, in agreement with the simulation, which shows a shift in direction in the vicinity of this site from northerly flow at 2100 MST to southerly at 2200 MST (Fig. 6.19). This southerly flow appears to be associated with the remnants of the surging southerly density current from the upper Arkansas Valley. In addition, large-scale adjustment processes, which begin in earnest after the onset of surface cooling and the decoupling of the deep mountain boundary layer from the surface (Blackadar 1957), are now beginning to strongly influence the circulation over the mountain region. By 2200 MST, all of the east slope and Front Range barrier stations are observed to rotate from a southerly direction toward a southwesterly direction. Thus, this hour marks the true onset of the nocturnal flow regime. The simulated wind fields also show the evolution of southwesterly flow between 2200 and 0100 MST (Fig. 6.20) along the entire Front Range.

On the western slope, the winds are highly variable during the initial onset of the nocturnal flow regime between 2100 and 0100 MST at all stations except VA, which maintains steady southeasterly flow. This suggests that VA is under the influence of the southerly density current during this period, while the other stations, all located farther north and west, undergo significant variations. Thus, while a steady nocturnal wind regime begins to appear at the east slope, Front Range barrier, and the VA station on the western slope, the outlying western slope stations do not experience a steady south-southeast nocturnal wind until 0200 MST. This wind variation can actually be found in the simulation, for example, in the vicinity of MW, where the wind shifts from east-southeast at 2200 MST to southwest from 2300 MST until 0200 MST, when it shifts back to a southeasterly direction. The steady nocturnal southeasterlies persist until the end of the simulation at 0500 MST (Figs. 6.20 and 6.21).

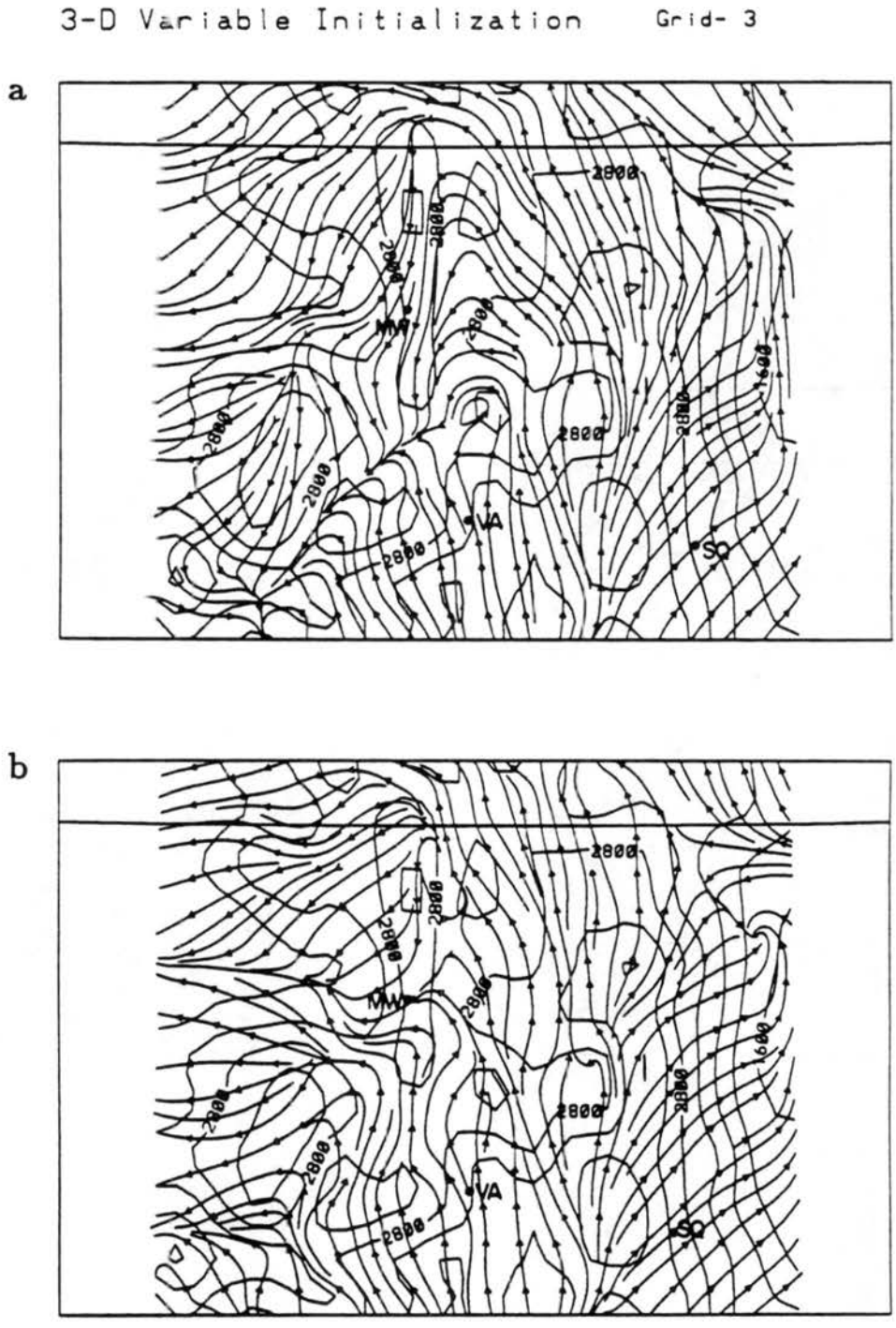

Figure 6.19: Streamlines on Grid 3 at 50 m above the surface for (a) 0400 UTC (2100 MST) and (b) 0500 UTC (2200 MST) 27 August 1985. Locations of the Mount Werner (MW), Vail Mountain (VA), and Squaw Mountain (SQ) stations indicated for reference.

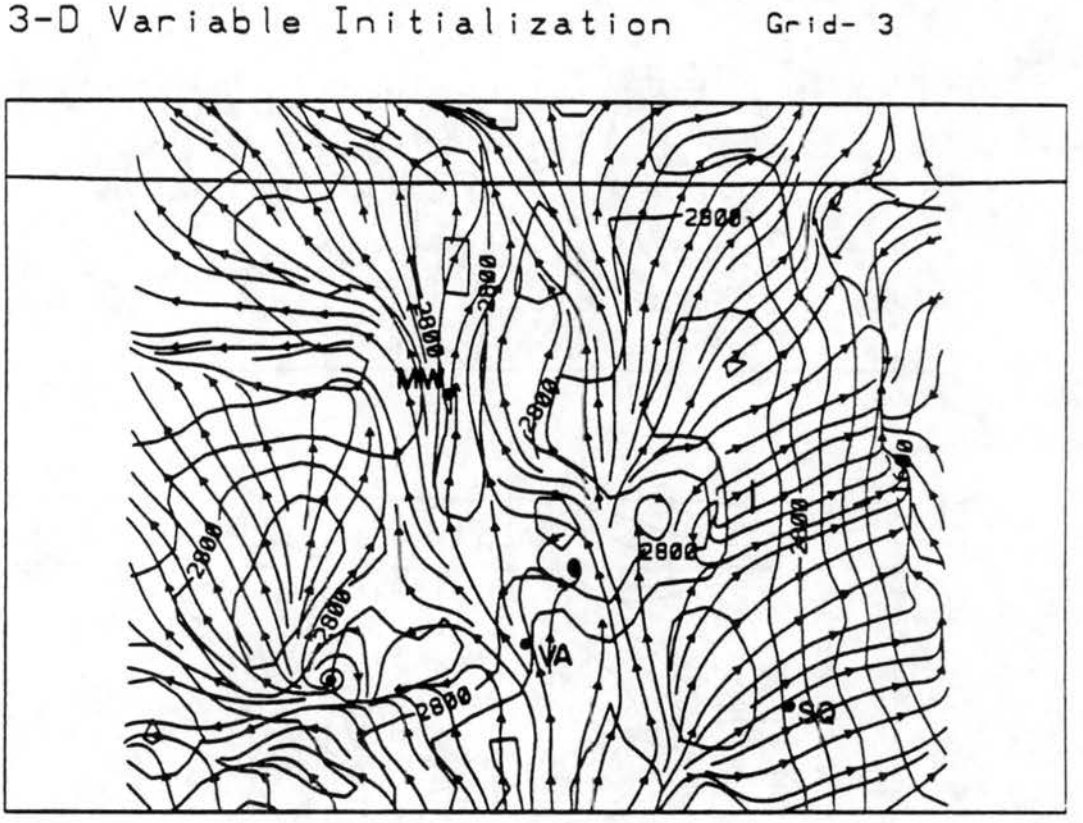

Figure 6.20: Streamlines on Grid 3 at 50 m above the surface for 0800 UTC (0100 MST) 27 August 1985. Locations of the Mount Werner (MW), Vail Mountain (VA), and Squaw Mountain (SQ) stations indicated for reference.

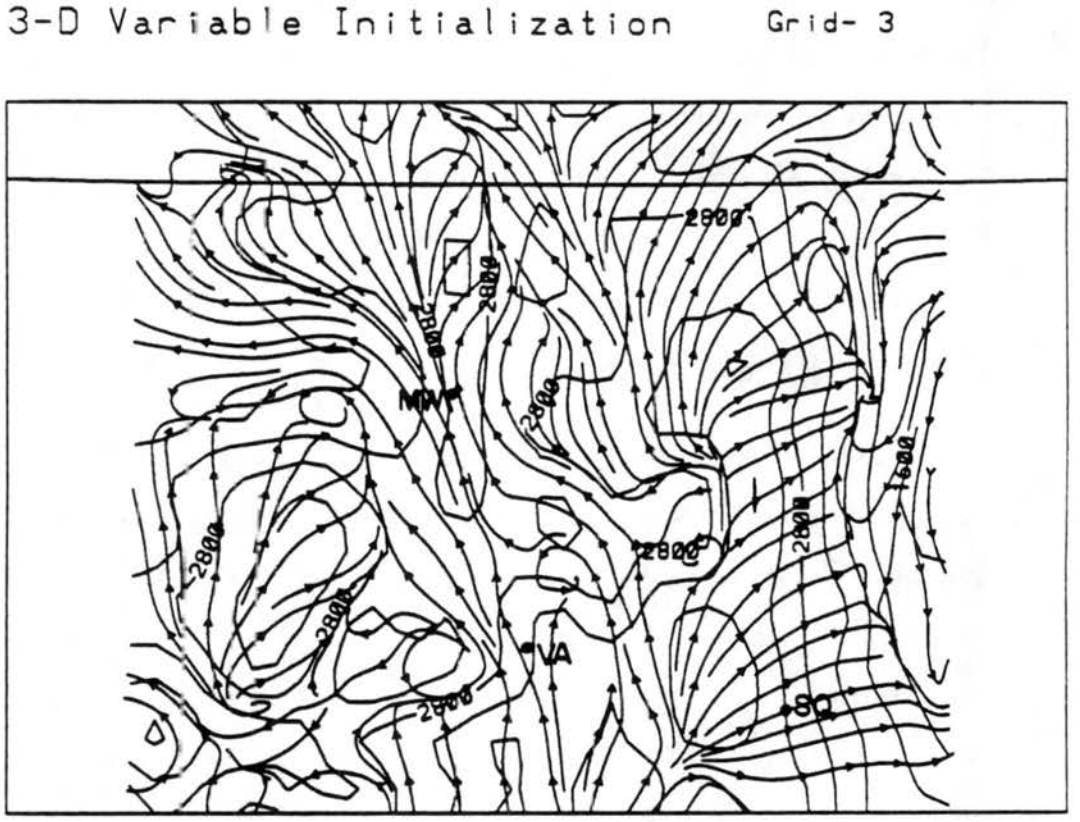

Figure 6.21: Streamlines on Grid 3 at 50 m above the surface for 1200 UTC (0500 MST) 27 August 1985. Locations of the Mount Werner (MW), Vail Mountain (VA), and Squaw Mountain (SQ) stations indicated for reference.

The simulation ends at 1200 UTC 27 August 1985. The streamline fields on the three grids at this time (Fig. 6.22a-c) show that the flow over the central Rocky Mountains is similar in many ways to that of the previous day (see Fig. 6.6), except that the general wind pattern is from a more south-southwest direction, due primarily to the movement during this 24-hour period of the upper-level ridge from west to east of the mountain barrier (Fig. 6.23). The simulated large-scale fields are in fairly good agreement with those observed (see Fig. 6.1b), which show some eastward movement of the upper level ridge, as indicated by the southwesterly winds at the two rawinsonde stations in Colorado, and in the low-levels by the position of the two high pressure cells over southern Illinois and in central Canada. The position of the surface front through Wyoming, northeastward toward Lake Superior is also handled well in the model, all suggesting that the model has done an adequate job of simulating the observed large-scale conditions over a 36-hour period.

6.4 Case Day Simulation Summary

This case day simulation has shown that many of the observed aspects of the diurnal evolution of regional-scale circulations over the central Rocky Mountains are simulated within the model. In particular, the model simulates well the low-level wind reversal over each slope of the mountain barrier from an outflow to an inflow direction with the onset of diurnal heating. The simulated afternoon propagation of the eastern slope mountain-plains solenoid over the crest of the barrier was also present in the observed data, and marks the transitional phase of the diurnally-evolving regional-scale wind regime. Of special interest in this case day simulation was the northwestward propagation of the mountain-plains solenoid located south of the Front Range within the upper Arkansas Valley. This branch of the circulation developed a particularly strong low-level south-southeast flow which appeared to be enhanced by large-scale forcing. Cold air advection within this particular region produced the most intense low-level nocturnal density current from the collapse of the daytime mountain-plains circulation. This southerly density current appeared in the simulation to be responsible for the abrupt shift observed in the evening winds at the VA station from an inflow to outflow direction, while over the Front Range it induced a similar shift to southwesterly outflow winds.

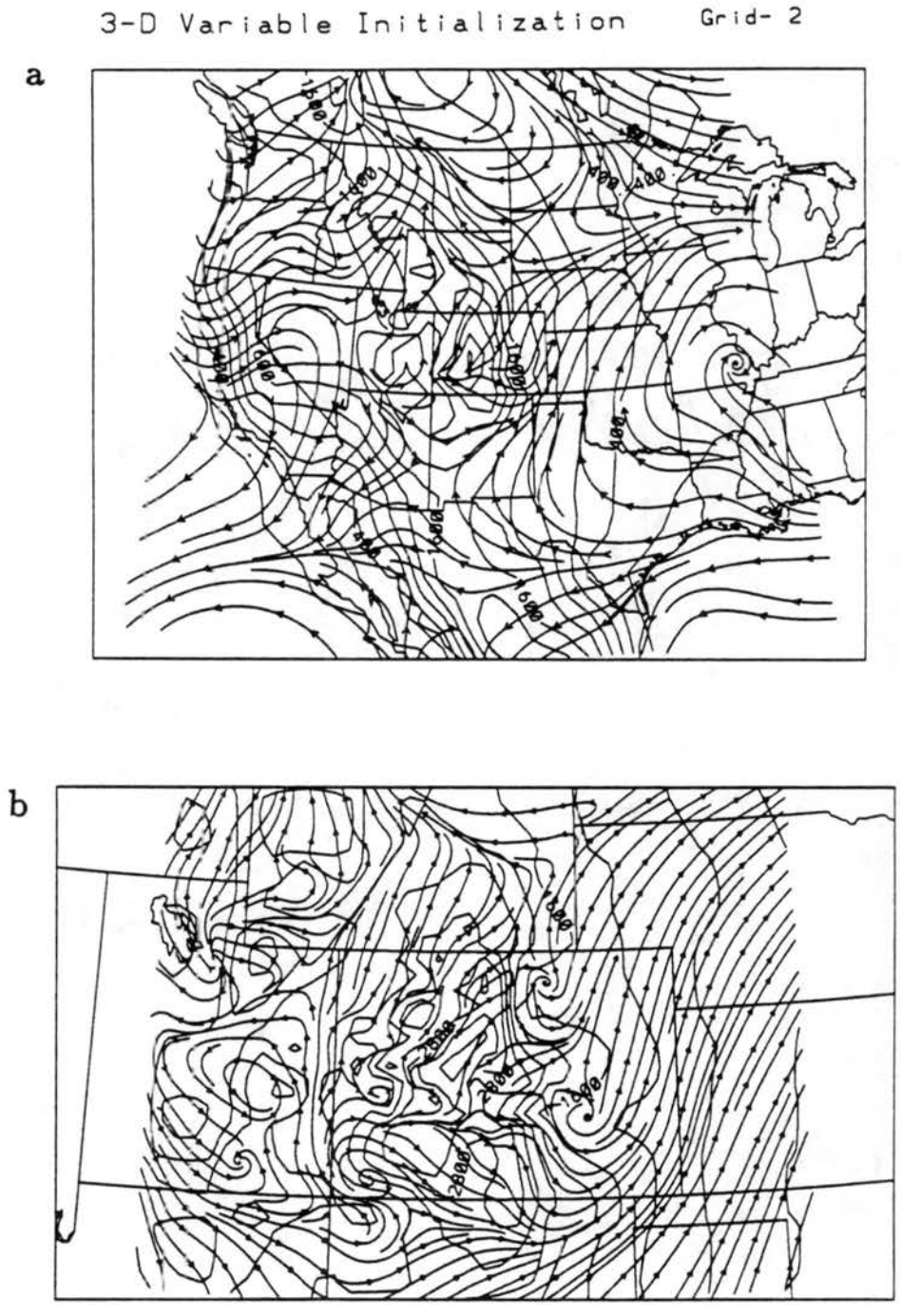

Figure 6.22: Streamlines on (a) Grid 1, (b) Grid 2, and (c) Grid 3 at 0.28 km above the surface for 1200 UTC (0500 MST) 27 August 1985.

c

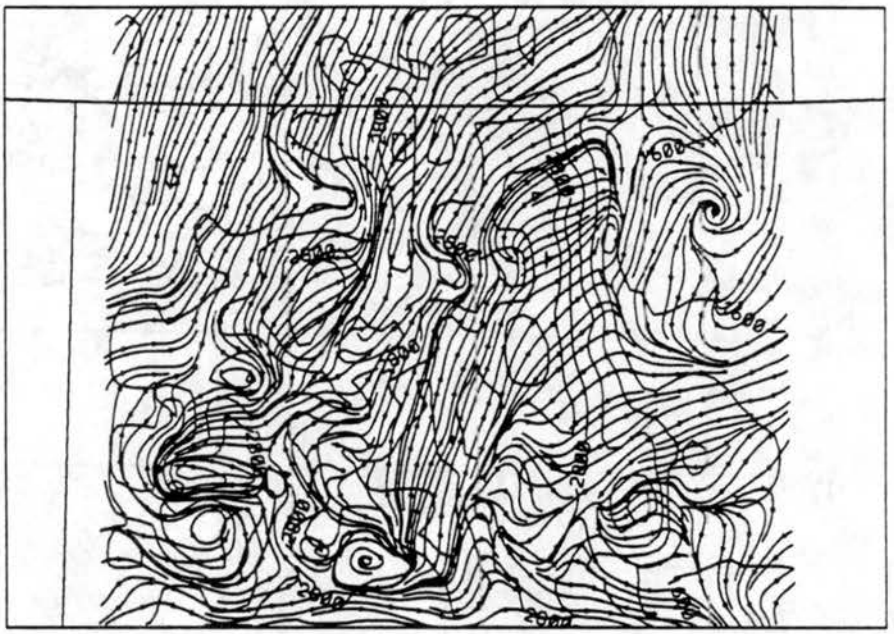

Figure 6.22: Continued.

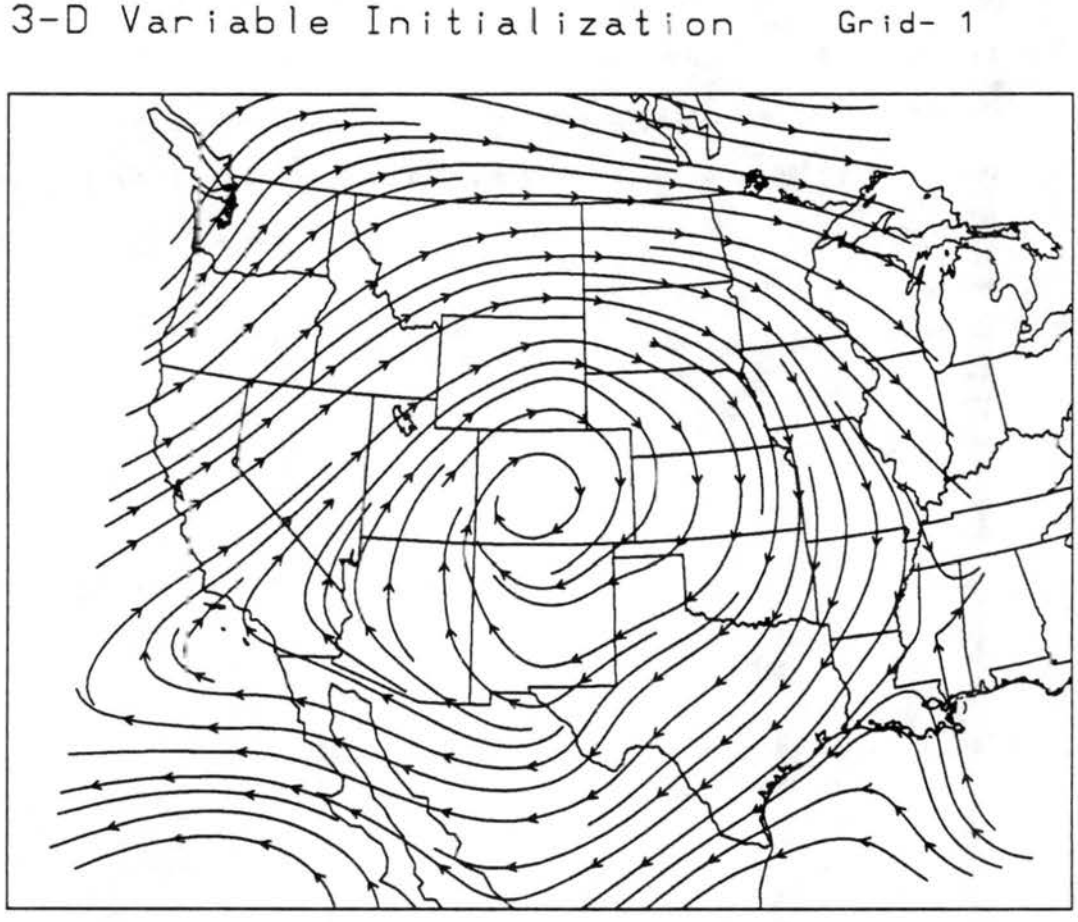

Figure 6.23: Streamlines on Grid 1 at 5.65 km above the surface for 1200 UTC (0500 MST) 27 August 1985.

The onset of the nocturnal outflow wind regime advanced from south to north within the simulation, as the strong southerly current merged over Middle Park with the somewhat weaker, more easterly current generated over the Front Range. This merging of discrete flows from different drainage basins along the eastern slope of the Colorado mountain barrier indicates the truly complex three-dimensional character of this flow phenomenon. The decay of the density currents from the southerly surge and from the Front Range was reflected in the unsteady late evening wind behavior at the MW station in both the simulation and the observations. The late night onset of steady southeasterly outflow winds at this site was another aspect where good agreement was found between the model and observations, and appears to result from the geostrophically-balanced response to the late night temperature distribution across the mountain barrier.

Chapter 7

SUMMARY AND CONCLUSIONS

This study has attempted to reveal the salient features associated with thermally driven meso-β to meso-α scale circulation systems across the Colorado mountain barrier. Through observational and numerical analyses, the research has identified the primary mechanisms forcing this largely unknown flow system. The purpose of this chapter is threefold; 1) to summarize the information presented in previous chapters and present a conceptual model which synthesizes the observations and numerical simulations, 2) describe the principal conclusions that were reached within this study, 3) discuss suggestions for future research.

7.1 Summary of Research Results

7.1.1 Initial observations

Results from a mountaintop measurement program conducted in the Colorado Rocky Mountains over the course of five summer seasons (1984-1988) have revealed the existence of a recurrent flow phenomenon across the mountain barrier. In the most basic sense, this phenomenon consists of a regional-scale (meso-β to meso-α scale) flow which operates on a diurnal time-scale, oscillating between daytime winds toward, and nocturnal outflow away, from the highest mountains. Of particular interest has been the observation of strong, nocturnal southeasterly winds at peaktop stations along the western slope. This previously undocumented flow regime was often observed to onset abruptly in early evening, replacing the prevalent west to northwest daytime flow. Outflow from convective storms over the high terrain of Colorado were shown to contribute to the southeasterly winds. Soundings have shown this nocturnal flow to be shallow over the peaktops ($\sim$ 500 m) with a low-level jet structure within a distinct stable layer. This southeasterly mountaintop flow is often observed with westerly upper level winds, determined from the Grand Junction, Colorado

rawinsonde. Thus, these nocturnal winds typically flow counter to the upper level wind direction, a surprising result considering that most of the stations used in this study are at exposed mountaintop locations, generally above the 70 kPa level. Of further interest, this southeasterly flow regime along the western slope of the mountain barrier occurs with enough frequency to appear in climatological averages of the station winds. An opposing circulation system with similar, though less dramatic characteristics is also found along the eastern slope, completing the inflow/outflow structure toward the high terrain across the entire mountain barrier.

7.1.2 Numerical experiment description

To facilitate the following summary of results from the numerical experiments, a brief description of each experiment included in the previous two Chapters is given in Table 7.1. All of the experiments used a nonhydrostatic version of the CSU-RAMS mesoscale model, and included a radiation parameterization with a prognostic soil model to realistically simulate surface forcing, which is the primary mechanism driving the flows of interest.

7.1.3 Simulated regional-scale wind characteristics

In an effort to understand more about the little studied regional-scale wind patterns across the Colorado mountains, two- and three-dimensional numerical simulations were conducted with the CSU-RAMS mesoscale model. Two three-dimensional experiments were conducted, one with zero initial winds, and the other using actual data. These experiments investigated the effects of surface heating over realistic three-dimensional topography at 7 km horizontal resolution and clearly demonstrated that many aspects of the observed winds at mountaintop could be attributed to intense summertime heating and cooling of the complex terrain on a diurnal temporal scale. From these two experiments, four primary stages of this diurnal circulation system can be identified.

Daytime mountain boundary layer development phase The most important thermally-forced flow feature was the development of a mountain-plains circulation along the eastern slope of the Front Range (Fig 7.1). This circulation system consists of a pressure-density solenoid (Holton, 1979) with a low-level upslope branch, vertical branch, and outflow, or

Table 7.1: SUMMARY OF NUMERICAL EXPERIMENTS

Exp.	Model Config.	Winds	Thermal Structure	Topography	Comments
3D1	3-D 2 grids (Δx=28, 7 km)	zero ambient flow	realistic	realistic on both grids	
T1	2-D 2 grids (Δx=32, 8 km)	" "	" "	idealized symmetric mountain	
T2	" "	" "	" "	low plateau	
T3	" "	" "	" "	high plateau	
T3a	" "	" "	" "	" "	no Coriolis
T3b	" "	" "	" "	" "	westerly shear
ZERO	" "	" "	" "	realistic	
AE1	" "	u= -1 m/s	" "	" "	
AE3	" "	u= -3 m/s	" "	" "	
AE6	" "	u= -6 m/s	" "	" "	
AW1	" "	u= +1 m/s	" "	" "	
AW3	" "	u= +3 m/s	" "	" "	
AW6	" "	u= +6 m/s	" "	" "	
S1	" "	zero ambient flow	neutral below 4.9 km	" "	compared with ZERO experiment
S2	" "	" "	isothermal below 4.9 km	" "	" "
M1	" "	" "	realistic	" "	dry soil east of Front Range, wet soil west
M2	" "	" "	" "	" "	dry soil west west soil east
M3	" "	" "	" "	" "	dry over low terrain, wet over high
3D2	3-D 3 grids (Δx= 111, 28, 7 km)	variable over domain	variable over domain	" "	initialized using NMC, rawinsonde, and surface info.

return branch at 5-6 km AGL. Similar, though generally weaker, thermally-direct circulation systems exist over the many smaller mountain ranges comprising the western slope of the Colorado Rocky Mountains, with a mean westerly inflow component toward the Continental Divide. The lower upslope branch of the mountain-plains solenoid along the Colorado Front Range has been intensively studied by Dirks (1969), Banta and Cotton (1981), Smith and McKee (1983), Toth and Johnson (1985), Abbs and Pielke (1986), and Tripoli and Cotton (1989 a,b).

The vertical branch of the mountain-plains circulation delineates the boundary between two differentially-heated air masses. A baroclinic zone results between the heated air over the intermountain region of the western slope and unheated air to the east of the Front Range barrier at a similar altitude. This thermal front is intensified throughout the late morning and early afternoon by convergence generated within the low-level regional-scale inflow circulation.

Late afternoon transition phase By late afternoon, the baroclinicity across the mountain-plains solenoid strengthens, with a temperature gradient of up to 2°C in 7 km of horizontal distance. Weakening of the convergent flow in the low-level branch of the system occurs concurrently from the diminished surface forcing. At this time, the pressure difference across the Front Range barrier forces the mountain-plains solenoid from its initial position near the Front Range crest, westward over the barrier and down the western slope (Fig. 7.2). Potentially cooler air from east of the mountain barrier is advected behind the leading edge of the low-level circulation, which has a slow propagation speed of 4-5 ms^{-1} at this time. Low-level winds (200-300 m agl) behind the interface are strong at 12-18 ms^{-1} and from a southeasterly direction, due to the prolonged influence of the Coriolis force. As the solenoid propagates over the barrier crest its vertical extent decreases from its negative buoyancy and the demise of surface heating, transforming into a shallow, intrusive current within the deep, well-mixed boundary layer over the intermountain region. The top of this low-level current is capped by a layer of high stability which is amplified during the day by subsidence associated with return flow in the upper branch of the solenoid.

Once the low-level circulation begins to propagate farther down the western slope of the Front Range, it takes on the physical characteristics of a density current as identified

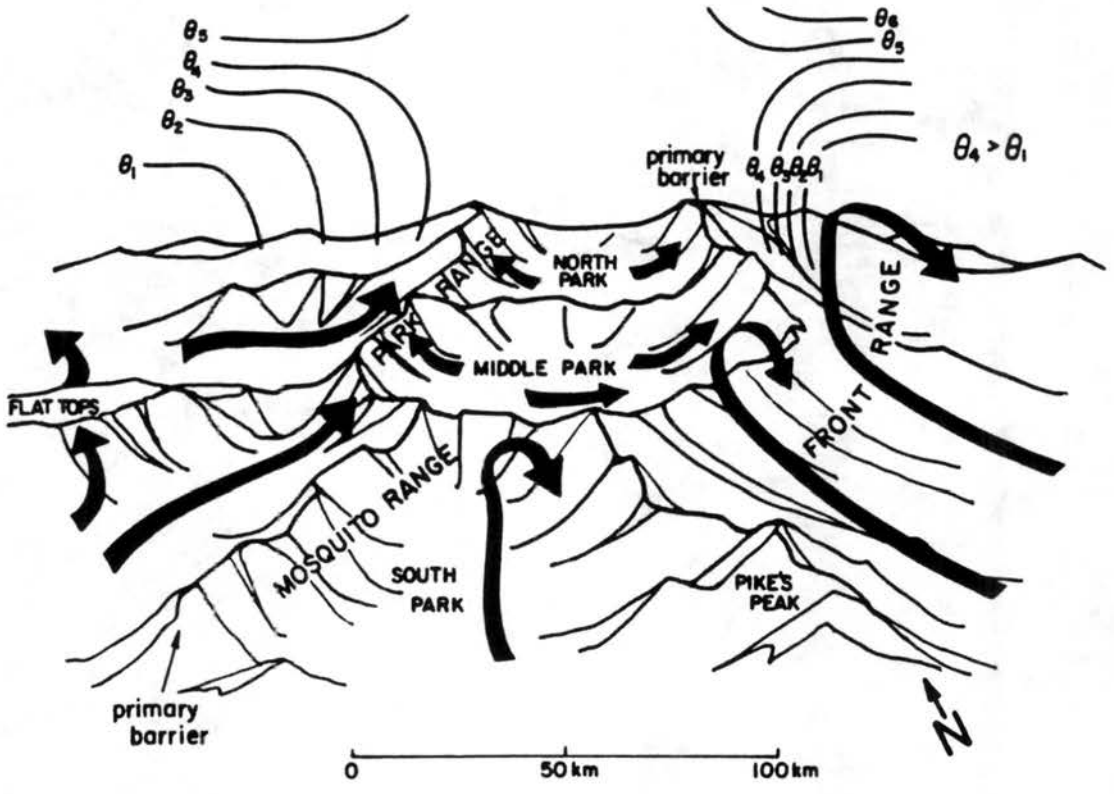

Figure 7.1: Conceptual model of the regional-scale daytime inflow circulation system over the north-central Colorado Rocky Mountains. (See text for details.)

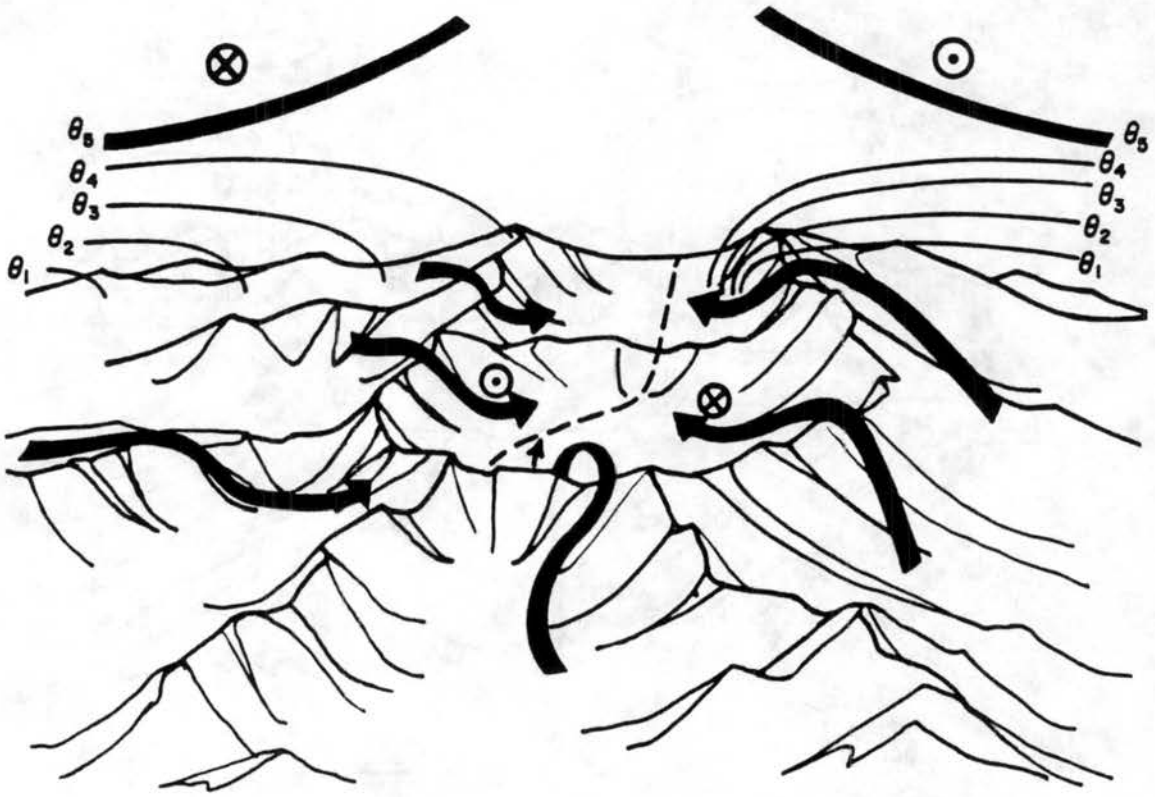

Figure 7.2: Transition phase conceptual model of the regional-scale circulation system over the north-central Colorado Rocky Mountains. (See text for details.)

by Benjamin (1968), Simpson (1969), Charba (1974), Goff (1976), and many others. The evolution of the mountain-plains solenoid into a shallow density current circulation is a widespread event and can encompass the entire north-south extent of the eastern slope of Colorado. Over these horizontal scales, the synoptic-scale wind and temperature structure become increasingly important, enhancing the development of regional-scale circulation systems in preferred regions.

Density currents initiated by the Front Range mountain-plains solenoid increase in velocity to 7-9 ms^{-1} as they propagate into the intermountain region. This effect is due to the additional gravitational acceleration down the western slope and the onset of surface cooling, which intensifies the thermal gradient across the interface. The powerful current causes an abrupt shift in the winds across its path from 7-12 ms^{-1} west-northwest flow, characteristic of the daytime wind regime over the western slope region, to strong southeasterly flow (15-20 ms^{-1} at 200 m agl), which marks the onset of the nocturnal wind regime. Thus, the abrupt wind shift appears as a progressive phenomenon in agreement with the ROMPEX observations over the western slope. Concurrent with the evolution of the density current, the upslope flow regime along the eastern slope decays, and with the onset of radiational surface cooling in the early evening, the flow begins to veer toward a downslope direction.

This unusual transitional flow behavior over the Colorado mountains appears to have an analog in northern Australia. There, the propagation of the east coast sea-breeze front over the crest of the Cape York Peninsula and its subsequent transformation into a density current has been described by Clarke (1972), Clarke (1983 a,b), Clarke (1984), and Crook and Miller (1985), among others. Moreover, this sea-breeze front has been found to collide with a similar, though weaker, front from the west coast of the peninsula. This collision initiates an undular bore which propagates southwestward for great distances during the night over the shallow sea breeze inversion of the Gulf of Carpentaria, and is occasionally witnessed along the south coast of the Gulf as the spectacular "Morning Glory" phenomenon (Clarke 1965).

Evening density current propagation phase This phase of the regional-scale circulation system over the Colorado mountain barrier includes the period during which the easterly density current propagates the length of the intermountain region. The flow interactions

associated with the low-level current appear to be similar in many respects to the sequence of events leading to the development of the Morning Glory phenomenon. This is demonstrated in Fig. 7.3 by the collision of the propagating easterly density current with a weaker westward moving current near the base of the Flat Tops Range. However, the wave response initiated by the collision is largely trapped by complex topography features within the intermountain region, a situation not found in tropical Australia. Meanwhile, north of the Flat Tops, the shallow density current progresses westward across the top of the intermountain ranges and through the lower passes. Topographic channeling and continuing Coriolis influence act to rotate the once southeasterly flow towards a more southerly direction. After it reaches the edge of the high terrain, the head of the current separates from the core of the flow and decays away over the lower terrain of western Colorado. The demise of the current over western Colorado appears similar to the decay of a far inland penetrating sea-breeze front, near dawn in northern Australia, into an isolated vortex, as described and simulated by Physick and Smith (1985).

Late night adjustment phase Late at night, the nocturnal flow over north-central Colorado adjusts to the influence of differential cooling across the mountain barrier, with the winds consisting of steady, shallow, downslope flows along the major slopes of the complex topography, and a regional-scale southerly flow through the intermountain region. While the downslope flows evolve in response to thermal imbalances induced by radiative cooling on a spatial-scale the order of individual slopes, the widespread southerly flow is the geostrophically-balanced response to the meso-α scale thermal gradient which continues to persist in the lower troposphere between the colder eastern and warmer western sides of the mountain barrier. This scenario of prevailing southerly winds over the center of the intermountain region in a quasi-balanced state, persists until the onset of heating the following morning. A rotation of the wind vector from southeast to south during the course of the night is also observed at the western slope ROMPEX stations (see Figs. 4.4 and 4.12).

Flow Sensitivity From the diverse array of sensitivity experiments (see Table 7.1) we can deduce that the development in summer of a deep mountain-plains circulation system over the crest of the high mountains, and its subsequent evolution in late afternoon into a shallow density current which propagates westward into the night is a fairly robust feature of the

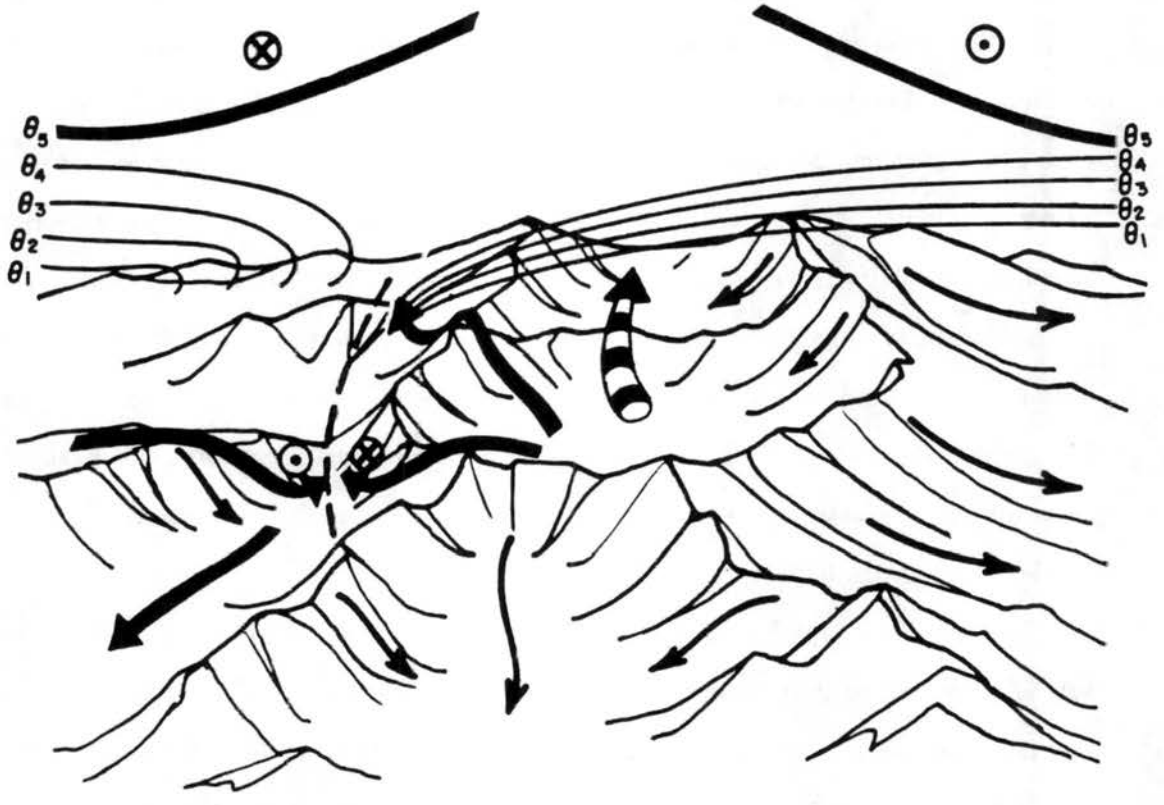

Figure 7.3: Conceptual model of the regional-scale nocturnal outflow circulation system over the north-central Colorado Rocky Mountains. (See text for details.)

summer climatology of the central Rocky Mountains. The initial experiments with differing topographic structures revealed that differential heating between an elevated plateau and lower plains is the primary mechanism by which the over barrier propagation of the solenoid occurs. The second experiment showed that the Coriolis force is responsible for maintaining a strong low-level southerly flow over the elevated plateau or intermountain region, which denotes the balanced atmospheric response to the baroclinicity generated during the day.

With strong westerly shear, the resulting low-level nocturnal density current still evolved over the plateau, due to the intense thermal front generated by differential temperature advection in the low-levels over the plateau. The propagation distance of the current is significantly reduced, however. Further experiments with differing direction and speed of initial flow revealed that mean easterly winds intensify the development of the low-level density current, whose westward propagation increases linearly with increasing initial easterly wind speed. These experiments also showed that the westward propagating current will still develop in initial westerly flow up to 3 ms^{-1}, but stronger westerly flow suppresses the growth of the mountain-plains solenoid to such an extent that no over the barrier propagation is possible.

The low-level variable stratification experiments showed that the mountain-plains solenoid and associated easterly density current will occur in all possible stratification regimes. The depth and upslope speeds obtained in the mountain-plains circulation are highly dependent on the initial stratification, with a neutral or weakly stable environment providing the most favorable conditions. However, despite the development of a weak solenoid, the westward propagation of the resulting density current was enhanced in an environment with isothermal stratification.

Soil moisture has a dramatic influence on the development of the mountain-plains circulation, with moist slopes and flat areas having greatly reduced thermally-driven winds. Dry conditions along the eastern slope and plains in combination with moist soil over the high terrain or western slope are unfavorable for the development of the strong nocturnal currents across western Colorado. On the other hand, the situation where the eastern slope experiences wet soil and the whole of western Colorado is dry, is very favorable for the development of a strong low-level westward propagating density current. In addition,

this latter scenario can supply eastern slope moisture for deep convective storms over the intermountain region.

7.2 Conclusions

While many of the conclusions reached in this study are discussed at length above, here we explicitly state several of the major findings of this research.

- A wind regime with distinct diurnally-reversing flow characteristics has been observed to occur with regularity over the Colorado mountain barrier. Coherent flow structure at mountaintop stations in similar topographic settings indicate this flow regime is of meso-β to meso-α scale proportions. Enveloping the smaller mountain-valley wind systems, yet contained within the larger plateau-scale circulation systems, this regional flow regime occupies a discrete scale within the hierarchical order of thermally-induced circulation systems over complex terrain. Perhaps the most revealing feature of this wind regime in Colorado are the strong, steady nocturnal outflow winds along the western slope of the mountain barrier, which generally flow counter to the upper level wind.

- The winds in summer over the high mountain terrain of Colorado are <u>not</u> controlled by large-scale winds (except on highly disturbed days), but by the intense surface forcing which generates pressure/density solenoids over the complex topography on regional-scales, including the deep mountain-plains solenoid over the Front Range. This result was clearly demonstrated in the climatological data from two mountaintop stations. In addition, comparisons of the afternoon flow between the two three-dimensional simulations, one with no initial flow and the other initialized with real wind and temperature data, showed striking similarities, revealing the dominant control of thermal forcing in producing the observed flows.

- The results from this study indicate that the diurnally-oscillating regional-scale circulation system observed at mountaintop over Colorado evolves from a fundamental potential to kinetic energy conversion process in response to thermal heating of the

complex topography. This result was demonstrated in a three-dimensional simulation with surface heating, and a realistic stratification, but no other external forcing. In the actual case day simulation, regional-scale circulations were generated whose wind direction, speed, and wind regime onset time were all in reasonable agreement with mountaintop wind observations, given the complex nature of the flow phenomenon.

- The reversal which occurs in the surface energy balance between the diurnal and nocturnal period transforms the thermally-driven circulation of interest from a deep mountain-plains solenoid to a shallow westward propagating density current. This density current is the forcing mechanism responsible for the strong nocturnal southeasterly winds observed at mountaintop over the western slope. The density current can also act as a triggering mechanism for late afternoon and early evening thunderstorm development over the western slope. The longevity of the observed southeast-south winds initiated by the density current is due to the larger-scale adjustment processes which sustain southerly winds over the mountain region west of the Front Range barrier throughout the nocturnal period.

7.3 Future Research Topics

While this study has revealed many aspects surrounding the diurnal evolution of meso-β to meso-α scale thermally-driven circulation systems in complex terrain, it has produced more questions than answers. Some of these unknown aspects pertain to the potential importance of physical processes which could not be adequately addressed here, while others concern the implications of regional-scale flows on the activities of man. With further investigation, based upon the results from this study, our understanding of these research problems and the impact of large mesoscale flow systems in general would be greatly enhanced. The most relevant of these problems are discussed below.

- In the course of this study we have suggested that the forcing associated with regional-scale flows could be an important triggering mechanism for deep convection over the Colorado mountains. In fact, Tripoli and Cotton (1989 a,b) have shown that the Front Range mountain-plains solenoid is the genesis mechanism for storms which propagate

eastward over the Great Plains and transform into long-lived mesoscale convective systems. Furthermore, these authors showed that the vertical and horizontal structure of the mountain-plain solenoid was strongly modulated by the deep convection. These results indicate that the structure of the dry regional-scale circulations described herein may be changed significantly through convective processes. In addition, it was shown in Section 4.2 that the outflows produced by strong convective storms over the western slope of Colorado can have a dramatic influence upon the resulting regional-scale flows.

Unfortunately, time and resource constraints precluded a numerical study of these effects within this particular research. Given these preliminary results and the frequency of deep moist convection over widespread regions of the Colorado mountains in summer (Klitch *et al.* 1985; Lopez and Holle 1986; Banta and Schaaf 1987), this problem certainly merits further research attention. This could be accomplished with the CSU-RAMS model in a three-dimensional framework with full microphysics to simulate cloud processes for a case day when strong storms were observed to influence the regional-scale circulations (e.g. 27 July 1987, see Section 4.2).

- Another problem not addressed within this research is the implication of regional-scale flows over the Colorado mountains on the transport and dispersion of pollutants. In the numerical results shown herein, atmospheric water vapor was used as a passive tracer, which revealed that east slope moisture was always entrained into the westward propagating density current. In a similar way, pollutants released near the ground within the populated regions along the Front Range could also be entrained into the low-level upslope branch of the mountain-plains solenoid and advected toward the barrier crest. While much of this material might be ejected within the vertical and return branches of this circulation system, some may become trapped within the evolving density current, during the transitional phase of the regional-scale flow, and advected westward into the intermountain region by this low-level circulation. The ensuing fallout of pollution particles over the western slope or re-entrainment into the developing boundary layer the following day over western Colorado, could have serious

implications for present pollution control policy. Given the variety and amounts of effluents released along the Front Range corridor, it appears that additional study to investigate these potential circulation effects with state of the art dispersion models and/or physical models is certainly warranted.

- The scale interaction of the regional-scale wind systems described here with wind systems on both larger- and smaller-scales deserves further research attention. In the case study simulation, it was shown that the synoptic-scale flow, influenced by the diurnal Western Plateau circulation system (Reiter and Tang 1984), affected the development of the east slope mountain-plain solenoid. This type of flow interaction between mesoscale and synoptic-scale thermally-driven circulations is largely unknown at present.

  At the other end of the spatial-scale, Barr and Orgill (1989) have discussed the influence of external winds upon the nocturnal downvalley circulation system within the Brush Creek Valley of western Colorado. In this study, we have simulated strong, nocturnal, near surface flows on the western slope, which could severely impact these valley circulation systems. In particular, the propagation of cold stable density current flow over a valley could easily "scour" the valley winds (Pielke 1985), entraining valley air (and possibly pollutants) into the density current, and interrupting the downvalley flow. A modeling study examining this effect could provide some insight into this multi-scale complex terrain problem.

- While in this chapter we have discussed an analog circulation system to the specific regional-scale flows described herein, thermally-forced circulation systems of meso-β to meso-α scales over complex terrain are little documented around the world. However, many regions around the globe possess similar terrain characteristics to that over the Colorado Front Range, with a large mountain slope separating a high plateau area from a lower plain. This appears to be the primary conditions necessary to generate a strong regional-scale flow response. Indeed, one of the few other observational studies related to the present is that conducted in South Africa by Tyson and Preston-Whyte (1972), who describe a diurnally-varying flow of regional-scale proportions between

the Drakensburg Plateau and the Indian Ocean. Detectable regional-scale circulations with analogous density currents might also be expected to occur within China in the vicinity of the Tibetan Plateau, in South America between the Pacific Ocean and the Peruvian and Bolivian high plateaus (see Lettau 1967, 1978), in Mexico between the coastal plains and the central plateau, and perhaps even in Arizona between the lower Sonoran Desert and the Mogollon Rim. Future observational and numerical studies might investigate the presence of similar thermally-driven regional-scale flows and their possible meteorological implications within these regions.

REFERENCES

Abbs, D.J., and R.A. Pielke, 1986: Thermally forced surface flow and convergence patterns over northeast Colorado. *Mon. Wea. Rev.*, **114**, 2281-2296.

Albrecht, B.A., and S.K. Cox, 1976: Pyrgeometer data reduction and calibration procedures. Atmos. Sci. Paper No. 251, Colorado State University, Dept. of Atmospheric Science, Fort Collins, CO 80523. 59 pp.

Arritt, R.W., and R.A. Pielke, 1986: Interactions of nocturnal slope flows with ambient winds. *Bound.-Layer Meteorol.*, **37**, 183-195.

Astling, E.G., 1984: On the relationship between diurnal mesoscale circulations and precipitation in a mountain-valley. *J. Climate Appl. Meteor.*, **23**, 1635-1644.

Atkinson, B.W., 1981: *Meso-scale Atmospheric Circulations*, Academic Press, London. 495 pp.

Ayer, H.S., 1961: On the dissipation of drainage wind systems in valleys in the morning hours. *J. Meteor.*, **18**, 560-563.

Bader, D.C., and T.B. McKee, 1983: Dynamical model simulation of the morning boundary layer development in deep mountain valleys. *J. Climate Appl. Meteor.*, **22**, 341-351.

—, — and G.J. Tripoli, 1987: Mesoscale boundary layer evolution over complex terrain. Part I: Numerical simulation of the diurnal cycle. *J. Atmos. Sci.*, **44**, 2823-2838.

Banta, R.M., 1984: Daytime boundary-layer evolution over mountainous terrain. Part I: Observations of the dry circulations. *Mon. Wea. Rev.*, **112**, 340-356.

—, 1986: Daytime boundary-layer evolution over mountainous terrain. Part II: Numerical studies of upslope flow duration. *Mon. Wea. Rev.*, **114**, 1112-1130.

—, and W.R. Cotton, 1981: An analysis of the structure of local wind systems in a broad mountain basin. *J. Appl. Meteor.*, **20**, 1255-1266.

—, and C.B. Schaaf, 1987: Thunderstorm genesis zones in the Colorado Rocky Mountains as determined by traceback of geosynchronous satellite images. *Mon. Wea. Rev.*, **115**, 463-476.

Barnes, S.L., 1973: Mesoscale objective map analysis using weighted time series observations. NOAA Tech. Memo. ERL NSSL-62, 66 pp. [NTIS COM-73-10781].

Barr, S., and W.E. Clements, 1981: Nocturnal wind characteristics in high terrain of the Piceance Basin, Colorado. Preprints, 2nd Conference on Mountain Meteorology, 9-12 November 1981, Steamboat Springs, Colorado, Amer. Meteor. Soc., Boston, MA. 325-330.

——, and M.M. Orgill, 1989: Influence of external meteorology on nocturnal valley drainage winds. *J. Appl. Meteor.*, **28**, 497-517.

Barry, R.G., 1981: *Mountain Weather and Climate.* Methuen and Co. Ltd., London, 313 pp.

Benjamin, S.G., 1986: Some effects of surface heating and topography on the regional severe storm environment. Part II: Two-dimensional idealized experiments. *Mon. Wea. Rev.*, **114**, 330-343.

——, and T.N. Carlson, 1986: Some effects of surface heating and topography on the regional severe storm environment. Part I: Three-dimensional simulations. *Mon. Wea. Rev.*, **114**, 307-329.

Benjamin, T.B, 1968: Gravity currents and related phenomena. *J. Fluid Mech.*, **31**, 209-248.

Betts, A.K., 1973: The thermodynamic transformation of the tropical subcloud layer by precipitation and downdrafts. *J. Atmos. Sci.*, **33**, 1008-1020.

——, 1982: Cloud thermodynamic models in saturation point coordinates. *J. Atmos. Sci.*, **39**, 2182-2190.

——, 1984: Boundary layer thermodynamics of a High Plains severe storm. *Mon. Wea. Rev.*, **112**, 2199-2211.

Blackadar, A.K., 1957: Boundary layer wind maxima and their significance for the growth of nocturnal inversions. *Bull. Amer. Meteor. Soc.*, **38**, 283-290.

Bolton, D., 1980: The computation of equivalent potential temperature. *Mon. Wea. Rev.*, **7**, 1046-1053.

Bonner, W.D., 1968: Climatology of the low level jet. *Mon. Wea. Rev.*, **96**, 833-850.

——, and J. Paegle, 1970: Diurnal variations in boundary layer winds over the south-central United States in summer. *Mon. Wea. Rev.*, **98**, 735-744.

Bossert, J.E., and E.R. Reiter, 1987: Observed characteristics of a mountain-plain circulation in Colorado. *Proc. AMS Fourth Conference on Mountain Meteorology*, Seattle, WA, Amer. Meteor. Soc., 20-21.

—, J.D. Sheaffer and E.R. Reiter, 1989: Aspects of regional-scale flows in mountainous terrain. *J. Appl. Meteor.*, **28**, 590-601.

Brehm, M., and C. Freytag, 1982: Erosion of the night-time thermal circulation in an alpine valley. *Arch. Meteor. Geophys. Bioklim.*, **31**, 331-352.

Brenner, I.S., 1974: A surge of maritime tropical air–Gulf of California to the southwestern United States. *Mon. Wea. Rev.*, **102**, 375-389.

Brown, J.M., 1979: Mesoscale unsaturated downdrafts driven by rainfall evaporation: A numerical study. *J. Atmos. Sci.*, **36**, 313-338.

Bryson, R.A., and W.P. Lowry, 1955: Synoptic climatology of the Arizona summer precipitation singularity. *Bull. Amer. Meteor. Soc.*, **36**, 329-339.

Buettner, K.J.K., and N. Thyer, 1966: Valley winds in the Mount Rainier area. *Arch. Meteor. Geophys. Bioklim., Ser. B.*, **14**, 125-147.

Burger, A., and E. Ekhart, 1937: Uber die tagliche Zirkulation der Atmosphare im Bereiche der Alpen. *Ger. Beitr. Geophys.*, **49**, 341-367.

Carlson, J.D., and M.R. Foster, 1986a: Numerical study of some neutrally and unstably stratified boundary-layer flows over a valley at small Richardson Number. *Tellus*, **38A**, 60-75.

—, and —, 1986b: Numerical study of some neutrally and unstably stratified boundary-layer flows over a valley at moderate Richardson Number. *J. Climate Appl. Meteor.*, **25**, 203-213.

Carlson, T.N., S.G. Benjamin, G.S. Forbes and Y.-F. Lin, 1983: Elevated mixed layers in the regional severe storm environment: Conceptual model and case studies. *Mon. Wea. Rev.*, **111**, 1453-1473.

Charba, J., 1974: Application of gravity current model to analysis of squall line gust front. *Mon. Wea. Rev.*, **102**, 140-156.

Chen, C., and W.R. Cotton, 1983: A one-dimensional simulation of the stratocumulus-capped mixed layer. *Bound.-Layer Meteor.*, **25**, 289-321.

Chen, L., E.R. Reiter and Z. Feng, 1985: The atmospheric heat source over the Tibetan Plateau; May - August 1979. *Mon. Wea. Rev.*, **113**, 1771-1790.

Clark, T.L., 1977: A small-scale dynamic model using a terrain-following coordinate transformation. *J. Comp. Phys.*, **24**, 186-215.

—, and R.D. Farley, 1984: Severe downslope windstorm calculations in two and three spatial dimensions using anelastic interactive grid nesting: A possible mechanism for gustiness. *J. Atmos. Sci.*, **41**, 329-350.

Clarke, R.H., 1965: Horizontal mesoscale vortices in the atmosphere. *Aust. Met. Mag.*, **50**, 1-25.

—, 1972: The morning glory: An atmospheric hydraulic jump. *J. Appl. Meteor.*, **11**, 304-311.

—, 1983a: Fair weather nocturnal inland wind surges and atmospheric bores. Part I: Nocturnal wind surges. *Aust. Met. Mag.*, **31**, 133-145.

—, 1983b: Fair weather nocturnal inland wind surges and atmospheric bores. Part II: Internal atmospheric bores in northern Australia. *Aust. Met. Mag.*, **31**, 147-160.

—, 1984: Colliding sea-breezes and the creation of internal atmospheric bore waves: Two-dimensional numerical studies. *Aust. Met. Mag.*, **32**, 207-226.

Clements, W.E., J.A. Archuleta and P.H. Gudiksen, 1989: Experimental design of the 1984 ASCOT Field Study. *J. Appl. Meteor.*, **28**, 405-413.

—, — and D.E. Hoard, 1989: Mean structure of the nocturnal drainage flow in a deep valley. *J. Appl. Meteor.*, **28**, 457-462.

Cotton, W.R., R.L. George and K.R. Knupp, 1982: An intense, quasi-steady thunderstorm over mountainous terrain. Part I: Evolution of the storm-initiating mesoscale circulation. *J. Atmos. Sci.*, **39**, 328-342.

—, —, P.J. Wetzel and R.L. McAnelly, 1983: A long-lived mesoscale convective complex. Part I: The mountain generated component. *Mon. Wea. Rev.*, **111**, 1893-1918.

—, C.J. Tremback, and R.L. Walko, 1988: CSU-RAMS - A cloud model goes regional. *Proc. NCAR Workshop on Limited-Area Modeling Intercomparison*, Nov. 15-18, NCAR, Boulder, CO, 202-211.

Coulter, R.L., M.M. Orgill and W.M. Porch, 1989: Tributary fluxes into Brush Creek Valley. *J. Appl. Meteor.*, **28**, 555-568.

Crook, N.A. and M.J. Miller, 1985: A numerical and analytical study of atmospheric undular bores. *Quart. J. R. Meteor. Soc.*, **111**, 225-242.

Crow, L.W., 1969: Relationships between hail and rain in Kansas, Nebraska and eastern Colorado. LWC Report No. 76, Final Report, Contract No. NSF C522, National Science Foundation, 18th and G Streets, N.W., Washington, D.C. 20550, 34 pp.

Culverwell, A.H., 1982: An analysis of moisture sources and circulation fields associated with an MCC episode. M.S. thesis, Colorado State University, Dept. of Atmospheric Science, Fort Collins, CO 80523, 291 pp.

Davidson, B., and P.K. Rao, 1958: Preliminary report on valley wind studies in Vermont. 1957. Final Report, Contract AF 19(604)-1971, AFCRC-TR-58-29, College of Engineering, New York University, 54 pp. (Available from NTIS as PB 138 594).

Defant, F., 1949: Zur Theorie der Hangwinde nebst Bemerkungen zur Theorie der Bergund Talwinde. [A theory of slope winds, along with remarks on the theory of mountain winds and valley winds.] *Arch. Meteor. Geophys. Bioklim, Ser. A*, **1**, 421-450. [English translation: Whiteman, C.D. and E. Dreiseitl, 1984: *Alpine Meterology.* Translations of classic contributions by A. Wagner, E. Ekhart and F. Defant. PNL-5141/ASCOT-84-3. Pacific Northwest Laboratory, Richland, Washington, 121 pp.]

Defant, F., 1951: Local winds. *Compendium of Meteorology*, Amer. Meteor. Soc., 655-672.

Dirks, R., 1969: A theoretical investigation of convective patterns in the lee of the Colorado Rockies. Ph.D. dissertation. Atmos. Sci. Paper No. 145. Dept. of Atmospheric Science, Colorado State University, Fort Collins, CO 80523, 122 pp.

Doran, J.C., and T.W. Horst, 1981: Velocity and temperature oscillations in drainage winds. *J. Appl. Meteor.*, **20**, 361-364.

——, and ——, 1983: Observations and models of simple nocturnal slope flows. *J. Atmos. Sci.*, **40**, 708-717.

Droegemeier, K.K., and R.B. Wilhelmson, 1987: Numerical simulation of thunderstorm outflow dynamics. Part I: Outflow sensitivity experiments and turbulence dynamics. *J. Atmos. Sci.*, **44**, 1180-1210.

Egger, J., 1981: On the linear two-dimensional theory of thermally induced slope winds. *Contrib. Atmos. Phys.*, **54**, 465-481.

——, 1983: Topographic forcing. *Mesoscale Meteorology-Theories, Observations and Models.* Lilly, D.K. and T. Gal-Chen, Eds., 321-337.

——, 1987: Valley winds and the diurnal circulation over plateaus. *Mon. Wea. Rev.*, **115**, 2177-2186.

Ekhart, E., 1934: Neuere Untersuchungen zur Aerologie der Talwinde: Die periodischen Tageswinde in einem Quertale der Alpen. [New studies of the aerology of valley winds: the periodic diurnal winds in a cross-valley of the Alps]. *Beitr. Physik fr. Atmos.*, **21**, 245-268.

Ekhart, E., 1944: Beitrage zur alpinen Meteorologie. [Contributions to Alpine meteorology]. *Meteor. Z.*, **61**, 217-231. [English translation: Whiteman, C.D. and E. Dreiseitl, 1984:

Alpine Meteorology. Translations of classic contributions by A. Wagner, E. Ekhart and F. Defant. PNL-5141/ASCOT-84-3. Pacific Northwest Laboratory, Richland, Washington, 121 pp.]

Ellison, T.H., and J.S. Turner, 1959: Turbulent entrainment in stratified flows. *J. Fluid Mech.*, **6**, 423-448.

Farrell, R.J., and T.N. Carlson, 1989: Evidence for the role of the lid and underrunning in an outbreak of tornadic thunderstorms. *Mon. Wea. Rev.*, **117**, 857-871.

Fitzjarrald, D.R., 1984: Katabatic wind in opposing flow. *J. Atmos. Sci.*, **41**, 1143-1158.

Flatau, P.J., G.J. Tripoli, J. Verlinde and W.R. Cotton, 1989: The CSU-RAMS Cloud Microphysics Module: General theory and code documentation. Atmos. Sci. Paper No. 451, Colorado State University, Dept. of Atmospheric Science, Fort Collins, CO 80523, 88 pp.

Fleagle, R.G., 1950: A theory of air drainage. *J. Meteor.*, **7**, 227-232.

Flohn, H., 1965: Thermal effects of the Tibetan Plateau during the Asian monsoon season. *Aust. Met. Mag.*, **49**, 55-57.

——, 1968: Contributions to a meteorology of the Tibetan Highlands. Atmos. Sci. Paper No. 130, Colorado State University, Dept. of Atmospheric Science, Fort Collins, CO 80523, 49 pp.

Fournet, M.J., 1840: Des brises de jour et de nuit autour des montagnes. *Annls. Chim. Phys.*, **74**, 337-401.

Freytag, C., 1985: MERKUR-Results: Aspects of the temperature field and the energy budget in a large alpine valley during mountain and valley wind. *Contrib. Atmos. Phys.*, **58**, 458-476.

Gao, Y.X., M.C. Tang, S.W. Luo, Z.B. Shen and C. Li, 1981: Some aspects of recent research on the Qinghai-Xizang Plateau meteorology. *Bull. Amer. Meteor. Soc.*, **62**, 31-35.

Gleeson, T.A., 1951: On the theory of cross-valley winds arising from differential heating of the slopes. *J. Meteor.*, **8**, 398-405.

——, 1953: Effects of various factors on valley winds. *J. Meteor.*, **10**, 262-269.

Goff, R.C., 1976: Vertical structure of thunderstorm outflows. *Mon. Wea. Rev.*, **104**, 1429-1440.

Green, C.R., and W.D. Sellers, 1964: *Arizona Climate.* Univ. of Arizona Press, 503 pp.

Gryning, S.-E., L. Mahrt and S. Larsen, 1985: Oscillating nocturnal slope flow in a coastal valley. *Tellus*, **37A**, 196-203.

Hahn, D.G., and S. Manabe, 1975: The role of mountains in the south Asian monsoon circulation. *J. Atmos. Sci.*, **32**, 1515-1541.

Hales, J.E., Jr., 1974: Southwestern United States summer monsoon source–Gulf of Mexico or Pacific Ocean? *J. Appl. Meteor.*, **13**, 331-342.

Haltiner, G.J., and R.T. Williams, 1980: *Numerical Prediction and Dynamic Meteorology.* 2nd ed., Wiley and Sons, 477 pp.

Hann, J. von, 1879: Zur theorie der berg- und talwinde. *Z. ost ges. Met.*, **14**, 444-448.

Hennemuth, B., 1985: Temperature field and energy budget of a small alpine valley. *Contrib. Atmos. Phys.*, **58**, 545-559.

—, and H. Schmidt, 1985: Wind phenomena in the Dischma Valley during DISKUS. *Arch. Meteor. Geophys. Bioclim., Ser. B.*, **35**, 361-387.

Henz, J., 1974: Colorado high plains thunderstorm systems - a descriptive radar-synoptic climatology. M.S. thesis, Department of Atmospheric Science, Colorado State University, Fort Collins, Colorado 80523, 82 pp.

Heywood, G.S.P., 1933: Katabatic winds in a valley. *Quart. J. Roy. Meteor. Soc.*, **59**, 47-58.

Holton, J.R., 1967: The diurnal boundary layer wind oscillation above sloping terrain. *Tellus*, **19**, 199-205.

—, 1979: *An Introduction to Dynamical Meteorology*, 2nd ed., Academic Press, 391 pp.

Horst, T.W., and J.C. Doran, 1986: Nocturnal drainage flow on simple slopes. *Bound.-Layer Meteorol.*, **34**, 263-286.

Houghton, J.G., 1979: A model for orographic precipitation in the north-central Great Basin. *Mon. Wea. Rev.*, **107**, 1462-1475.

Hunt, J.C.R., W.H. Snyder and R.E. Lawson, R., 1978: Flow structure and turbulent diffusion around a three-dimensional hill: Fluid modeling study on effects of stratification. Part I: Flow structure. U.S. Environmental Protection Agency, EPA-600/4-78-041, Research Triangle Park, NC.

Jeffreys, H., 1922: On the dynamics of the wind. *Quart. J. Roy. Meteor. Soc.*, **48**, 29-47.

Jelinek, A., 1937a: Beitrag zur Mechanik der periodischen Hangwinde. [Contributions on the mechanics of periodic slope winds]. *Beitr. Phys. fr. Atmos.*, **24**, 60-84.

Jelinek, A., 1937b: Uber den thermischen Aufbau der periodischen Hangwinde.[On the thermal buildup of periodic slope winds]. *Beitr. Phys. fr. Atmos.*, **24**, 85-97.

Johnson, R.H., 1976: The role of convective-scale precipitation downdrafts in cumulus and synoptic-scale interactions. *J. Atmos. Sci.*, **33**, 1890-1910.

Kamburova, P.L., and F.H. Ludlam, 1966: Rainfall evaporation in thunderstorm downdraughts. *Quart. J. Roy. Meteor. Soc.*, **92**, 510-518.

Klemp, J.B., and R.B. Wilhelmson, 1978a: The simulation of three-dimensional convective storm dynamics. *J. Atmos. Sci.*, **35**, 1070-1096.

—, and —, 1978b: Simulations of right- and left-moving storms produced through storm splitting. *J. Atmos. Sci.*, **35**, 1097-1110.

Klitch, M.A., J.F. Weaver, F.P. Kelly and T.H. VonderHaar, 1985: Convective cloud climatologies constructed from satellite imagery. *Mon. Wea. Rev.*, **113**, 326-337.

Knupp, K.R., 1985: Precipitating convective cloud downdraft structure: A synthesis of observations and modeling. Ph.D. dissertation, Atmos. Sci. Paper No. 387, Colorado State University, Dept. of Atmospheric Science, Fort Collins, CO 80523. 296 pp.

—, 1987: Downdrafts within High Plains cumulonimbi. Part I: General kinematic structure. *J. Atmos. Sci.*, **44**, 987-1008.

—, and W.R. Cotton, 1982a: An intense, quasi-steady thunderstorm over mountainous terrain. Part II: Doppler radar observations of the storm morphological structure. *J. Atmos. Sci.*, **39**, 343-358.

—, and W.R. Cotton, 1982b: An intense, quasi-steady thunderstorm over mountainous terrain. Part III: Doppler radar observations of the turbulent structure. *J. Atmos. Sci.*, **39**, 359-368.

Kondo, J., and T. Sato, 1988: A simple model of drainage flow on a slope. *Bound.-Layer Meteorol.*, **43**, 103-123.

Koteswaram, P., 1958: The Easterly jet stream in the Tropics. *Tellus*, **10**, 43-57.

Kuo, H.L., and Y.F. Qian, 1981: Influence of the Tibetan Plateau on cumulative and diurnal changes of weather and climate in summer. *Mon. Wea. Rev.*, **109**, 2337-2356.

—, and —, 1982: Numerical simulation of the development of mean monsoon circulation in July. *Mon. Wea. Rev.*, **110**, 1879-1897.

Lee, J.T., R.E. Lawson, Jr. and G.L. Marsh, 1987: Flow visualization experiments on stably stratified flow over ridges. *Meteor. Atmos. Phys.*, **37**, 183-194.

Lenschow, D.H., B.B. Stankov and L. Mahrt, 1979: The rapid morning boundary-layer transition. *J. Atmos. Sci.*, **36**, 2108-2124.

Lettau, H.H., 1967: Small to large-scale features of boundary layer structure over mountain slopes. *Proceedings of the Symposium on Mountain Meteorology*, Atmos. Sci. Paper No. 122, Colorado State University, Dept. of Atmospheric Science, Fort Collins, CO 80523, 74 pp.

—, and K. Lettau, Eds., 1978: *Exploring the world's driest climate.* Rep. 101, Inst. Environ. Studies, University of Wisconsin, Madison, 264 pp.

Lopez, R.E., and R.L. Holle, 1986: Diurnal and spatial variability of lightning activity in northeastern Colorado and central Florida during the summer. *Mon. Wea. Rev.*, **114**, 1288-1312.

Louis, J.F., 1979: A parametric model of vertical eddy fluxes in the atmosphere. *Bound.-Layer Meteorol.*, **17**, 187-202.

Luo, H., and M. Yanai, 1983: The large-scale circulation and heat sources over the Tibetan Plateau and surrounding areas during the early summer of 1979. Part I: Precipitation and kinematic analyses. *Mon. Wea. Rev.*, **111**, 922-944.

—, and —, 1984: The large-scale circulation and heat sources over the Tibetan Plateau and surrounding areas during the early summer of 1979. Part II: Heat and moisture budgets. *Mon. Wea. Rev.*, **112**, 966-989.

Maddox, R.A., 1981: The structure and life-cycle of midlatitude mesoscale convective complexes. Ph.D. dissertation. Atmos. Sci. Paper No. 336, Dept. of Atmospheric Science, Colorado State University, Fort Collins, CO 80523, 311 pp.

Mahrer, Y., and R. Pielke, 1977a: A numerical study of airflow over irregular terrain. *Beitr. Phys. Atmos.*, **50**, 98-113.

—, and —, 1977b: The effects of topography on sea and land breezes in a two-dimensional numerical model. *Mon. Wea. Rev.*, **105**, 1151-1162.

Mahrt, L., 1982: Momentum balance of gravity flows. *J. Atmos. Sci.*, **39**, 2701-2711.

—, and S. Larsen, 1982: Small scale drainage flow. *Tellus*, **34**, 579-587.

Manins, P.C., and B.L. Sawford, 1979a: Katabatic winds: A field case study. *Quart. J. Roy. Meteor. Soc.*, **105**, 1011-1025.

—, and —, 1979b: A model of katabatic winds. *J. Atmos. Sci.*, **36**, 619-630.

Mannouji, N., 1982: A numerical experiment on the mountain and valley winds. *J. Meteor. Soc. Japan*, **60**, 1085-1105.

Mass, C., 1982: The topographically forced circulations of western Washington state and their influence on precipitation. *Mon. Wea. Rev.*, **110**, 170-183.

McKee, T.B., and R.D. O'Neal, 1989: The role of valley geometry and energy budget in the formation of nocturnal valley winds. *J. Appl. Meteor.*, **28**, 445-456.

McNider, R.T., 1982: A note on velocity fluctuations in drainage flows. *J. Atmos. Sci.*, **39**, 1658-1660.

——, and R.A. Pielke, 1981: Diurnal boundary-layer development over sloping terrain. *J. Atmos. Sci.*, **38**, 2198-2212.

——, and ——, 1984: Numerical simulation of slope and mountain flows. *J. Climate Appl. Meteor.*, **23**, 1441-1453.

Means, L.L., 1954: A study of the mean southerly wind maxima in low levels associated with a period of summer precipitation in the middle west. *Bull. Amer. Meteor. Soc.*, **35**, 166-170.

Mesinger, F., Z.A. Janjic, S. Nickovic, D. Gavrilov and D.G. Deaven, 1988: The step-mountain coordinate: Model description and performance for cases of alpine lee cyclogenesis and for a case of an Appalachian redevelopment. *Mon. Wea. Rev.*, **116**, 1493-1518.

Mitchell, K.E., and J.B. Hovermale, 1977: A numerical investigation of a severe thunderstorm gust front. *Mon. Wea. Rev.*, **105**, 657-675.

Moll, E., 1935: Aerologische Untersuchung periodischer Gebirgswinde in V-formigen Alpentalern. [Aerological study of periodic mountain winds in V-shaped alpine valleys.] *Beitr. Phys. fr. Atmos.*, **22**, 177-197.

Neff, W.D., and C.W. King, 1989: The accumulation and pooling of drainage flows in a large basin. *J. Appl. Meteor.*, **28**, 518-529.

Newton C.W., 1950: Structure and mechanism of the prefrontal squall line. *J. Meteor.*, **8**, 210-222.

Nitta, T., 1983: Observational study of heat sources over the eastern Tibetan Plateau during the summer monsoon. *J. Meteor. Soc. Japan*, **61**, 590-605.

Ookouchi, Y., M. Segal, R.C. Kessler and R.A. Pielke, 1984: Evaluation of soil moisture effects on the generation and modification of mesoscale circulations. *Mon. Wea. Rev.*, **112**, 2281-2292.

Orville, H.D., 1968: Ambient wind effects on the initiation of development of cumulus clouds over mountains. *J. Atmos. Sci.*, **25**, 385-403.

Petkovsek, Z., and A. Hocevar, 1971: Night drainage winds. *Arch. Meteor. Geophys. Bioklim., Ser. A.*, **20**, 353-360.

Phillips, N.A., and J. Shukla, 1973: On the strategy of combining coarse and find grid meshes in numerical weather prediction. *J. Appl. Meteor.*, **12**, 763-770.

Physick, W.L., and R.K. Smith, 1985: Observations and dynamics of sea-breezes in northern Australia. *Aust. Met. Mag.*, **33**, 51-63.

Pielke, R.A., 1974: A three dimensional model of the sea breezes over South Florida. *Mon. Wea. Rev.*, **102**, 115-139.

——, 1985: The use of mesoscale numerical models to assess wind distribution and boundary-layer structure in complex terrain. *Bound. -Layer Meteorol.*, **31**, 217-232.

Porch, W.M., R.B. Fritz, R.L. Coulter and P.H. Gudiksen, 1989: Tributary, valley and sidewall air flow interactions in a deep valley. *J. Appl. Meteor.*, **28**, 578-589.

Prandtl, L., 1942: *Fuhrer durch die Stromungslehre.* Braunschweig Vieweg und Sohn, 382 pp.

——, 1952: *Essentials of Fluid Dynamics*, Blackie and Son Ltd., London [translation of Prandtl (1942)].

Rangarajan, S., 1963: Thermal effects of the Tibetan Plateau during the Asian monsoon season. *Aust. Met. Mag.*, **42**, 24-34.

Reiter, E.R., and Deng-yi Gao, 1982: Heating of the Tibet Plateau and movements of the south Asian high during spring. *Mon. Wea. Rev.*, **110**, 1964-1711.

——, and M. Tang, 1984: Plateau effects on diurnal circulation patterns. *Mon. Wea. Rev.*, **112**, 638-651.

——, J.D. Sheaffer, J.E. Bossert, R.C. Fleming, W.E. Clements, J.T. Lee, S. Barr, J.A. Archuleta and D.E. Hoard, 1987a: ROMPEX–The Rocky Mountain Peaks Experiment of 1985: Preliminary assessment. *Bull. Amer. Meteor. Soc.*, **68**, 321-328.

——, ——, ——, E.A. Smith, G. Stone, R. McBeth and Q. Zheng, 1987b: Tibet revisited–TIPMEX-86. *Bull. Amer. Meteor. Soc.*, **68**, 607-615.

Sang, J., and E.R. Reiter, 1982a: Model-derived effects of large-scale diurnal thermal forcing on meteorological fields. *Arch. Meteor. Geoph. Biokl., Ser. A.*, **31**, 185-203.

——, and ——, 1982b: Numerical model for a large-scale mountain-valley breeze on a plateau. *Proc. Symp. Mountain Meteorology, Beijing*, Reiter *et al.*, Eds., Science Press, Beijing, and Amer. Meteor. Soc., 609-631.

Segal, M., J.R. Garratt, G. Kallos and R.A. Pielke, 1989: The impact of wet soil and canopy temperatures on daytime boundary-layer growth. *J. Atmos. Sci.*, **46**, 3673-3684.

Sheaffer, J.D., and E.R. Reiter, 1987: Measurements of surface energy budgets in the Rocky Mountains of Colorado. *J. Geophys. Res.*, **92**, 4145-4162.

Shen, R., E.R. Reiter, and J.F. Bresch, 1986: Some aspects of the effects of sensible heating on the development of summer weather systems over the Tibetan Plateau. *J. Atmos. Sci.*, **43**, 2241-2260.

Shinn, J.H., R.T. Cederwall, F.J. Gouveia and K.R. Chapman, 1989: Micrometeorology of slope flows in a tributary canyon during the 1984 ASCOT Experiment. *J. Appl. Meteor.*, **28**, 569-577.

Simpson, J.E., 1969: A comparison between laboratory and atmospheric density currents. *Quart. J. Roy. Meteor. Soc.*, **95**, 754-765.

——, and R.E. Britter, 1980: A laboratory model of an atmospheric meso-front. *Quart. J. Roy. Meteor. Soc.*, **106**, 485-500.

——, D.A. Mansfield and J.R. Milford, 1977: Inland penetration of sea-breeze fronts. *Quart. J. Roy. Meteor. Soc.*, **103**, 47-76.

Smith, E.A., 1986a: The structure of the Arabian heat low. Part I: Surface energy budget. *Mon. Wea. Rev.*, **114**, 1067-1083.

——, 1986b: The structure of the Arabian heat low. Part II: Bulk tropospheric heat budget and implications. *Mon. Wea. Rev.*, **114**, 1084-1102.

Smith, E.A., E.R. Reiter and Y. Gao, 1986: Transition of the surface energy budget in the Gobi Desert between spring and summer seasons. *J. Climate Appl. Meteor.*, **24**, 1725-1740.

Smith, J.K., and T.B. McKee, 1983: Undisturbed clear day diurnal wind and temperature pattern in northeastern Colorado. Atmos. Sci. Paper No. 365, Colorado State University, Dept. of Atmospheric Science, Fort Collins, CO 80523, 103 pp.

Staley, D.O., 1957: The low-level sea breeze of northwest Washington. *J. Meteor.*, **14**, 458-470.

Steinacker, R., 1984: Area-height distribution of a valley and its relation to the valley wind. *Contrib. Atmos. Phys.*, **57**, 64-71.

Stone, G.L., and D.E. Hoard, 1989: Low-frequency velocity and temperature fluctuations in katabatic valley flows. *J. Appl. Meteor.*, **28**, 477-488.

Tang, M., and E.R. Reiter, 1984: Plateau monsoons of the Northern Hemisphere: A comparison between North America and Tibet. *Mon. Wea. Rev.*, **112**, 617-637.

Tang, W., 1976: Theoretical study of cross-valley wind circulations. *Arch. Meteor. Geophys. Bioklim., Ser. A*, **25**, 1-18.

Tao, S.Y., and Y.H. Ding, 1981: Observational evidence of the influence of the Qinghai-Xizang (Tibet) plateau on the occurence of heavy rain and severe convective storms in China. *Bull. Amer. Meteor. Soc.*, **62**, 23-30.

Thyer, N.H.: 1966: A theoretical explanation of mountain and valley winds by a numerical method. *Arch. Meteor. Geophys. Bioklim., Ser. A*, **15**, 318-348.

Toth, J.J., 1987: Interaction of shallow cold surges with topography on scales of 100-1000 kilometers. Ph.D. dissertation. Cooperative Institute for Research in the Atmosphere, ISSN No. 0737-5352-8, Colorado State University, Fort Collins, CO 80523, 135 pp.

—, and R.H. Johnson, 1985: Summer surface flow characteristics over northeast Colorado. *Mon. Wea. Rev.*, **113**, 1458-1469.

Tremback, C.J., 1990: Numerical simulation of a mesoscale convective complex: Model development and numerical results. Ph.D. dissertation, Atmos. Sci. Paper No. 465, Colorado State University, Dept. of Atmospheric Science, Fort Collins, CO 80523, 247 pp.

—, and R. Kessler, 1985: A surface temperature and moisture parameterization for use in mesoscale numerical models. Preprints, 7th Conference on Numerical Weather Prediction, 17-20 June 1985, Montreal, Canada, Amer. Meteor. Soc.

—, G.J. Tripoli, R. Arritt, W.R. Cotton, and R.A. Pielke, 1986: The Regional Atmospheric Modelling System. *Proc. Internat. Conf. Development and Application of Computer Techniques to Environmental Studies*, November, Los Angeles, California, P. Zannetti, Ed., Computational Mechanics Publications, Boston, 601-607.

—, G.J. Tripoli and W.R. Cotton, 1985: A regional scale atmospheric numerical model including explicit moist physics and a hydrostatic time-split scheme. Preprints, 7th Conference in Numerical Weather Prediction, 17-20 June 1985, Montreal, Quebec, Amer. Meteor. Soc.

Tripoli, G.J., 1986: A numerical investigation of an orogenic mesoscale convective system. Ph.D. disseration, Atmos. Sci. Paper No. 401, Colorado State University, Dept. of Atmospheric Science, Fort Collins, Colorado 80523, 290 pp.

—, and W.R. Cotton, 1980: A numerical investigation of several factors contributing to the observed variable intensity of deep convective over South Florida. *J. Appl. Meteor.*, **19**, 1037-1063.

—, and —, 1982: The Colorado State University three-dimensional cloud/mesoscale model-1982. Part I: General theoretical framework and sensitivity experiments. *J. Rech. Atmos.*, **16**, 185-220.

—, and —, 1989a: A numerical study of an observed orogenic mesoscale convective system. Part I: Simulated genesis and comparison with observations. *Mon. Wea. Rev.*, **117**, 273-304.

—, and —, 1989b: A numerical study of an observed orogenic mesoscale convective system. Part II: Analysis of governing dynamics. *Mon. Wea. Rev.*, **117**, 305-328.

Tyson, P.D., and R.A. Preston-Whyte, 1972: Observations of regional topographically-induced wind systems in Natal. *J. Appl. Meteor.*, **11**, 643-650.

Urfer-Henneberger, C., 1970: Neure Beobachtungen uber die Entwicklung des Schonwetter-winds systems in einem V-formigen Aplental (Dischmatal bie Davos). [New observations of the development of a clear weather wind system in a V-shaped mountain valley (Dischma Valley near Davos).] *Arch. Meteor. Geophys. Bioklim., Ser. B*, **18**, 21-42.

Vergeiner, I., and E. Dreiseitl, 1987: Valley winds and slope winds-observations and elementary thoughts. *Meteor. Atmos. Phys.*, **36**, 264-286.

Wagner, A., 1938: Theorie und Beobachtung der periodischen Gebirgswinde. [Theory and observation of periodic mountain winds.] *Gerlands Beitr. Geophys. (Leipzig)*, **52**, 408-449. [English translation: Whiteman, C.D. and E. Dreiseitl, 1984: Alpine Meteorology. Translations of classic contributions by A. Wagner, E. Ekhart and F. Defant. PNL-5141/ASCOT-84-3. Pacific Northwest Laboratory, Richland, Washington, 121 pp.]

Wallace, J.M., S. Tibaldi and A.J. Simmons, 1983: Reduction of systematic forecast errors in the ECMWF model through the introduction of an envelope orography. *Quart. J. Roy. Meteor. Soc.*, **109**, 683-717.

Wenger, R., 1923: Zur Theorie der Berg- und Talwinde. *Met. Z.*, **40**, 193-204.

Wetzel, P.J., 1973: Moisture sources and flow patterns during the northeast Colorado hail season. M.S. thesis, Dept. of Atmospheric Science, Colorado State University, Fort Collins, Colorado 80523.

—, W.R. Cotton and R.L. McAnelly, 1983: A long-lived mesoscale convective complex. Part II: Evolution and structure of the mature complex. *Mon. Wea. Rev.*, **111**, 1919-1937.

Wexler, H., 1961: A boundary layer interpretation of the low-level jet. *Tellus*, **13A**, 368-378.

Whiteman, C.D., 1980: Breakup of temperature inversions in Colorado mountain valleys. Ph.D. dissertation. Atmos. Sci. Paper No. 328, Climatology Report No. 80-2, Colorado State University, Dept. of Atmospheric Science, Fort Collins, CO 80523. 250 pp.

—, and T.B. McKee, 1977: Observations of vertical atmospheric structure in a deep mountain valley. *Arch. Meteor. Geophys. Bioklim, Ser. A.*, **26**, 29-50.

—, and T.B. McKee, 1982: Breakup of temperature inversions in deep mountain valleys. Part II: Thermodynamic model. *J. Appl. Meteor.*, **21**, 290-302.

—, and S. Barr, 1986: Atmospheric mass transport by along-valley wind systems in a deep Colorado valley. *J. Climate Appl. Meteor.*, **25**, 1205-1212.

—, K.J. Allwine, L.J. Fritschen, M.M. Orgill and J.R. Simpson, 1989a: Deep valley radiation and surface energy budget microclimates. Part I: Radiation. *J. Appl. Meteor.*, **28**, 414-426.

—, —, —, — and —, 1989b: Deep valley radiation and surface energy budget microclimates. Part II: Energy budget. *J. Appl. Meteor.*, **28**, 427-437.

Ye, Z.J., M. Segal and R.A. Pielke, 1987: Effects of atmospheric thermal stability and slope steepness on the development of daytime thermally induced upslope flow. *J. Atmos. Sci.*, **44**, 3341-3354.

Yeh, D.Zh., 1981: Some characteristics of the summer circulation over the Qinghai-Xizang (Tibet) Plateau and its neighborhood. *Bull. Amer. Meteor. Soc.*, **62**, 14-35.

—, Y.X. Gao, M.C. Tang, S.W. Lo, C.B. Shen, D.Y. Gao, Z.S. Song, Y.F. Qian, F.M. Yuan, G.Q. Li, Y.H. Ding, Z.T. Chen, M.Y. Zhou, K.J. Yang and Q.Q. Wang, 1979: *Meteorology of Qinghai-Xizang (Tibet) Plateau.* Science Press, Beijing (in Chinese).